Advanced quantum mechanics

Sylvain Nascimbene

M2 ICFP - École Normale Supérieure

These lecture notes are intended for the Master 2 course *Advanced quantum mechanics* at the École Normale Supérieure, Paris, France. They cover the full content of the course, and include additional material that is not covered in the lectures, marked by the symbol $(*)$ in the table of contents and the main text.

Contents

1 Effective dynamics of quantum systems **5**
1.1 Effective description and separation of energy scales 5
1.1.1 Formal expression of the effective Hamiltonian 5
1.1.2 Perturbative expansion of the effective Hamiltonian. 7
1.1.3 $(*)$ Projected dynamics in Landau levels 8
1.1.4 Two-photon transitions 11
1.1.5 $(*)$ Third-order virtual processes in the triangular Hubbard model 17
1.2 Adiabatic particle motion and Berry phase 20
1.2.1 The geometric Berry phase 20
1.2.2 Berry phase of a spinful particle 24
1.2.3 Engineering a synthetic magnetic monopole 25
1.3 Resonant coupling to a continuum 26
1.3.1 Short-time dynamics: reminder on Fermi's golden rule 26
1.3.2 The resolvent operator 28
1.3.3 Emergence of exponentially decaying dynamics 32
1.3.4 The Wigner and Weisskopf model and its variations 37
1.3.5 Spontaneous emission in a structured medium 43
1.4 From effective Hamiltonians to open quantum systems 48
1.4.1 Lindblad equation for a two-level system coupled to a continuum 49
1.4.2 The Lindblad equation from the Wigner–Weisskopf model . . . 50
1.4.3 Extending the Lindblad equation to the general case 55
1.4.4 $(*)$ Derivation of the Lindblad equation 56
1.4.5 Alternative description: quantum trajectories 63
1.4.6 Example of a decaying electromagnetic field in an optical cavity 65

2 Indistinguishable particles **71**
2.1 The symmetrization postulate . . . 71
2.2 Symmetric states in first quantization . . . 74
2.2.1 Restriction to the symmetric subspace . . . 74
2.2.2 Fermionic states . . . 75
2.2.3 Bosonic states . . . 77
2.2.4 Explicit expressions of few-body wave-functions . . . 78
2.2.5 Two-particle interference: the Hong–Ou–Mandel effect . . . 79
2.3 Second quantization . . . 84
2.3.1 Fock space . . . 84
2.3.2 Creation and annihilation operators . . . 85
2.3.3 Field operators . . . 88
2.3.4 Observables . . . 88
2.3.5 Evolution of quantum fields . . . 91
2.4 Quantum statistics of composite particles . . . 92
2.5 (∗) From classical to quantum fields: a vibrating string . . . 96
2.6 Gaussian quantum states and Wick theorem . . . 100

3 Coherence and correlations in many-body systems **104**
3.1 First-order correlation function and coherence properties . . . 104
3.1.1 Definition and basic properties . . . 104
3.1.2 Link with the momentum distribution. . . . 105
3.2 Pair-distribution function and particle fluctuations . . . 106
3.3 Example 1: ideal Bose and Fermi gases. . . . 107
3.3.1 First-order coherence . . . 107
3.3.2 Particle correlations and fluctuations . . . 110
3.4 Example 2: impenetrable bosons in one dimension . . . 113
3.4.1 Definition and mapping to free fermions . . . 113
3.4.2 Many-body ground state . . . 115
3.5 Example 3: superfluid helium . . . 119
3.5.1 Coherence properties and condensed fraction . . . 119
3.5.2 Pair distribution function . . . 119

4 Describing interactions: quantum scattering **121**
4.1 The two-body problem: definitions . . . 121
4.2 The Lippmann-Schwinger equation . . . 124
4.3 Born approximation and perturbative expansion . . . 126
4.3.1 Born approximation . . . 126
4.3.2 Extending the Born expansion . . . 127
4.4 Partial wave decomposition . . . 129
4.4.1 Definition of the partial wave decomposition . . . 129
4.4.2 Bound states and poles of the scattering amplitude . . . 131
4.4.3 Low-energy limit and scattering length . . . 131
4.5 Scattering between identical particles . . . 133
4.6 Examples . . . 136
4.6.1 Hard-sphere potential . . . 136
4.6.2 Square-well potential . . . 137

4.7 Scattering resonances . . . 139
4.7.1 Bound states, virtual states and resonances . . . 139
4.7.2 Feshbach resonances . . . 140
4.8 Zero-range model: the Fermi-Huang pseudopotential . . . 142
4.8.1 Definition of the pseudopotential . . . 142
4.8.2 Momentum-space representation . . . 144
4.8.3 Bound state of the pseudo-potential . . . 145
4.8.4 Born expansion of the scattering amplitude . . . 146
4.8.5 Equivalence with a renormalized coupling constant . . . 147

5 Diagonalization of quadratic many-body systems 148
5.1 A warm-up: a single bosonic mode . . . 149
5.2 General formalism . . . 153
5.3 Bogoliubov transformation for fermions . . . 155
5.4 Bogoliubov transformation for bosons . . . 157
5.5 Summary: fermions versus bosons . . . 159

6 Bogoliubov theory of Bose-Einstein condensation 160
6.1 Framework of Bogoliubov theory . . . 160
6.2 Order zero: Gross-Pitaevskii equation . . . 161
6.3 Cancellation of the first order of Bogoliubov expansion . . . 164
6.4 Order two: Bogoliubov Hamiltonian . . . 165
6.5 Bogoliubov excitation spectrum . . . 166
6.6 Density fluctuations and static structure factor . . . 169
6.7 Quantum depletion . . . 170
6.8 Zero-point energy . . . 172
6.9 Superfluidity . . . 174
6.9.1 Superfluid fraction of an interacting Bose-Einstein condensate . 174
6.9.2 Landau's criterion and critical velocity . . . 176

7 BCS theory of superconductivity 178
7.1 Introduction to the BCS ansatz . . . 178
7.2 Diagonalization of the BCS mean-field Hamiltonian . . . 180
7.3 Ground-state properties in the BEC-BCS crossover . . . 182
7.4 Gapped excitation spectrum and superfluidity *à la Landau* . . . 185
7.5 Collective excitations in a neutral superfluid . . . 186
7.6 Meissner effect and superconductivity . . . 187

8 Lattice models 189
8.1 Derivation of the Hubbard model . . . 189
8.1.1 Reminder: Bloch theorem . . . 189
8.1.2 Wannier functions and tight-binding model . . . 189
8.1.3 Localized interactions and Hubbard model . . . 191
8.2 Bose-Hubbard model . . . 192
8.2.1 Bogoliubov theory of the condensed phase . . . 192
8.2.2 Superfluid to Mott insulator transition . . . 195
8.3 Fermi-Hubbard model . . . 198
8.3.1 Introduction and symmetry considerations . . . 198

8.3.2 Magnetic instabilities of itinerant electrons 200
8.3.3 Quantum magnetism from superexchange in a Mott insulator . 202

9 Quantum magnetism **207**
9.1 Heisenberg model with ferromagnetic interaction 207
9.1.1 Ferromagnetic ground state 207
9.1.2 Spin-wave excitations 208
9.2 Heisenberg model with antiferromagnetic interaction 209
9.2.1 Frustration effects 209
9.2.2 Antiferromagnet on the square lattice 210

A Density matrix of a quantum system **214**
A.1 Density matrix of a quantum system 214
A.2 Subsystems and the reduced density matrix 215
A.3 Reduced state of an entangled pure state 215
A.4 Populations, coherences, and entropy 216

References **218**

1 Effective dynamics of quantum systems

The Schrödinger equation provides, in principle, a complete description of the dynamics of an isolated quantum system. In practice, however, the full microscopic description is often neither necessary nor useful. A physical system may contain degrees of freedom that are inaccessible to measurement, evolve on very different time scales, or interact only weakly with the degrees of freedom of interest. In such situations, we seek a simpler description that retains the relevant physics while eliminating unnecessary details.

This idea of an effective description is ubiquitous in quantum mechanics. We may, for example, follow a system while its Hamiltonian is slowly varied and find that its dynamics is governed by the instantaneous eigenstates of the Hamiltonian. We may eliminate weakly coupled excited states and obtain an effective interaction between low-energy states. Or we may describe a small quantum system coupled to a large environment, in which case its evolution is no longer described by a wave function evolving unitarily, but by an effective equation for its density matrix.

These apparently different situations share a common structure: we start from a more complete quantum description and identify a regime in which a reduced description emerges. The purpose of this chapter is to develop several of the main tools used to construct and understand such descriptions. Along the way, we will encounter geometric phases, effective Hamiltonians, spontaneous emission, and Markovian open-system dynamics.

1.1 Effective description and separation of energy scales

A central strategy in quantum mechanics is to replace a complicated description by a simpler one that captures the physics relevant at a given energy or time scale. The basic idea is to separate the degrees of freedom of a system into a set of states that we want to keep (subspace A) and another set that can, under suitable conditions, be eliminated (complementary subset B).

The full Hilbert space can then be decomposed into the direct sum $A \oplus B$, and we define the projectors $\hat{P}$ and $\hat{Q} = 1 - \hat{P}$ onto the two subspaces A and B, respectively. The dynamics of the system is governed by a Hamiltonian $\hat{H}$, which can be decomposed as a block matrix in the $A \oplus B$ basis:

$$\hat{H} = \begin{pmatrix} \hat{H}_{AA} & \hat{H}_{AB} \\ \hat{H}_{BA} & \hat{H}_{BB} \end{pmatrix} \tag{1.1}$$

where $\hat{H}_{AA} = \hat{P}\hat{H}\hat{P}$, $\hat{H}_{AB} = \hat{P}\hat{H}\hat{Q}$, $\hat{H}_{BA} = \hat{Q}\hat{H}\hat{P}$, and $\hat{H}_{BB} = \hat{Q}\hat{H}\hat{Q}$. The diagonal blocks describe the dynamics within each subspace, while the coupling $\hat{H}_{AB}$ and $\hat{H}_{BA} = \hat{H}_{AB}^{\dagger}$ describe the coupling between the two subspaces.

1.1.1 Formal expression of the effective Hamiltonian

Our objective is to establish an effective description of the dynamics within the A subspace, which is valid when the energy scales associated with the B subspace are well separated from those of the A subspace. More specifically, considering an eigenstate $|\psi\rangle$ of energy E, which satisfies the Schrödinger equation

$$\hat{H}|\psi\rangle = E|\psi\rangle, \tag{1.2}$$

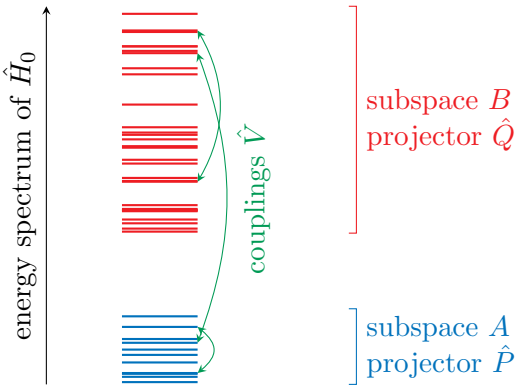


Figure 1: Scheme of the level structure of the unperturbed Hamiltonian $\hat{H}_0$, which exhibits a subspace A well separated in energy from the complementary subspace B. We are interested in deriving the effective dynamics within A under the action of the perturbation $\hat{V}$, which couples together states within each subspace, as well as states of different subspaces.

we aim at finding the Schrödinger equation for $\hat{P}|\psi\rangle$ as

$$\hat{H}_{\text{eff}}\hat{P}|\psi\rangle = E\hat{P}|\psi\rangle. \tag{1.3}$$

The energy E should be chosen within the energy range of the A subspace.

The Schrödinger equation $\hat{H}|\psi\rangle = E|\psi\rangle$ gives two coupled equations projected onto the A and B subspaces:

$$E\hat{P}|\psi\rangle = \hat{H}_{AA}\hat{P}|\psi\rangle + \hat{H}_{AB}\hat{Q}|\psi\rangle, \tag{1.4}$$

$$E\hat{Q}|\psi\rangle = \hat{H}_{BA}\hat{P}|\psi\rangle + \hat{H}_{BB}\hat{Q}|\psi\rangle. \tag{1.5}$$

The second equation can be formally solved for the component in the eliminated subspace:

$$\hat{Q}|\psi\rangle = \frac{1}{E - \hat{Q}\hat{H}\hat{Q}}\hat{Q}\hat{H}\hat{P}|\psi\rangle. \tag{1.6}$$

This expression assumes that the energy E is chosen away from the energy range of the B subspace, so that the operator $E - \hat{Q}\hat{H}\hat{Q}$ is invertible.

Substituting this expression into the first equation, we obtain an effective Schrödinger equation for the component in the A subspace:

$$\hat{H}_{\text{eff}}(E)\hat{P}|\psi\rangle = E\hat{P}|\psi\rangle, \tag{1.7}$$

where we introduce the effective Hamiltonian

$$\hat{H}_{\text{eff}}(E) = \hat{P}\hat{H}\hat{P} + \hat{P}\hat{H}\hat{Q}\frac{1}{E - \hat{Q}\hat{H}\hat{Q}}\hat{Q}\hat{H}\hat{P}. \tag{1.8}$$

It is important to stress that the effective Hamiltonian is parametrized by the energy E. The eigen-energies E of the system are therefore the solutions of the implicit equation

$$\det[E - \hat{H}_{\text{eff}}(E)] = 0. \tag{1.9}$$

The operator $1/(E - \hat{Q}\hat{H}\hat{Q})$ is a resolvent of the eliminated subspace. It describes, in a compact way, the virtual propagation of the system through the states that have been removed from the effective description. This observation will become particularly useful when we consider perturbative expansions.

1.1.2 Perturbative expansion of the effective Hamiltonian.

We now consider the case in which the Hamiltonian can be decomposed as $\hat{H} = \hat{H}_0 + \hat{V}$, where $\hat{H}_0$ does not couple A and B subspaces, and $\hat{V}$ is a perturbation that couples the two subspaces.

We assume the spectrum of $\hat{H}_0$ such that the characteristic energies of $\hat{H}_0$ in the A and B subspaces are well separated, and we define the energy difference $\hbar\Delta = E_A - E_B$, where E_A and E_B are typical energies in subspaces A and B, respectively. In that case, the effective Hamiltonian can be expressed more explicitly as a perturbative expansion in powers of $\hat{V}$.

Expansion to second order in $\hat{V}$. We first consider the expansion up to second order, which requires the evaluation of the resolvent $1/(E - \hat{Q}\hat{H}\hat{Q})$ up to zero order in $\hat{V}$. Assuming the energy E is chosen within the energy range of the A subspace, and that the spread of the energies of $\hat{H}_0$ within each subspace is small compared with $|\hbar\Delta|$ (so that $\hat{Q}\hat{H}_0\hat{Q} \simeq E_B\hat{Q}$), it is simply given by $1/(E - \hat{Q}\hat{H}\hat{Q}) = 1/(\hbar\Delta) + \mathcal{O}(\hat{V})$. One then obtains the effective Hamiltonian up to second order in $\hat{V}$ as

$$\hat{H}_{\text{eff}} = \hat{P}\hat{H}_0\hat{P} + \hat{P}\hat{V}\hat{P} + \frac{\hat{P}\hat{V}\hat{Q}\hat{V}\hat{P}}{\hbar\Delta} + \mathcal{O}(\hat{V}^3). \tag{1.10}$$

In the simplest case in which $\hat{P}$ projects on a single eigenstate $|\psi_0\rangle$ of energy E_0 in the absence of the perturbation, keeping the full resolvent of $\hat{H}_0$ in B (i.e. without assuming B to be quasi-degenerate), we recover the standard result from perturbation theory

$$E = E_0 + \langle\psi_0|\hat{V}|\psi_0\rangle + \langle\psi_0|\hat{V}\hat{Q}\frac{1}{E_0 - \hat{Q}\hat{H}_0\hat{Q}}\hat{Q}\hat{V}|\psi_0\rangle. \tag{1.11}$$

(∗) **Expansion to third order in $\hat{V}$.** The expansion can be extended to higher orders in $\hat{V}$, but it requires more care. Indeed, the evaluation of the resolvent $1/(E - \hat{Q}\hat{H}\hat{Q})$ needs to take into account the fact that the energy E is shifted from its unperturbed value, such that the resolvent $1/(E - \hat{Q}\hat{H}\hat{Q})$ cannot be simply replaced by the expansion of $1/(\hbar\Delta - \hat{Q}\hat{V}\hat{Q})$ in powers of $\hat{V}$.

To get the perturbative expansion of the effective Hamiltonian at third order in $\hat{V}$, we assume for simplicity that both subspaces are degenerate for $\hat{H}_0$, i.e. $\hat{P}\hat{H}_0\hat{P} = E_A\hat{P}$ and $\hat{Q}\hat{H}_0\hat{Q} = E_B\hat{Q}$. One then writes the resolvent as:

$$\frac{1}{E - \hat{Q}\hat{H}\hat{Q}} = \frac{1}{\hbar\Delta + E - E_A - \hat{Q}\hat{V}\hat{Q}}. \tag{1.12}$$

The energy difference $E - E_A$ is of order $\hat{V}$, such that the resolvent can be expanded in powers of $\hat{V}$ as

$$\frac{1}{E - \hat{Q}\hat{H}\hat{Q}} = \frac{1}{\hbar\Delta} + \frac{\hat{Q}\hat{V}\hat{Q} - (E - E_A)}{(\hbar\Delta)^2} + \mathcal{O}(\hat{V}^2). \tag{1.13}$$

The effective Hamiltonian can then be expressed as

$$\hat{H}_{\text{eff}} = \hat{P}\hat{H}_0\hat{P} + \hat{P}\hat{V}\hat{P} + \frac{\hat{P}\hat{V}\hat{Q}\hat{V}\hat{P}}{\hbar\Delta} + \frac{\hat{P}\hat{V}\hat{Q}\hat{V}\hat{Q}\hat{V}\hat{P}}{(\hbar\Delta)^2} - \frac{(E - E_A)\hat{P}\hat{V}\hat{Q}\hat{V}\hat{P}}{(\hbar\Delta)^2} + \mathcal{O}(\hat{V}^4). \tag{1.14}$$

The energy difference $E - E_A$ can be replaced by its operator expression at first order in $\hat{V}$, which is given by $E - E_A = \hat{P}\hat{V}\hat{P} + \mathcal{O}(\hat{V}^2)$. The Hermitian character of the effective Hamiltonian is ensured by taking the anti-commutator of this operator with the other factor $\hat{P}\hat{V}\hat{Q}\hat{V}\hat{P}$. We then obtain the final expression of the effective Hamiltonian up to third order in $\hat{V}$ as

$$\hat{H}_{\text{eff}} = \hat{P}\hat{H}_0\hat{P} + \hat{P}\hat{V}\hat{P} + \frac{\hat{P}\hat{V}\hat{Q}\hat{V}\hat{P}}{\hbar\Delta} + \frac{1}{(\hbar\Delta)^2}\left(\hat{P}\hat{V}\hat{Q}\hat{V}\hat{Q}\hat{V}\hat{P} - \frac{1}{2}\{\hat{P}\hat{V}\hat{P}, \hat{P}\hat{V}\hat{Q}\hat{V}\hat{P}\}\right) + \mathcal{O}(\hat{V}^4). \tag{1.15}$$

1.1.3 (∗) Projected dynamics in Landau levels

The perturbative expansion of the effective Hamiltonian is particularly interesting when the subspace A is highly degenerate. A paradigmatic example is provided by the Landau levels of a charged particle moving in two dimensions in a perpendicular magnetic field. Each Landau level is a flat band containing a macroscopic number of states, and the projection of a perturbation onto such a band leads to a nontrivial effective dynamics.

We consider a spinless particle of charge q and mass m, confined to the xy plane and subjected to a uniform magnetic field $\mathbf{B} = B\mathbf{e}_z$. The unperturbed dynamics is governed by the Landau Hamiltonian

$$\hat{H}_0 = \frac{[\hat{\mathbf{p}} - q\mathbf{A}(\hat{\mathbf{r}})]^2}{2m}, \tag{1.16}$$

where the vector potential satisfies

$$\nabla \times \mathbf{A} = B\mathbf{e}_z. \tag{1.17}$$

It is useful to separate the position of the particle into two independent contributions,

$$\hat{\mathbf{r}} = \hat{\mathbf{R}} + \hat{\mathbf{r}}_{\text{c}}, \tag{1.18}$$

where $\hat{\mathbf{R}}$ is the guiding-center coordinate and $\hat{\mathbf{r}}_{\text{c}}$ describes the cyclotron motion. We define

$$\hat{\mathbf{r}}_{\text{c}} = \frac{1}{qB}\,\mathbf{e}_z \times [\hat{\mathbf{p}} - q\mathbf{A}(\hat{\mathbf{r}})]. \tag{1.19}$$

The velocity is related to the cyclotron coordinate according to

$$\hat{\boldsymbol{v}} = \frac{qB}{m}\,\hat{\mathbf{r}}_{\text{c}} \times \mathbf{e}_z, \tag{1.20}$$

so that the Heisenberg equation gives

$$\partial_t \hat{\mathbf{r}}_{\text{c}} = \omega_{\text{c}}\,\hat{\mathbf{r}}_{\text{c}} \times \mathbf{e}_z, \qquad \omega_{\text{c}} = \frac{qB}{m}. \tag{1.21}$$

The cyclotron coordinate therefore rotates at the cyclotron frequency ω_{c} around the guiding center.

The two sets of coordinates have nontrivial commutation relations,

$$[\hat{X}, \hat{Y}] = -\mathrm{i}\ell_{\text{c}}^2, \tag{1.22}$$

$$[\hat{x}_{\text{c}}, \hat{y}_{\text{c}}] = \mathrm{i}\ell_{\text{c}}^2, \tag{1.23}$$

while all commutators between guiding-center and cyclotron coordinates vanish. Here

$$\ell_{\mathrm{c}} = \sqrt{\frac{\hbar}{qB}} \tag{1.24}$$

is the magnetic length. The Landau Hamiltonian depends only on the cyclotron coordinates,

$$\hat{H}_0 = \frac{\hbar\omega_{\mathrm{c}}}{2\ell_{\mathrm{c}}^2}\left(\hat{x}_{\mathrm{c}}^2 + \hat{y}_{\mathrm{c}}^2\right). \tag{1.25}$$

Since $\hat{x}_{\mathrm{c}}$ and $\hat{y}_{\mathrm{c}}$ form a conjugate pair, this Hamiltonian is equivalent to a harmonic oscillator. Its spectrum is therefore

$$E_{n_{\mathrm{c}}} = \hbar\omega_{\mathrm{c}}\left(n_{\mathrm{c}} + \frac{1}{2}\right), \tag{1.26}$$

where $n_{\mathrm{c}} = 0, 1, 2, \ldots$ is the cyclotron excitation number.

Importantly, $\hat{H}_0$ contains no guiding-center coordinate. The quantum number n_{c} therefore labels a highly degenerate eigenspace: each n_{c} defines a flat band known as the n_{c}th Landau level. The degeneracy of these levels is at the heart of the integer quantum Hall effect.

We now consider a weak external potential $V(\mathbf{r})$ and treat it as a perturbation,

$$\hat{V} = V(\hat{\mathbf{r}}). \tag{1.27}$$

We focus on the lowest Landau level, $n_{\mathrm{c}} = 0$, and denote by $\hat{P}$ the corresponding projector. To first order in the perturbation, the effective Hamiltonian within this subspace is simply

$$\hat{H}_{\mathrm{eff}} = \hat{P}\hat{H}_0\hat{P} + \hat{P}\hat{V}\hat{P}. \tag{1.28}$$

Since $\hat{H}_0$ is constant within a Landau level, the nontrivial part is the projected potential,

$$\hat{V}_{\mathrm{eff}} = \hat{P}V(\hat{\mathbf{R}} + \hat{\mathbf{r}}_{\mathrm{c}})\hat{P}. \tag{1.29}$$

The projection has an interesting physical consequence: the potential is no longer evaluated at the particle position, but is averaged over the cyclotron wave function. To make this explicit, we write the potential in Fourier space,

$$V(\mathbf{r}) = \int \tilde{V}(\mathbf{q})\mathrm{e}^{\mathrm{i}\mathbf{q}\cdot\mathbf{r}}\,\mathrm{d}^2q. \tag{1.30}$$

Since the guiding-center and cyclotron coordinates commute, we can factorize

$$\mathrm{e}^{\mathrm{i}\mathbf{q}\cdot\hat{\mathbf{r}}} = \mathrm{e}^{\mathrm{i}\mathbf{q}\cdot\hat{\mathbf{R}}}\mathrm{e}^{\mathrm{i}\mathbf{q}\cdot\hat{\mathbf{r}}_{\mathrm{c}}}. \tag{1.31}$$

Consequently,

$$\hat{V}_{\mathrm{eff}} = \int \tilde{V}(\mathbf{q})\mathrm{e}^{\mathrm{i}\mathbf{q}\cdot\hat{\mathbf{R}}}\hat{P}\mathrm{e}^{\mathrm{i}\mathbf{q}\cdot\hat{\mathbf{r}}_{\mathrm{c}}}\hat{P}\,\mathrm{d}^2q, \tag{1.32}$$

where we used the fact that $\hat{P}$ commutes with $\hat{\mathbf{R}}$, since it projects on the ground state of the cyclotron motion.

The operator $\mathrm{e}^{\mathrm{i}\mathbf{q}\cdot\hat{\mathbf{r}}_{\mathrm{c}}}$ acts only on the cyclotron degree of freedom. In the lowest Landau level, the cyclotron wavefunction is a Gaussian, hence the matrix element is

$$\langle n_{\mathrm{c}} = 0|\mathrm{e}^{\mathrm{i}\mathbf{q}\cdot\hat{\mathbf{r}}_{\mathrm{c}}}|n_{\mathrm{c}} = 0\rangle = \mathrm{e}^{-(q\ell_{\mathrm{c}})^2/4}. \tag{1.33}$$

The projected potential can therefore be written solely in terms of the guiding-center coordinate,

$$\hat{V}_{\text{eff}} = \hat{P}\left[\int \tilde{V}(\mathbf{q})\mathrm{e}^{-(q\ell_{\mathrm{c}})^2/4}\mathrm{e}^{\mathrm{i}\mathbf{q}\cdot\hat{\mathbf{R}}}\,\mathrm{d}^2q\right]\hat{P}. \tag{1.34}$$

Thus, projection onto the lowest Landau level amounts to filtering the Fourier components of the potential by the Gaussian factor $\mathrm{e}^{-(q\ell_{\mathrm{c}})^2/4}$. Equivalently, the effective potential is a smoothed version of the original potential,

$$V_{\text{eff}}(\mathbf{R}) = (V * K)(\mathbf{R}), \tag{1.35}$$

where

$$K(\mathbf{R}) = \frac{1}{\pi\ell_{\mathrm{c}}^2}\mathrm{e}^{-(R/\ell_{\mathrm{c}})^2}. \tag{1.36}$$

The cyclotron motion therefore averages the external potential over a region of characteristic size ℓ_{c}. In particular, spatial variations of V on length scales much shorter than ℓ_{c} are strongly suppressed after projection.

The effective Hamiltonian within the lowest Landau level is consequently

$$\hat{H}_{\text{eff}} = \hat{P}\left[\frac{\hbar\omega_{\mathrm{c}}}{2} + V_{\text{eff}}(\hat{\mathbf{R}})\right]\hat{P}. \tag{1.37}$$

Although the kinetic energy is frozen within the Landau level, the guiding-center coordinates remain dynamical because they do not commute:

$$[\hat{X}, \hat{Y}] = -\mathrm{i}\ell_{\mathrm{c}}^2. \tag{1.38}$$

The Heisenberg equations therefore give

$$\partial_t\hat{\mathbf{R}} = \frac{1}{\mathrm{i}\hbar}[\hat{\mathbf{R}}, \hat{H}_{\text{eff}}] = \frac{1}{qB}\mathbf{e}_z \times \nabla V_{\text{eff}}(\hat{\mathbf{R}}). \tag{1.39}$$

Thus, in the semiclassical limit, the guiding center drifts along the equipotential lines of V_{eff}. This is the quantum version of the classical $\boldsymbol{E} \times \boldsymbol{B}$ drift: the cyclotron motion averages the potential over the finite spatial extent of the cyclotron orbit, while the guiding center subsequently drifts along the resulting equipotential contours.

For a uniform electric field, the potential is linear,

$$V(\mathbf{r}) = -q\mathbf{E}\cdot\mathbf{r}. \tag{1.40}$$

A Gaussian convolution leaves a linear function unchanged, so that

$$V_{\text{eff}}(\mathbf{R}) = -q\mathbf{E}\cdot\mathbf{R}. \tag{1.41}$$

Equation (1.39) then gives

$$\partial_t\hat{\mathbf{R}} = \frac{\mathbf{E}\times\mathbf{B}}{B^2}, \tag{1.42}$$

which is the familiar Hall drift velocity. For a nonuniform potential, however, the projection onto a Landau level modifies the potential at length scales comparable to the magnetic length, providing a simple example of how projection onto a degenerate subspace can qualitatively modify the dynamics generated by a perturbation.

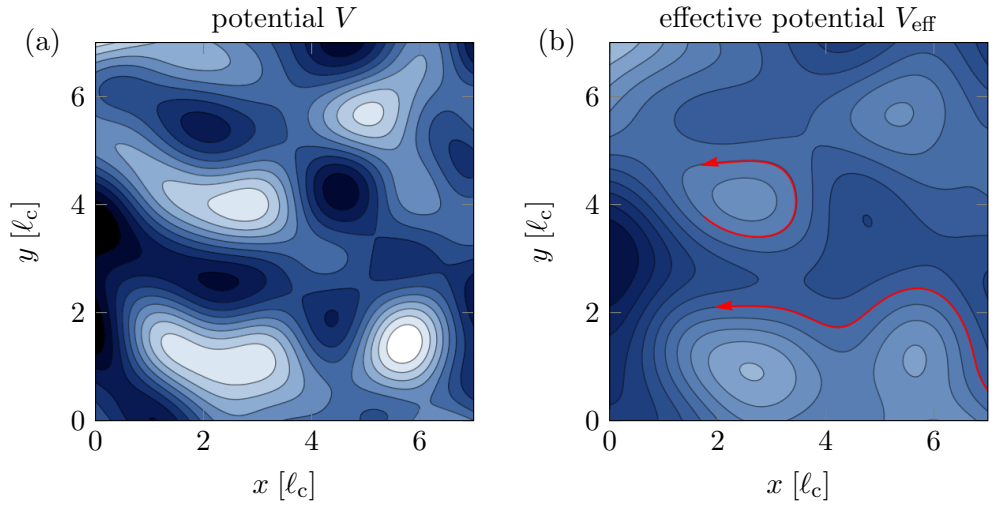


Figure 2: (a) Example of equipotential lines of a disorder potential $V(x, y)$ acting on a charged particle subjected to a perpendicular magnetic field. (b) Effective potential $V_{\text{eff}}(x, y)$ obtained by smoothing the potential $V(x, y)$ over the magnetic length, as given by (1.35). The guiding-center dynamics follows the equipotential lines of $V_{\text{eff}}(x, y)$, as illustrated by the two trajectories.

1.1.4 Two-photon transitions

A particularly important application of the effective Hamiltonian formalism is provided by two-photon transitions. They arise when a light field couples a low-energy manifold to an excited electronic state, while the light is sufficiently far detuned from the corresponding optical transition. The excited state is then only virtually populated and can be eliminated, resulting in an effective coupling between states within the ground-state manifold.

We consider a simple example in which the ground electronic manifold has angular momentum $J = 1$, while the excited electronic level $|e\rangle$ is non-degenerate ($J_e = 0$), as illustrated in Fig. 3. We denote by $\hbar\omega_0$ the energy of $|e\rangle$ relative to the ground manifold, by $\hat{P}$ the projector onto the ground manifold, and by $\hat{Q} = \mathbb{1} - \hat{P} = |e\rangle\langle e|$ the projector onto the excited state.

Atom–light coupling. The ground-state manifold is coupled to the excited state by a monochromatic electric field, which we write as

$$\mathbf{E}(t) = \mathcal{E}\,\boldsymbol{\epsilon}\,\mathrm{e}^{-\mathrm{i}\omega t} + \mathcal{E}^*\,\boldsymbol{\epsilon}^*\,\mathrm{e}^{\mathrm{i}\omega t}, \tag{1.43}$$

where $\mathcal{E}$ is a complex amplitude and $\boldsymbol{\epsilon}$ a complex unit vector, $\boldsymbol{\epsilon}^* \cdot \boldsymbol{\epsilon} = 1$, which specifies the polarization. The field $\mathbf{E}(t)$ is real, as it must be. Its splitting into a positive-frequency part, varying as $\mathrm{e}^{-\mathrm{i}\omega t}$, and its complex conjugate plays an essential role in what follows: only the former drives absorption towards the excited state.

Within the electric-dipole approximation, the atom–light interaction is

$$\hat{V}(t) = -\hat{\mathbf{d}} \cdot \mathbf{E}(t), \tag{1.44}$$

where $\hat{\mathbf{d}}$ is the atomic dipole operator, a Hermitian vector operator.

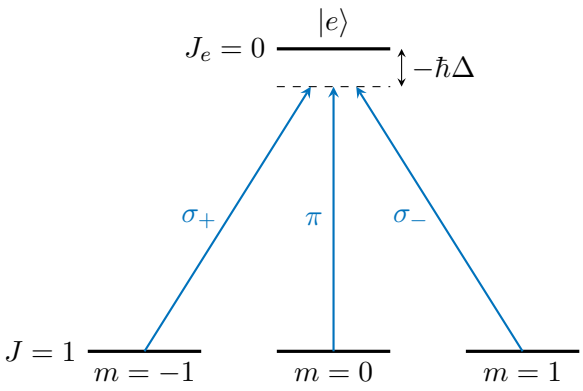


Figure 3: Scheme of the level structure considered in the text. The ground manifold has angular momentum $J = 1$ and is coupled to a non-degenerate excited state by an off-resonant light field. The relative coupling amplitudes between the ground states and the excited state are determined by the polarization of the light field. The dashed line indicates the energy $\hbar\omega$ of the light field, detuned by $\Delta = \omega - \omega_0$ from the excited state (here $\Delta < 0$).

It is convenient to decompose vectors in the spherical basis, defined by the three unit vectors

$$\mathbf{e}_{+1} = \frac{1}{\sqrt{2}}(\mathbf{e}_x + \mathrm{i}\mathbf{e}_y), \tag{1.45}$$

$$\mathbf{e}_0 = \mathbf{e}_z, \tag{1.46}$$

$$\mathbf{e}_{-1} = \frac{1}{\sqrt{2}}(\mathbf{e}_x - \mathrm{i}\mathbf{e}_y), \tag{1.47}$$

where $\mathbf{e}_x$, $\mathbf{e}_y$, and $\mathbf{e}_z$ are the Cartesian unit vectors. This basis is orthonormal in the sense

$$\mathbf{e}_q^* \cdot \mathbf{e}_{q'} = \delta_{qq'}, \qquad \mathbf{e}_q^* = \mathbf{e}_{-q}. \tag{1.48}$$

The vectors $\mathbf{e}_{\pm1}$ describe the circular polarizations $\sigma^\pm$, while $\mathbf{e}_0$ describes linear polarization along the z axis (π polarization). One checks directly from (1.43) that, for $\boldsymbol{\epsilon} = \mathbf{e}_{+1}$ and real $\mathcal{E}$, the field rotates from $\mathbf{e}_x$ towards $\mathbf{e}_y$, i.e. carries an angular momentum $+\hbar$ along z per photon.

The Cartesian basis and the dipole operator. Since $|e\rangle$ is a scalar ($J_e = 0$) and $\hat{\mathbf{d}}$ is a vector operator, the Wigner–Eckart theorem fixes all dipole matrix elements between the two manifolds in terms of a single reduced matrix element d. The statement takes its simplest form in a *Cartesian* basis $\{|x\rangle, |y\rangle, |z\rangle\}$ of the ground manifold, defined as the basis in which

$$\langle e|\, \mathbf{e}_i \cdot \hat{\mathbf{d}}\, |j\rangle = d\, \delta_{ij}, \qquad i, j \in \{x, y, z\}, \tag{1.49}$$

with d real, which fixes the phase of $|e\rangle$. The state $|i\rangle$ is the state of the ground manifold that transforms as the Cartesian component i of a vector; equivalently, $|i\rangle = |m = 0\rangle_i$, the state of vanishing angular-momentum projection along the axis i. The part of the dipole operator connecting the two manifolds then reads

$$\hat{\mathbf{d}} = d \sum_{i=x,y,z} \mathbf{e}_i \left(|e\rangle\langle i| + |i\rangle\langle e|\right). \tag{1.50}$$

The Cartesian states are related to the eigenstates $|m\rangle_z$ of $\hat{J}_z$ by exactly the same coefficients that relate the spherical basis vectors to the Cartesian unit vectors,

$$|m\rangle_z = \sum_i (\mathbf{e}_m)_i \, |i\rangle, \tag{1.51}$$

that is,

$$|m = \pm 1\rangle_z = \frac{1}{\sqrt{2}} \left(|x\rangle \pm \mathrm{i}|y\rangle \right), \tag{1.52}$$

$$|m = 0\rangle_z = |z\rangle, \tag{1.53}$$

or, inversely,

$$|x\rangle = \frac{1}{\sqrt{2}} \left(|m = 1\rangle_z + |m = -1\rangle_z \right), \tag{1.54}$$

$$|y\rangle = -\frac{\mathrm{i}}{\sqrt{2}} \left(|m = 1\rangle_z - |m = -1\rangle_z \right), \tag{1.55}$$

$$|z\rangle = |m = 0\rangle_z. \tag{1.56}$$

Inserting (1.51) into (1.50) gives the equivalent spherical form

$$\hat{\mathbf{d}} = d \sum_{m=-1}^{1} \left(\mathbf{e}_m |e\rangle\langle m|_z + \mathbf{e}_m^* |m\rangle_z \langle e| \right). \tag{1.57}$$

Rotating-wave approximation. We now insert the field (1.43) and the dipole operator (1.50) into $\hat{V}(t)$. It is useful to introduce, for any complex vector $\mathbf{v}$, the ground-state superposition

$$|\mathbf{v}\rangle = \sum_i v_i |i\rangle, \qquad \text{so that} \qquad \langle \mathbf{v}| = \sum_i v_i^* \langle i|. \tag{1.58}$$

Using $\mathbf{e}_i \cdot \boldsymbol{\epsilon} = \epsilon_i$, we obtain

$$\hat{\mathbf{d}} \cdot \boldsymbol{\epsilon} = d \left(|e\rangle\langle \boldsymbol{\epsilon}^*| + |\boldsymbol{\epsilon}\rangle\langle e| \right), \tag{1.59}$$

$$\hat{\mathbf{d}} \cdot \boldsymbol{\epsilon}^* = d \left(|e\rangle\langle \boldsymbol{\epsilon}| + |\boldsymbol{\epsilon}^*\rangle\langle e| \right), \tag{1.60}$$

where the appearance of $\langle \boldsymbol{\epsilon}^*| = \sum_i \epsilon_i \langle i|$ in the first line should be noted carefully. The interaction therefore reads

$$\begin{aligned} \hat{V}(t) = & - d\,\mathcal{E}\, \mathrm{e}^{-\mathrm{i}\omega t} \left(|e\rangle\langle \boldsymbol{\epsilon}^*| + |\boldsymbol{\epsilon}\rangle\langle e| \right) \\ & - d\,\mathcal{E}^*\, \mathrm{e}^{\mathrm{i}\omega t} \left(|e\rangle\langle \boldsymbol{\epsilon}| + |\boldsymbol{\epsilon}^*\rangle\langle e| \right). \end{aligned} \tag{1.61}$$

The four terms differ by their time dependence in the interaction picture. There, the excited state carries a phase $\mathrm{e}^{-\mathrm{i}\omega_0 t}$ relative to the ground manifold, so that any operator of the form $|e\rangle\langle g|$ acquires a factor $\mathrm{e}^{\mathrm{i}\omega_0 t}$, and $|g\rangle\langle e|$ a factor $\mathrm{e}^{-\mathrm{i}\omega_0 t}$. The two terms

$$\mathrm{e}^{-\mathrm{i}\omega t} |e\rangle\langle \boldsymbol{\epsilon}^*|, \qquad \mathrm{e}^{\mathrm{i}\omega t} |\boldsymbol{\epsilon}^*\rangle\langle e| \tag{1.62}$$

then oscillate slowly, at the detuning $\Delta = \omega - \omega_0$, whereas the two remaining terms oscillate rapidly, at $\omega + \omega_0$. For a near-resonant drive, $|\Delta| \ll \omega_0$, the latter average

to zero over the time scales of interest and can be dropped. This is the *rotating-wave approximation*. Its leading correction is an energy shift of order $|\Omega|^2/\omega_0$, the Bloch–Siegert shift, negligible in the regime considered here.

It is worth emphasizing that the counter-rotating terms discarded in this step are precisely those involving $|\boldsymbol{\epsilon}\rangle$, whereas the retained, co-rotating terms involve $|\boldsymbol{\epsilon}^*\rangle$. The rotating-wave approximation is thus what singles out one of the two conjugate superpositions.

Introducing the Rabi frequency

$$\Omega = -\frac{d\,\mathcal{E}}{\hbar}, \tag{1.63}$$

the retained part of (1.61) becomes

$$\hat{V}(t) = \hbar\Omega\, \mathrm{e}^{-\mathrm{i}\omega t}|e\rangle\langle\boldsymbol{\epsilon}^*| + \hbar\Omega^*\, \mathrm{e}^{\mathrm{i}\omega t}|\boldsymbol{\epsilon}^*\rangle\langle e|. \tag{1.64}$$

The residual time dependence is removed by the unitary transformation

$$\hat{U}(t) = \hat{P} + \mathrm{e}^{\mathrm{i}\omega t}|e\rangle\langle e| \tag{1.65}$$

to the frame rotating at the laser frequency. Using $\hat{U}\hat{H}\hat{U}^\dagger + \mathrm{i}\hbar(\partial_t\hat{U})\hat{U}^\dagger$, the Hamiltonian becomes time-independent,

$$\hat{H}_0 = -\hbar\Delta\,\hat{Q}, \tag{1.66}$$

$$\hat{V} = \hbar\Omega|e\rangle\langle\boldsymbol{\epsilon}^*| + \hbar\Omega^*|\boldsymbol{\epsilon}^*\rangle\langle e|, \tag{1.67}$$

the ground manifold having energy zero and the excited state energy $-\hbar\Delta$.

Bright and dark states. The essential structural feature of (1.67) is that the light couples the excited state to a *single* ground-state superposition,

$$|\boldsymbol{\epsilon}^*\rangle = \epsilon_x^*|x\rangle + \epsilon_y^*|y\rangle + \epsilon_z^*|z\rangle, \tag{1.68}$$

called the *bright state*. The complex conjugation is essential: the bright state carries the components of $\boldsymbol{\epsilon}^*$, not those of $\boldsymbol{\epsilon}$, in the Cartesian basis. It originates from the fact that absorption is driven by the positive-frequency part of the field, which enters the coupling through the bra $\langle\boldsymbol{\epsilon}^*| = \sum_i \epsilon_i\langle i|$. For linear polarizations $\boldsymbol{\epsilon}$ may be chosen real and the distinction is immaterial; for elliptical or circular polarizations it is not.

Because $|e\rangle$ is non-degenerate, the coupling operator $|e\rangle\langle\boldsymbol{\epsilon}^*|$ has rank one. The two-dimensional subspace orthogonal to $|\boldsymbol{\epsilon}^*\rangle$ is therefore entirely decoupled from the light and forms a *dark subspace*. The polarization thus selects one direction in the three-dimensional ground manifold, leaving the two orthogonal directions unaffected.

As a check, consider a pure circular or linear polarization $\boldsymbol{\epsilon} = \mathbf{e}_q$. Using $\mathbf{e}_q^* = \mathbf{e}_{-q}$ together with (1.51),

$$|\boldsymbol{\epsilon}^*\rangle = \sum_i (\mathbf{e}_{-q})_i|i\rangle = |m = -q\rangle_z. \tag{1.69}$$

A σ^+ field ($q = +1$) therefore couples the excited state to $|m = -1\rangle_z$, a σ^- field to $|m = +1\rangle_z$, and π light to $|m = 0\rangle_z$. This is precisely the usual selection rule: absorbing a σ^+ photon raises the magnetic quantum number by one unit, and since the excited state has $m_e = 0$, the only ground state that can be reached is $m = -1$.

Adiabatic elimination: the light shift. We now derive the effective dynamics generated by the off-resonant light, taking the ground-state manifold as the low-energy subspace A and the excited state as the eliminated subspace B.

For $|\Omega| \ll |\Delta|$, the excited state is only virtually populated and can be eliminated perturbatively. Since the perturbation (1.67) only couples the two manifolds, $\hat{P}\hat{V}\hat{P} = 0$ and the leading contribution to the effective Hamiltonian is of second order,

$$\hat{H}^{(2)}_{\text{eff}} = \hat{P}\hat{V}\hat{Q}\frac{1}{E_A - \hat{H}^{(0)}_{BB}}\hat{Q}\hat{V}\hat{P}. \tag{1.70}$$

Taking $E_A = 0$ and $\hat{H}^{(0)}_{BB} = -\hbar\Delta$, this becomes

$$\hat{H}^{(2)}_{\text{eff}} = \frac{1}{\hbar\Delta}\hat{P}\hat{V}\hat{Q}\hat{V}\hat{P}, \tag{1.71}$$

and, inserting (1.67),

$$\hat{H}_{\text{eff}} = \frac{\hbar|\Omega|^2}{\Delta}|\boldsymbol{\epsilon}^*\rangle\langle\boldsymbol{\epsilon}^*|. \tag{1.72}$$

The bright state therefore acquires a light shift $\hbar|\Omega|^2/\Delta$, while the dark states remain unaffected. The energy shift results from a virtual process in which the atom is transferred to the excited state and subsequently returns to the ground manifold. Its sign is set by that of the detuning: a red-detuned field ($\Delta < 0$) lowers the energy of the bright state, which is the basis of optical trapping.

This mechanism is known as an *AC Stark shift* or *light shift*. It provides the basis for optical manipulation of atoms and other polarizable systems (so-called optical tweezers).

Raman coupling between two ground states. So far the three ground states have been degenerate. We now apply a static magnetic field along z, which lifts this degeneracy and, at the same time, defines the quantization axis used throughout. The ground manifold acquires the Zeeman Hamiltonian

$$\hat{H}_{\text{Z}} = \hbar\omega_{\text{Z}}\sum_{m=-1}^{1} m\,|m\rangle_z\langle m|_z, \tag{1.73}$$

where $\hbar\omega_{\text{Z}}$ is the splitting between adjacent sublevels. The excited state, having $J_e = 0$, carries no magnetic moment and remains unshifted. We assume that the Zeeman splitting is small compared with the detuning, $|\omega_{\text{Z}}| \ll |\Delta|$, so that all sublevels may be assigned a common detuning from the excited state.

We now couple two sublevels of this manifold by a Raman transition. To make the discussion concrete, we choose the two polarizations

$$\boldsymbol{\epsilon}_1 = \mathbf{e}_0, \qquad \boldsymbol{\epsilon}_2 = \mathbf{e}_{+1}, \tag{1.74}$$

that is, one π-polarized and one σ^+-polarized beam. According to the selection rule established above, the corresponding bright states are

$$|\boldsymbol{\epsilon}_1^*\rangle = |m = 0\rangle_z, \qquad |\boldsymbol{\epsilon}_2^*\rangle = |m = -1\rangle_z, \tag{1.75}$$

of energies 0 and $-\hbar\omega_{\text{Z}}$ respectively. The third sublevel $|m = +1\rangle_z$ is orthogonal to both and therefore remains dark: the dynamics is confined to a closed two-level system.

The electric field must now contain two frequency components, so that the energy difference between the two sublevels can be supplied by the field,

$$\mathbf{E}(t) = \mathcal{E}_1 \boldsymbol{\epsilon}_1 \mathrm{e}^{-\mathrm{i}\omega_1 t} + \mathcal{E}_2 \boldsymbol{\epsilon}_2 \mathrm{e}^{-\mathrm{i}\omega_2 t} + \mathrm{c.c.}, \tag{1.76}$$

with the corresponding Rabi frequencies $\Omega_j = -d\,\mathcal{E}_j/\hbar$. We denote the frequency difference by

$$\delta = \omega_2 - \omega_1, \tag{1.77}$$

and choose it equal to the Zeeman splitting,

$$\omega_2 = \omega_1 + \omega_{\mathrm{Z}}. \tag{1.78}$$

The reason for this choice will become apparent below: the transition proceeds by absorbing a photon from beam 2 and re-emitting one into beam 1, so that the atom gains the energy $\hbar\delta$, which must match the energy $\hbar\omega_{\mathrm{Z}}$ separating $|m=-1\rangle_z$ from $|m=0\rangle_z$. We assume $|\delta| \ll |\Delta|$, so that both virtual paths share the common detuning $\Delta = \omega_1 - \omega_0$.

Repeating the rotating-wave treatment and working in the frame rotating at ω_1, the interaction reads

$$\hat{V}(t) = \hbar \left(\Omega_1 |e\rangle\langle \boldsymbol{\epsilon}_1^*| + \Omega_2\, \mathrm{e}^{-\mathrm{i}\delta t} |e\rangle\langle \boldsymbol{\epsilon}_2^*| + \mathrm{h.c.} \right). \tag{1.79}$$

Applying the same second-order expression, and retaining the Zeeman term, gives $\hat{H}_{\mathrm{eff}} = \hat{H}_{\mathrm{Z}} + \hat{H}_{\mathrm{eff}}^{(2)}$ with

$$\hat{H}_{\mathrm{eff}}^{(2)} = \frac{\hbar|\Omega_1|^2}{\Delta} |\boldsymbol{\epsilon}_1^*\rangle\langle\boldsymbol{\epsilon}_1^*| + \frac{\hbar|\Omega_2|^2}{\Delta} |\boldsymbol{\epsilon}_2^*\rangle\langle\boldsymbol{\epsilon}_2^*| \tag{1.80}$$

$$+ \frac{\hbar\Omega_1^*\Omega_2}{\Delta}\, \mathrm{e}^{-\mathrm{i}\delta t}\, |\boldsymbol{\epsilon}_1^*\rangle\langle\boldsymbol{\epsilon}_2^*| + \frac{\hbar\Omega_1\Omega_2^*}{\Delta}\, \mathrm{e}^{\mathrm{i}\delta t}\, |\boldsymbol{\epsilon}_2^*\rangle\langle\boldsymbol{\epsilon}_1^*|. \tag{1.81}$$

The first two terms are the individual light shifts, while the last two terms describe an effective coupling between the two ground-state superpositions, oscillating at the frequency difference δ of the two beams.

This coupling can be understood as a two-step virtual process,

$$|\boldsymbol{\epsilon}_2^*\rangle \longrightarrow |e\rangle \longrightarrow |\boldsymbol{\epsilon}_1^*\rangle, \tag{1.82}$$

that is, $|m=-1\rangle_z \to |e\rangle \to |m=0\rangle_z$, in which a σ^+ photon is absorbed from beam 2 and a π photon is re-emitted into beam 1. The angular-momentum budget is consistent: the absorbed photon carries $+\hbar$ and the emitted one carries none, so that the atom gains one unit of angular momentum, $\Delta m = +1$. The excited state is never significantly populated, but it mediates a coherent transition between the two ground states. The corresponding coupling strength is

$$\Omega_{2\mathrm{ph}} = \frac{\Omega_1^*\Omega_2}{\Delta}, \tag{1.83}$$

up to the convention used for defining the Rabi frequency. This is the basic mechanism of a *two-photon* or *Raman* transition.

It remains to verify that the choice (1.78) indeed makes this coupling resonant. The remaining time dependence is removed by a further transformation within the ground manifold,

$$\hat{U}_2(t) = |\boldsymbol{\epsilon}_1^*\rangle\langle\boldsymbol{\epsilon}_1^*| + \mathrm{e}^{-\mathrm{i}\delta t}|\boldsymbol{\epsilon}_2^*\rangle\langle\boldsymbol{\epsilon}_2^*|, \tag{1.84}$$

which cancels the factors $\mathrm{e}^{\mp\mathrm{i}\delta t}$ in (1.81) and adds $\hbar\delta|\boldsymbol{\epsilon}_2^*\rangle\langle\boldsymbol{\epsilon}_2^*|$ to the Hamiltonian. Since $|\boldsymbol{\epsilon}_2^*\rangle = |m=-1\rangle_z$ has Zeeman energy $-\hbar\omega_{\mathrm{Z}}$, the two diagonal entries become

$$E_1 = \frac{\hbar|\Omega_1|^2}{\Delta}, \tag{1.85}$$

$$E_2 = \hbar(\delta - \omega_{\mathrm{Z}}) + \frac{\hbar|\Omega_2|^2}{\Delta}, \tag{1.86}$$

and the effective Hamiltonian is static,

$$\hat{H}_{\mathrm{eff}} = E_1|\boldsymbol{\epsilon}_1^*\rangle\langle\boldsymbol{\epsilon}_1^*| + E_2|\boldsymbol{\epsilon}_2^*\rangle\langle\boldsymbol{\epsilon}_2^*| + (\hbar\Omega_{2\mathrm{ph}}|\boldsymbol{\epsilon}_1^*\rangle\langle\boldsymbol{\epsilon}_2^*| + \mathrm{h.c.})\,. \tag{1.87}$$

This is the Hamiltonian of a driven two-level system. With the choice (1.78), $\delta = \omega_{\mathrm{Z}}$, the Zeeman term is exactly compensated and the two levels are degenerate up to their light shifts: the atom then undergoes complete Rabi oscillations between $|m=-1\rangle_z$ and $|m=0\rangle_z$ at the frequency $|\Omega_{2\mathrm{ph}}|$.

The light shifts nevertheless survive in E_1 and E_2, and their difference acts as a residual two-photon detuning. Exact resonance therefore requires the slightly corrected condition

$$\delta = \omega_{\mathrm{Z}} + \frac{|\Omega_1|^2 - |\Omega_2|^2}{\Delta}, \tag{1.88}$$

a differential light shift that must be compensated in practice, for instance by adjusting the frequency difference or by balancing the two intensities.

Finally, if the ground manifold were degenerate, $\omega_{\mathrm{Z}} = 0$, the resonance condition would reduce to $\delta = 0$: the two beams could then be taken at the same frequency, and a single field whose polarization combines $\boldsymbol{\epsilon}_1$ and $\boldsymbol{\epsilon}_2$ would suffice to drive the transition.

1.1.5 (∗) Third-order virtual processes in the triangular Hubbard model

> **Warning.** This example assumes some familiarity with second quantization and the Hubbard model, which are introduced later in these lecture notes. The reader may therefore skip this section on a first reading and return to it after the corresponding material has been covered. Nevertheless, the discussion can be followed at a qualitative level using only the effective-Hamiltonian formalism developed above.

The third-order contribution to an effective Hamiltonian becomes particularly interesting in systems where the lowest-order virtual processes do not capture all the symmetries of the problem. A paradigmatic example is the Hubbard model on a triangular plaquette in the presence of a magnetic flux. In this case, third-order virtual hopping processes generate a three-spin interaction that is absent at second order.

We consider three sites arranged on a triangle and described by the Hubbard Hamiltonian

$$\hat{H} = \hat{H}_0 + \hat{V}, \tag{1.89}$$

with

$$\hat{H}_0 = U \sum_{i=1}^{3} \hat{n}_{i\uparrow}\hat{n}_{i\downarrow}, \tag{1.90}$$

$$\hat{V} = -t \sum_{\langle i,j\rangle,\sigma} \left(\mathrm{e}^{\mathrm{i}\phi_{ij}} \hat{c}^{\dagger}_{i\sigma}\hat{c}_{j\sigma} + \mathrm{h.c.} \right). \tag{1.91}$$

The phases ϕ_{ij} are the Peierls phases associated with the magnetic vector potential. Their sum around the triangle is related to the magnetic flux through the plaquette,

$$\Phi = \phi_{12} + \phi_{23} + \phi_{31}. \tag{1.92}$$

We consider the regime

$$t \ll U \tag{1.93}$$

at half filling, with one particle per site. The low-energy subspace A then consists of all states with exactly one particle on each site. The complementary subspace B contains states with at least one doubly occupied site. Since a doubly occupied site costs an energy U, the two subspaces are well separated in energy and the hopping can be treated perturbatively.

At first order, the hopping does not connect states within the low-energy subspace:

$$\hat{P}\hat{V}\hat{P} = 0. \tag{1.94}$$

The leading contribution to the effective Hamiltonian therefore occurs at second order,

$$\hat{H}^{(2)}_{\mathrm{eff}} = \hat{P}\hat{V}\hat{Q}\frac{1}{-\hat{H}^{(0)}_{BB}}\hat{Q}\hat{V}\hat{P}. \tag{1.95}$$

Since the intermediate states contain one doubly occupied site, the energy denominator is $-U$, and one obtains the familiar antiferromagnetic superexchange Hamiltonian

$$\hat{H}^{(2)}_{\mathrm{eff}} = J \sum_{\langle i,j\rangle} \left(\mathbf{S}_i \cdot \mathbf{S}_j - \frac{1}{4} \right), \qquad J = \frac{4t^2}{U}. \tag{1.96}$$

Thus, at second order, the Hubbard model reduces to a Heisenberg model acting within the singly occupied subspace.

On a triangular lattice, however, there are also virtual processes involving three successive hoppings. A particle can hop around the entire triangle and return to the low-energy subspace,

$$A \longrightarrow B \longrightarrow B \longrightarrow A. \tag{1.97}$$

These processes are third order in the hopping and are described by the term

$$\hat{H}^{(3)}_{\mathrm{eff}} = \hat{V}_{AB}\hat{R}_A\hat{V}_{BB}\hat{R}_A\hat{V}_{BA}, \tag{1.98}$$

where, to the required order,

$$\hat{R}_A = \frac{1}{-\hat{H}^{(0)}_{BB}}. \tag{1.99}$$

Since each intermediate state contains one doublon, each resolvent contributes a factor $-1/U$, so that the amplitude of a three-step virtual process scales as

$$\hat{H}_{\text{eff}}^{(3)} \sim \frac{t^3}{U^2}. \tag{1.100}$$

The physical processes can be represented schematically as

$$1 \to 2 \to 3 \to 1 \tag{1.101}$$

and

$$1 \to 3 \to 2 \to 1. \tag{1.102}$$

The first process acquires the phase

$$\mathrm{e}^{\mathrm{i}\Phi}, \tag{1.103}$$

while the reverse process acquires the phase $\mathrm{e}^{-\mathrm{i}\Phi}$. Their sum therefore contains

$$\mathrm{e}^{\mathrm{i}\Phi} + \mathrm{e}^{-\mathrm{i}\Phi} = 2\cos\Phi, \tag{1.104}$$

while their difference contains

$$\mathrm{e}^{\mathrm{i}\Phi} - \mathrm{e}^{-\mathrm{i}\Phi} = 2\mathrm{i}\sin\Phi. \tag{1.105}$$

It is useful to express the result in terms of cyclic permutation operators. Let $\hat{P}_{123}$ denote the operator that cyclically permutes the three spins,

$$\hat{P}_{123}|\sigma_1, \sigma_2, \sigma_3\rangle = |\sigma_3, \sigma_1, \sigma_2\rangle, \tag{1.106}$$

and let $\hat{P}_{321} = \hat{P}_{123}^{\dagger}$ denote the opposite cyclic permutation. The third-order contribution has the form

$$\hat{H}_{\text{eff}}^{(3)} = K\left(\mathrm{e}^{\mathrm{i}\Phi}\hat{P}_{123} + \mathrm{e}^{-\mathrm{i}\Phi}\hat{P}_{321}\right), \tag{1.107}$$

where K is proportional to t^3/U^2.

The two cyclic permutation operators can be decomposed into time-reversal-even and time-reversal-odd parts. For spin-1/2 particles,

$$\hat{P}_{123} + \hat{P}_{321} = \frac{1}{2} + 2\left(\mathbf{S}_1\cdot\mathbf{S}_2 + \mathbf{S}_2\cdot\mathbf{S}_3 + \mathbf{S}_3\cdot\mathbf{S}_1\right), \tag{1.108}$$

$$\hat{P}_{123} - \hat{P}_{321} = -4\mathrm{i}\,\mathbf{S}_1\cdot(\mathbf{S}_2\times\mathbf{S}_3). \tag{1.109}$$

Consequently, the third-order Hamiltonian splits into a flux-dependent correction to the Heisenberg exchange and a genuinely new scalar spin-chirality interaction,

$$\hat{H}_{\text{eff}}^{(3)} = K\cos\Phi\left[\frac{1}{2} + 2\sum_{\langle i,j\rangle}\mathbf{S}_i\cdot\mathbf{S}_j\right] + J_\chi\,\mathbf{S}_1\cdot(\mathbf{S}_2\times\mathbf{S}_3), \tag{1.110}$$

with

$$J_\chi = 4K\sin\Phi \propto \frac{t^3}{U^2}\sin\Phi. \tag{1.111}$$

Only the second term is new: the first one merely renormalizes the superexchange already obtained at second order. With the convention used above, the standard Hubbard-model result is

$$J_\chi = 24\frac{t^3}{U^2}\sin\Phi, \tag{1.112}$$

up to the sign convention chosen for the Peierls phases and for the orientation of the triangle.

This result illustrates why higher-order terms in an effective Hamiltonian can be qualitatively important. The second-order contribution produces the conventional Heisenberg exchange, whereas the third-order virtual processes generate a new interaction that couples the three spins through their scalar chirality,

$$\chi = \mathbf{S}_1 \cdot (\mathbf{S}_2 \times \mathbf{S}_3)\,. \tag{1.113}$$

This quantity changes sign under time reversal. The corresponding interaction is therefore allowed only when time-reversal symmetry is broken, here by the magnetic flux through the triangle.

The third-order term provides a direct example of how virtual processes can retain information about the geometry and gauge field of the microscopic problem. The phase accumulated by a particle during a closed virtual trajectory is the magnetic flux enclosed by that trajectory, and this phase appears directly in the effective Hamiltonian.

For $\Phi = 0$, the clockwise and counter-clockwise processes are equivalent and the scalar-chirality contribution vanishes. A finite magnetic flux makes the two processes inequivalent and produces a nonzero chiral interaction. The magnitude of this interaction is smaller than the usual superexchange by a factor of order t/U,

$$\frac{J_\chi}{J} \sim \frac{t}{U}, \tag{1.114}$$

but its qualitative importance can be much greater because it introduces a new symmetry-breaking interaction that is absent at second order.

1.2 Adiabatic particle motion and Berry phase

We now consider an important situation in which the subspace retained in the effective description depends on the position of the particle. This occurs when a particle possesses an internal degree of freedom whose local eigenstates vary in space. If the internal state follows adiabatically one of these local eigenstates, the particle acquires an effective dynamics within a single dressed band.

A remarkable consequence of this projection is the appearance of a geometric vector potential, known as the Berry connection. Its circulation gives rise to a geometric phase, and its curl acts on the particle in the same way as a magnetic field acts on a charged particle. The projection also produces a scalar potential, which is sometimes called the geometric scalar potential.

1.2.1 The geometric Berry phase

We first derive these effects for a particle whose internal state is locked to a non-degenerate local eigenstate. The wave function can then be written as

$$|\Psi\rangle = \int \psi(\mathbf{r})|\mathbf{r}\rangle \otimes |\phi(\mathbf{r})\rangle\, \mathrm{d}^3 r, \tag{1.115}$$

where $\psi(\mathbf{r})$ is the spatial wave function and $|\phi(\mathbf{r})\rangle$ is a normalized internal state that depends on position.

The retained subspace is therefore spanned by the position-dependent dressed states $|\mathbf{r}\rangle \otimes |\phi(\mathbf{r})\rangle$, and the projector onto it reads

$$\hat{P} = \int |\mathbf{r}\rangle\langle\mathbf{r}| \otimes \hat{\Pi}(\mathbf{r})\, \mathrm{d}^3 r, \qquad \hat{\Pi}(\mathbf{r}) = |\phi(\mathbf{r})\rangle\langle\phi(\mathbf{r})|, \tag{1.116}$$

where $\hat{\Pi}(\mathbf{r})$ acts on the internal degree of freedom alone. The assumption of adiabaticity means that transitions to the other local internal states can be neglected. The internal degree of freedom therefore remains locked to $|\phi(\mathbf{r})\rangle$ as the particle moves through space.

A natural realization is provided by a spinful particle subjected to a position-dependent magnetic field. We consider the spin-field coupling

$$\hat{H}_0 = -g\mu_{\mathrm{B}} \hat{\mathbf{J}} \cdot \mathbf{B}(\mathbf{r}), \tag{1.117}$$

where μ_{B} is the Bohr magneton and $g > 0$ is the Landé factor. With this sign convention, the spin of the ground state points along $\mathbf{B}$; it is opposite to the usual convention for the electron, whose magnetic moment is antiparallel to its spin. If the magnetic field is sufficiently strong and varies sufficiently slowly in space, the spin remains in the local ground state

$$|\phi(\mathbf{r})\rangle = |m = J\rangle_{\mathbf{n}(\mathbf{r})}, \tag{1.118}$$

where

$$\mathbf{n}(\mathbf{r}) = \frac{\mathbf{B}(\mathbf{r})}{B(\mathbf{r})}. \tag{1.119}$$

The corresponding local energy is

$$E_0(\mathbf{r}) = -g\mu_{\mathrm{B}} J B(\mathbf{r}). \tag{1.120}$$

We now derive the effective Hamiltonian within this adiabatic subspace. The kinetic energy,

$$\hat{V} = -\frac{\hbar^2}{2m}\nabla^2, \tag{1.121}$$

acts not only on the spatial wave function but also on the position-dependent internal state. It is convenient to work in the position representation, where

$$\langle\mathbf{r}|\hat{V}|\Psi\rangle = -\frac{\hbar^2}{2m}\nabla^2 \left[\psi(\mathbf{r})|\phi(\mathbf{r})\rangle\right], \tag{1.122}$$

the remaining ket referring to the internal degree of freedom alone. Expanding the Laplacian of this product gives three terms,

$$\langle\mathbf{r}|\hat{V}|\Psi\rangle = -\frac{\hbar^2}{2m}\Big[\left(\nabla^2\psi\right)|\phi\rangle + 2\left(\nabla\psi\right)\cdot\nabla|\phi\rangle + \psi\,\nabla^2|\phi\rangle\Big], \tag{1.123}$$

and projecting onto the local internal state yields

$$\left(\langle\mathbf{r}| \otimes \langle\phi(\mathbf{r})|\right)\hat{V}|\Psi\rangle = -\frac{\hbar^2}{2m}\Big[\nabla^2\psi + 2\langle\phi|\nabla|\phi\rangle\cdot\nabla\psi + \langle\phi|\nabla^2|\phi\rangle\,\psi\Big]. \tag{1.124}$$

Before rearranging this result, we note a key property of the matrix element appearing in the cross term. The normalization condition

$$\langle\phi(\mathbf{r})|\phi(\mathbf{r})\rangle = 1 \tag{1.125}$$

holds at every position, so that its gradient vanishes,

$$\langle\phi(\mathbf{r})|\nabla|\phi(\mathbf{r})\rangle + [\langle\phi(\mathbf{r})|\nabla|\phi(\mathbf{r})\rangle]^* = 0. \tag{1.126}$$

The quantity $\langle\phi|\nabla|\phi\rangle$ is therefore *purely imaginary*, which motivates the definition of the Berry connection

$$\mathbf{A}(\mathbf{r}) = \mathrm{i}\hbar\langle\phi(\mathbf{r})|\nabla|\phi(\mathbf{r})\rangle, \tag{1.127}$$

a real vector field.

We now compare with the expansion of a covariant kinetic term

$$\frac{1}{2m}\left[\frac{\hbar}{\mathrm{i}}\nabla - \mathbf{A}\right]^2\psi = -\frac{\hbar^2}{2m}\nabla^2\psi + \frac{\mathrm{i}\hbar}{m}\mathbf{A}\cdot\nabla\psi + \frac{\mathrm{i}\hbar}{2m}(\nabla\cdot\mathbf{A})\,\psi + \frac{A^2}{2m}\psi. \tag{1.128}$$

The first two terms of (1.128) reproduce exactly the first two terms of (1.124). The projected kinetic energy can therefore be written as

$$(\langle\mathbf{r}|\otimes\langle\phi(\mathbf{r})|)\,\hat{V}|\Psi\rangle = \frac{1}{2m}\left[\frac{\hbar}{\mathrm{i}}\nabla - \mathbf{A}(\mathbf{r})\right]^2\psi(\mathbf{r}) + W(\mathbf{r})\psi(\mathbf{r}), \tag{1.129}$$

where the scalar term collects the leftover contributions,

$$W = -\frac{\hbar^2}{2m}\langle\phi|\nabla^2|\phi\rangle - \frac{\mathrm{i}\hbar}{2m}\nabla\cdot\mathbf{A} - \frac{A^2}{2m}. \tag{1.130}$$

This expression simplifies considerably. Taking the divergence of (1.127),

$$\nabla\cdot\mathbf{A} = \mathrm{i}\hbar\left[\langle\nabla\phi|\nabla\phi\rangle + \langle\phi|\nabla^2|\phi\rangle\right], \tag{1.131}$$

the second term of (1.130) becomes $+\frac{\hbar^2}{2m}[\langle\nabla\phi|\nabla\phi\rangle + \langle\phi|\nabla^2|\phi\rangle]$, whose second piece cancels the first term of (1.130). Using in addition $A^2 = \hbar^2|\langle\phi|\nabla|\phi\rangle|^2$, we obtain the geometric scalar potential

$$W(\mathbf{r}) = \frac{\hbar^2}{2m}\left[\langle\nabla\phi|\nabla\phi\rangle - |\langle\phi|\nabla|\phi\rangle|^2\right] \tag{1.132}$$

$$= \frac{\hbar^2}{2m}(\nabla\langle\phi|)\,[\mathbb{1} - |\phi\rangle\langle\phi|]\,(\nabla|\phi\rangle) \tag{1.133}$$

$$= \frac{\hbar^2}{2m}\left\|\hat{Q}\nabla|\phi\rangle\right\|^2, \tag{1.134}$$

where

$$\hat{Q}(\mathbf{r}) = \mathbb{1} - \hat{\Pi}(\mathbf{r}) \tag{1.135}$$

projects, within the internal Hilbert space, onto the local states that have been eliminated.

The effective Hamiltonian within the adiabatic subspace is therefore

$$\hat{H}_{\text{eff}} = \frac{[\hat{\mathbf{p}} - \mathbf{A}(\hat{\mathbf{r}})]^2}{2m} + U(\hat{\mathbf{r}}), \tag{1.136}$$

where

$$U(\mathbf{r}) = E_0(\mathbf{r}) + W(\mathbf{r}). \tag{1.137}$$

Thus, after the internal degree of freedom has been adiabatically eliminated, the particle behaves as an effective spinless particle coupled to a vector potential $\mathbf{A}(\mathbf{r})$ and a scalar potential $U(\mathbf{r})$.

The vector potential $\mathbf{A}$ is not an ordinary electromagnetic vector potential: it originates entirely from the spatial variation of the internal eigenstate. It is therefore referred to as a *geometric* or *Berry* connection.

It is important to point out that the Berry connection itself is not gauge invariant. Indeed, the local eigenstate can be redefined by an arbitrary smooth position-dependent phase,

$$|\phi(\mathbf{r})\rangle \longrightarrow \mathrm{e}^{\mathrm{i}\alpha(\mathbf{r})}|\phi(\mathbf{r})\rangle. \tag{1.138}$$

The spatial wave function must simultaneously transform as

$$\psi(\mathbf{r}) \longrightarrow \mathrm{e}^{-\mathrm{i}\alpha(\mathbf{r})}\psi(\mathbf{r}), \tag{1.139}$$

so that the physical state $|\Psi\rangle$ remains unchanged. Under this transformation, the Berry connection changes according to

$$\mathbf{A}(\mathbf{r}) \longrightarrow \mathbf{A}(\mathbf{r}) - \hbar\nabla\alpha(\mathbf{r}). \tag{1.140}$$

This is precisely the gauge transformation law of an electromagnetic vector potential.

Gauge-invariant information is instead contained in the Berry curvature,

$$\mathbf{\Omega}(\mathbf{r}) = \nabla \times \mathbf{A}(\mathbf{r}). \tag{1.141}$$

Similarly, when the particle is transported adiabatically along a closed contour $\mathcal{C}$, its state acquires, besides the dynamical phase, a factor $\mathrm{e}^{\mathrm{i}\gamma(\mathcal{C})}$, with the Berry phase

$$\gamma(\mathcal{C}) = \frac{1}{\hbar}\oint_{\mathcal{C}} \mathbf{A}\cdot\mathrm{d}\mathbf{l}. \tag{1.142}$$

Equivalently, $\gamma(\mathcal{C}) = \mathrm{i}\oint_{\mathcal{C}}\langle\phi|\nabla|\phi\rangle\cdot\mathrm{d}\mathbf{l}$. Since $|\phi(\mathbf{r})\rangle$ must be single-valued, α can only change by a multiple of 2π around $\mathcal{C}$: the Berry phase of a closed loop is gauge invariant modulo 2π. If $\mathbf{A}$ is smooth on a surface $\mathcal{S}$ bounded by $\mathcal{C}$, Stokes' theorem gives

$$\gamma(\mathcal{C}) = \frac{1}{\hbar}\int_{\mathcal{S}} \mathbf{\Omega}\cdot\mathrm{d}\mathbf{S}, \qquad \mathcal{C} = \partial\mathcal{S}. \tag{1.143}$$

The Berry phase therefore has exactly the same mathematical structure as the Aharonov–Bohm phase acquired by a charged particle moving around a magnetic flux.

The analogy is particularly useful: $\mathbf{A}$ plays the role of a vector potential, while $\mathbf{\Omega}$ plays the role of a magnetic field. The difference is that here both quantities emerge from the geometry of the internal Hilbert space rather than from a physical electromagnetic field acting on the particle's orbital motion.

1.2.2 Berry phase of a spinful particle

We now return to the spinful particle subjected to a position-dependent magnetic field. The local adiabatic state is

$$|\phi(\mathbf{r})\rangle = |m = J\rangle_{\mathbf{n}(\mathbf{r})}. \tag{1.144}$$

The Berry connection and curvature can be calculated explicitly from the spatial variation of the magnetic-field orientation.

For a spin-1/2 particle, a convenient choice of local eigenstate is

$$|\tfrac{1}{2}\rangle_{\mathbf{n}} = \begin{pmatrix} \cos(\theta/2) \\ \sin(\theta/2)\mathrm{e}^{\mathrm{i}\varphi} \end{pmatrix}, \tag{1.145}$$

where (θ, φ) are the polar angles of $\mathbf{n}$. The corresponding Berry connection is

$$\mathbf{A} = -\hbar \sin^2\left(\frac{\theta}{2}\right) \nabla\varphi, \tag{1.146}$$

and the Berry curvature is

$$\mathbf{\Omega} = -\frac{\hbar}{2} \nabla\theta \times (\sin\theta \, \nabla\varphi) \,. \tag{1.147}$$

The connection $\mathbf{A}$ is singular on the line $\theta = \pi$, where φ is undefined while $\sin^2(\theta/2) = 1$. This Dirac string is an artifact of the gauge choice, and the curvature $\mathbf{\Omega}$ remains regular there. Stokes' theorem can only be applied with this gauge on surfaces $\mathcal{S}$ that avoid it.

The result for an arbitrary spin J follows particularly simply for the stretched state $|m = J\rangle_{\mathbf{n}}$. Such a state can be viewed as the symmetric tensor product of $2J$ spin-1/2 states pointing along $\mathbf{n}$. The Berry curvature is therefore multiplied by a factor $2J$,

$$\mathbf{\Omega} = -J\hbar \nabla\theta \times (\sin\theta \, \nabla\varphi) \,. \tag{1.148}$$

Consequently, the Berry phase accumulated along a closed trajectory $\mathcal{C} = \partial\mathcal{S}$ is

$$\gamma(\mathcal{C}) = -J \int_{\mathcal{S}} \sin\theta \, \nabla\theta \times \nabla\varphi \cdot \mathrm{d}\mathbf{S}. \tag{1.149}$$

The integral measures the area swept on the unit sphere by the field orientation $\mathbf{n}$, counted with the orientation inherited from $\mathcal{S}$. Denoting this *signed* solid angle by $\Omega(\mathcal{C})$, we obtain

$$\gamma(\mathcal{C}) = -J \, \Omega(\mathcal{C}). \tag{1.150}$$

It is essential that $\Omega(\mathcal{C})$ carries a sign: it is negative whenever $\mathbf{n}$ sweeps the corresponding area with the orientation opposite to that of $\mathcal{S}$. As the example of the quadrupolar field below shows, this sign cannot be inferred from the swept area alone.

This result provides a particularly simple geometrical interpretation of the Berry phase: as the particle moves through space, the direction of the local magnetic field traces a path on the Bloch sphere. The geometric phase is proportional to the solid angle enclosed by this path.

1.2.3 Engineering a synthetic magnetic monopole

The Berry curvature can exhibit structures that have no counterpart in ordinary magnetic fields. In particular, it is possible to engineer a monopole of Berry curvature even though isolated magnetic monopoles have not been observed as ordinary electromagnetic sources. Consider, for example, a spinful particle subjected to the quadrupolar magnetic field

$$\mathbf{B}(\mathbf{r}) = b'(x, y, -2z), \tag{1.151}$$

with $b' > 0$. This field is divergence-free, as any magnetostatic field must be, and vanishes only at the origin.

Away from the origin, the direction $\mathbf{n}(\mathbf{r})$ is well defined. As a closed surface $\mathcal{S}$ enclosing the origin is traversed, the magnetic-field orientation covers the unit sphere exactly once, so that the solid angle swept has magnitude 4π. Its *sign* requires care, because the solid angle entering $\gamma = -J\Omega$ is a signed quantity. The linear map $\mathbf{r} \mapsto (x, y, -2z)$ has determinant $-2 < 0$ and therefore reverses orientation, so that the map $\mathbf{r} \mapsto \mathbf{n}(\mathbf{r})$ from $\mathcal{S}$ to the unit sphere has degree -1 rather than $+1$.

This is readily verified explicitly. Parametrizing $\mathcal{S}$ as a sphere of radius R with polar angles (α, β), the field orientation has azimuthal angle $\varphi = \beta$ and polar angle

$$\cos\theta = \frac{-2\cos\alpha}{\sqrt{\sin^2\alpha + 4\cos^2\alpha}}. \tag{1.152}$$

As α increases from 0 to π, $\cos\theta$ increases from -1 to $+1$: the north pole of $\mathcal{S}$ is mapped onto the *south* pole of the Bloch sphere, and conversely. Since (α, β) is positively oriented with respect to the outward normal of $\mathcal{S}$, the signed solid angle is

$$\Omega = \int_0^{2\pi} \mathrm{d}\beta \int_0^{\pi} \sin\theta \, \frac{\mathrm{d}\theta}{\mathrm{d}\alpha} \, \mathrm{d}\alpha = -2\pi \Big[\cos\theta \Big]_{\alpha=0}^{\alpha=\pi} = -4\pi. \tag{1.153}$$

The total flux of Berry curvature through $\mathcal{S}$ then follows from $\gamma = -J\Omega$,

$$\int_{\mathcal{S}} \mathbf{\Omega} \cdot \mathrm{d}\mathbf{S} = \hbar\gamma = -J\hbar\,\Omega = 4\pi J\hbar, \tag{1.154}$$

which is positive, i.e. an outward flux, as shown in Figure 4(b). The two minus signs – the one in $\gamma = -J\Omega$ and the orientation reversal $\Omega = -4\pi$ – thus compensate each other. Reversing the sign of b' maps $\mathbf{n} \to -\mathbf{n}$ and flips the sign of the monopole charge.

Equivalently, the Berry curvature has a nonzero flux through any closed surface surrounding the origin, characteristic of a magnetic monopole.

The origin of this monopole can be understood directly from the adiabatic construction. At $\mathbf{r} = \mathbf{0}$, the magnetic field vanishes and its direction is undefined. Consequently, the local eigenstate $|\phi(\mathbf{r})\rangle$ cannot be defined smoothly at the origin. The adiabatic band therefore contains a singular point, and the Berry curvature can have a nonzero flux through a closed surface surrounding it.

This illustrates an important distinction between the Berry curvature and an ordinary magnetic field. Away from degeneracies, the Berry curvature is locally divergence-free, just as a magnetic field is in the absence of magnetic monopoles. A nonzero total flux can nevertheless emerge when the enclosed region contains a point at which the adiabatic eigenstate becomes ill-defined, corresponding here to a degeneracy of the internal Hamiltonian.

Synthetic magnetic monopoles of this type have been realized experimentally with ultracold atoms possessing a magnetic moment and subjected to a quadrupolar magnetic field [1].

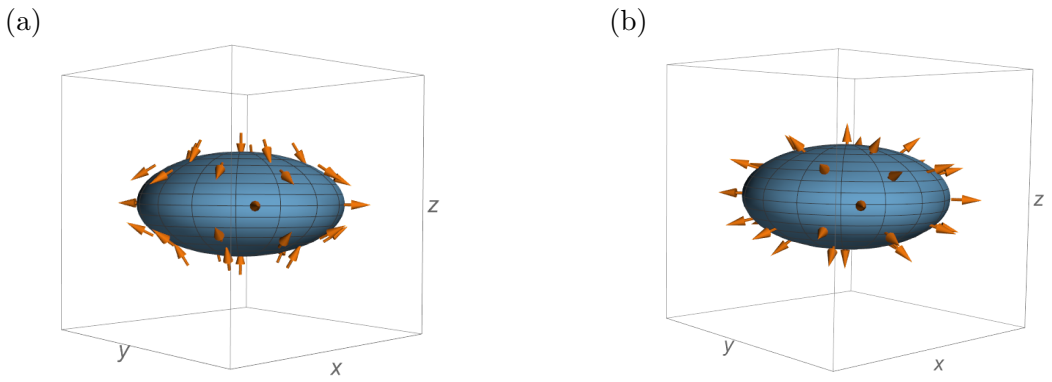


Figure 4: (a) Structure of a quadrupolar magnetic field $\mathbf{B} = b'(x, y, -2z)$. The ellipsoid represents a surface of constant magnetic-field magnitude, while the vectors show the spatial variation of the field orientation. (b) Berry curvature $\mathbf{\Omega}$ on the same surface. The curvature points outward and has a nonzero total flux through the surface, corresponding to a synthetic Berry-curvature monopole at the origin.

1.3 Resonant coupling to a continuum

The situation changes qualitatively when the subspace that is eliminated is not separated in energy from the state of interest, but instead contains a continuum of resonant states. In that case, the resolvent

$$\frac{1}{E - \hat{Q}\hat{H}\hat{Q}}$$

cannot be evaluated as an ordinary inverse at energies belonging to the continuous spectrum. More importantly, the coupling to the continuum leads to irreversible dynamics: a state initially localized in the discrete subspace can progressively lose its population by emitting amplitude into the continuum. The effective Hamiltonian formalism can nevertheless be extended to this situation by treating the energy as a complex variable and using the analytic properties of the resolvent. The resulting effective Hamiltonian becomes complex-valued when evaluated close to the continuum, with its real part describing the energy shift induced by the coupling and its imaginary part describing the decay rate. We develop this connection in the following, starting with the short-time dynamics and Fermi's golden rule.

1.3.1 Short-time dynamics: reminder on Fermi's golden rule

We first recall the derivation of Fermi's golden rule and clarify the regime in which it applies. Consider a discrete state $|\psi_0\rangle$ of the unperturbed Hamiltonian $\hat{H}_0$, with energy E_0, coupled by a weak perturbation $\hat{V}$ to a continuum of states $|\psi_f\rangle$ of energy E_f. We assume that the system is initially prepared in $|\psi_0\rangle$. The full evolution operator satisfies

$$\mathrm{i}\hbar\partial_t\hat{U}(t) = (\hat{H}_0 + \hat{V})\hat{U}(t), \tag{1.155}$$

and can be formally rewritten as the integral equation

$$\hat{U}(t) = \hat{U}_0(t) + \frac{1}{\mathrm{i}\hbar}\int_0^t \hat{U}_0(t-\tau)\hat{V}\hat{U}(\tau)\,\mathrm{d}\tau, \tag{1.156}$$

where

$$\hat{U}_0(t) = \mathrm{e}^{-\mathrm{i}\hat{H}_0 t/\hbar} \tag{1.157}$$

is the evolution operator associated with $\hat{H}_0$.

For a sufficiently weak perturbation, we can obtain the lowest-order transition amplitude by replacing $\hat{U}(\tau)$ by $\hat{U}_0(\tau)$ in the integral. This gives

$$\hat{U}(t) \simeq \hat{U}_0(t) + \frac{1}{\mathrm{i}\hbar}\int_0^t \hat{U}_0(t-\tau)\hat{V}\hat{U}_0(\tau)\,\mathrm{d}\tau. \tag{1.158}$$

The transition amplitude from the initial state $|\psi_0\rangle$ to a continuum state $|\psi_f\rangle$ is therefore

$$\langle\psi_f|\psi(t)\rangle = \frac{\langle\psi_f|\hat{V}|\psi_0\rangle}{\mathrm{i}\hbar}\int_0^t \mathrm{e}^{-\mathrm{i}E_f(t-\tau)/\hbar}\mathrm{e}^{-\mathrm{i}E_0\tau/\hbar}\,\mathrm{d}\tau \tag{1.159}$$

$$= \frac{\langle\psi_f|\hat{V}|\psi_0\rangle}{E_0 - E_f}\mathrm{e}^{-\mathrm{i}E_f t/\hbar}\left[\mathrm{e}^{-\mathrm{i}(E_0-E_f)t/\hbar} - 1\right]. \tag{1.160}$$

The overall phase $\mathrm{e}^{-\mathrm{i}E_f t/\hbar}$ has no physical consequence, and the corresponding transition probability is

$$P_{\psi_f}(t) = \frac{4|\langle\psi_f|\hat{V}|\psi_0\rangle|^2}{(E_0-E_f)^2}\sin^2\left(\frac{(E_0-E_f)t}{2\hbar}\right). \tag{1.161}$$

Equivalently,

$$P_{\psi_f}(t) = \frac{|\langle\psi_f|\hat{V}|\psi_0\rangle|^2 t^2}{\hbar^2}\operatorname{sinc}^2\left(\frac{(E_0-E_f)t}{2\hbar}\right), \tag{1.162}$$

where throughout we use the unnormalized convention $\operatorname{sinc} u = \sin u/u$.

At sufficiently long times, the function $\operatorname{sinc}^2[(E_0-E_f)t/(2\hbar)]$ becomes sharply peaked around $E_f = E_0$. More precisely, in the sense of distributions,

$$\lim_{t\to\infty} t\,\operatorname{sinc}^2\left(\frac{(E_0-E_f)t}{2\hbar}\right) = 2\pi\hbar\,\delta(E_0-E_f). \tag{1.163}$$

Provided that the density of states and the matrix elements vary slowly over the corresponding energy width $\hbar/t$, we can therefore write

$$P_{\psi_f}(t) \simeq \frac{2\pi t}{\hbar}|\langle\psi_f|\hat{V}|\psi_0\rangle|^2\delta(E_0-E_f). \tag{1.164}$$

Summing over the continuum states gives the total probability of leaving the initial state,

$$P_{\mathrm{dec}}(t) \simeq \Gamma t, \tag{1.165}$$

where

$$\Gamma = \frac{2\pi}{\hbar}\sum_f |\langle\psi_f|\hat{V}|\psi_0\rangle|^2\delta(E_0-E_f). \tag{1.166}$$

Introducing the density of states $\rho_E(E)$ and denoting by $\overline{|\langle\psi_f|\hat{V}|\psi_0\rangle|^2}$ the average squared matrix element at fixed energy, this becomes

$$\Gamma = \frac{2\pi}{\hbar}\overline{|\langle\psi_f|\hat{V}|\psi_0\rangle|^2}\,\rho_E(E_0). \tag{1.167}$$

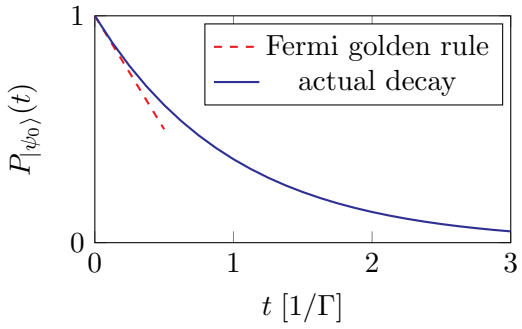


Figure 5: Example of dynamics describing the irreversible departure from a discrete state $|\psi_0\rangle$ resonantly coupled to a broad continuum. While the decay is typically exponential, the Fermi golden rule only predicts the small-time (linear) dynamics.

This is Fermi's golden rule.

The corresponding survival probability is therefore

$$P_{\psi_0}(t) \simeq 1 - \Gamma t. \tag{1.168}$$

This expression holds at times long enough for the above δ-function limit to apply, but short compared with the decay time, $\Gamma t \ll 1$, so that the depletion of the initial state remains negligible. It is important to emphasize that this result is not, by itself, an exponential decay law. Fermi's golden rule gives the rate at which probability initially flows from the discrete state into the continuum. Determining the subsequent dynamics requires keeping track of the back-action of the continuum on the initial state. Under appropriate conditions, this back-action leads to an exponential decay,

$$P_{\psi_0}(t) \simeq \mathrm{e}^{-\Gamma t}, \tag{1.169}$$

but this behavior does not follow from Fermi's golden rule alone.

In the following, we use the resolvent formalism to determine when and why such an exponential decay emerges, and to describe deviations from it when the continuum has a nontrivial energy dependence.

1.3.2 The resolvent operator

The resolvent operator provides a convenient way of describing the spectral properties of a Hamiltonian and, in particular, of studying its time evolution. It is defined for a complex energy z by

$$\hat{G}(z) = \frac{1}{z - \hat{H}}, \tag{1.170}$$

whenever the inverse exists. The resolvent is therefore well defined away from the spectrum of the Hamiltonian. Its singularities encode the spectral properties of $\hat{H}$: isolated eigenvalues appear as poles, while continuous spectra give rise to branch cuts.

The connection between the resolvent and the time-evolution operator can be established by considering the retarded Green function. We define $\hat{U}_+(t)$ as the solution of

$$\mathrm{i}\hbar\partial_t \hat{U}_+(t) = \hat{H}\hat{U}_+(t) + \mathrm{i}\hbar\,\delta(t), \tag{1.171}$$

with the retarded boundary condition

$$\hat{U}_+(t) = 0 \qquad \text{for} \qquad t < 0. \tag{1.172}$$

For a time-independent Hamiltonian, this Green function is related to the usual evolution operator

$$\hat{U}(t) = \mathrm{e}^{-\mathrm{i}\hat{H}t/\hbar} \tag{1.173}$$

through

$$\hat{U}_+(t) = \hat{U}(t)\Theta(t), \tag{1.174}$$

where $\Theta(t)$ is the Heaviside function.

We introduce the Fourier transform

$$\hat{G}(E + \mathrm{i}\eta) = \frac{1}{\mathrm{i}\hbar} \int_{-\infty}^{\infty} \hat{U}_+(t) \mathrm{e}^{\mathrm{i}(E+\mathrm{i}\eta)t/\hbar} \, \mathrm{d}t, \tag{1.175}$$

where $\eta > 0$ is an infinitesimal positive real number. Using the expression for $\hat{U}_+(t)$, we obtain

$$\hat{G}(E + \mathrm{i}\eta) = \frac{1}{\mathrm{i}\hbar} \int_{0}^{\infty} \mathrm{e}^{\mathrm{i}(E+\mathrm{i}\eta-\hat{H})t/\hbar} \, \mathrm{d}t \tag{1.176}$$

$$= \frac{1}{E + \mathrm{i}\eta - \hat{H}}. \tag{1.177}$$

Thus, the Fourier transform of the retarded time-evolution operator is precisely the resolvent evaluated just above the real energy axis. The infinitesimal positive imaginary part ensures convergence of the integral at large times.

It is useful to regard the energy as a general complex variable,

$$z = E + \mathrm{i}\eta, \tag{1.178}$$

and to write simply

$$\hat{G}(z) = \frac{1}{z - \hat{H}}. \tag{1.179}$$

The relation can be inverted to recover the time evolution. Introducing the frequency $\omega = E/\hbar$, the definition of $\hat{G}$ given above is an ordinary Fourier transform of the damped evolution operator $\hat{U}_+(t)\mathrm{e}^{-\eta t/\hbar}$,

$$\mathrm{i}\hbar \, \hat{G}(E + \mathrm{i}\eta) = \int_{-\infty}^{\infty} \left[\hat{U}_+(t) \, \mathrm{e}^{-\eta t/\hbar}\right] \mathrm{e}^{\mathrm{i}\omega t} \, \mathrm{d}t, \tag{1.180}$$

whose inversion reads

$$\hat{U}_+(t) \, \mathrm{e}^{-\eta t/\hbar} = \frac{1}{2\pi} \int_{-\infty}^{\infty} \mathrm{i}\hbar \, \hat{G}(E + \mathrm{i}\eta) \, \mathrm{e}^{-\mathrm{i}\omega t} \, \mathrm{d}\omega. \tag{1.181}$$

Substituting $\mathrm{d}\omega = \mathrm{d}E/\hbar$ and absorbing the damping factor into the exponential, we obtain

$$\hat{U}_+(t) = \frac{\mathrm{i}}{2\pi} \int_{-\infty}^{\infty} \mathrm{e}^{-\mathrm{i}(E+\mathrm{i}\eta)t/\hbar} \hat{G}(E + \mathrm{i}\eta) \, \mathrm{d}E. \tag{1.182}$$

It is natural to express this integral in terms of the complex variable $z = E + \mathrm{i}\eta$. As E runs over the real axis, z runs over the horizontal line $\mathrm{Im}\, z = \eta$, located just above the real axis and therefore above the whole spectrum of $\hat{H}$. Since $\mathrm{d}z = \mathrm{d}E$,

$$\hat{U}_+(t) = \frac{\mathrm{i}}{2\pi} \int_{-\infty+\mathrm{i}\eta}^{+\infty+\mathrm{i}\eta} \mathrm{e}^{-\mathrm{i}zt/\hbar} \hat{G}(z)\, \mathrm{d}z. \tag{1.183}$$

Finally, using $\mathrm{i}/(2\pi) = -1/(2\mathrm{i}\pi)$, the minus sign can be absorbed by reversing the orientation of the path. Denoting by $\mathcal{C}_+$ this same line traversed from $+\infty$ to $-\infty$, we arrive at

$$\hat{U}_+(t) = \int_{\mathcal{C}_+} \mathrm{e}^{-\mathrm{i}zt/\hbar} \hat{G}(z) \frac{\mathrm{d}z}{2\mathrm{i}\pi}. \tag{1.184}$$

The orientation of $\mathcal{C}_+$ is not a matter of taste: it is precisely the convention for which the residue theorem applies with a positive sign. Consider $t > 0$ and write $z = x + \mathrm{i}y$, so that

$$\left|\mathrm{e}^{-\mathrm{i}zt/\hbar}\right| = \mathrm{e}^{yt/\hbar} \tag{1.185}$$

decays in the lower half plane. The contour may then be closed by a large semicircle below the axis, whose contribution vanishes because $\hat{G}(z)$ behaves as $1/z$ at large $|z|$. Travelling along the top from right to left leaves the enclosed region on the left, so that the closed contour encircles the lower half plane counterclockwise, and the residue theorem gives

$$\hat{U}_+(t) = \sum_j \operatorname*{Res}_{z=z_j} \left[\mathrm{e}^{-\mathrm{i}zt/\hbar} \hat{G}(z)\right] \qquad (t > 0), \tag{1.186}$$

with no additional sign or numerical factor. This is the form that will be used repeatedly in the following.

For $t < 0$, the same exponential decays instead in the upper half plane, and the contour must be closed above. Since the line $\mathrm{Im}\, z = \eta$ lies above the entire spectrum of $\hat{H}$, the region enclosed in that case contains no singularity, and

$$\hat{U}_+(t) = 0 \qquad (t < 0), \tag{1.187}$$

which is exactly the retarded condition imposed at the outset. The infinitesimal η, introduced to ensure convergence of the direct transform, is thus also what encodes causality in the inverse one.

As an elementary check, consider a single discrete level of energy E_1, for which $\hat{G}(z) = |\phi_1\rangle\langle\phi_1|/(z - E_1)$. The integrand has a single pole at $z = E_1$, with residue $\mathrm{e}^{-\mathrm{i}E_1 t/\hbar}|\phi_1\rangle\langle\phi_1|$, and we recover the expected free evolution $\hat{U}_+(t) = \mathrm{e}^{-\mathrm{i}E_1 t/\hbar}|\phi_1\rangle\langle\phi_1|$ for $t > 0$.

The usefulness of the resolvent follows from the fact that its analytical structure contains information about the spectrum of the Hamiltonian. To see this explicitly, consider first a purely discrete spectrum, with eigenstates $|\phi_n\rangle$ and energies E_n. Using the spectral decomposition of the Hamiltonian, one obtains

$$\hat{G}(z) = \sum_n \frac{|\phi_n\rangle\langle\phi_n|}{z - E_n}. \tag{1.188}$$

Each eigenvalue therefore appears as a simple pole of the resolvent. The residue at the pole is the projector onto the corresponding eigenstate,

$$\operatorname*{Res}_{z=E_n} \hat{G}(z) = |\phi_n\rangle\langle\phi_n|. \tag{1.189}$$

Equation (1.184) then shows directly how these poles contribute to the time evolution.

The situation is different in the presence of a continuous spectrum. Introducing continuum eigenstates $|\psi_E\rangle$ normalized according to

$$\langle\psi_E|\psi_{E'}\rangle = \delta(E - E'), \tag{1.190}$$

where for simplicity we assume the continuum to be non-degenerate, a degeneracy index being otherwise carried along without changing any of the following, the spectral decomposition takes the form

$$\hat{G}(z) = \sum_n \frac{|\phi_n\rangle\langle\phi_n|}{z - E_n} + \int \frac{|\psi_E\rangle\langle\psi_E|}{z - E}\,\mathrm{d}E. \tag{1.191}$$

The second term is singular when z approaches the real axis within the continuous spectrum. The two limiting values from above and below are different, as follows from the distribution identity

$$\frac{1}{E - E' \pm \mathrm{i}\eta} = \mathcal{P}\frac{1}{E - E'} \mp \mathrm{i}\pi\delta(E - E'), \tag{1.192}$$

understood, here and throughout, in the sense of distributions and for the infinitesimal $\eta > 0$ introduced above.

Here $\mathcal{P}$ denotes the Cauchy principal value, not to be confused with the projector $\hat{P}$. We remind that it is defined, for an integral whose integrand has a simple pole at $E' = E$, by excluding a symmetric interval of half-width $\varepsilon > 0$ around the pole and letting ε tend to zero at the end,

$$\mathcal{P}\int \frac{f(E')}{E - E'}\,\mathrm{d}E' = \lim_{\varepsilon\to 0}\left[\int^{E-\varepsilon} \frac{f(E')}{E - E'}\,\mathrm{d}E' + \int_{E+\varepsilon} \frac{f(E')}{E - E'}\,\mathrm{d}E'\right]. \tag{1.193}$$

The resolvent can then be recast as

$$\hat{G}(E + \mathrm{i}\eta) = \sum_n \frac{|\phi_n\rangle\langle\phi_n|}{E - E_n} + \int \left[\mathcal{P}\frac{1}{E - E'} - \mathrm{i}\pi\delta(E - E')\right]|\psi_{E'}\rangle\langle\psi_{E'}|\,\mathrm{d}E'. \tag{1.194}$$

Similarly,

$$\hat{G}(E - \mathrm{i}\eta) = \sum_n \frac{|\phi_n\rangle\langle\phi_n|}{E - E_n} + \int \left[\mathcal{P}\frac{1}{E - E'} + \mathrm{i}\pi\delta(E - E')\right]|\psi_{E'}\rangle\langle\psi_{E'}|\,\mathrm{d}E'. \tag{1.195}$$

The resolvent therefore has two distinct boundary values on the continuous spectrum. In the complex-energy plane, the continuum appears as a branch cut along the corresponding interval of real energies, while isolated discrete states appear as poles. This analytical structure will be central to the description of resonant decay. In particular, when a discrete state is coupled to a continuum, the pole associated with that state can be continued away from the real axis. The resulting complex resonance pole will provide a direct description of the energy shift and the decay rate.

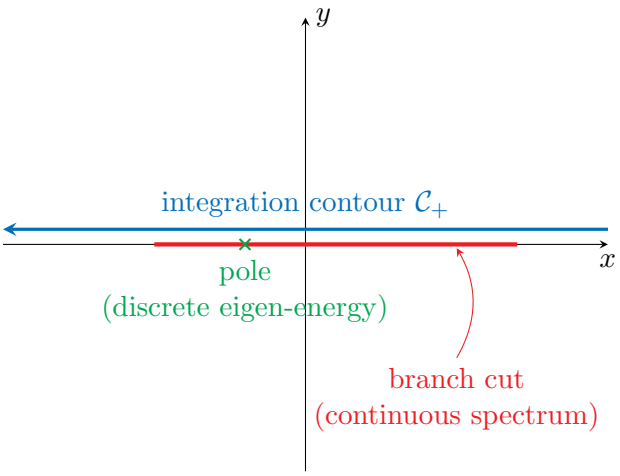


Figure 6: Scheme of the complex-energy plane defining the argument z of the resolvent operator $\hat{G}(z)$. Since the Hamiltonian $\hat{H}$ is Hermitian, its spectrum is real and the resolvent is analytic away from the real axis. Isolated discrete eigenvalues appear as poles on the real axis (green crosses), while a continuous spectrum gives rise to a branch cut (red segment). The contour $\mathcal{C}_+$ used in the inverse transform (1.184) is shown in blue.

1.3.3 Emergence of exponentially decaying dynamics

We now return to the physical problem of a discrete state coupled to a continuum. We consider a discrete eigenstate $|\psi_0\rangle$ of the unperturbed Hamiltonian $\hat{H}_0$, with energy E_0, and assume that E_0 lies within the continuous spectrum of $\hat{Q}\hat{H}_0\hat{Q}$. The perturbation $\hat{V}$ couples $|\psi_0\rangle$ to the continuum, so that the state is no longer an eigenstate of the full Hamiltonian $\hat{H} = \hat{H}_0 + \hat{V}$. We are interested in the survival amplitude

$$A(t) = \langle\psi_0|\hat{U}(t)|\psi_0\rangle, \tag{1.196}$$

and in particular in the corresponding survival probability

$$P_{\psi_0}(t) = |A(t)|^2. \tag{1.197}$$

Using the retarded evolution operator introduced above, the survival amplitude can be written as

$$A(t) = \langle\psi_0|\hat{U}_+(t)|\psi_0\rangle = \int_{\mathcal{C}_+} \mathrm{e}^{-\mathrm{i}zt/\hbar}\langle\psi_0|\hat{G}(z)|\psi_0\rangle\frac{\mathrm{d}z}{2\mathrm{i}\pi}. \tag{1.198}$$

The long-time behavior is therefore determined by the analytical structure of the projected resolvent $\langle\psi_0|\hat{G}(z)|\psi_0\rangle$.

Before the coupling is introduced, the resolvent of $\hat{H}_0$ contains a pole at the real energy E_0, associated with the discrete state $|\psi_0\rangle$. Since E_0 lies inside the continuous spectrum, however, this pole is embedded in the continuum. Once the perturbation $\hat{V}$ is introduced, the discrete state is no longer an exact eigenstate and the pole disappears from the physical sheet of the resolvent. The spectral weight associated with the initial state is instead distributed over the continuum.

The decay can nevertheless be described in terms of a resonance pole by analytically continuing the resolvent through the branch cut associated with the continuum. We

denote this analytically continued resolvent by $\hat{G}'(z)$. On the second Riemann sheet, the pole associated with the initial discrete state is displaced away from the real axis into the lower half of the complex-energy plane, as illustrated in Fig. 7. We denote its position by

$$E_0' = E_0 + \hbar\left(\Delta_0 - \mathrm{i}\frac{\Gamma_0}{2}\right). \tag{1.199}$$

The real part of the displacement, $\hbar\Delta_0$, describes the energy shift induced by the coupling to the continuum, while the negative imaginary part determines the decay rate Γ_0.

It is important to emphasize that E_0' is not an eigenvalue of the Hermitian Hamiltonian $\hat{H}$. The spectrum of $\hat{H}$ remains real. Rather, E_0' is a pole of the analytically continued resolvent and is therefore called a resonance pole. Its imaginary part encodes the irreversible decay of the metastable state.

To evaluate the integral in (1.198), we deform the contour $\mathcal{C}_+$ into the lower half of the complex plane, as illustrated in Fig. 7. This deformation is possible because the exponential factor $\mathrm{e}^{-\mathrm{i}zt/\hbar}$ decreases in the lower half plane for $t > 0$. The original branch cut is replaced by a contour running along the analytically continued branch cut, and the deformation encloses the resonance poles.

Under suitable assumptions, the contribution from the deformed branch-cut contour can be neglected. In particular, this requires that the relevant continuum be sufficiently broad and that the contribution from the large semicircle vanish. The integral can then be evaluated using the residue theorem. If several resonance poles are present, one obtains

$$A(t) \simeq \sum_n Z_n \mathrm{e}^{-\mathrm{i}E_n t/\hbar}\mathrm{e}^{-\mathrm{i}\Delta_n t}\mathrm{e}^{-\Gamma_n t/2}, \tag{1.200}$$

where Z_n is the residue of the corresponding pole in the projected resolvent.

For a single isolated resonance, the survival amplitude therefore takes the simple form

$$A(t) \simeq Z_0 \mathrm{e}^{-\mathrm{i}(E_0/\hbar+\Delta_0)t}\mathrm{e}^{-\Gamma_0 t/2}. \tag{1.201}$$

In the weak-coupling regime, the resonance state remains close to the original discrete state, so that $Z_0 \simeq 1$. We then obtain

$$A(t) \simeq \mathrm{e}^{-\mathrm{i}(E_0/\hbar+\Delta_0)t}\mathrm{e}^{-\Gamma_0 t/2}, \tag{1.202}$$

and hence

$$P_{\psi_0}(t) \simeq \mathrm{e}^{-\Gamma_0 t}. \tag{1.203}$$

We thus recover the exponential decay law anticipated from the phenomenological picture. The decay rate is determined by the imaginary part of the resonance pole, while the real part gives the shift of the energy of the initial state. The connection between these quantities and the effective Hamiltonian derived earlier will be established below.

Effective Hamiltonian. The position of the resonance poles can be determined using the effective Hamiltonian introduced earlier. The key observation is that the same projection formalism used to eliminate the complementary subspace can be applied directly to the resolvent. We introduce the projector

$$\hat{P} = |\psi_0\rangle\langle\psi_0|, \qquad \hat{Q} = \mathbb{1} - \hat{P}, \tag{1.204}$$

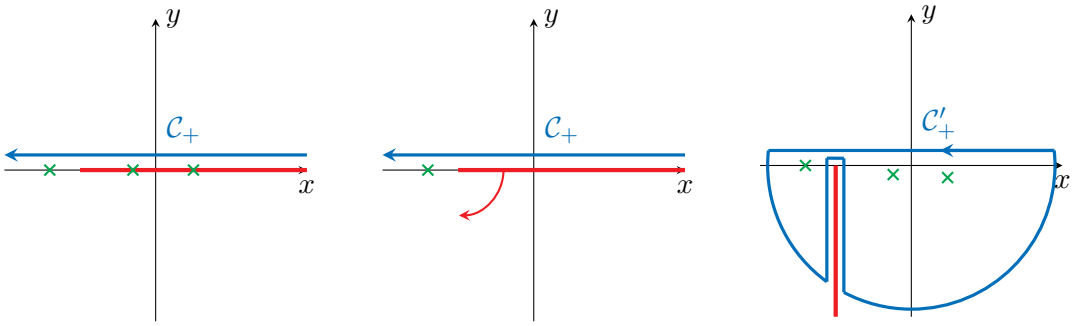


Figure 7: Analytic continuation of the resolvent into the lower half plane. (a) For the unperturbed Hamiltonian $\hat{H}_0$, the resolvent $\hat{G}_0(z)$ has poles on the real axis corresponding to discrete eigenstates (green crosses), together with a branch cut associated with the continuous spectrum (red segment). (b) When the coupling $\hat{V}$ is introduced, a discrete state embedded in the continuum is no longer an isolated eigenstate. (c) The resolvent can be analytically continued through the branch cut into the lower half plane. The resonant states then appear as poles of the continued resolvent $\hat{G}'(z)$, shifted away from the real axis (green crosses). The blue contour $\mathcal{C}'_+$ illustrates the deformed integration contour used to evaluate the time evolution.

where $|\psi_0\rangle$ is the discrete state of $\hat{H}_0$. We are interested in the component of the resolvent that acts within the initial subspace,

$$\hat{P}\hat{G}(z)\hat{P}, \tag{1.205}$$

where $\hat{G}(z) = (z - \hat{H})^{-1}$ and $\hat{H} = \hat{H}_0 + \hat{V}$.

Using the same block decomposition of the Schrödinger equation as in the derivation of the effective Hamiltonian, one obtains the exact identity

$$\hat{P}\hat{G}(z)\hat{P} = \hat{P}\frac{1}{z - \hat{H}_{\text{eff}}(z)}\hat{P}, \tag{1.206}$$

where the energy-dependent effective Hamiltonian acting within the subspace P is

$$\hat{H}_{\text{eff}}(z) = \hat{P}\hat{H}\hat{P} + \hat{P}\hat{V}\hat{Q}\frac{1}{z - \hat{Q}\hat{H}\hat{Q}}\hat{Q}\hat{V}\hat{P}. \tag{1.207}$$

This expression is exact. In particular, no perturbative approximation has been made at this stage. The poles of the projected resolvent, and therefore the resonances associated with the initial discrete state, are determined by the self-consistent equation

$$z = \text{eigenvalue of } \hat{H}_{\text{eff}}(z). \tag{1.208}$$

For a one-dimensional subspace P, this simply reduces to

$$z = \langle\psi_0|\hat{H}_{\text{eff}}(z)|\psi_0\rangle. \tag{1.209}$$

The effective Hamiltonian in (1.207) differs in an important way from the effective Hamiltonians considered for a discrete, well-isolated subspace. Since z is now taken close to the continuous spectrum, the resolvent of the Q subspace has different limits

when approached from the upper or lower half plane. Consequently, $\hat{H}_{\text{eff}}(z)$ acquires an imaginary part. For $z = E + \mathrm{i}\eta$ approaching the real axis from above, the operator form of (1.192),

$$\frac{1}{E - \hat{Q}\hat{H}\hat{Q} + \mathrm{i}\eta} = \mathcal{P}\frac{1}{E - \hat{Q}\hat{H}\hat{Q}} - \mathrm{i}\pi\delta(E - \hat{Q}\hat{H}\hat{Q}), \tag{1.210}$$

gives

$$\hat{H}_{\text{eff}}(E + \mathrm{i}\eta) = \hat{P}\hat{H}\hat{P} + \hbar\hat{\Delta}(E) - \frac{\mathrm{i}\hbar}{2}\hat{\Gamma}(E), \tag{1.211}$$

where

$$\hbar\hat{\Delta}(E) = \hat{P}\hat{V}\hat{Q}\,\mathcal{P}\left(\frac{1}{E - \hat{Q}\hat{H}\hat{Q}}\right)\hat{Q}\hat{V}\hat{P}, \tag{1.212}$$

$$\hat{\Gamma}(E) = \frac{2\pi}{\hbar}\hat{P}\hat{V}\hat{Q}\,\delta(E - \hat{Q}\hat{H}\hat{Q})\hat{Q}\hat{V}\hat{P}. \tag{1.213}$$

The Hermitian operator $\hat{\Delta}(E)$ describes the energy shift induced by the coupling to the continuum, while the positive operator $\hat{\Gamma}(E)$ describes the decay into continuum states. The effective Hamiltonian therefore becomes non-Hermitian when evaluated on the real axis. This non-Hermiticity does not indicate that the underlying Hamiltonian $\hat{H}$ is non-Hermitian: it results from eliminating the continuum degrees of freedom, which act as an effective reservoir for the projected dynamics.

The two operators are not independent. Writing the principal value in (1.212) as an integral over the spectral decomposition of $\hat{Q}\hat{H}\hat{Q}$, one finds that the reactive response $\hat{\Delta}$ is the Hilbert transform of the dissipative one $\hat{\Gamma}$,

$$\hat{\Delta}(E) = \frac{1}{2\pi}\int_{-\infty}^{\infty}\mathcal{P}\left(\frac{1}{E - E'}\right)\hat{\Gamma}(E')\,\mathrm{d}E'. \tag{1.214}$$

This is a Kramers–Kronig relation: the energy shift and the decay rate are the real and imaginary parts of a single analytic response function, and cannot be specified independently.

The resonance poles are obtained by analytically continuing this effective Hamiltonian into the lower half plane and solving the corresponding self-consistent equation. In the weak-coupling regime, the pole close to the unperturbed energy E_0, denoted z_0 in the following (it is the resonance pole E_0' introduced above), can be written as

$$z_0 = E_0 + \hbar\left(\Delta_0 - \frac{\mathrm{i}}{2}\Gamma_0\right), \tag{1.215}$$

so that its imaginary part directly determines the decay rate. The projected time evolution consequently contains the factor

$$\mathrm{e}^{-\mathrm{i}z_0 t/\hbar} = \mathrm{e}^{-\mathrm{i}(E_0/\hbar + \Delta_0)t}\mathrm{e}^{-\Gamma_0 t/2}. \tag{1.216}$$

Thus, the exponential decay of the discrete state can be understood as the dynamical manifestation of a resonance pole displaced into the lower half of the complex-energy plane.

Evaluation of the Lamb shift and decay rate. The expressions (1.212) and (1.213) still depend on the energy E. In principle, the position of the resonance pole must therefore be determined self-consistently from

$$z_0 = \langle\psi_0|\hat{H}_{\text{eff}}(z_0)|\psi_0\rangle, \tag{1.217}$$

with $\hat{H}_{\text{eff}}(z)$ analytically continued into the lower half plane. This equation accounts not only for the shift and decay of the discrete state, but also for their dependence on the energy at which the continuum is sampled.

A particularly simple approximation is obtained when the continuum is sufficiently broad and smooth around the unperturbed energy E_0. In this case, the Lamb shift and decay rate vary slowly over the energy scale of the resonance width, and one can evaluate them at the unperturbed energy,

$$\hat{\Delta}(E) \simeq \hat{\Delta}(E_0), \qquad \hat{\Gamma}(E) \simeq \hat{\Gamma}(E_0). \tag{1.218}$$

This is sometimes referred to as the *broad-continuum* or *on-shell* approximation. In addition, if the coupling $\hat{V}$ is weak, the operators in (1.212) and (1.213) can be evaluated to second order in $\hat{V}$ by replacing $\hat{Q}\hat{H}\hat{Q}$ with $\hat{Q}\hat{H}_0\hat{Q}$. For the one-dimensional subspace spanned by $|\psi_0\rangle$, this gives

$$\hbar\Delta_0 = \int \left|\langle\psi_k|\hat{V}|\psi_0\rangle\right|^2 \mathcal{P}\frac{1}{E_0 - E_k}\,\mathrm{d}k, \tag{1.219}$$

$$\Gamma_0 = \frac{2\pi}{\hbar}\int \left|\langle\psi_k|\hat{V}|\psi_0\rangle\right|^2 \delta(E_0 - E_k)\,\mathrm{d}k. \tag{1.220}$$

The first expression is the familiar second-order energy shift, here commonly called the *Lamb shift*, while the second one is precisely Fermi's golden rule.

The physical origin of the two terms is particularly transparent from the decomposition

$$\frac{1}{E_0 - E_k + \mathrm{i}\eta} = \mathcal{P}\frac{1}{E_0 - E_k} - \mathrm{i}\pi\delta(E_0 - E_k). \tag{1.221}$$

Virtual transitions to off-resonant continuum states contribute to the real part and shift the energy of the discrete state. On-shell transitions into continuum states contribute to the imaginary part and produce irreversible decay. The two effects are therefore two components of the same self-energy.

Within the broad-continuum approximation, the effective Hamiltonian can consequently be replaced by the constant complex energy

$$\hat{H}_{\text{eff}}(E) \simeq \left[E_0 + \hbar\Delta_0 - \frac{\mathrm{i}\hbar\Gamma_0}{2}\right]|\psi_0\rangle\langle\psi_0|. \tag{1.222}$$

The corresponding projected resolvent takes the Breit–Wigner form

$$\langle\psi_0|\hat{G}(E + \mathrm{i}\eta)|\psi_0\rangle \simeq \frac{1}{E - E_0 - \hbar\Delta_0 + \mathrm{i}\hbar\Gamma_0/2}. \tag{1.223}$$

Its pole is located at

$$z_0 = E_0 + \hbar\Delta_0 - \frac{\mathrm{i}\hbar\Gamma_0}{2}, \tag{1.224}$$

and the inverse Fourier transform therefore gives

$$\langle\psi_0|\hat{U}(t)|\psi_0\rangle \simeq \mathrm{e}^{-\mathrm{i}(E_0/\hbar+\Delta_0)t}\mathrm{e}^{-\Gamma_0 t/2}. \tag{1.225}$$

The survival probability consequently decays exponentially,

$$P_{\psi_0}(t) \simeq \mathrm{e}^{-\Gamma_0 t}. \tag{1.226}$$

This result makes explicit the connection between the short-time Fermi golden rule and the long-time exponential decay: under the broad-continuum and weak-coupling assumptions, the golden-rule rate is precisely the imaginary part of the resonance pole. When these assumptions fail—for instance near a band edge, a sharp resonance, or a photonic bandgap—$\Delta(E)$ and $\Gamma(E)$ can vary significantly over the resonance width. The self-consistent energy dependence of $\hat{H}_{\mathrm{eff}}(z)$ must then be retained, and the decay generally ceases to be purely exponential.

1.3.4 The Wigner and Weisskopf model and its variations

The Wigner–Weisskopf model provides a simple exactly solvable example of a discrete quantum state coupled to a continuum. It is particularly useful for illustrating the physical meaning of the resonance pole and for identifying the conditions under which the exponential decay obtained in the previous section is a good approximation [2].

We consider a single discrete state $|\phi\rangle$ of unperturbed energy E_0, coupled to a continuum of states $|\psi_E\rangle$ with energy E. We choose the continuum states to satisfy the energy normalization

$$\langle\psi_E|\psi_{E'}\rangle = \delta(E-E'), \tag{1.227}$$

so that the density of states is absorbed into the energy normalization of the continuum states. The unperturbed Hamiltonian is then

$$\hat{H}_0 = E_0|\phi\rangle\langle\phi| + \int_{E_{\min}}^{E_{\max}} E|\psi_E\rangle\langle\psi_E|\,\mathrm{d}E. \tag{1.228}$$

The coupling between the discrete state and the continuum is taken of the form

$$\hat{V} = \int_{E_{\min}}^{E_{\max}} [V_0(E)|\psi_E\rangle\langle\phi| + V_0^*(E)|\phi\rangle\langle\psi_E|]\,\mathrm{d}E. \tag{1.229}$$

The simplest Wigner–Weisskopf model corresponds to $V_0(E) = V_0$, independent of energy.

The projector on the discrete state is

$$\hat{P} = |\phi\rangle\langle\phi|, \qquad \hat{Q} = \mathbb{1} - \hat{P}. \tag{1.230}$$

Since $\hat{Q}\hat{V}\hat{Q} = 0$, the energy-dependent effective Hamiltonian introduced above reduces to

$$\hat{H}_{\mathrm{eff}}(z) = E_0|\phi\rangle\langle\phi| + \hat{P}\hat{V}\hat{Q}\frac{1}{z-\hat{Q}\hat{H}_0\hat{Q}}\hat{Q}\hat{V}\hat{P}. \tag{1.231}$$

Its matrix element in the discrete state is therefore

$$\langle\phi|\hat{H}_{\mathrm{eff}}(z)|\phi\rangle = E_0 + \int_{E_{\min}}^{E_{\max}} \frac{|V_0(E)|^2}{z-E}\,\mathrm{d}E. \tag{1.232}$$

For a constant coupling V_0, this becomes

$$\langle\phi|\hat{H}_{\text{eff}}(z)|\phi\rangle = E_0 + |V_0|^2 \log\left(\frac{E_{\min} - z}{E_{\max} - z}\right), \tag{1.233}$$

where the appropriate branch of the logarithm is chosen according to the analytic continuation of the resolvent.

The projected resolvent consequently takes the simple form

$$\langle\phi|\hat{G}(z)|\phi\rangle = \frac{1}{z - E_0 - |V_0|^2 \log\left(\frac{E_{\min} - z}{E_{\max} - z}\right)}. \tag{1.234}$$

This expression already contains the full dynamics of the discrete state. In particular, its poles determine the dressed eigenstates or resonances, while its branch cut reflects the presence of the continuum.

Infinite-band limit. We first consider the idealized limit in which the continuum extends over the entire real axis,

$$E_{\min} \to -\infty, \qquad E_{\max} \to +\infty. \tag{1.235}$$

The limit must be taken symmetrically, $E_{\min} = -E_{\max} \to -\infty$; otherwise the real part of the self-energy diverges logarithmically. In this limit, the logarithm in (1.233) approaches a constant on each side of the branch cut. For z in the upper half plane,

$$\log\left(\frac{E_{\min} - z}{E_{\max} - z}\right) \longrightarrow -\mathrm{i}\pi, \tag{1.236}$$

whereas, evaluating the same expression directly for z in the lower half plane,

$$\log\left(\frac{E_{\min} - z}{E_{\max} - z}\right) \longrightarrow +\mathrm{i}\pi. \tag{1.237}$$

The jump of $2\mathrm{i}\pi$ across the real axis is precisely the branch cut associated with the continuum.

It is essential not to confuse this discontinuity with the analytic continuation. The continued function $\hat{G}'(z)$, obtained by prolonging the upper-half-plane resolvent *through* the cut, is not the resolvent evaluated below the cut. Since the logarithm is constant on the upper sheet in this limit, its continuation retains the value $-\mathrm{i}\pi$ in the lower half plane. It is this continued function, and not $\hat{G}(z)$ itself, that carries the resonance pole.

On the physical sheet, the resolvent therefore becomes

$$\langle\phi|\hat{G}(z)|\phi\rangle = \frac{1}{z - E_0 + \mathrm{i}\pi|V_0|^2}. \tag{1.238}$$

Introducing

$$\Gamma = \frac{2\pi}{\hbar}|V_0|^2, \tag{1.239}$$

we obtain

$$\langle\phi|\hat{G}(z)|\phi\rangle = \frac{1}{z - E_0 + \mathrm{i}\hbar\Gamma/2}. \tag{1.240}$$

This expression, valid for $\mathrm{Im}\, z > 0$, is a rational function of z, so its analytic continuation into the lower half plane is given by the same formula. The continued resolvent therefore possesses a single resonance pole, located below the real axis at

$$z_0 = E_0 - \frac{\mathrm{i}\hbar\Gamma}{2}. \tag{1.241}$$

Note that $\hat{G}(z)$ itself has no pole there: evaluated directly in the lower half plane it equals $1/(z - E_0 - \mathrm{i}\hbar\Gamma/2)$, whose pole lies in the upper half plane and is therefore never reached. The resonance is a property of the second sheet alone. There is no Lamb shift in this idealized model: the continuum is perfectly symmetric and extends to arbitrarily high and low energies.

The inverse Fourier transform can now be evaluated by closing the contour in the lower half plane for $t > 0$. The pole gives

$$\langle\phi|\hat{U}(t)|\phi\rangle = \mathrm{e}^{-\mathrm{i}E_0 t/\hbar}\mathrm{e}^{-\Gamma t/2}, \tag{1.242}$$

and hence

$$P_\phi(t) = \left|\langle\phi|\hat{U}(t)|\phi\rangle\right|^2 = \mathrm{e}^{-\Gamma t}. \tag{1.243}$$

The exponential decay is therefore exact in this infinite-band model.

The result also illustrates particularly clearly the connection with Fermi's golden rule. The golden-rule rate is

$$\Gamma = \frac{2\pi}{\hbar}|V_0|^2, \tag{1.244}$$

while the same quantity appears as the imaginary part of the resonance pole. In this sense, the exponential decay rate is not an additional assumption: it follows exactly from the analytic structure of the resolvent in the infinite-band limit.

Finite bandwidth and energy shift. A realistic continuum is always restricted to a finite energy range. We therefore return to finite $E_{\min}$ and $E_{\max}$. Even in the weak-coupling regime, the finite bandwidth has two important consequences. First, the real part of the self-energy produces a Lamb shift. Second, the branch points at $E_{\min}$ and $E_{\max}$ modify the long-time dynamics and can lead to deviations from exponential decay.

Suppose first that the unperturbed level lies outside the continuum. For definiteness, consider

$$E_0 < E_{\min}. \tag{1.245}$$

Since there are no continuum states resonant with E_0, the imaginary part of the self-energy vanishes:

$$\Gamma_0 = 0. \tag{1.246}$$

The coupling nevertheless shifts the discrete level. To second order in V_0,

$$\Delta_0 = \frac{|V_0|^2}{\hbar}\int_{E_{\min}}^{E_{\max}} \frac{\mathrm{d}E}{E_0 - E} = \frac{|V_0|^2}{\hbar}\log\left|\frac{E_{\min} - E_0}{E_{\max} - E_0}\right|. \tag{1.247}$$

The dressed state remains a true discrete eigenstate, now shifted away from its unperturbed energy. The same phenomenon occurs above the upper edge of the continuum.

When E_0 lies inside the continuum,

$$E_{\min} < E_0 < E_{\max}, \tag{1.248}$$

the self-energy has both a real and an imaginary part. In the weak-coupling, broad-continuum approximation one obtains

$$\Delta_0 = \frac{|V_0|^2}{\hbar}\mathcal{P}\int_{E_{\min}}^{E_{\max}} \frac{\mathrm{d}E}{E_0 - E} = \frac{|V_0|^2}{\hbar}\log\left|\frac{E_0 - E_{\min}}{E_{\max} - E_0}\right|, \tag{1.249}$$

$$\Gamma_0 = \frac{2\pi}{\hbar}|V_0|^2. \tag{1.250}$$

The decay rate thus coincides with the infinite-band value, $\Gamma_0 = \Gamma$, and the corresponding resonance pole is approximately

$$z_0 \simeq E_0 + \hbar\Delta_0 - \frac{\mathrm{i}\hbar\Gamma_0}{2}. \tag{1.251}$$

The pole is now located on the second sheet of the analytically continued resolvent rather than on the physical real axis. This is the characteristic signature of a resonance: the original discrete eigenstate has become a metastable state with a finite lifetime.

The approximation leading to these expressions requires the resonance to remain well separated from the band edges. More precisely, the energy scale associated with the pole shift and linewidth should be small compared with the distance from E_0 to the nearest edge,

$$\hbar|\Delta_0|,\ \hbar\Gamma_0 \ll \min(E_0 - E_{\min}, E_{\max} - E_0). \tag{1.252}$$

When this condition is not satisfied, the energy dependence of the self-energy cannot be neglected and the simple Breit–Wigner description breaks down.

Beyond the exponential regime. The finite-band model provides a simple way to understand why exponential decay cannot hold at arbitrarily long times in a realistic system. The resolvent contains branch points at the edges of the continuum, and therefore the inverse Fourier transform contains contributions from the vicinity of these branch points in addition to the resonance pole.

At intermediate times, if the resonance is sufficiently far from the band edges, the pole contribution dominates and one observes the familiar exponential decay,

$$P_\phi(t) \simeq \mathrm{e}^{-\Gamma_0 t}. \tag{1.253}$$

At very long times, however, the branch-cut contribution eventually becomes important. It generally produces a non-exponential, typically algebraic, decay. Thus the exponential law should be understood as an intermediate-time regime rather than an exact universal law.

A second important consequence is the existence of a real pole of the resolvent outside the continuum. Its weight is significant when the discrete state lies outside the continuum or within a distance of order $|V_0|^2$ of one of its edges, and it becomes exponentially small for a state deep inside the band (see below). Such a pole corresponds to a genuine dressed bound state and therefore does not decay. The initial state has a finite overlap with this bound state, implying

$$\lim_{t\to\infty}\left|\langle\phi|\hat{U}(t)|\phi\rangle\right|^2 > 0. \tag{1.254}$$

The remaining part of the initial state decays into the continuum, while the component associated with the bound-state pole survives indefinitely.

For the present model, a real bound-state energy E_b outside the continuum satisfies the self-consistent equation

$$E_b - E_0 - |V_0|^2 \log \left| \frac{E_{\min} - E_b}{E_{\max} - E_b} \right| = 0. \tag{1.255}$$

The residue of the corresponding pole determines the overlap of the dressed bound state with the original discrete state. Denoting this residue by Z_b, the long-time survival probability contains the contribution

$$P_\phi(\infty) = |Z_b|^2. \tag{1.256}$$

The existence of such a non-decaying component is particularly important near a continuum edge, where the assumption of a broad continuum is most strongly violated.

A solvable band-edge model. This last situation can be worked out completely analytically, which is worth doing because it is the case in which the Markovian description fails most dramatically. We place the continuum on

$$[E_{\min}, E_{\max}] = [0, W] \tag{1.257}$$

and put the discrete state exactly at its lower edge, $E_0 = E_{\min} = 0$. The self-energy appearing in (1.233) is then

$$\Sigma(z) = |V_0|^2 \int_0^W \frac{\mathrm{d}E}{z - E} = |V_0|^2 \log \frac{z}{z - W}. \tag{1.258}$$

The dressed bound state. We look for a real pole below the band, $z = E_b = -\epsilon$ with $\epsilon > 0$. The pole condition $z = E_0 + \Sigma(z)$ gives

$$\epsilon = |V_0|^2 \log \left(\frac{\epsilon + W}{\epsilon} \right). \tag{1.259}$$

As ϵ grows from 0 to ∞, the left-hand side increases from 0 to ∞ while the right-hand side decreases from ∞ to 0. The equation therefore admits exactly one solution, and it does so *for arbitrarily weak coupling*: a bound state is always pulled out below the band edge. Being a real eigenvalue of the Hermitian Hamiltonian $\hat{H}$ lying outside the continuous spectrum, it does not decay at all.

Ordinary perturbation theory fails here. Evaluating the second-order shift at $E_0 = 0$ would give $|V_0|^2 \, \mathcal{P} \int_0^W \mathrm{d}E/(0 - E)$, which diverges logarithmically at the lower edge. The divergence is cured self-consistently: the level moves down by ϵ, and this displacement is precisely what cuts off the logarithm. For $|V_0|^2 \ll W$, (1.259) reduces to $\epsilon \simeq |V_0|^2 \log(W/\epsilon)$, so that

$$\epsilon \simeq |V_0|^2 \log \frac{W}{|V_0|^2} \tag{1.260}$$

to leading logarithmic accuracy. The binding energy is of first order in $|V_0|^2$, but enhanced by a large logarithm.

Residue and trapped population. The residue of the projected resolvent (1.234) at a simple pole E_b is

$$Z_b = \frac{1}{1 - \Sigma'(E_b)}. \tag{1.261}$$

Differentiating (1.258),

$$\Sigma'(z) = -\frac{|V_0|^2 W}{z(z-W)}, \qquad \Sigma'(-\epsilon) = -\frac{|V_0|^2 W}{\epsilon(\epsilon+W)}, \tag{1.262}$$

so that

$$Z_b = \frac{\epsilon(\epsilon+W)}{\epsilon(\epsilon+W) + |V_0|^2 W}, \tag{1.263}$$

which indeed lies between 0 and 1. For $\epsilon \ll W$ this simplifies to

$$Z_b \simeq \frac{\epsilon}{\epsilon + |V_0|^2} \simeq \frac{L}{L+1}, \qquad L = \log\frac{W}{|V_0|^2}. \tag{1.264}$$

The residue approaches 1 only *logarithmically* slowly as the coupling is reduced: a state sitting at a band edge remains strongly dressed however weak the coupling. Since the asymptotic survival probability is $P_\phi(\infty) = |Z_b|^2$, a large fraction of the population never decays. Taking for instance $W = 100\,|V_0|^2$, (1.259) gives $\epsilon \simeq 3.41\,|V_0|^2$ and $Z_b \simeq 0.78$, hence

$$P_\phi(\infty) \simeq 0.61, \tag{1.265}$$

although the coupling is a hundred times smaller than the bandwidth.

Decay of the remaining weight. The complementary weight $1 - Z_b$ is carried by the continuum and does decay, but not exponentially. Its spectral density follows from (1.234), using $\log[z/(z-W)] = \log[E/(W-E)] - \mathrm{i}\pi$ for $z = E + \mathrm{i}\eta$ inside the band,

$$\rho(E) = -\frac{1}{\pi}\,\mathrm{Im}\langle\phi|\hat{G}(E+\mathrm{i}\eta)|\phi\rangle = \frac{|V_0|^2}{\left[E + |V_0|^2 \log\dfrac{W-E}{E}\right]^2 + \pi^2 |V_0|^4}. \tag{1.266}$$

Instead of the Lorentzian of the broad-band case, this distribution is *suppressed* at the edge: as $E \to 0$ the logarithm diverges and

$$\rho(E) \simeq \frac{1}{|V_0|^2 \log^2(W/E)} \longrightarrow 0, \tag{1.267}$$

although only logarithmically slowly. There is no pole close to the real axis, and hence no exponential regime at all. Since the survival amplitude is the Fourier transform of ρ, its long-time behaviour is controlled by the window $E \lesssim \hbar/t$, over which ρ is essentially constant, giving

$$\left|A(t) - Z_b\,\mathrm{e}^{-\mathrm{i}E_b t/\hbar}\right| \sim \frac{\hbar}{|V_0|^2\, t\, \log^2(Wt/\hbar)}. \tag{1.268}$$

The survival probability therefore approaches its plateau $|Z_b|^2$ algebraically, as $1/t$ up to logarithmic factors, with oscillations at the binding frequency $\epsilon/\hbar$ produced by the interference between the bound-state and continuum contributions. This is precisely the behaviour displayed in Fig. 8(b).

Why the effect disappears inside the band. The same calculation explains why no such plateau is visible in Fig. 8(a). For a discrete state well inside the band, a bound state is still pulled below the lower edge — the logarithmic divergence of Σ there guarantees it — but it is now exponentially weakly bound. Setting $E_b = -\epsilon$ in the general pole condition (1.255) gives $-\epsilon - E_0 = |V_0|^2 \log[\epsilon/(\epsilon + W)]$, and neglecting ϵ against both E_0 and W one finds

$$\epsilon \simeq W\, \mathrm{e}^{-E_0/|V_0|^2}, \qquad Z_b \simeq \frac{\epsilon}{|V_0|^2} = \frac{W}{|V_0|^2}\, \mathrm{e}^{-E_0/|V_0|^2}. \tag{1.269}$$

The trapped fraction is exponentially small in $E_0/|V_0|^2$, and entirely negligible for a state far from the edges. The Markovian, exponential description is then recovered, and the bound state reveals itself only when the discrete level approaches a band edge.

Physical interpretation. The Wigner–Weisskopf model therefore provides a useful hierarchy of descriptions. In the broad-band weak-coupling regime, the continuum acts as an effectively memoryless environment: the self-energy can be evaluated at E_0, the resonance pole is approximately

$$z_0 = E_0 + \hbar\Delta_0 - \frac{\mathrm{i}\hbar\Gamma_0}{2}, \tag{1.270}$$

and the decay is exponential. This is the regime in which Fermi's golden rule gives the correct long-time decay rate.

When the density of states or coupling varies significantly around E_0, the self-energy becomes strongly energy-dependent. The continuum then retains a memory of the emitted amplitude, and the dynamics is no longer described by a single exponential. Band edges provide a particularly simple realization of this situation. They can lead to non-exponential decay and, when a real pole is pulled out of the continuum, to a dressed bound state with an infinite lifetime.

The Wigner–Weisskopf model thus makes explicit the relation between three equivalent descriptions of decay: the golden-rule transition rate, the imaginary part of the effective Hamiltonian, and the position of a resonance pole of the analytically continued resolvent.

1.3.5 Spontaneous emission in a structured medium

The decay of a discrete quantum state into a continuum is particularly important in quantum optics, where it describes spontaneous emission of an excited atom into the electromagnetic field. The decay rate obtained from Fermi's golden rule,

$$\Gamma_0 = \frac{2\pi}{\hbar}\overline{|\langle\psi_f|\hat{V}|\psi_0\rangle|^2}\rho_E(E_0), \tag{1.271}$$

depends both on the coupling matrix elements and on the density of available final states at the transition energy. The electromagnetic environment can therefore strongly modify spontaneous emission by modifying its density of states.

We illustrate this idea with three examples. In free space, the electromagnetic modes form a broad continuum and lead to the familiar exponential decay. An optical resonator concentrates the density of states around a resonant frequency and can enhance the decay, an effect known as the Purcell effect. Conversely, a photonic bandgap suppresses the density of states over a range of frequencies and can inhibit spontaneous emission.

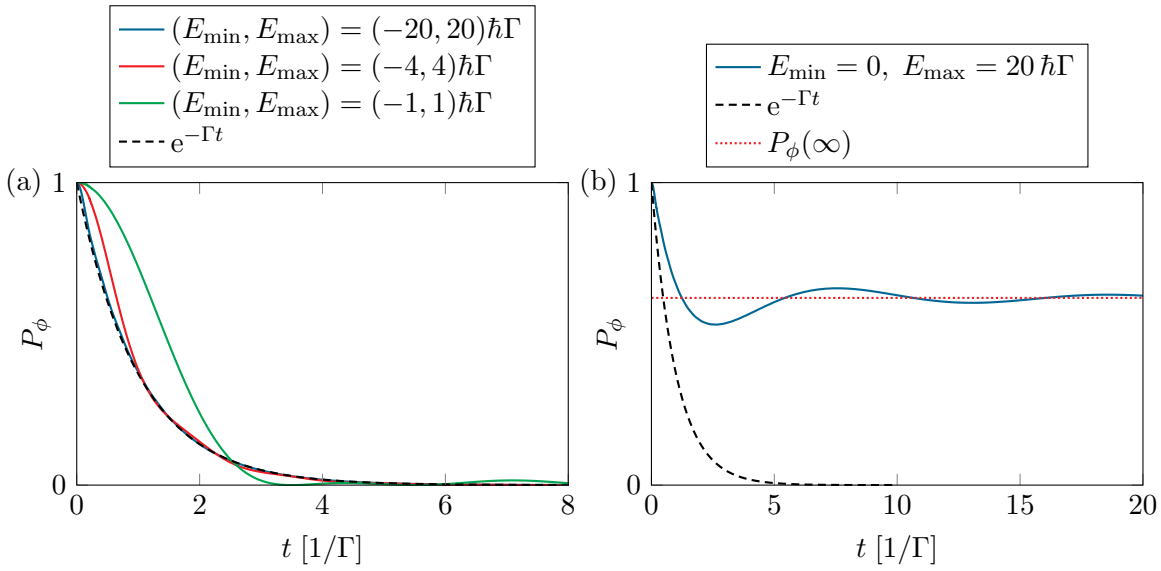


Figure 8: Decay of the probability P_ϕ to remain in the discrete state $|\phi\rangle$ after it is coupled to a continuum. In (a), the discrete-state energy lies in the middle of the continuum, whereas in (b) it lies at its lower edge. The dashed black line shows the purely exponential decay $P_\phi(t) = \mathrm{e}^{-\Gamma t}$ obtained for an infinitely broad continuum. For a finite bandwidth, deviations from exponential decay appear at long times. In (b), the horizontal dotted line indicates the nonzero asymptotic probability $P_\phi(\infty) = |Z_b|^2$ associated with the real pole of the resolvent, corresponding to a bound state dressed by the continuum.

Close to a band edge, the density of states varies rapidly with energy, so that the broad-continuum approximation breaks down and the full resolvent description becomes necessary.

Spontaneous emission to free space. We first recall how to compute the spontaneous emission rate for an excited atomic level coupled to the electromagnetic vacuum. For simplicity, we consider the level structure of a spinless particle, whose ground state is a non-degenerate S orbital (angular momentum $L = 0$) and whose excited state belongs to a P orbital ($L = 1$, three-fold degenerate). We consider an initial state in which the atom occupies a state $|e\rangle$ of the excited manifold, while the electromagnetic field is in the vacuum state $|\mathbf{0}\rangle$.

The excited state $|e\rangle$ is defined within the P manifold by the polarization $\boldsymbol{\epsilon}_{\mathrm{exc}}$ that was used to promote the particle to the excited state. Spontaneous emission couples this state to a continuum of states in which the atom has returned to the ground state $|g\rangle$ and one photon has been created. These final states are indexed by the photon wavevector $\mathbf{k}$ and polarization $\boldsymbol{\epsilon}$, with $\boldsymbol{\epsilon} \perp \mathbf{k}$.

The interaction is given by the electric-dipole coupling

$$\hat{V} = -\hat{\mathbf{d}} \cdot \hat{\mathbf{E}}, \tag{1.272}$$

and the corresponding matrix element is

$$\langle e, \mathbf{0}|(-\hat{\mathbf{d}} \cdot \hat{\mathbf{E}})|g, 1_{\mathbf{k},\boldsymbol{\epsilon}}\rangle = -d\, \mathcal{E}_\omega\, \boldsymbol{\epsilon}^*_{\mathrm{exc}} \cdot \boldsymbol{\epsilon}, \tag{1.273}$$

where $\omega = ck$ is the photon frequency and

$$\mathcal{E}_\omega = \sqrt{\frac{\hbar\omega}{2\epsilon_0 V}} \tag{1.274}$$

is the rms electric field associated with a single photon in the quantization volume V. We write it $\mathcal{E}_\omega$ rather than $E_0(\omega)$ to avoid any confusion with the unperturbed energy E_0 of the discrete state.

The photon modes form a continuum. Taking into account the two transverse polarizations, their density of states per unit energy is

$$\rho_E(E) = \frac{V E^2}{\pi^2 \hbar^3 c^3}. \tag{1.275}$$

Fermi's golden rule then gives

$$\Gamma_0 = \frac{2\pi}{\hbar} \overline{\left|\langle e, \mathbf{0}|(-\hat{\mathbf{d}} \cdot \hat{\mathbf{E}})|g, 1_{\mathbf{k},\boldsymbol{\epsilon}}\rangle\right|^2} \rho_E(\hbar\omega_0), \tag{1.276}$$

where the average is taken over photon modes resonant with the atomic transition. Using

$$\overline{|\boldsymbol{\epsilon}^*_{\mathrm{exc}} \cdot \boldsymbol{\epsilon}|^2} = \frac{1}{3}, \tag{1.277}$$

we obtain the standard expression

$$\Gamma_0 = \frac{\omega_0^3 d^2}{3\pi\epsilon_0 \hbar c^3}. \tag{1.278}$$

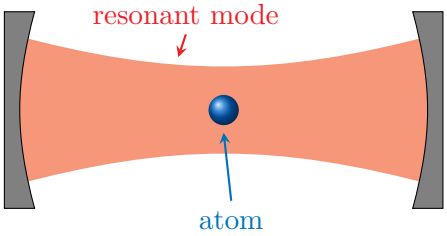


Figure 9: Scheme of an atom placed inside an optical cavity. The resonator modifies the electromagnetic density of states and can enhance spontaneous emission when a cavity resonance is close to the atomic transition frequency. This enhancement is known as the Purcell effect.

Since $\hbar\Gamma_0 \ll \hbar\omega_0$ and the density of states varies smoothly on the scale $\hbar\omega_0$, the broad-continuum approximation is very well satisfied and the decay is exponential. This result already illustrates the two ingredients controlling spontaneous emission: the coupling between the atom and the electromagnetic field, and the density of available photon states at the transition frequency. Modifying the electromagnetic environment therefore provides a way of controlling the decay of the atom.

Purcell effect in an optical resonator. One way to modify the electromagnetic density of states is to place the atom inside an optical resonator [3, 4], as illustrated in Fig. 9.

A given resonant mode of the cavity, of frequency $\omega_{\rm cav}$, gives rise to a resonance in the density of states. Assuming that the photon losses are characterized by a decay rate κ, this contribution can be approximated by a Lorentzian,

$$\rho_E(E) = \frac{1}{\pi}\frac{\hbar\kappa/2}{(E-\hbar\omega_{\rm cav})^2 + (\hbar\kappa/2)^2}. \tag{1.279}$$

At resonance with the atomic transition,

$$\omega_{\rm cav} = \omega_0, \tag{1.280}$$

one has

$$\rho_E(\hbar\omega_0) = \frac{2}{\pi\hbar\kappa}. \tag{1.281}$$

The spontaneous decay rate into the resonant mode is therefore

$$\Gamma = \frac{4d^2}{\hbar^2\kappa}\left|\boldsymbol{\epsilon}^*_{\rm exc}\cdot\mathbf{E}_{\rm cav}(\mathbf{r}_0)\right|^2, \tag{1.282}$$

where $\mathbf{E}_{\rm cav}(\mathbf{r}_0)$ is the electric field of the resonant mode at the atom position.

It is convenient to introduce an effective cavity mode volume $V_{\rm cav}$ through

$$V_{\rm cav}\,\epsilon_0 E_{\rm cav}(\mathbf{r}_0)^2 = \frac{\hbar\omega_0}{2}, \tag{1.283}$$

the subscript distinguishing it from the coupling amplitude V_0 of the Wigner–Weisskopf model. Assuming that the atomic dipole and cavity mode have the same polarization, we obtain

$$\Gamma = \frac{2d^2\omega_0}{\epsilon_0\hbar\kappa V_{\rm cav}}. \tag{1.284}$$

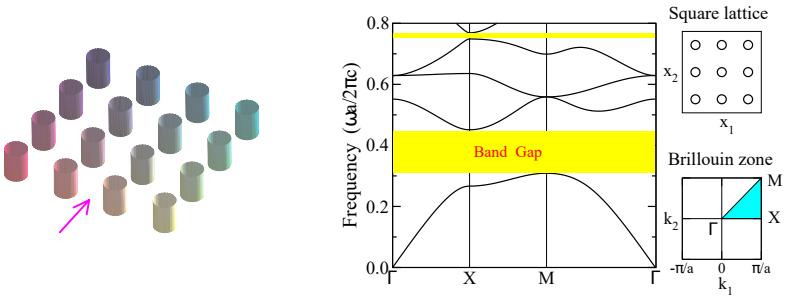


Figure 10: Scheme of a two-dimensional photonic crystal consisting of a regular array of dielectric rods. The periodic structure modifies the electromagnetic density of states and produces photonic bandgaps (yellow regions in the dispersion relation), in which light cannot propagate. Spontaneous emission is inhibited when the atomic transition frequency lies inside a photonic bandgap. Near a band edge, the strong energy dependence of the density of states can lead to non-exponential decay and the formation of photon bound states.

Comparing this result with the free-space decay rate gives the Purcell factor

$$\frac{\Gamma}{\Gamma_0} = \frac{3}{4\pi^2}\frac{\lambda_0^3}{V_{\text{cav}}}Q, \tag{1.285}$$

where λ_0 is the resonant wavelength and

$$Q = \frac{\omega_0}{\kappa} \tag{1.286}$$

is the quality factor of the cavity.

The Purcell effect thus provides a direct example of the role of the continuum density of states: concentrating electromagnetic modes around the transition frequency enhances the decay rate. This enhancement has been observed in a wide range of systems, from Rydberg atoms in microwave cavities [5] to quantum dots in optical microcavities [6], where it plays an important role in the realization of semiconductor single-photon sources [7].

Inhibition of spontaneous emission in a photonic bandgap. The opposite effect can be obtained by suppressing the density of electromagnetic states. A periodic modulation of the refractive properties of a material can produce photonic bandgaps, frequency intervals in which electromagnetic waves cannot propagate through the structure (see Fig. 10).

When an atomic transition frequency ω_0 lies inside such a bandgap, there are no propagating photon modes at the transition energy. Fermi's golden rule therefore predicts a suppression of spontaneous emission,

$$\Gamma_0 = 0. \tag{1.287}$$

This phenomenon, known as inhibition of spontaneous emission, has been observed in a variety of physical systems, from single atoms [8, 9] to solid-state systems [10, 11].

The vanishing of the golden-rule decay rate, however, does not imply that the atom is completely decoupled from the electromagnetic field. Virtual transitions to off-resonant

photon modes can still produce an energy shift, corresponding to the real part of the self-energy. Moreover, close to the edge of a photonic bandgap, the density of states varies rapidly with energy. In this situation, the broad-continuum approximation used to derive exponential decay is no longer justified.

When the atomic transition is close to a band edge, the energy dependence of the effective Hamiltonian becomes important. The resulting dynamics can deviate strongly from exponential decay, and a finite fraction of the initial excitation can remain localized around the emitter. In the resolvent description, this behavior can be associated with the appearance of a real pole outside the continuous spectrum. The corresponding eigenstate is a bound state dressed by the electromagnetic field, often called a photon bound state in photonic structures with a bandgap.

Such non-exponential decay and dressed bound states have been predicted and observed in a wide range of platforms [12, 13, 14, 15, 16, 17]. They provide a particularly clear physical realization of the limitations of Fermi's golden rule and motivate the resolvent approach developed in this section.

1.4 From effective Hamiltonians to open quantum systems

So far, we have mainly considered situations in which the Hilbert space can be separated into two complementary subspaces,

$$\mathcal{H} = \mathcal{H}_A \oplus \mathcal{H}_B, \tag{1.288}$$

with the projector $\hat{P}$ selecting the subspace of interest and $\hat{Q} = \mathbb{1} - \hat{P}$ its complement. The degrees of freedom associated with $\mathcal{H}_B$ can then be eliminated, leading to an effective Hamiltonian acting within $\mathcal{H}_A$. This construction has allowed us to describe, for instance, virtual transitions to excited states, effective couplings between degenerate levels, and the decay of a discrete state into a continuum.

A qualitatively different situation arises when the degrees of freedom that we wish to describe form a *subsystem* coupled to an environment (see Figure 11). The total Hilbert space is then a tensor product,

$$\mathcal{H} = \mathcal{H}_S \otimes \mathcal{H}_E, \tag{1.289}$$

where $\mathcal{H}_S$ describes the subsystem of interest and $\mathcal{H}_E$ the environmental degrees of freedom. Unlike the direct-sum decomposition considered previously, both sets of degrees of freedom are present simultaneously: the environment does not represent an alternative state of the subsystem, but rather additional physical degrees of freedom that become entangled with it.

The total Hamiltonian can generally be written as

$$\hat{H} = \hat{H}_S \otimes \mathbb{1}_E + \mathbb{1}_S \otimes \hat{H}_E + \hat{V}, \tag{1.290}$$

where $\hat{V}$ describes the coupling between the subsystem and its environment. Even though the evolution generated by $\hat{H}$ is unitary, we are often interested only in the subsystem. Its state is therefore described by the reduced density operator

$$\hat{\rho}_S = \mathrm{Tr}_E(\hat{\rho}), \tag{1.291}$$

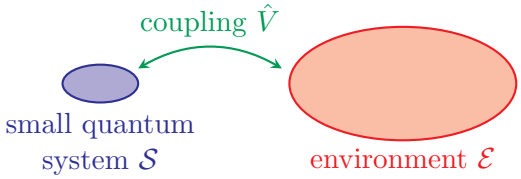


Figure 11: Scheme of the open system considered here. A small quantum system $\mathcal{S}$ is coupled to a large environment, or reservoir, $\mathcal{E}$ by a coupling $\hat{V}$.

obtained by tracing out the environmental degrees of freedom. A reminder of the properties of the reduced density operator is given in Appendix A.

In general, the reduced state $\hat{\rho}_S$ does not evolve according to a unitary Schrödinger equation, nor can its dynamics be described by an effective Hermitian Hamiltonian alone. Information and energy can be exchanged with the environment, and the subsystem can become entangled with degrees of freedom that are no longer explicitly retained. The resulting dynamics can therefore exhibit irreversible phenomena such as relaxation and decoherence.

There is nevertheless a close connection with the effective-Hamiltonian approach developed above. In both cases, we eliminate degrees of freedom that are not explicitly observed. The difference is that, for an open quantum system, the eliminated degrees of freedom constitute an environment with its own dynamics and generally retain information about the subsystem. Their elimination consequently produces not only energy shifts, but also dissipation and decoherence.

We first illustrate this idea with the simplest possible example: a two-level subsystem coupled to a continuum. This example provides a direct bridge between the resolvent treatment of resonant decay developed above and the more general framework of open quantum systems. We then generalize the construction to an arbitrary subsystem coupled to an environment and introduce, under suitable approximations, the Lindblad equation.

1.4.1 Lindblad equation for a two-level system coupled to a continuum

We consider a two-level subsystem coupled to a continuum, which can be solved quasi-analytically. This will allow us to reveal the type of evolution followed by the reduced density matrix of an open system and to identify the conditions under which it takes the Lindblad form.

Description of the model. Consider a two-level subsystem with ground state $|g\rangle$ and excited state $|e\rangle$, coupled to an environment initially in a state $|0_E\rangle$. The total Hilbert space is

$$\mathcal{H} = \mathcal{H}_S \otimes \mathcal{H}_E, \tag{1.292}$$

and we assume that the interaction allows the excitation of the subsystem to be transferred to the environment. A typical interaction Hamiltonian can be written as

$$\hat{V} = \hbar \int \left[g_\omega \, \hat{\sigma}_- \otimes \hat{b}_\omega^\dagger + g_\omega^* \, \hat{\sigma}_+ \otimes \hat{b}_\omega \right] \mathrm{d}\omega, \tag{1.293}$$

where

$$\hat{\sigma}_- = |g\rangle\langle e|, \qquad \hat{\sigma}_+ = |e\rangle\langle g|, \tag{1.294}$$

and $\hat{b}_\omega^\dagger$ creates an excitation in the environmental mode labelled by ω, where ω is the frequency of the mode. With the normalization $[\hat{b}_\omega, \hat{b}_{\omega'}^\dagger] = \delta(\omega - \omega')$, $|g_\omega|^2$ has the dimension of a rate.

If the total system initially contains a single excitation,

$$|\Psi(0)\rangle = |e\rangle \otimes |0_E\rangle, \tag{1.295}$$

the dynamics remains in the single-excitation sector. The relevant states are then

$$|e, 0_E\rangle \qquad \text{and} \qquad |g, 1_\omega\rangle, \tag{1.296}$$

where $|1_\omega\rangle$ denotes an environment containing one excitation in mode ω. Within this restricted sector, the Hilbert space therefore takes the direct-sum form

$$\mathcal{H}_1 = \mathrm{span}\{|e, 0_E\rangle\} \oplus \mathrm{span}\{|g, 1_\omega\rangle\}_\omega. \tag{1.297}$$

We thus recover precisely the structure considered in the previous section: a discrete state coupled to a continuum.

From the point of view of the subsystem, however, the physical interpretation is different. The transition

$$|e, 0_E\rangle \longrightarrow |g, 1_\omega\rangle \tag{1.298}$$

corresponds to the decay of the excited state and the emission of an excitation into the environment. The continuum is therefore not merely a complementary subspace of the subsystem, but consists of additional environmental degrees of freedom.

In the weak-coupling and broad-continuum regime, the resolvent calculation gives

$$\langle e, 0_E|\hat{U}(t)|e, 0_E\rangle \simeq \mathrm{e}^{-\mathrm{i}(E_e/\hbar+\Delta)t}\mathrm{e}^{-\Gamma t/2}, \tag{1.299}$$

and hence

$$P_e(t) = \mathrm{e}^{-\Gamma t}. \tag{1.300}$$

At the level of the reduced subsystem, this describes an irreversible transition

$$|e\rangle \longrightarrow |g\rangle. \tag{1.301}$$

The same physics can be expressed directly in terms of the density matrix of the two-level subsystem. Starting from the initial state $|e\rangle$, the exponential decay obtained above implies

$$\rho_{ee}(t) = \langle e|\hat{\rho}_S(t)|e\rangle = \mathrm{e}^{-\Gamma t}. \tag{1.302}$$

A natural question is then how to describe the dynamics of the density matrix $\hat{\rho}_S(t)$ itself. Establishing such a description is the goal of our introduction to open quantum systems.

1.4.2 The Lindblad equation from the Wigner–Weisskopf model

The evolution of the density matrix $\hat{\rho}_S(t)$ can be pushed analytically under the simplifying assumptions underlying the Wigner–Weisskopf model. As in Section 1.3.4, it is convenient to measure the continuum label ω relative to the atomic transition frequency ω_0, so that ω denotes the *detuning* of a mode from resonance rather than its absolute frequency: the excited level $|e\rangle$ then plays the role of the discrete state placed at zero energy, exactly as $E_0 = 0$ there. We assume that the coupling g_ω is uniform (equal to $g > 0$) over a band

of width W centred on resonance, $-W/2 < \omega < W/2$, and vanishes outside it. The continuum is assumed to be broad in the sense that it is much wider than the decay rate it will be found to produce – a condition we make precise once that rate, Γ, has been computed.

The state evolution can be written exactly as

$$|\Psi(t)\rangle = c_e(t)|e,0\rangle + \int_{-W/2}^{W/2} \mathrm{d}\omega\; c_\omega(t)\mathrm{e}^{-\mathrm{i}\omega t}|g,1_\omega\rangle, \tag{1.303}$$

where the free phases have been factored out. Inserting (1.303) in the Schrödinger equation gives the coupled amplitude equations

$$\dot{c}_e(t) = -\mathrm{i}\; g \int_{-W/2}^{W/2} \mathrm{d}\omega\, c_\omega(t)\, \mathrm{e}^{-\mathrm{i}\omega t}, \tag{1.304}$$

$$\dot{c}_\omega(t) = -\mathrm{i}\, g\, c_e(t)\, \mathrm{e}^{+\mathrm{i}\omega t}. \tag{1.305}$$

Equation (1.305) can be integrated exactly with the initial condition $c_\omega(0) = 0$,

$$c_\omega(t) = -\mathrm{i}\, g \int_0^t \mathrm{d}\tau\; c_e(\tau)\, \mathrm{e}^{+\mathrm{i}\omega\tau}, \tag{1.306}$$

and substituted back into (1.304). We obtain a closed, still exact, integro-differential equation for the atomic amplitude alone,

$$\dot{c}_e(t) = -\int_0^t \mathrm{d}\tau\; K(t-\tau)\, c_e(\tau), \tag{1.307}$$

with the *memory kernel*

$$K(s) = g^2 \int_{-W/2}^{W/2} \mathrm{d}\omega\, \mathrm{e}^{-\mathrm{i}\omega s} = \frac{2g^2}{s}\sin\!\Big(\frac{Ws}{2}\Big) = g^2 W\; \mathrm{sinc}\left(\frac{Ws}{2}\right). \tag{1.308}$$

The whole influence of the environment on the subsystem is then encoded in the single function $K(s)$.

Where the Markov approximation enters. Equation (1.307) is non-local in time: the evolution at time t depends on the whole history of the atom. The kernel (1.308) decays over the *correlation time* set by the width of the sinc function,

$$\tau_E \sim \frac{1}{W}. \tag{1.309}$$

Its total weight, on the other hand, is fixed by the coupling exactly at resonance and does not depend on W: using $\int_{-\infty}^{\infty} \mathrm{d}s\, \mathrm{e}^{-\mathrm{i}\omega s} = 2\pi\delta(\omega)$,

$$\int_{-\infty}^{\infty} \mathrm{d}s\; K(s) = g^2 \int_{-W/2}^{W/2} \mathrm{d}\omega\; 2\pi\delta(\omega) = 2\pi g^2, \tag{1.310}$$

and, since $K(s)$ is even in s, half of this weight lies at $s > 0$. In the broad-band limit $W \to \infty$, the kernel itself becomes a delta function,

$$K(s) \;\xrightarrow[W\to\infty]{}\; 2\pi g^2\, \delta(s), \tag{1.311}$$

using the standard representation $\sin(as)/(\pi s) \to \delta(s)$ for $a \to \infty$.

The *Markov approximation* is most transparent once the integration variable in (1.307) is changed from the absolute time τ to the delay $s = t - \tau$,

$$\dot{c}_e(t) = -\int_0^t \mathrm{d}s\; K(s)\, c_e(t-s). \tag{1.312}$$

It then consists of two steps: replacing $c_e(t-s)$ by $c_e(t)$, and extending the upper limit of the delay integral from t to infinity. Equation (1.307) then becomes local in time,

$$\dot{c}_e(t) = -\left[\int_0^\infty \mathrm{d}s\, K(s)\right] c_e(t) = -\frac{\Gamma}{2}\, c_e(t), \qquad \Gamma \equiv 2\pi g^2, \tag{1.313}$$

so that the broad-continuum condition reads precisely $W \gg \Gamma = 2\pi g^2$: the continuum must be broad compared with the decay rate it produces. We recognize in Γ Fermi's golden rule for the resonant transition. There is, moreover, no Lamb shift here, $\Delta = 0$: because the band is exactly symmetric about the atomic transition. Equation (1.313) integrates to the exponential decay

$$c_e(t) = \mathrm{e}^{-\Gamma t/2}. \tag{1.314}$$

It is worth stressing that this exponential law cannot hold at arbitrarily short times. Expanding (1.307) for $t \to 0$ gives the quadratic, so-called Zeno, behaviour

$$|c_e(t)|^2 \simeq 1 - K(0)\, t^2, \qquad K(0) = g^2 W, \tag{1.315}$$

which crosses over to the exponential decay (1.314) only once $t \gtrsim \tau_E \sim 1/W$. Any Markovian description is therefore implicitly *coarse-grained* in time.

From amplitudes to the reduced density matrix. So far we have only followed the atom initially in $|e\rangle$, working throughout in the frame in which the atomic energy has been set to zero (Section 1.3.4). To treat an arbitrary initial state we must restore the trivial phase associated with the true atomic transition frequency ω_0, and use the linearity of the Schrödinger equation. Starting from a general product state

$$|\Psi(0)\rangle = (c_g|g\rangle + c_e|e\rangle) \otimes |0\rangle, \tag{1.316}$$

the state $|g,0\rangle$ has zero energy and is not coupled to anything: it is stationary. The excited-state survival amplitude is

$$A(t) \equiv \langle e,0|\hat{U}(t)|e,0\rangle = \mathrm{e}^{-\mathrm{i}\omega_0 t}\, c_e(t), \tag{1.317}$$

where $c_e(t)$ is the solution of (1.307) obtained above, equal to $\mathrm{e}^{-\Gamma t/2}$ in the Markovian regime, (1.314). The exact state at time t reads

$$|\Psi(t)\rangle = c_g|g,0\rangle + c_e\, A(t)|e,0\rangle + c_e|g\rangle \otimes |\varphi(t)\rangle, \tag{1.318}$$

where $|\varphi(t)\rangle = \int \mathrm{d}\omega\, c_\omega(t)\mathrm{e}^{-\mathrm{i}\omega t}|1_\omega\rangle$ is the one-excitation state of the environment. Unitarity imposes

$$\langle\varphi(t)|\varphi(t)\rangle = 1 - |A(t)|^2, \qquad \langle 0|\varphi(t)\rangle = 0. \tag{1.319}$$

The key point is that the environment ends up in only *two* orthogonal states: the vacuum $|0\rangle$, and the normalized one-excitation state

$$|\hat{\varphi}(t)\rangle = \frac{|\varphi(t)\rangle}{\sqrt{1-|A(t)|^2}}. \tag{1.320}$$

It is therefore natural to regroup the terms of the state according to the state of the environment,

$$|\Psi(t)\rangle = |\chi_0(t)\rangle \otimes |0\rangle + |\chi_1(t)\rangle \otimes |\hat{\varphi}(t)\rangle, \tag{1.321}$$

with the two *unnormalized* atomic states

$$|\chi_0(t)\rangle = c_g|g\rangle + c_e\, A(t)|e\rangle, \tag{1.322}$$

$$|\chi_1(t)\rangle = c_e\sqrt{1-|A(t)|^2}\;|g\rangle. \tag{1.323}$$

The first describes the branch in which no photon has been emitted, the second the branch in which one photon has been emitted.

The partial trace over the environment is now immediate. Expanding the projector on (1.321),

$$\begin{aligned}|\Psi(t)\rangle\langle\Psi(t)| = {}& |\chi_0\rangle\langle\chi_0| \otimes |0\rangle\langle 0| + |\chi_1\rangle\langle\chi_1| \otimes |\hat{\varphi}\rangle\langle\hat{\varphi}| \\ & + |\chi_0\rangle\langle\chi_1| \otimes |0\rangle\langle\hat{\varphi}| + |\chi_1\rangle\langle\chi_0| \otimes |\hat{\varphi}\rangle\langle 0|,\end{aligned} \tag{1.324}$$

and using $\mathrm{Tr}_E\,[|a\rangle\langle b|] = \langle b|a\rangle$ for the environment factors, the two diagonal terms contribute with weight $\langle 0|0\rangle = \langle\hat{\varphi}|\hat{\varphi}\rangle = 1$, whereas the two cross terms vanish because $\langle\hat{\varphi}|0\rangle = 0$. We are left with

$$\hat{\rho}_S(t) = \mathrm{Tr}_E|\Psi(t)\rangle\langle\Psi(t)| = |\chi_0(t)\rangle\langle\chi_0(t)| + |\chi_1(t)\rangle\langle\chi_1(t)|. \tag{1.325}$$

The orthogonality of the two environment states is what makes the reduced density matrix a *sum* of two branches, with no interference between them: the environment has kept a record of which branch occurred.

It remains to express this result in terms of the initial atomic state $\hat{\rho}_S(0) = |\psi_0\rangle\langle\psi_0|$, with $|\psi_0\rangle = c_g|g\rangle + c_e|e\rangle$. Both $|\chi_0\rangle$ and $|\chi_1\rangle$ are linear in $|\psi_0\rangle$, and can therefore be written as operators acting on it,

$$|\chi_0(t)\rangle = \hat{M}_0(t)|\psi_0\rangle, \qquad |\chi_1(t)\rangle = \hat{M}_1(t)|\psi_0\rangle, \tag{1.326}$$

with

$$\hat{M}_0 = |g\rangle\langle g| + A(t)|e\rangle\langle e|, \qquad \hat{M}_1 = \sqrt{1-|A(t)|^2}\;\hat{\sigma}_-. \tag{1.327}$$

Substituting into (1.325) gives

$$\hat{\rho}_S(t) = \hat{M}_0(t)\,\hat{\rho}_S(0)\,\hat{M}_0^\dagger(t) + \hat{M}_1(t)\,\hat{\rho}_S(0)\,\hat{M}_1^\dagger(t). \tag{1.328}$$

Although obtained here for a pure initial state, this relation is linear in $\hat{\rho}_S(0)$ and therefore holds for an arbitrary initial atomic density matrix, provided the atom and the field start in a product state with the field in its vacuum.

The two operators satisfy

$$\begin{aligned}\hat{M}_0^\dagger\hat{M}_0 + \hat{M}_1^\dagger\hat{M}_1 &= |g\rangle\langle g| + |A|^2|e\rangle\langle e| + \left(1-|A|^2\right)\hat{\sigma}_+\hat{\sigma}_- \\ &= |g\rangle\langle g| + |e\rangle\langle e| = \mathbb{1},\end{aligned} \tag{1.329}$$

which guarantees that the trace is preserved. Equation (1.328) is an example of a *Kraus decomposition*; any map of this form is automatically completely positive and trace preserving, so that $\hat{\rho}_S(t)$ is a legitimate density matrix. Explicitly, the matrix elements evolve as

$$\rho_{ee}(t) = |A(t)|^2\,\rho_{ee}(0), \tag{1.330}$$

$$\rho_{eg}(t) = A(t)\,\rho_{eg}(0), \tag{1.331}$$

$$\rho_{gg}(t) = \rho_{gg}(0) + \left[1 - |A(t)|^2\right]\rho_{ee}(0). \tag{1.332}$$

The two operators have a transparent physical meaning. The operator $\hat{M}_1 \propto \hat{\sigma}_-$ describes the branch in which an excitation has been emitted into the environment: it is the *quantum jump*. The operator $\hat{M}_0$ describes the complementary branch, in which no excitation has been emitted; it is not unitary, since $|A| < 1$, and it reduces the weight of $|e\rangle$ accordingly. This is the microscopic origin of the non-Hermitian effective Hamiltonian encountered in the resolvent approach, and the starting point of the quantum-trajectory description discussed below.

Infinitesimal time step and the Lindblad equation. Expanding (1.327) to first order in a small time increment $\mathrm{d}t$,

$$\hat{M}_0 = \mathbb{1} - \left[\mathrm{i}\omega_0 + \frac{\Gamma}{2}\right]\hat{\sigma}_+\hat{\sigma}_-\,\mathrm{d}t = \mathbb{1} - \frac{\mathrm{i}}{\hbar}\hat{H}_{\mathrm{eff}}\,\mathrm{d}t, \tag{1.333}$$

$$\hat{M}_1 = \sqrt{\Gamma\,\mathrm{d}t}\;\hat{\sigma}_- = \sqrt{\mathrm{d}t}\;\hat{L}, \tag{1.334}$$

where we have introduced the non-Hermitian effective Hamiltonian and the jump operator

$$\hat{H}_{\mathrm{eff}} = \hbar\omega_0\,\hat{\sigma}_+\hat{\sigma}_- - \frac{\mathrm{i}\hbar\Gamma}{2}\hat{\sigma}_+\hat{\sigma}_-, \qquad \hat{L} = \sqrt{\Gamma}\,\hat{\sigma}_-. \tag{1.335}$$

The characteristic $\sqrt{\mathrm{d}t}$ scaling of the jump operator is the signature of the Markovian limit: it is precisely what makes the jump term $\hat{M}_1\hat{\rho}_S\hat{M}_1^\dagger$ contribute at first order in $\mathrm{d}t$. Had the kernel possessed a finite correlation time, the jump probability would have been quadratic in $\mathrm{d}t$ at short times, as in the Zeno regime discussed above, and no such expansion would exist.

Inserting (1.333) and (1.334) into (1.328) and keeping the terms linear in $\mathrm{d}t$ gives, with $\hat{H}_S = \hbar\omega_0\hat{\sigma}_+\hat{\sigma}_-$,

$$\begin{aligned}\hat{\rho}_S(t+\mathrm{d}t) = \hat{\rho}_S &- \frac{\mathrm{i}}{\hbar}\left[\hat{H}_S, \hat{\rho}_S\right]\mathrm{d}t \\ &+ \Gamma\left(\hat{\sigma}_-\hat{\rho}_S\hat{\sigma}_+ - \frac{1}{2}\left\{\hat{\sigma}_+\hat{\sigma}_-, \hat{\rho}_S\right\}\right)\mathrm{d}t,\end{aligned} \tag{1.336}$$

that is, the Lindblad equation

$$\partial_t\hat{\rho}_S = -\frac{\mathrm{i}}{\hbar}\left[\hat{H}_S, \hat{\rho}_S\right] + \hat{L}\hat{\rho}_S\hat{L}^\dagger - \frac{1}{2}\left\{\hat{L}^\dagger\hat{L}, \hat{\rho}_S\right\}, \tag{1.337}$$

with the single jump operator $\hat{L} = \sqrt{\Gamma}\,\hat{\sigma}_-$ and, in this symmetric example, *no* Lamb-shift correction to $\hat{H}_S$ – a direct consequence of $\Delta = 0$. For a band not centred on resonance,

the same calculation would add a Lamb-shift term $\hat{H}_{\mathrm{LS}} = \hbar\Delta\,\hat{\sigma}_+\hat{\sigma}_-$ to the coherent part, with Δ given by (1.249). The populations and coherences obey

$$\partial_t \rho_{ee} = -\Gamma\rho_{ee}, \qquad \partial_t \rho_{eg} = -\left(\frac{\Gamma}{2} + \mathrm{i}\omega_0\right)\rho_{eg}, \tag{1.338}$$

so that the coherence decays twice as slowly as the population. This factor of two, which is a direct consequence of $\rho_{eg} \propto A$ while $\rho_{ee} \propto |A|^2$, is one of the most useful predictions of the Lindblad description: it is not contained in the survival probability alone.

1.4.3 Extending the Lindblad equation to the general case

The Wigner–Weisskopf example produced a Lindblad equation with a single jump operator, associated with the one decay channel available to the two-level system. A generic subsystem $\mathcal{S}$ coupled to a generic environment typically possesses several independent irreversible channels – one jump operator per pair of energy levels, say, or per polarization of an emitted photon – each expected to contribute dissipative dynamics of the same structure. This suggests postulating, for an arbitrary subsystem, the generator

$$\partial_t \hat{\rho}_S = -\frac{\mathrm{i}}{\hbar}\left[\hat{H}_S, \hat{\rho}_S\right] + \sum_k \left(\hat{L}_k \hat{\rho}_S \hat{L}_k^\dagger - \frac{1}{2}\left\{\hat{L}_k^\dagger \hat{L}_k, \hat{\rho}_S\right\}\right), \tag{1.339}$$

with $\hat{H}_S$ Hermitian and $\{\hat{L}_k\}$ an arbitrary family of operators on $\mathcal{H}_S$, one per channel. Rather than deriving (1.339) from a microscopic model, as we did above, let us check directly that it meets the requirements demanded of the evolution of an open quantum system: linearity, trace preservation, preservation of Hermiticity, and complete positivity.

Linearity is manifest. Hermiticity is preserved because every term on the right-hand side is separately Hermitian whenever $\hat{\rho}_S$ is: $[\hat{H}_S, \hat{\rho}_S]$ is anti-Hermitian, so that $-\mathrm{i}[\hat{H}_S, \hat{\rho}_S]/\hbar$ is Hermitian, while $\hat{L}_k\hat{\rho}_S\hat{L}_k^\dagger$ and $\{\hat{L}_k^\dagger\hat{L}_k, \hat{\rho}_S\}$ are manifestly so. Trace preservation follows exactly as in the single-channel case, using the cyclic property of the trace separately for each k,

$$\mathrm{Tr}\left(\hat{L}_k\hat{\rho}_S\hat{L}_k^\dagger\right) = \mathrm{Tr}\left(\hat{L}_k^\dagger\hat{L}_k\hat{\rho}_S\right) = \mathrm{Tr}\left[\frac{1}{2}\left\{\hat{L}_k^\dagger\hat{L}_k, \hat{\rho}_S\right\}\right], \tag{1.340}$$

so that the two contributions cancel in $\partial_t \,\mathrm{Tr}\,\hat{\rho}_S$.

Complete positivity is the one property that is not obvious by inspection, and it is precisely where the Markov approximation enters. As for the two-level example, consider the evolution over an infinitesimal step $\mathrm{d}t$, and introduce the non-Hermitian effective Hamiltonian

$$\hat{H}_{\mathrm{eff}} = \hat{H}_S - \frac{\mathrm{i}\hbar}{2}\sum_k \hat{L}_k^\dagger\hat{L}_k. \tag{1.341}$$

Defining $\hat{M}_0 = \mathbb{1} - \frac{\mathrm{i}}{\hbar}\hat{H}_{\mathrm{eff}}\,\mathrm{d}t$ and $\hat{M}_k = \sqrt{\mathrm{d}t}\,\hat{L}_k$, a short calculation gives, to first order in $\mathrm{d}t$,

$$\hat{M}_0^\dagger\hat{M}_0 + \sum_k \hat{M}_k^\dagger\hat{M}_k = \mathbb{1} - \mathrm{d}t\sum_k \hat{L}_k^\dagger\hat{L}_k + \mathrm{d}t\sum_k \hat{L}_k^\dagger\hat{L}_k + O(\mathrm{d}t^2) = \mathbb{1} + O(\mathrm{d}t^2), \tag{1.342}$$

and

$$\hat{M}_0\hat{\rho}_S\hat{M}_0^\dagger + \sum_k \hat{M}_k\hat{\rho}_S\hat{M}_k^\dagger = \hat{\rho}_S + \mathrm{d}t\left[-\frac{\mathrm{i}}{\hbar}[\hat{H}_S,\hat{\rho}_S] + \sum_k\left(\hat{L}_k\hat{\rho}_S\hat{L}_k^\dagger - \frac{1}{2}\left\{\hat{L}_k^\dagger\hat{L}_k,\hat{\rho}_S\right\}\right)\right], \tag{1.343}$$

which is exactly $\hat{\rho}_S(t+\mathrm{d}t)$ as generated by (1.339). In other words, to the order required, the evolution over $\mathrm{d}t$ is a genuine Kraus map $\hat{\rho}_S \mapsto \sum_i \hat{M}_i\hat{\rho}_S\hat{M}_i^\dagger$ with $\sum_i \hat{M}_i^\dagger\hat{M}_i = \mathbb{1}$. Any map of this form is automatically completely positive and trace preserving, for any choice and any number of the operators $\hat{M}_i$, whether or not $\mathcal{S}$ is entangled with another system.

We have thus verified that (1.339) satisfies every mathematical requirement placed on the generator of a Markovian open-system evolution, generalizing to an arbitrary number of jump operators the single-channel result (1.337) obtained explicitly above. What remains open is the converse question: is (1.339) the *most general* generator with these properties? This is the content of the Gorini–Kossakowski–Sudarshan–Lindblad theorem; a sketch of its microscopic derivation, spelling out the weak-coupling, Born–Markov and secular approximations only sketched here, is given in the next, optional, section.

1.4.4 (∗) Derivation of the Lindblad equation

This section is optional reading. It provides a justification of the Lindblad equation following the standard weak-coupling, Born–Markov and secular approximations.

The quantum master equation. We consider a quantum system $\mathcal{S}$ coupled to a reservoir $\mathcal{E}$, with total Hamiltonian

$$\hat{H} = \hat{H}_S + \hat{H}_E + \hat{V}. \tag{1.344}$$

The first two terms describe the independent dynamics of the system and reservoir, while $\hat{V}$ describes their coupling.

For an isolated system, the density matrix obeys the Liouville–von Neumann equation

$$\mathrm{i}\hbar\,\partial_t\hat{\rho}_S = [\hat{H}_S,\hat{\rho}_S], \tag{1.345}$$

and therefore evolves unitarily according to

$$\hat{\rho}_S(t) = \hat{U}_S(t)\hat{\rho}_S(0)\hat{U}_S^\dagger(t). \tag{1.346}$$

In particular, the eigenvalues of $\hat{\rho}_S$ are conserved: an isolated quantum system cannot become mixed through its own unitary evolution.

The situation changes when $\mathcal{S}$ is coupled to an environment. Although the total system $\mathcal{S}+\mathcal{E}$ still evolves unitarily, the reduced density matrix

$$\hat{\rho}_S = \mathrm{Tr}_E\,\hat{\rho} \tag{1.347}$$

can evolve non-unitarily.

We derive an approximate equation for this reduced dynamics by moving to the interaction picture with respect to

$$\hat{H}_0 = \hat{H}_S + \hat{H}_E. \tag{1.348}$$

The interaction-picture density matrix obeys

$$\mathrm{i}\hbar\,\partial_t\tilde{\rho}(t) = [\tilde{V}(t), \tilde{\rho}(t)]. \tag{1.349}$$

Integrating once gives

$$\tilde{\rho}(t) = \tilde{\rho}(0) + \frac{1}{\mathrm{i}\hbar}\int_0^t [\tilde{V}(\tau), \tilde{\rho}(\tau)]\,\mathrm{d}\tau. \tag{1.350}$$

Substitution into the equation of motion and tracing over the reservoir gives the exact second-order identity

$$\begin{aligned}\partial_t\tilde{\rho}_S(t) = {} & \frac{1}{\mathrm{i}\hbar}\,\mathrm{Tr}_E[\tilde{V}(t), \tilde{\rho}(0)] \\ & - \frac{1}{\hbar^2}\int_0^t \mathrm{Tr}_E\left[\tilde{V}(t), [\tilde{V}(\tau), \tilde{\rho}(\tau)]\right]\,\mathrm{d}\tau.\end{aligned} \tag{1.351}$$

We now introduce the approximations that allow this exact equation to be converted into a local equation for the reduced density matrix.

Initial state and vanishing first-order contribution. We assume that initially the system and reservoir are uncorrelated,

$$\tilde{\rho}(0) = \tilde{\rho}_S(0) \otimes \hat{\rho}_E, \tag{1.352}$$

where $\hat{\rho}_E$ is stationary with respect to $\hat{H}_E$. We also choose the interaction such that

$$\mathrm{Tr}_E(\tilde{V}(t)\hat{\rho}_E) = 0. \tag{1.353}$$

A non-zero average of $\hat{V}$ could in any case be absorbed into a redefinition of $\hat{H}_S$. Equation (1.351) then reduces to

$$\partial_t\tilde{\rho}_S(t) = -\frac{1}{\hbar^2}\int_0^t \mathrm{Tr}_E\left[\tilde{V}(t), [\tilde{V}(\tau), \tilde{\rho}(\tau)]\right]\,\mathrm{d}\tau. \tag{1.354}$$

Born approximation. We assume that the reservoir is sufficiently large that its state is not significantly modified by the interaction. Moreover, correlations generated between system and reservoir are assumed to remain small. We therefore approximate

$$\tilde{\rho}(t) \simeq \tilde{\rho}_S(t) \otimes \hat{\rho}_E. \tag{1.355}$$

This gives

$$\partial_t\tilde{\rho}_S(t) = -\frac{1}{\hbar^2}\int_0^t \mathrm{Tr}_E\left[\tilde{V}(t), [\tilde{V}(\tau), \tilde{\rho}_S(\tau) \otimes \hat{\rho}_E]\right]\,\mathrm{d}\tau. \tag{1.356}$$

Markov approximation. The remaining equation contains memory: the derivative of $\tilde{\rho}_S$ at time t depends on its values at earlier times. To eliminate this memory, we assume that the reservoir correlation function decays on a timescale τ_E much shorter than the characteristic evolution time τ_S of the system,

$$\tau_E \ll \tau_S. \tag{1.357}$$

During the short interval over which the reservoir retains memory, the reduced density matrix therefore changes only negligibly, so that

$$\tilde{\rho}_S(t-\tau) \simeq \tilde{\rho}_S(t). \tag{1.358}$$

Furthermore, because the reservoir correlation has essentially vanished for $\tau \gg \tau_E$, the upper limit of the integral can be extended to infinity.

To make this explicit, consider for simplicity an interaction of the form

$$\hat{V} = \hat{S} \otimes \hat{R}. \tag{1.359}$$

The more general case is obtained by writing the interaction as a sum of such terms. Introducing the reservoir correlation function

$$g(\tau) = \mathrm{Tr}_E \left[\tilde{R}(\tau)\tilde{R}(0)\hat{\rho}_E \right], \tag{1.360}$$

one obtains a time-local master equation of the form

$$\begin{aligned} \partial_t \tilde{\rho}_S = -\frac{1}{\hbar^2} \int_0^\infty \Big[& g(\tau)\tilde{S}(t)\tilde{S}(t-\tau)\tilde{\rho}_S + g(-\tau)\tilde{\rho}_S\tilde{S}(t-\tau)\tilde{S}(t) \\ & - g(\tau)\tilde{S}(t-\tau)\tilde{\rho}_S\tilde{S}(t) - g(-\tau)\tilde{S}(t)\tilde{\rho}_S\tilde{S}(t-\tau) \Big] \, \mathrm{d}\tau. \end{aligned} \tag{1.361}$$

The Markov approximation is therefore the step that converts the exact non-local evolution into a differential equation involving only the density matrix at the current time. It is the density-matrix analogue of the short-memory or broad-continuum approximation that led to exponential decay in the resolvent treatment.

Secular approximation. The Markov approximation removes the memory of the reservoir, but the resulting master equation (1.361) does not yet have the mathematical structure required to guarantee that the reduced density matrix remains a physical density operator at all times. In particular, it is not manifest that the evolution preserves the positivity of $\hat{\rho}_S$. A further approximation is therefore required to separate the different characteristic frequencies of the system.

To see how this arises, let us expand the interaction-picture system operator in the eigenbasis of $\hat{H}_S$,

$$\tilde{S}(t) = \sum_{n,n'} S_{nn'} \mathrm{e}^{\mathrm{i}\omega_{nn'}t} |\psi_{n'}\rangle\langle\psi_n|, \tag{1.362}$$

where

$$\omega_{nn'} = \frac{E^S_{n'} - E^S_n}{\hbar}. \tag{1.363}$$

The terms appearing in the master equation then contain oscillating factors involving differences of these transition frequencies. For example, products of two components of $\tilde{S}$ contain terms proportional to

$$\mathrm{e}^{\mathrm{i}(\omega_{n_1 n'_1} - \omega_{n_2 n'_2})t}. \tag{1.364}$$

When the corresponding frequencies are different, these terms oscillate rapidly compared with the slow dissipative evolution generated by the weak coupling. Their contribution therefore averages to zero on the timescale over which the reduced density matrix evolves.

The *secular approximation* consists in retaining only the terms for which

$$\omega_{n_1 n_1'} = \omega_{n_2 n_2'}. \tag{1.365}$$

For a non-degenerate spectrum, this condition reduces to

$$n_1 = n_2, \qquad n_1' = n_2'. \tag{1.366}$$

The different transition frequencies then evolve independently. This approximation is justified when the frequency differences between distinct transitions are large compared with the dissipative rates, so that the corresponding oscillations are effectively averaged out.

The importance of this step is that the resulting equation can be reorganized into a sum of independent contributions, each associated with a particular transition frequency. The coefficients multiplying these contributions are Fourier transforms of the reservoir correlation function. As we shall see, these coefficients are positive, which allows the resulting evolution to be written in the completely positive Lindblad form.

Decomposition into transition operators. It is useful to reorganize the system operator according to the different transition frequencies of the subsystem. We define

$$\hat{\mathfrak{S}}(\omega) = \sum_{\substack{n,n' \\ \omega_{nn'}=\omega}} S_{nn'} |\psi_{n'}\rangle\langle\psi_n|, \tag{1.367}$$

so that

$$\tilde{S}(t) = \sum_{\omega} \mathrm{e}^{\mathrm{i}\omega t} \hat{\mathfrak{S}}(\omega). \tag{1.368}$$

For a non-degenerate spectrum, each $\hat{\mathfrak{S}}(\omega)$ corresponds to a single transition $|\psi_n\rangle \to |\psi_{n'}\rangle$. These operators satisfy

$$\hat{\mathfrak{S}}^\dagger(\omega) = \hat{\mathfrak{S}}(-\omega). \tag{1.369}$$

After inserting this decomposition into (1.361), the secular approximation eliminates terms involving different transition frequencies. The master equation can therefore be written as a sum over independent frequencies. Introducing the one-sided Fourier transform of the reservoir correlation function (a complex quantity, not a rate),

$$\Phi(\omega) = \int_0^\infty \mathrm{e}^{-\mathrm{i}\omega\tau} g(\tau)\, \mathrm{d}\tau, \tag{1.370}$$

one obtains

$$\begin{aligned} \partial_t \tilde{\rho}_S = -\frac{1}{\hbar^2} \sum_{\omega} \Big[& \Phi(\omega) \hat{\mathfrak{S}}^\dagger(\omega) \hat{\mathfrak{S}}(\omega) \tilde{\rho}_S + \Phi^*(\omega) \tilde{\rho}_S \hat{\mathfrak{S}}^\dagger(\omega) \hat{\mathfrak{S}}(\omega) \\ & - \big(\Phi(\omega) + \Phi^*(\omega)\big) \hat{\mathfrak{S}}(\omega) \tilde{\rho}_S \hat{\mathfrak{S}}^\dagger(\omega) \Big]. \end{aligned} \tag{1.371}$$

The real and imaginary parts of $\Phi(\omega)$ have distinct physical roles. We write

$$\Phi(\omega) = \mathrm{Re}\,\Phi(\omega) + \mathrm{i}\,\mathrm{Im}\,\Phi(\omega), \tag{1.372}$$

and define

$$\gamma(\omega) = \frac{2\,\mathrm{Re}\,\Phi(\omega)}{\hbar^2}, \tag{1.373}$$

together with the Lamb-shift Hamiltonian

$$\hat{H}_{\mathrm{LS}} = \sum_{\omega} \frac{\mathrm{Im}\,\Phi(\omega)}{\hbar} \hat{\mathfrak{S}}^{\dagger}(\omega)\hat{\mathfrak{S}}(\omega). \tag{1.374}$$

Equation (1.371) can then be rearranged as

$$\begin{aligned}\partial_t \tilde{\rho}_S = &\frac{1}{\mathrm{i}\hbar}[\hat{H}_{\mathrm{LS}}, \tilde{\rho}_S] \\ &+ \sum_{\omega} \gamma(\omega) \left[\hat{\mathfrak{S}}(\omega)\tilde{\rho}_S\hat{\mathfrak{S}}^{\dagger}(\omega) - \frac{1}{2}\left\{\hat{\mathfrak{S}}^{\dagger}(\omega)\hat{\mathfrak{S}}(\omega), \tilde{\rho}_S\right\}\right].\end{aligned} \tag{1.375}$$

Identification of the Lindblad equation. We have thus obtained an equation of the form

$$\partial_t \tilde{\rho}_S = \frac{1}{\mathrm{i}\hbar}[\hat{H}_{\mathrm{LS}}, \tilde{\rho}_S] + \sum_{\omega} \left[\hat{L}_{\omega}\tilde{\rho}_S\hat{L}_{\omega}^{\dagger} - \frac{1}{2}\left\{\hat{L}_{\omega}^{\dagger}\hat{L}_{\omega}, \tilde{\rho}_S\right\}\right], \tag{1.376}$$

where

$$\hat{L}_{\omega} = \sqrt{\gamma(\omega)}\hat{\mathfrak{S}}(\omega). \tag{1.377}$$

This is precisely the Lindblad form of a Markovian quantum master equation.

An important check is that the rates $\gamma(\omega)$ are positive. This follows from the fact that they are Fourier transforms of the reservoir correlation function

$$g(\tau) = \sum_{m,m'=1}^{\dim(\mathcal{H}_E)} \Pi_m |R_{mm'}|^2 \mathrm{e}^{-\mathrm{i}\omega^E_{mm'}\tau}, \tag{1.378}$$

which clearly only has positive Fourier components. The positivity of the rates is crucial for the complete positivity of the resulting evolution.

Returning to the Schrödinger picture simply adds the free Hamiltonian $\hat{H}_S$ to the coherent part of the evolution, giving the final form of the Lindblad equation

$$\partial_t \hat{\rho}_S = \frac{1}{\mathrm{i}\hbar}[\hat{H}_S + \hat{H}_{\mathrm{LS}}, \hat{\rho}_S] + \sum_{\omega} \left[\hat{L}_{\omega}\hat{\rho}_S\hat{L}_{\omega}^{\dagger} - \frac{1}{2}\left\{\hat{L}_{\omega}^{\dagger}\hat{L}_{\omega}, \hat{\rho}_S\right\}\right]. \tag{1.379}$$

The structure of this equation is important. The first term describes the unitary evolution generated by the system Hamiltonian, including the Lamb shift induced by the reservoir. The remaining terms describe irreversible processes associated with the different transition frequencies of the system. The operators $\hat{L}_{\omega}$ are therefore naturally interpreted as *jump operators*: they map one system state onto another while transferring information and energy to the reservoir.

It is worth emphasizing, however, that the Lindblad equation is not an exact consequence of the Hamiltonian dynamics. Its validity relies on the hierarchy of timescales underlying the approximations made above: the reservoir must lose its correlations rapidly compared with the evolution of the subsystem, the coupling must be sufficiently weak for the Born approximation to remain valid, and distinct system transition frequencies must be sufficiently well separated for the secular approximation to apply. When these conditions fail, memory effects or non-secular couplings can become important and the reduced dynamics need not be described by a time-independent Lindblad generator.

Non-Hermitian effective Hamiltonian and jump operators The Lindblad equation (1.379) can be rewritten in terms of a non-Hermitian effective Hamiltonian. We define

$$\hat{H}_{\text{eff}} = \hat{H}_S + \hat{H}_{\text{LS}} - \frac{\mathrm{i}\hbar}{2}\sum_{\omega} \hat{L}_\omega^\dagger \hat{L}_\omega. \tag{1.380}$$

The master equation then takes the form

$$\partial_t \hat{\rho}_S = \frac{1}{\mathrm{i}\hbar}\left(\hat{H}_{\text{eff}}\hat{\rho}_S - \hat{\rho}_S \hat{H}_{\text{eff}}^\dagger\right) + \sum_{\omega} \hat{L}_\omega \hat{\rho}_S \hat{L}_\omega^\dagger. \tag{1.381}$$

The last term in (1.380) is purely anti-Hermitian and is responsible for the loss of probability associated with irreversible transitions into the reservoir.

Let us first consider the jump contribution in (1.381). For a transition frequency $\omega_{nn'}$, the corresponding jump operator is

$$\hat{L}_{nn'} = \sqrt{\gamma(\omega_{nn'})}\langle\psi_{n'}|\hat{S}|\psi_n\rangle|\psi_{n'}\rangle\langle\psi_n|, \tag{1.382}$$

where, for simplicity, we have assumed non-degenerate transition frequencies. Its contribution to the density matrix is

$$\hat{L}_{nn'}\hat{\rho}_S\hat{L}_{nn'}^\dagger = \gamma(\omega_{nn'})\left|\langle\psi_{n'}|\hat{S}|\psi_n\rangle\right|^2\langle\psi_n|\hat{\rho}_S|\psi_n\rangle|\psi_{n'}\rangle\langle\psi_{n'}|. \tag{1.383}$$

This expression makes the physical interpretation particularly transparent. The process removes population from $|\psi_n\rangle$ and transfers it to $|\psi_{n'}\rangle$. Its rate is proportional to the population initially present in $|\psi_n\rangle$, to the square of the corresponding matrix element of the coupling operator, and to the reservoir spectral density $\gamma(\omega_{nn'})$. The resulting state is the projector onto $|\psi_{n'}\rangle$. Such a process is called a *quantum jump* from $|\psi_n\rangle$ to $|\psi_{n'}\rangle$.

The anti-Hermitian part of $\hat{H}_{\text{eff}}$ provides the complementary description of the same process. Indeed,

$$-\frac{\mathrm{i}\hbar}{2}\hat{L}_{nn'}^\dagger\hat{L}_{nn'} = -\frac{\mathrm{i}\hbar}{2}\gamma(\omega_{nn'})\left|\langle\psi_{n'}|\hat{S}|\psi_n\rangle\right|^2|\psi_n\rangle\langle\psi_n|. \tag{1.384}$$

It therefore produces a decay of the amplitude associated with $|\psi_n\rangle$, corresponding to the probability that a jump towards $|\psi_{n'}\rangle$ will occur. The non-Hermitian evolution thus describes the dynamics conditioned on the absence of a detected jump, while the terms $\hat{L}_\omega\hat{\rho}_S\hat{L}_\omega^\dagger$ restore the probability associated with the corresponding jump processes.

This interpretation also establishes a direct connection with the exponential decay obtained previously from the resolvent formalism. For example, if there is a single decay channel $|e\rangle \to |g\rangle$ with

$$\hat{L} = \sqrt{\Gamma}|g\rangle\langle e|, \tag{1.385}$$

the effective Hamiltonian contains

$$\hat{H}_{\text{eff}} = \hat{H}_S + \hat{H}_{\text{LS}} - \frac{\mathrm{i}\hbar\Gamma}{2}|e\rangle\langle e|. \tag{1.386}$$

The excited-state amplitude therefore evolves as

$$\langle e|\psi(t)\rangle \propto \mathrm{e}^{-\mathrm{i}(E_e+\Delta E_{\text{LS}})t/\hbar}\mathrm{e}^{-\Gamma t/2}, \tag{1.387}$$

and its population decays as $\mathrm{e}^{-\Gamma t}$, in agreement with the pole of the analytically continued resolvent.

Connection with the resolvent effective Hamiltonian. The relation with the effective Hamiltonian introduced earlier can be made more explicit. Using

$$\Phi(\omega) = \int_0^\infty \mathrm{e}^{-\mathrm{i}\omega\tau} g(\tau)\,\mathrm{d}\tau, \tag{1.388}$$

the coherent and dissipative contributions can be combined into

$$\hat{H}_{\mathrm{eff}} = \hat{H}_S + \frac{1}{\mathrm{i}\hbar}\sum_{\omega} \Phi(\omega)\hat{\mathfrak{S}}^\dagger(\omega)\hat{\mathfrak{S}}(\omega). \tag{1.389}$$

This expression has the same structure as the second-order effective Hamiltonian obtained from the resolvent formalism. To make the connection explicit, consider a system eigenstate $|\psi_n\rangle$ and a stationary reservoir described by

$$\hat{\rho}_E = \sum_m \Pi_m |\chi_m\rangle\langle\chi_m|. \tag{1.390}$$

For a factorized interaction

$$\hat{V} = \hat{S} \otimes \hat{R}, \tag{1.391}$$

the diagonal matrix element of (1.389) can be written as

$$\begin{aligned}\langle\psi_n|\hat{H}_{\mathrm{eff}}|\psi_n\rangle = E_n^S + \frac{1}{\mathrm{i}\hbar}\sum_m \Pi_m \langle\psi_n,\chi_m|\hat{V} \\ \times \int_0^\infty \mathrm{e}^{\mathrm{i}(E_n^S+E_m^E-\hat{H}_S-\hat{H}_E)\tau/\hbar}\,\mathrm{d}\tau\,\hat{V}|\psi_n,\chi_m\rangle.\end{aligned} \tag{1.392}$$

Using the standard integral representation of the resolvent,

$$\frac{1}{\mathrm{i}\hbar}\int_0^\infty \mathrm{e}^{\mathrm{i}(E-\hat{H})\tau/\hbar}\mathrm{e}^{-\eta\tau/\hbar}\,\mathrm{d}\tau = \frac{1}{E+\mathrm{i}\eta-\hat{H}}, \tag{1.393}$$

with $\eta > 0$ the same infinitesimal convergence factor as above, this becomes

$$\langle\psi_n|\hat{H}_{\mathrm{eff}}|\psi_n\rangle = E_n^S + \sum_m \Pi_m \langle\psi_n,\chi_m|\hat{V}\frac{1}{E_n^S+E_m^E+\mathrm{i}\eta-\hat{H}_S-\hat{H}_E}\hat{V}|\psi_n,\chi_m\rangle. \tag{1.394}$$

The second term in (1.394) is precisely the second-order effective Hamiltonian obtained previously from the $\hat{P}\hat{G}(z)\hat{P}$ construction, with the projector $\hat{P}$ now selecting the state $|\psi_n,\chi_m\rangle$. The effective Hamiltonian governing the reduced subsystem can therefore be interpreted as the reservoir average of the energy-dependent effective Hamiltonians obtained in the resolvent approach:

$$\hat{H}_{\mathrm{eff}} \simeq \sum_m \Pi_m \hat{H}_{\mathrm{eff}}^{(m)}. \tag{1.395}$$

The real part of this effective Hamiltonian produces the energy renormalization, or Lamb shift, while its imaginary part gives the decay rates. The Lindblad description thus provides the density-matrix counterpart of the non-Hermitian resolvent description.

1.4.5 Alternative description: quantum trajectories

The notion of quantum jump introduced above also provides an alternative description of the evolution of an open quantum system, in terms of *quantum trajectories*. Instead of solving directly for the reduced density matrix, one represents the dynamics by an ensemble of pure states, each evolving under a non-Hermitian effective Hamiltonian and undergoing random quantum jumps. The density matrix is then recovered by averaging over a large number of such trajectories.

We take as our starting point the Lindblad equation in the general form obtained in Section 1.4.3,

$$\partial_t \hat{\rho}_S = -\frac{\mathrm{i}}{\hbar}\left[\hat{H}_S, \hat{\rho}_S\right] + \sum_k \left(\hat{L}_k \hat{\rho}_S \hat{L}_k^\dagger - \frac{1}{2}\left\{\hat{L}_k^\dagger \hat{L}_k, \hat{\rho}_S\right\}\right), \tag{1.396}$$

with one jump operator $\hat{L}_k$ per dissipation channel. Introducing the non-Hermitian effective Hamiltonian

$$\hat{H}_{\text{eff}} = \hat{H}_S - \frac{\mathrm{i}\hbar}{2}\sum_k \hat{L}_k^\dagger \hat{L}_k, \tag{1.397}$$

the anticommutator can be absorbed into the commutator term, and (1.396) takes the strictly equivalent form

$$\partial_t \hat{\rho}_S = \frac{1}{\mathrm{i}\hbar}\left(\hat{H}_{\text{eff}}\hat{\rho}_S - \hat{\rho}_S \hat{H}_{\text{eff}}^\dagger\right) + \sum_k \hat{L}_k \hat{\rho}_S \hat{L}_k^\dagger. \tag{1.398}$$

This splitting is the starting point of the trajectory description: the first term generates a deterministic evolution that does not conserve the norm, while the second restores the probability that the first one loses.

The two branches over an infinitesimal step. The rules governing a trajectory follow directly from the Kraus form established in Section 1.4.3. Over an infinitesimal step $\mathrm{d}t$, the evolution is generated by the operators

$$\hat{M}_0 = \mathbb{1} - \frac{\mathrm{i}}{\hbar}\hat{H}_{\text{eff}}\,\mathrm{d}t, \qquad \hat{M}_k = \sqrt{\mathrm{d}t}\,\hat{L}_k, \tag{1.399}$$

which satisfy $\hat{M}_0^\dagger \hat{M}_0 + \sum_k \hat{M}_k^\dagger \hat{M}_k = \mathbb{1}$ to first order in $\mathrm{d}t$. Read as a statement about probabilities, this completeness relation invites us to interpret each $\hat{M}_i$ as one possible outcome of a measurement performed on the environment: either nothing is detected, and the state is acted upon by $\hat{M}_0$, or a quantum of type k is detected, and the state is acted upon by $\hat{M}_k$. Averaging over unread outcomes reproduces the Lindblad equation; following one particular sequence of outcomes defines a *quantum trajectory*.

Starting from a normalized state $|\psi(t)\rangle$, the probability that the jump k occurs during $\mathrm{d}t$ is

$$\mathrm{d}p_k(t) = \left\|\hat{M}_k|\psi(t)\rangle\right\|^2 = \mathrm{d}t\,\langle\psi(t)|\hat{L}_k^\dagger \hat{L}_k|\psi(t)\rangle, \tag{1.400}$$

of first order in $\mathrm{d}t$ precisely because of the $\sqrt{\mathrm{d}t}$ scaling of $\hat{M}_k$. With the complementary probability $1 - \sum_k \mathrm{d}p_k$, no jump occurs and the state evolves under $\hat{M}_0$, that is, according to the non-unitary Schrödinger equation

$$\mathrm{i}\hbar\,\partial_t|\psi(t)\rangle = \hat{H}_{\text{eff}}|\psi(t)\rangle. \tag{1.401}$$

Because $\hat{H}_{\text{eff}}$ is non-Hermitian, the norm of the state is not preserved. This loss of norm has a direct probabilistic interpretation: it is the accumulated probability that a jump has occurred, so that the state has to be renormalized after each step. When a jump of type k does occur, the state is replaced by

$$|\psi\rangle \longrightarrow \frac{\hat{L}_k|\psi\rangle}{\sqrt{\langle\psi|\hat{L}_k^\dagger\hat{L}_k|\psi\rangle}}. \tag{1.402}$$

Thus the non-Hermitian evolution describes the continuous dynamics between jumps, while the operators $\hat{L}_k$ describe the discrete stochastic events induced by the coupling to the environment.

The dynamics of a single trajectory is therefore governed by the following rules:

1. the system evolves deterministically under the non-Hermitian Hamiltonian $\hat{H}_{\text{eff}}$ of (1.397) between jumps, the state being renormalized at each step;
2. a jump of type k occurs randomly with instantaneous rate $\langle\psi|\hat{L}_k^\dagger\hat{L}_k|\psi\rangle$;
3. following the jump, the state is replaced and renormalized according to

$$|\psi\rangle \to \frac{\hat{L}_k|\psi\rangle}{\sqrt{\langle\psi|\hat{L}_k^\dagger\hat{L}_k|\psi\rangle}}. \tag{1.403}$$

Although each trajectory describes a pure state, an individual trajectory does not represent the full reduced state of the open system. Rather, the density matrix is obtained by averaging over the ensemble of possible trajectories,

$$\hat{\rho}_S(t) = \mathbb{E}_{\text{traj}}\left[|\psi(t)\rangle\langle\psi(t)|\right]. \tag{1.404}$$

The ensemble average of any observable can consequently be evaluated as

$$\langle\hat{O}_S\rangle = \mathbb{E}_{\text{traj}}\left[\langle\psi(t)|\hat{O}_S|\psi(t)\rangle\right]. \tag{1.405}$$

One can show that this stochastic evolution is exactly equivalent, upon ensemble averaging, to the evolution generated by the Lindblad master equation (1.396) [18, 19]. Quantum trajectories thus provide an intuitive interpretation of the different terms of the Lindblad equation: the non-Hermitian effective Hamiltonian describes the evolution conditioned on the absence of an environmental detection event, while the jump operators describe the possible detection events themselves.

Readers who have gone through the optional Section 1.4.4 may identify the channel index k with the transition frequencies ω of the subsystem, the jump operators with the $\hat{L}_\omega$ obtained there, and the Hamiltonian $\hat{H}_S$ of (1.396) with $\hat{H}_S + \hat{H}_{\text{LS}}$, i.e. the bare system Hamiltonian corrected by the Lamb shift induced by the reservoir. Nothing in the present section depends on that identification.

This interpretation also provides a useful connection with the resolvent approach developed earlier. The same non-Hermitian effective Hamiltonian that emerges from the analytic continuation of the resolvent now governs the conditional evolution between quantum jumps, while the jump terms restore the probability lost through its non-Hermitian part. The interested reader can find further details on the foundations and applications of quantum trajectories and non-Hermitian quantum mechanics in Refs. [18, 19, 20].

1.4.6 Example of a decaying electromagnetic field in an optical cavity

We now consider a slightly more complex example than the two-level system discussed above: a single electromagnetic mode in an optical cavity, where the subsystem is the cavity mode, which can contain an arbitrary number of photons, and is therefore of infinite dimension. The reservoir is the continuum of electromagnetic modes outside the cavity, which can absorb photons that escape through the imperfect mirrors.

In an idealized lossless cavity, the Hamiltonian of a single mode is

$$\hat{H}_S = \hbar\omega\, \hat{a}^\dagger \hat{a}, \tag{1.406}$$

where ω is the resonance frequency and $\hat{a}$ and $\hat{a}^\dagger$ are the annihilation and creation operators of the cavity mode.

In a real cavity, the coupling to the electromagnetic modes outside the cavity makes the cavity mode an open quantum system. A single dissipation channel is at play, so that the sum over k in (1.396) reduces to a single term. The corresponding quantum jump removes one photon from the cavity, which fixes the jump operator to be proportional to $\hat{a}$,

$$\hat{L} = \sqrt{\kappa}\, \hat{a}, \tag{1.407}$$

the constant κ being determined below by the rate at which the mean photon number decays. The Lindblad equation for the reduced density matrix of the cavity mode is consequently

$$\partial_t \hat{\rho}_S = \frac{1}{\mathrm{i}\hbar}[\hat{H}_S, \hat{\rho}_S] + \kappa \left(\hat{a}\hat{\rho}_S \hat{a}^\dagger - \frac{1}{2} \left\{ \hat{a}^\dagger \hat{a}, \hat{\rho}_S \right\} \right). \tag{1.408}$$

It should be stressed that this describes a reservoir in its vacuum state: the only elementary process retained is the loss of a photon. At finite temperature a second channel opens, described by $\hat{L}' = \sqrt{\kappa\, \bar{n}_{\mathrm{th}}}\, \hat{a}^\dagger$, in which a thermal photon is absorbed from the environment, and the steady state is then a thermal state rather than the vacuum. For an optical cavity, $\bar{n}_{\mathrm{th}}$ is entirely negligible at room temperature and the description above is excellent; for a microwave resonator it is not, unless the device is cooled well below $\hbar\omega/k_{\mathrm{B}}$.

The exponential decay of the mean photon number follows directly from this equation. Introducing the photon-number operator $\hat{n} = \hat{a}^\dagger \hat{a}$, one finds the exact evolution

$$\langle \hat{n} \rangle(t) = \mathrm{Tr}[\hat{n}\hat{\rho}_S(t)] = \langle \hat{n} \rangle(0) \mathrm{e}^{-\kappa t}, \tag{1.409}$$

which identifies κ as the photon loss rate. It coincides with the cavity linewidth introduced in the discussion of the Purcell effect.

It is instructive to consider more specifically an initial Fock state $|n_0\rangle$. Since the Hamiltonian does not couple different photon-number states and the jump operator simply removes one photon,

$$\hat{a}|n\rangle = \sqrt{n}|n-1\rangle, \tag{1.410}$$

the density matrix remains diagonal in the Fock basis. Writing

$$\hat{\rho}_S(t) = \sum_{n=0}^{n_0} \Pi_n(t) |n\rangle\langle n|, \tag{1.411}$$

the populations are given by the binomial distribution

$$\Pi_n(t) = \binom{n_0}{n} \mathrm{e}^{-n\kappa t} \left(1 - \mathrm{e}^{-\kappa t}\right)^{n_0 - n}, \qquad n \leq n_0. \tag{1.412}$$

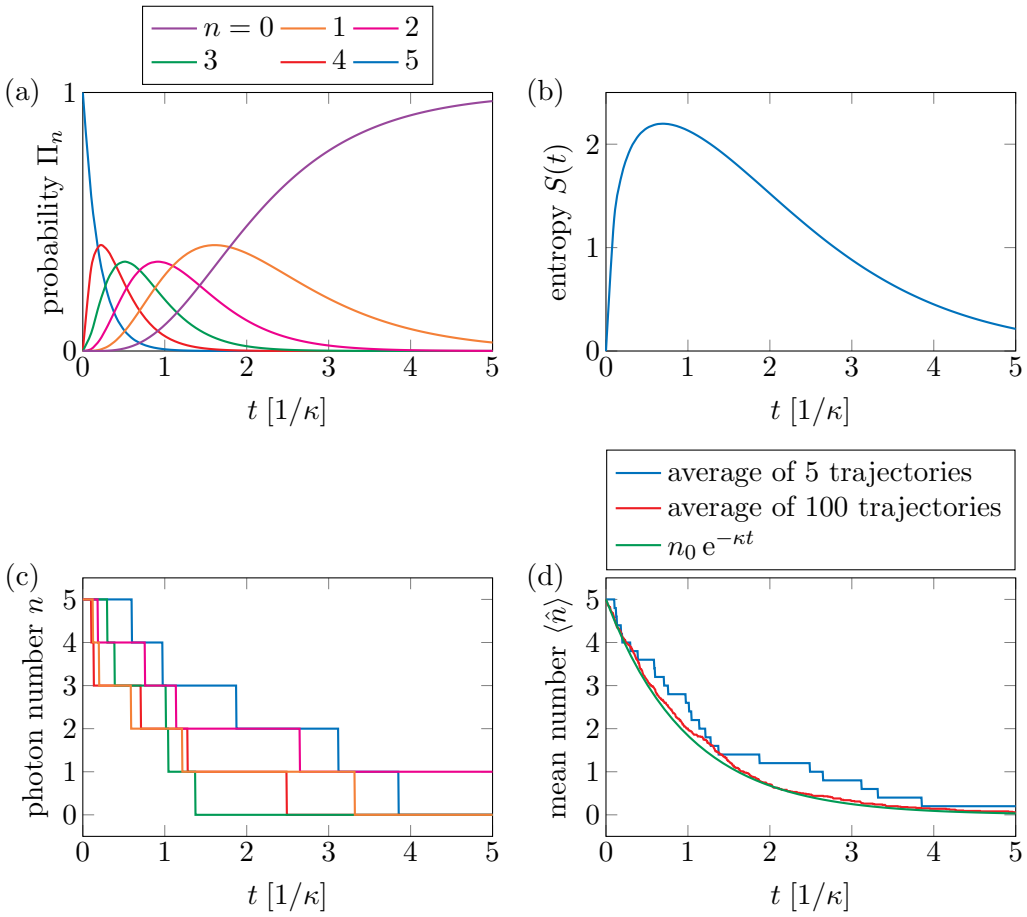


Figure 12: (a) Time evolution of the probabilities Π_n to measure a photon number n in a lossy cavity, starting in the Fock state $|n_0 = 5\rangle$. (b) Evolution of the von Neumann entropy, which quantifies the degree of mixing resulting from the photon loss towards the environment. (c) 5 examples of quantum trajectories, where the system remains in a pure Fock state at all times and undergoes quantum jumps at random times. (d) Mean photon number obtained by averaging quantum trajectories.

For example, the evolution for an initial state $|n_0 = 5\rangle$ is shown in Fig. 12a.

At long times, $t \gg 1/\kappa$, all photons eventually escape and the cavity approaches the vacuum state,

$$\hat{\rho}_S(t) \longrightarrow |0\rangle\langle 0|. \tag{1.413}$$

At intermediate times, however, several photon-number states are populated incoherently. The reduced state of the cavity is therefore mixed, even though the initial state was pure. This is reflected in the von Neumann entropy, shown in Fig. 12b. The entropy initially increases as information about the intracavity field is transferred to the environment, before eventually returning to zero when the cavity reaches the pure vacuum state.

The same dynamics admits a particularly intuitive description in terms of quantum trajectories. A single trajectory remains in a pure Fock state and undergoes stochastic jumps

$$|n\rangle \longrightarrow |n-1\rangle \tag{1.414}$$

at the rate

$$\langle n|\hat{L}^\dagger \hat{L}|n\rangle = \kappa n. \tag{1.415}$$

Thus, the larger the number of photons in the cavity, the more likely a photon-loss event is to occur. Between jumps, the state evolves under the non-Hermitian effective Hamiltonian (1.397), which here reads

$$\hat{H}_{\text{eff}} = \hbar\omega\,\hat{n} - \frac{\mathrm{i}\hbar\kappa}{2}\hat{n} = \hbar\left(\omega - \frac{\mathrm{i}\kappa}{2}\right)\hat{n}. \tag{1.416}$$

Being diagonal in the Fock basis, it only multiplies $|n\rangle$ by a number: the no-jump evolution reduces the norm, by the factor $\mathrm{e}^{-n\kappa t/2}$, without altering the state once it is renormalized. This is why a trajectory started in a Fock state remains in a Fock state at all times, and why the decrease of the norm reproduces the exponential waiting-time distribution of rate κn. Five example trajectories computed numerically by randomly drawing the jump events are shown in Fig. 12c.

Each trajectory remains a pure state and therefore does not by itself reproduce the mixed density matrix obtained from the Lindblad equation. Rather, the latter is recovered by averaging over many independent trajectories. In particular, averaging the photon number over an ensemble of trajectories gives

$$\langle\hat{n}\rangle(t) = \mathbb{E}_{\text{traj}}[n(t)], \tag{1.417}$$

which converges to the exponential decay of (1.409) as the number of trajectories is increased. An illustration is given in Fig. 12d. This simple example makes explicit the equivalence between the density-matrix description of open-system dynamics and the stochastic description in terms of quantum trajectories.

Coherent states are immune to decoherence. The Fock state is, in this respect, the least favourable initial condition: it is rapidly turned into a statistical mixture. It is instructive to contrast it with a coherent state $|\alpha_0\rangle$, for which the trajectory picture gives the answer almost without calculation. Since a coherent state is an eigenstate of the annihilation operator,

$$\hat{a}|\alpha\rangle = \alpha|\alpha\rangle, \tag{1.418}$$

a quantum jump leaves it strictly *unchanged*. Indeed, the renormalized post-jump state is

$$\frac{\hat{L}|\alpha\rangle}{\big\|\hat{L}|\alpha\rangle\big\|} = \frac{\sqrt{\kappa}\,\alpha|\alpha\rangle}{\sqrt{\kappa}\,|\alpha|} = \mathrm{e}^{\mathrm{i}\arg\alpha}|\alpha\rangle, \tag{1.419}$$

that is, the same physical state. Losing a photon from a coherent state teaches us nothing about the field, because the photon number was never definite in the first place.

The no-jump evolution is almost as simple. The effective Hamiltonian is diagonal in the Fock basis, so that

$$\mathrm{e}^{-\mathrm{i}\hat{H}_{\text{eff}}t/\hbar} = \mathrm{e}^{-\lambda\hat{n}}, \qquad \lambda = \mathrm{i}\omega t + \frac{\kappa t}{2}. \tag{1.420}$$

Acting on the Fock expansion of a coherent state,

$$\begin{aligned}\mathrm{e}^{-\lambda\hat{n}}|\alpha\rangle &= \mathrm{e}^{-|\alpha|^2/2}\sum_n \frac{\alpha^n\,\mathrm{e}^{-\lambda n}}{\sqrt{n!}}|n\rangle \\ &= \mathrm{e}^{-|\alpha|^2/2}\sum_n \frac{\left(\alpha\mathrm{e}^{-\lambda}\right)^n}{\sqrt{n!}}|n\rangle \;\propto\; |\alpha\,\mathrm{e}^{-\lambda}\rangle,\end{aligned} \tag{1.421}$$

since the series is again that of a coherent state, of amplitude $\alpha e^{-\lambda}$, the prefactor differing only by a real positive number that is absorbed in the normalization. The conditional evolution therefore maps coherent states onto coherent states, and simply damps the amplitude,

$$\alpha \longrightarrow \alpha\, \mathrm{e}^{-\mathrm{i}\omega t}\, \mathrm{e}^{-\kappa t/2}. \tag{1.422}$$

Both branches of the evolution thus preserve the coherent character of the state, and neither depends on the history: whatever the number of jumps and whatever the times at which they occur, the state at time t is the *same* coherent state. Averaging over trajectories then leaves a single pure state,

$$\hat{\rho}_S(t) = |\alpha(t)\rangle\langle\alpha(t)|, \qquad \alpha(t) = \alpha_0\, \mathrm{e}^{-\mathrm{i}\omega t}\, \mathrm{e}^{-\kappa t/2}. \tag{1.423}$$

The state stays pure throughout, its von Neumann entropy remains zero, and only the amplitude is damped. One checks that the mean photon number $|\alpha(t)|^2 = |\alpha_0|^2 \mathrm{e}^{-\kappa t}$ again obeys (1.409), as it must.

It is worth insisting that this does not mean that no photon is lost. Jumps do occur, at the instantaneous rate $\kappa|\alpha(t)|^2$; they simply carry no information about the state, and therefore leave it unchanged. This is visible in the norm of the no-jump branch, which follows from the calculation above,

$$\left\| \mathrm{e}^{-\lambda\hat{n}} |\alpha_0\rangle \right\|^2 = \exp\left[-|\alpha_0|^2 \left(1 - \mathrm{e}^{-\kappa t}\right) \right]. \tag{1.424}$$

This is precisely the Poisson probability of detecting no photon at all, the mean number emitted up to time t being $|\alpha_0|^2(1 - \mathrm{e}^{-\kappa t})$, in agreement with (1.409).

Finally, (1.423) can be confirmed without any reference to trajectories. Taking the expectation value of $\hat{a}$ in the master equation (1.408) gives, for an arbitrary state,

$$\frac{\mathrm{d}\langle\hat{a}\rangle}{\mathrm{d}t} = \left(-\mathrm{i}\omega - \frac{\kappa}{2} \right) \langle\hat{a}\rangle, \tag{1.425}$$

where the dissipative contribution follows from $\hat{a}^\dagger\hat{a}\hat{a} - \frac{1}{2}\hat{a}\hat{a}^\dagger\hat{a} - \frac{1}{2}\hat{a}^\dagger\hat{a}\hat{a} = -\frac{1}{2}\hat{a}$. The field amplitude therefore decays at the rate $\kappa/2$, half the rate of the photon number, exactly as in (1.423).

Coherent states are thus singled out by the coupling to the environment as the states that are *not* degraded by it. They are the *pointer states* of the damped harmonic oscillator. A superposition of two coherent states, by contrast, decoheres towards a statistical mixture of the two, at a rate that grows with their separation in phase space – which is why the quasi-classical states of a field are precisely the coherent ones.

Observing individual trajectories: quantum jumps of light. The individual trajectories of Fig. 12c are not merely a computational device: they have been observed directly. In the experiments performed by the group of S. Haroche, a microwave photon is stored in a superconducting Fabry–Pérot cavity of extremely high quality factor, $Q \simeq 4 \times 10^{10}$ at $\omega/2\pi = 51\,\mathrm{GHz}$, corresponding to a photon lifetime $1/\kappa \simeq 0.13\,\mathrm{s}$ [21, 22]. Circular Rydberg atoms are sent one by one through the cavity and act as *meters* for the intracavity photon number.

The essential point is that the atoms are tuned far from resonance with the cavity mode. They therefore cannot absorb or emit a photon: the interaction is purely dispersive

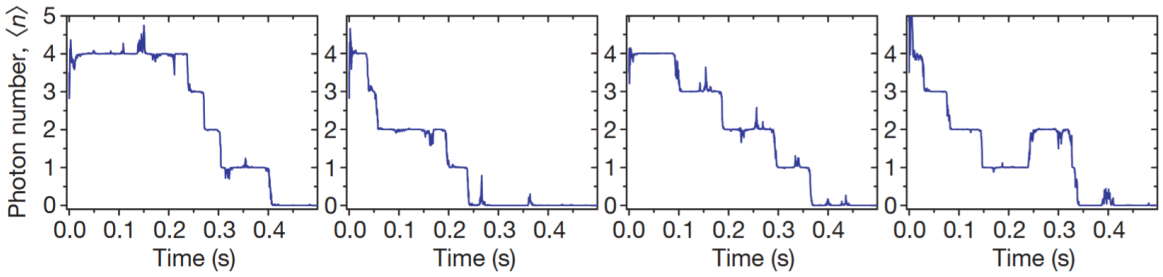


Figure 13: Individual quantum trajectories of a microwave field stored in a high-finesse superconducting cavity, monitored by quantum non-demolition measurements performed with a stream of circular Rydberg atoms. Each panel shows the photon number inferred from the running measurement record in a single realization, the cavity being initially prepared in a coherent state containing of the order of four photons. During the first few milliseconds, the repeated measurements project the field onto a Fock state of well-defined photon number, visible as the rapid initial transient. The field then decays towards the vacuum through a staircase of quantum jumps $|n\rangle \to |n-1\rangle$ occurring at random times, the plateaus becoming longer as n decreases, in agreement with the jump rate κn. In the rightmost panel, an upward step is also visible around $t \simeq 0.25\,\mathrm{s}$: it corresponds to the creation of a photon by the residual thermal field, a process described by the additional jump operator $\hat{L}' = \sqrt{\kappa\,\bar{n}_{\mathrm{th}}}\,\hat{a}^\dagger$ mentioned above. These records are the direct experimental counterpart of the simulated trajectories of Fig. 12c. Figure from [22].

and simply imprints on the atomic state a phase shift proportional to the photon number, which is read out interferometrically after the atom has left the cavity. Each atom thus measures $\hat{n}$ without changing it. This is a *quantum non-demolition* (QND) measurement.

A stream of such atoms provides a continuous record of the photon number. What is observed, reproduced in Fig. 13, is precisely the staircase of Fig. 12c: the photon number stays constant for random durations and then drops by one unit at unpredictable times, revealing the individual quantum jumps $|n\rangle \to |n-1\rangle$ associated with the loss of a photon through the mirrors. Starting from a coherent state, one sees in addition the repeated measurements progressively projecting the field onto a Fock state of well-defined photon number, which only then begins its staircase of jumps [22]. Averaging many such records reproduces the smooth exponential decay (1.409), exactly as in Fig. 12d.

These experiments, together with the trapped-ion work of D. Wineland, were recognized by the 2012 Nobel Prize in Physics [23]; a detailed account of the field can be found in [24].

It is worth emphasizing that this continuous monitoring does not perturb the decay dynamics. Three ingredients guarantee it. First, the measured observable is the photon number, which commutes with the cavity Hamiltonian, $[\hat{n}, \hat{H}_S] = 0$: this is the defining property of a QND observable, and it ensures that the measurement induces no transitions between number states. Second, the meter atoms are not the cause of the decay, which originates in the coupling to the continuum of modes outside the cavity; being far detuned, the atoms exchange no energy with the field. Third, and most tellingly in the present language, the trajectory evolves between jumps under the effective Hamiltonian $\hat{H}_{\mathrm{eff}} = \hbar(\omega - \mathrm{i}\kappa/2)\hat{n}$, which is diagonal in the Fock basis: a state of definite photon number is left unchanged by the no-jump evolution. The quantity measured by the

atoms is therefore already a constant of the conditional evolution, so that projecting onto it repeatedly changes nothing.

One might worry that frequent measurements should freeze the decay, by the quantum Zeno effect. They do not, for the reason discussed in Section 1.4.2: the quadratic, Zeno-like behaviour of the survival probability is confined to times shorter than the correlation time τ_E of the environment, which here is exceedingly short compared with the interval between successive atoms. The measurements probe the dynamics well inside the Markovian regime, where the jump probability grows linearly in time and repeated projections leave the decay rate untouched. Reading out the environment record, which is what the QND measurement does, unravels the Lindblad evolution into trajectories without modifying the ensemble average.

2 Indistinguishable particles

The description of a system containing several identical quantum particles requires an important modification of the usual tensor-product construction. It involves the symmetrization postulate, which states that the state of a system of identical particles must be either symmetric or antisymmetric under the exchange of any two particles. This postulate is a fundamental consequence of the indistinguishability of identical particles in quantum mechanics and leads to the classification of particles into bosons and fermions. The description of many-body systems of identical particles is then greatly simplified by the formalism of second quantization, which we also introduce in this chapter.

2.1 The symmetrization postulate

Let us first recall the role of particle labels in classical and quantum mechanics.

In classical mechanics, a system of N particles is fully characterized at a given time t by the position and velocity of each particle,

$$\Big(\mathbf{r}_i(t), \mathbf{v}_i(t)\Big)_{1\le i\le N},$$

or, equivalently, by a point in the $6N$-dimensional phase space. We may assign a label i to each particle and follow this label continuously as the system evolves. The labelling becomes somewhat arbitrary when two particles meet at the same position, but this ambiguity has no physical consequences: exchanging the labels of two identical classical particles does not change any observable prediction.

Quantum mechanics is more subtle. For identical particles, there is no physical observable that can distinguish one particle from another. If $|\Psi\rangle$ is a many-body state, then $|\Psi\rangle$ and $\hat{P}_\sigma|\Psi\rangle$ must therefore give identical predictions for every observable, where $\hat{P}_\sigma$ is the operator implementing the permutation σ of the particles. Its action on a product basis is defined by

$$\hat{P}_\sigma|k_1\rangle \otimes \cdots \otimes |k_N\rangle = |k_{\sigma(1)}\rangle \otimes \cdots \otimes |k_{\sigma(N)}\rangle. \tag{2.1}$$

Indistinguishability then requires that, for any observable $\hat{A}$,

$$\langle\Psi|\hat{A}|\Psi\rangle = \langle\Psi|\hat{P}_\sigma^{-1}\hat{A}\hat{P}_\sigma|\Psi\rangle. \tag{2.2}$$

Since this must hold for arbitrary states, we obtain

$$[\hat{P}_\sigma, \hat{A}] = 0. \tag{2.3}$$

In particular, the Hamiltonian must be invariant under permutations of identical particles.

At first sight, this requirement might seem sufficient to account for indistinguishability. It is not. The invariance of observables under permutations constrains the *operators*, but places no constraint whatsoever on the *state*. As we now show, this leaves the theory genuinely underdetermined: a complete specification of a physical preparation no longer suffices to predict the outcome of a measurement.

Consider two identical spin-1/2 particles occupying the same spatial orbital, one with spin up and one with spin down. Since no observable can distinguish the particles, this

sentence is the most complete physical specification of the preparation that can possibly be given. It is nevertheless compatible with any state of the two-dimensional family

$$|\Psi_{\alpha\beta}\rangle = \alpha\,|+\rangle \otimes |-\rangle + \beta\,|-\rangle \otimes |+\rangle, \qquad |\alpha|^2 + |\beta|^2 = 1. \tag{2.4}$$

Indeed, the two product states are physically equivalent to each other: for any observable $\hat{A}$ commuting with $\hat{P}_{\tau_{12}}$,

$$\langle -,+|\hat{A}|-,+\rangle = \langle +,-|\hat{P}_{\tau_{12}}^{-1}\hat{A}\hat{P}_{\tau_{12}}|+,-\rangle = \langle +,-|\hat{A}|+,-\rangle, \tag{2.5}$$

and the same identity, applied to the spectral projectors of $\hat{A}$, shows that the two states give identical probability distributions for *every* measurement. No experiment can therefore single out one of them.

The difficulty is that the states (2.4) are *not* physically equivalent to one another. Consider the total spin $\hat{\mathbf{S}} = \hat{\mathbf{s}}_1 + \hat{\mathbf{s}}_2$, which is manifestly symmetric under exchange and is therefore a legitimate observable. Within the family (2.4), the only state of total spin $S = 1$ is the symmetric combination $|T_0\rangle = (|+,-\rangle + |-,+\rangle)/\sqrt{2}$, so that a measurement of $\hat{\mathbf{S}}^2$ yields the triplet value with probability

$$P(S=1) = |\langle T_0|\Psi_{\alpha\beta}\rangle|^2 = \frac{|\alpha+\beta|^2}{2}. \tag{2.6}$$

This equals 1 for the symmetric combination $\alpha = \beta = 1/\sqrt{2}$, 0 for the antisymmetric one $\alpha = -\beta = 1/\sqrt{2}$, and $1/2$ for the product state $|+\rangle \otimes |-\rangle$ itself, which is shared equally between the singlet and the $m = 0$ triplet. One and the same complete specification of the preparation is thus compatible with a continuum of mutually incompatible predictions.

This ambiguity is known as *exchange degeneracy*. Its origin is worth stating plainly: because every observable commutes with the permutation operators, no set of commuting observables, however large, can lift the degeneracy between states related by a permutation. The state is therefore never fully determined by what can be measured. Note also that one cannot escape the difficulty by simply declaring the two product states to be "the same state". Physical equivalence between two vectors does not propagate through superposition, exactly as a global phase leaves $|a\rangle$ unchanged while making $|a\rangle + |c\rangle$ and $\mathrm{e}^{\mathrm{i}\theta}|a\rangle + |c\rangle$ two different states.

The resolution is provided by the *symmetrization postulate* [25]. As an additional postulate of quantum mechanics, it states that the state of a system of identical particles must transform according to a one-dimensional representation of the permutation group. In the present notation,

$$\hat{P}_\sigma|\Psi\rangle = c(\sigma)|\Psi\rangle, \qquad |c(\sigma)| = 1, \tag{2.7}$$

where $c(\sigma)$ is a complex phase that may depend on the permutation σ.

Restricting the state space in this way removes the exchange degeneracy. In the example above, the family (2.4) contains exactly one state satisfying the postulate for each sign of $c(\tau_{12})$: the symmetric combination, of total spin $S = 1$, and the antisymmetric one, of total spin $S = 0$. Once the sign is fixed, the specification of the preparation again determines every prediction uniquely.

It should be stressed that demanding a *one-dimensional* representation is part of the postulate, not a consequence of it. Higher-dimensional representations of the permutation

group would describe so-called parastatistics, which are excluded here by assumption rather than by any argument given below.

We now show that the permutation group admits exactly two one-dimensional representations: $c(\sigma) = 1$ for all permutations, corresponding to bosons, or $c(\sigma) = \varepsilon(\sigma)$, the signature of the permutation, corresponding to fermions.

The composition of two permutations satisfies

$$\hat{P}_{\sigma\circ\sigma'} = \hat{P}_{\sigma'}\hat{P}_{\sigma}, \tag{2.8}$$

The reversed order follows from our convention for $\hat{P}_\sigma$: if $\hat{P}_\sigma|\Psi\rangle$ carries $k_{\sigma(i)}$ in its i-th slot, then applying $\hat{P}_{\sigma'}$ leaves there $k_{\sigma(\sigma'(i))} = k_{(\sigma\circ\sigma')(i)}$. It is in any case immaterial in what follows, since the $c(\sigma)$ are numbers and commute. Consequently,

$$c(\sigma \circ \sigma') = c(\sigma)c(\sigma'). \tag{2.9}$$

Now decompose an arbitrary permutation into transpositions,

$$\sigma = \tau_{i_1 j_1} \circ \cdots \circ \tau_{i_k j_k}, \tag{2.10}$$

where τ_{ij} exchanges particles i and j while leaving all others unchanged. We then have

$$c(\sigma) = c(\tau_{i_1 j_1}) \cdots c(\tau_{i_k j_k}). \tag{2.11}$$

All transpositions must have the same value of c. Indeed, any transposition can be related to τ_{12} by conjugation. For example,

$$\tau_{ij} = \rho^{-1} \circ \tau_{12} \circ \rho, \qquad \rho = \tau_{1i} \circ \tau_{2j}, \tag{2.12}$$

and therefore

$$c(\tau_{ij}) = c(\tau_{12}). \tag{2.13}$$

Moreover, since exchanging the same two particles twice gives the identity,

$$\tau_{12} \circ \tau_{12} = \mathbb{1}, \tag{2.14}$$

we obtain

$$c(\tau_{12})^2 = 1. \tag{2.15}$$

Thus

$$c(\tau_{12}) = \pm 1. \tag{2.16}$$

This last step is the one that carries the assumption about spatial dimension. The argument is purely group-theoretical and holds for any number of particles, but it relies on $\tau_{12} \circ \tau_{12}$ being the identity, that is, on the statement that exchanging two particles twice amounts to doing nothing. This is true in three dimensions, where the two exchange paths can be continuously deformed into one another; it fails in one and two dimensions, as discussed at the end of this section.

There are consequently two possibilities:

- **Bosons:** if $c(\tau_{12}) = +1$, then $c(\sigma) = 1$ for every permutation σ. The many-body wave-function is therefore totally symmetric under particle exchange.

- **Fermions:** if $c(\tau_{12}) = -1$, then $c(\sigma) = \varepsilon(\sigma)$, where $\varepsilon(\sigma)$ is the signature of the permutation. The many-body wave-function is therefore totally antisymmetric under particle exchange.

The distinction between bosons and fermions is related to the spin of the particles through the *spin-statistics theorem*. In three spatial dimensions, the theorem states that particles with integer spin,

$$S = 0, 1, 2, \ldots,$$

are bosons, whereas particles with half-integer spin,

$$S = \frac{1}{2}, \frac{3}{2}, \ldots,$$

are fermions [26]. A proper proof of this result requires relativistic quantum field theory and will not be discussed here.[1]

Finally, the boson/fermion classification is not completely universal. In one and two spatial dimensions, particles can exhibit more general exchange statistics that are not captured by simple symmetric or antisymmetric wave-functions. Such systems are associated with, for example, anyonic and braid-group statistics [28, 29, 30]. These cases will not be considered in the following, where we restrict ourselves to ordinary bosonic and fermionic particles.

2.2 Symmetric states in first quantization

2.2.1 Restriction to the symmetric subspace

For a system of N distinguishable particles, the Hilbert space is the tensor product of the individual single-particle Hilbert spaces. If $|k\rangle$ denotes a basis of the single-particle Hilbert space, a corresponding basis of the many-body Hilbert space is given by

$$|k_1\rangle \otimes \ldots \otimes |k_N\rangle. \tag{2.17}$$

For simplicity, we assume that the single-particle Hilbert space has finite dimension d. The Hilbert space of N distinguishable particles then has dimension d^N.

For identical particles, the symmetrization postulate restricts the physical Hilbert space to either the fully symmetric subspace, for bosons, or the fully anti-symmetric subspace, for fermions. The dimension of these subspaces is much smaller than d^N. In this section, we construct convenient bases for these subspaces within the first-quantization formalism. In the next section, we will see how the same states arise naturally from the second-quantization formalism.

We introduce the symmetrization and anti-symmetrization operators

$$\hat{S} = \frac{1}{N!} \sum_\sigma \hat{P}_\sigma, \tag{2.18}$$

$$\hat{A} = \frac{1}{N!} \sum_\sigma \varepsilon(\sigma) \hat{P}_\sigma, \tag{2.19}$$

[1] The precise assumptions entering the spin-statistics theorem are important; see, for example, the pedagogical discussion in [27].

where the sums run over all permutations of N particles and $\varepsilon(\sigma)$ denotes the signature of the permutation. These operators are orthogonal projectors onto the symmetric and anti-symmetric subspaces, respectively:

$$\hat{S}^2 = \hat{S}, \qquad \hat{A}^2 = \hat{A}, \qquad \hat{S}^\dagger = \hat{S}, \qquad \hat{A}^\dagger = \hat{A}. \tag{2.20}$$

Hermiticity follows from $\hat{P}_\sigma^\dagger = \hat{P}_\sigma^{-1} = \hat{P}_{\sigma^{-1}}$ together with $\varepsilon(\sigma^{-1}) = \varepsilon(\sigma)$, the sum over σ being unchanged by the relabelling $\sigma \to \sigma^{-1}$. It will be used repeatedly below, when norms are computed as $\|\hat{A}|\Psi\rangle\|^2 = \langle\Psi|\hat{A}^2|\Psi\rangle = \langle\Psi|\hat{A}|\Psi\rangle$. The two subspaces are orthogonal, so that

$$\hat{S}\hat{A} = \hat{A}\hat{S} = 0. \tag{2.21}$$

They also satisfy

$$\hat{S}\hat{P}_\sigma = \hat{P}_\sigma\hat{S} = \hat{S}, \tag{2.22}$$

$$\hat{A}\hat{P}_\sigma = \hat{P}_\sigma\hat{A} = \varepsilon(\sigma)\hat{A}. \tag{2.23}$$

It should be stressed that these two projectors do not exhaust the Hilbert space as soon as $N \geq 3$:

$$\hat{S} + \hat{A} \neq \mathbb{1} \qquad (N \geq 3). \tag{2.24}$$

For two particles, any state splits into a symmetric and an anti-symmetric part, and $\hat{S} + \hat{A} = \mathbb{1}$. For three or more particles, the tensor-product space also contains subspaces of mixed symmetry, which transform according to higher-dimensional representations of the permutation group. These are precisely the parastatistics excluded by the symmetrization postulate: they are discarded by assumption, not by any property of $\hat{S}$ and $\hat{A}$.

A basis of the physical Hilbert space can now be constructed by applying either $\hat{S}$ or $\hat{A}$ to the product states $|k_1\rangle \otimes \ldots \otimes |k_N\rangle$. The resulting state does not depend on the ordering of the single-particle states for bosons, while for fermions changing the ordering can only change the overall sign. The physical state is therefore characterized by the occupation numbers n_k, i.e. by the number of particles occupying each single-particle state $|k\rangle$.

The allowed occupation numbers and the normalization of the corresponding states differ between fermions and bosons. We discuss the two cases separately.

2.2.2 Fermionic states

For fermions, the occupation number of every single-particle state can only be 0 or 1. To see this, consider a product state

$$|\Psi\rangle = |k_1\rangle \otimes \ldots \otimes |k_N\rangle \tag{2.25}$$

in which the same single-particle state $|k\rangle$ occurs for two different particle labels i and j. Exchanging these two particles leaves the state unchanged:

$$\hat{P}_{\tau_{ij}}|\Psi\rangle = |\Psi\rangle, \tag{2.26}$$

where τ_{ij} denotes, as above, the transposition exchanging particles i and j. On the other hand, the anti-symmetrizer satisfies

$$\hat{A}\hat{P}_{\tau_{ij}} = \varepsilon(\tau_{ij})\hat{A} = -\hat{A}, \tag{2.27}$$

and therefore

$$\hat{A}|\Psi\rangle = \hat{A}\hat{P}_{\tau_{ij}}|\Psi\rangle = -\hat{A}|\Psi\rangle. \tag{2.28}$$

Hence

$$\hat{A}|\Psi\rangle = 0. \tag{2.29}$$

This is the Pauli exclusion principle: two identical fermions cannot occupy the same single-particle quantum state.

Let us therefore consider N distinct single-particle states $|k_1\rangle, \ldots, |k_N\rangle$. We define the corresponding anti-symmetrized state as

$$|k_1, \ldots, k_N\rangle \equiv \mathcal{N}\hat{A}|k_1\rangle \otimes \ldots \otimes |k_N\rangle, \tag{2.30}$$

where $\mathcal{N}$ is a normalization factor. Assuming that the single-particle states form an orthonormal basis, the product state

$$|\Psi\rangle = |k_1\rangle \otimes \ldots \otimes |k_N\rangle \tag{2.31}$$

is normalized. We then have

$$\left\|\hat{A}|\Psi\rangle\right\|^2 = \langle\Psi|\hat{A}^2|\Psi\rangle = \langle\Psi|\hat{A}|\Psi\rangle \tag{2.32}$$

$$= \frac{1}{N!}\sum_\sigma \varepsilon(\sigma)\langle\Psi|\hat{P}_\sigma|\Psi\rangle. \tag{2.33}$$

Since all the k_i are distinct, the product state $|\Psi\rangle$ is orthogonal to all its non-trivial permutations. Hence

$$\langle\Psi|\hat{P}_\sigma|\Psi\rangle = \delta_{\sigma,\mathbb{1}}, \tag{2.34}$$

and therefore

$$\left\|\hat{A}|\Psi\rangle\right\|^2 = \frac{1}{N!}. \tag{2.35}$$

The normalized state is consequently

$$|k_1, \ldots, k_N\rangle = \sqrt{N!}\,\hat{A}|k_1\rangle \otimes \cdots \otimes |k_N\rangle. \tag{2.36}$$

In the position representation, this state takes the familiar form of a Slater determinant. The many-body wave-function is

$$\Psi(\mathbf{r}_1, \ldots, \mathbf{r}_N) \equiv \langle\mathbf{r}_1| \otimes \cdots \otimes \langle\mathbf{r}_N||k_1, \ldots, k_N\rangle \tag{2.37}$$

$$= \frac{1}{\sqrt{N!}}\sum_\sigma \varepsilon(\sigma)\langle\mathbf{r}_1|k_{\sigma(1)}\rangle \cdots \langle\mathbf{r}_N|k_{\sigma(N)}\rangle \tag{2.38}$$

$$= \frac{1}{\sqrt{N!}}\begin{vmatrix} \langle\mathbf{r}_1|k_1\rangle & \cdots & \langle\mathbf{r}_1|k_N\rangle \\ \vdots & \ddots & \vdots \\ \langle\mathbf{r}_N|k_1\rangle & \cdots & \langle\mathbf{r}_N|k_N\rangle \end{vmatrix}. \tag{2.39}$$

The ordering of the occupied states in the notation $|k_1, \ldots, k_N\rangle$ is therefore meaningful up to an overall sign. Exchanging two occupied states changes the sign of the state:

$$|k_2, k_1, \ldots, k_N\rangle = -|k_1, k_2, \ldots, k_N\rangle. \tag{2.40}$$

Of course, this overall sign has no physical consequence. The important information contained in the state is the set of occupied single-particle states.

This observation immediately gives the dimension of the physical Hilbert space. We denote by $\mathcal{E}_N^{\mathrm{F}}$ the anti-symmetric Hilbert space of N identical fermions, and by $\mathcal{E}_N^{\mathrm{B}}$ its symmetric counterpart for bosons, a notation we keep throughout. A fermionic basis state is specified by choosing which N of the d single-particle states are occupied, so that

$$\dim \mathcal{E}_N^{\mathrm{F}} = \binom{d}{N}. \tag{2.41}$$

In particular, the space is empty for $N > d$: no more than d fermions can be accommodated in d single-particle states.

2.2.3 Bosonic states

For bosons, there is no restriction on the occupation numbers: a single-particle state $|k\rangle$ can be occupied by any number $n_k = 0, 1, 2, \ldots$ of particles.

Consider a configuration with p occupied single-particle states $|k_1\rangle, \ldots, |k_p\rangle$ and occupation numbers $n_{k_1}, \ldots, n_{k_p}$ satisfying

$$\sum_{i=1}^{p} n_{k_i} = N. \tag{2.42}$$

Since the particles are bosons, their ordering is irrelevant. We can therefore choose the convenient representative

$$|\Psi\rangle = |k_1\rangle^{\otimes n_{k_1}} \otimes \cdots \otimes |k_p\rangle^{\otimes n_{k_p}}. \tag{2.43}$$

We again determine the normalization by calculating the norm of the symmetrized state:

$$\left\|\hat{S}|\Psi\rangle\right\|^2 = \langle\Psi|\hat{S}^2|\Psi\rangle = \langle\Psi|\hat{S}|\Psi\rangle \tag{2.44}$$

$$= \frac{1}{N!}\sum_{\sigma}\langle\Psi|\hat{P}_\sigma|\Psi\rangle. \tag{2.45}$$

The overlap is non-zero precisely for permutations that only exchange particles occupying the same single-particle state. There are

$$\prod_{i=1}^{p} n_{k_i}! \tag{2.46}$$

such permutations. We therefore obtain

$$\left\|\hat{S}|\Psi\rangle\right\|^2 = \frac{\prod_{i=1}^{p} n_{k_i}!}{N!}. \tag{2.47}$$

The normalized bosonic state is consequently

$$|n_{k_1} : k_1, \ldots, n_{k_p} : k_p\rangle = \sqrt{\frac{N!}{\prod_{i=1}^{p} n_{k_i}!}}\hat{S}|k_1\rangle^{\otimes n_{k_1}} \otimes \cdots \otimes |k_p\rangle^{\otimes n_{k_p}}. \tag{2.48}$$

In contrast to the fermionic case, there is no sign associated with exchanging two occupied states. A bosonic many-body state is therefore completely specified by its

occupation numbers n_k. This observation will become central in the second-quantization formalism.

Counting the basis states again gives the dimension of the Hilbert space. A basis state corresponds to a choice of d occupation numbers $n_k \geq 0$ summing to N, and the number of such choices is

$$\dim \mathcal{H}_N^{\text{bos}} = \binom{d+N-1}{N}. \tag{2.49}$$

This is the classic problem of distributing N indistinguishable balls among d boxes, solved by lining up the N balls together with $d-1$ separators and choosing which N of the $d+N-1$ objects are balls.

It is instructive to compare these dimensions with the value d^N obtained for distinguishable particles. For $N=5$ particles in $d=10$ single-particle states, for example, one finds $10^5 = 100\,000$ for distinguishable particles, against $\binom{14}{5} = 2002$ for bosons and $\binom{10}{5} = 252$ for fermions. The symmetrization postulate therefore reduces the size of the Hilbert space enormously.

2.2.4 Explicit expressions of few-body wave-functions

Let us now apply the formalism above to a few simple examples. These examples illustrate directly how the exchange symmetry of identical particles affects observable probabilities.

Two identical particles in the same internal state. We first consider two identical particles prepared in the same internal state, so that only their motional degrees of freedom need to be considered. Suppose that the two particles occupy orthogonal single-particle states $|\phi_1\rangle$ and $|\phi_2\rangle$. Their two-particle wave-function is

$$\psi(\mathbf{r}_1, \mathbf{r}_2) = \frac{\phi_1(\mathbf{r}_1)\phi_2(\mathbf{r}_2) + \varepsilon\, \phi_1(\mathbf{r}_2)\phi_2(\mathbf{r}_1)}{\sqrt{2}}, \tag{2.50}$$

where $\varepsilon = 1$ for bosons and $\varepsilon = -1$ for fermions.

For fermions, anti-symmetry immediately implies

$$\psi(\mathbf{r}, \mathbf{r}) = 0. \tag{2.51}$$

Thus, two identical fermions in the same internal state have zero probability amplitude to be found at the same position. This is the simplest manifestation of fermionic anti-bunching.

For bosons, the opposite behavior occurs: the two amplitudes associated with the two possible assignments of the particles to the positions interfere constructively. To illustrate this, consider two plane-wave orbitals

$$\phi_i(\mathbf{r}) = \frac{\mathrm{e}^{\mathrm{i}\mathbf{k}_i\cdot\mathbf{r}}}{\sqrt{V}}, \qquad i = 1, 2, \tag{2.52}$$

with $\mathbf{k}_1 \neq \mathbf{k}_2$, where V is the volume of the quantization box. The two-particle wave-function is then

$$\psi(\mathbf{r}_1, \mathbf{r}_2) = \frac{\mathrm{e}^{\mathrm{i}(\mathbf{k}_1\cdot\mathbf{r}_1 + \mathbf{k}_2\cdot\mathbf{r}_2)} + \mathrm{e}^{\mathrm{i}(\mathbf{k}_1\cdot\mathbf{r}_2 + \mathbf{k}_2\cdot\mathbf{r}_1)}}{\sqrt{2}V} \tag{2.53}$$

for bosons. At equal positions,

$$|\psi(\mathbf{r},\mathbf{r})|^2 = \frac{2}{V^2}, \tag{2.54}$$

which is twice the corresponding value for distinguishable particles. Thus, identical bosons tend to be found together: they exhibit bunching.

These bunching and anti-bunching effects are manifestations of exchange statistics and can be observed experimentally through temporal correlations in particle beams. Examples include the Hanbury Brown–Twiss effect for light [31] and the observation of fermionic anti-correlations in electronic conduction channels [32, 33]. We discuss these effects in more detail below.

2.2.5 Two-particle interference: the Hong–Ou–Mandel effect

A particularly striking manifestation of quantum statistics occurs when two identical particles are sent into the two input ports of a 50:50 beam splitter. This is known as the Hong–Ou–Mandel (HOM) effect, originally demonstrated with photons [34].

Suppose that one particle enters each of the two incoming ports a and b. We ask how the particles are distributed between the two outgoing ports a' and b'.

If the particles are distinguishable, each particle has an independent probability $1/2$ of exiting through either port. The four possible outcomes therefore have equal probabilities,

$$P(1:a',2:a') = P(1:a',2:b') = P(1:b',2:a') = P(1:b',2:b') = \frac{1}{4}. \tag{2.55}$$

For indistinguishable particles, however, the two possible paths leading to a given output configuration interfere, and the result depends dramatically on the exchange statistics.

To model the beam splitter, we introduce two propagation directions x and y, associated with the mode pairs a, a' and b, b' respectively, and divide space into an incoming region $\mathcal{E}_{\text{in}}$ with $x+y<0$ and an outgoing region $\mathcal{E}_{\text{out}}$ with $x+y>0$ (see Fig. 14a).

The whole calculation rests on a single ingredient: the way the beam splitter transforms the incoming modes. We denote by $\phi_a^{(0)}(\mathbf{r},t)$ and $\phi_b^{(0)}(\mathbf{r},t)$ two normalized wavepackets of spatial width w, propagating along x and y respectively. The first is localized in the incoming port a at early times and in the outgoing port a' at late times, while the second connects b to b'. This localization is what allows the number of particles in each port to be defined unambiguously. An explicit construction of these wavepackets is given at the end of this section; none of its details will be needed.

A particle entering through port a is then described by

$$\begin{aligned}\phi_a(\mathbf{r},t) &= \phi_a^{(0)}(\mathbf{r},t) \qquad \text{in } \mathcal{E}_{\text{in}},\\ &= \frac{1}{\sqrt{2}}\left[\phi_a^{(0)}(\mathbf{r},t) + \mathrm{i}\,\phi_b^{(0)}(\mathbf{r},t)\right] \qquad \text{in } \mathcal{E}_{\text{out}},\end{aligned}$$

and, symmetrically, a particle entering through port b by

$$\begin{aligned}\phi_b(\mathbf{r},t) &= \phi_b^{(0)}(\mathbf{r},t) \qquad \text{in } \mathcal{E}_{\text{in}},\\ &= \frac{1}{\sqrt{2}}\left[\phi_b^{(0)}(\mathbf{r},t) + \mathrm{i}\,\phi_a^{(0)}(\mathbf{r},t)\right] \qquad \text{in } \mathcal{E}_{\text{out}}.\end{aligned}$$

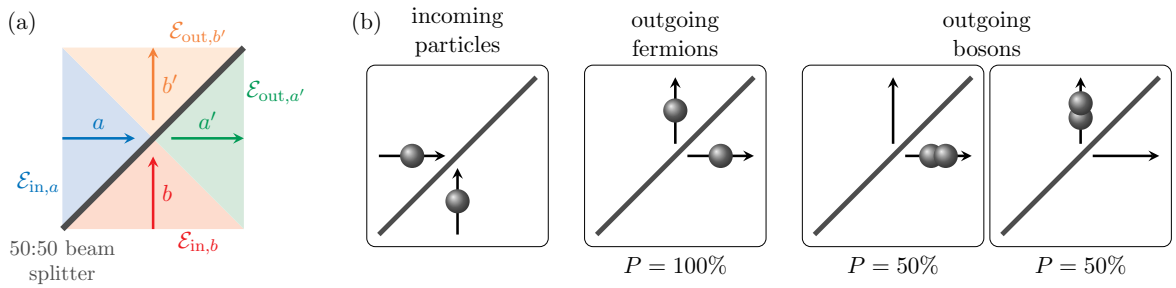


Figure 14: (a) Scheme of the incoming and outgoing ports of a particle beam splitter involved in the Hong–Ou–Mandel experiment. We divide the plane into regions allowing for an unambiguous definition of the particle number in each port. (b) Expected outgoing particle-number probabilities for two incoming particles, one in each input port. While two fermions always exit through different ports, two bosons always leave through the same output port.

The factor $1/\sqrt{2}$ expresses the balanced splitting, and the relative factor i the phase shift of $\pi/2$ acquired upon reflection; together they make the transformation unitary, which is the only property we shall use. For a single incoming particle, this reproduces the expected output probabilities

$$P(n_{a'} = 1, n_{b'} = 0) = P(n_{a'} = 0, n_{b'} = 1) = \frac{1}{2}. \tag{2.56}$$

We can now consider the HOM experiment with one particle entering through each input port. The two-particle state is described by the symmetrized or anti-symmetrized wave-function

$$\psi(\mathbf{r}_1, \mathbf{r}_2) = \frac{\phi_a(\mathbf{r}_1)\phi_b(\mathbf{r}_2) + \varepsilon\, \phi_a(\mathbf{r}_2)\phi_b(\mathbf{r}_1)}{\sqrt{2}}, \tag{2.57}$$

where $\varepsilon = 1$ for bosons and $\varepsilon = -1$ for fermions.

In the outgoing region, this becomes

$$\begin{aligned}\psi(\mathbf{r}_1, \mathbf{r}_2) = \frac{1}{2\sqrt{2}}\Big\{ & \mathrm{i}(1+\varepsilon)\phi_a^{(0)}(\mathbf{r}_1, t)\phi_a^{(0)}(\mathbf{r}_2, t) \\ & + \mathrm{i}(1+\varepsilon)\phi_b^{(0)}(\mathbf{r}_1, t)\phi_b^{(0)}(\mathbf{r}_2, t) \\ & + (1-\varepsilon)\left[\phi_a^{(0)}(\mathbf{r}_1, t)\phi_b^{(0)}(\mathbf{r}_2, t) - \phi_a^{(0)}(\mathbf{r}_2, t)\phi_b^{(0)}(\mathbf{r}_1, t)\right]\Big\}. \end{aligned} \tag{2.58}$$

The three terms correspond respectively to both particles exiting through a', both particles exiting through b', and one particle exiting through each port. The corresponding probabilities are

$$P(n_{a'} = 2, n_{b'} = 0) = P(n_{a'} = 0, n_{b'} = 2) = \frac{(1+\varepsilon)^2}{8} = \begin{cases} \frac{1}{2}, & \text{bosons}, \\ 0, & \text{fermions}, \end{cases} \tag{2.59}$$

$$P(n_{a'} = 1, n_{b'} = 1) = \frac{(1-\varepsilon)^2}{4} = \begin{cases} 0, & \text{bosons}, \\ 1, & \text{fermions}. \end{cases} \tag{2.60}$$

Thus, two identical bosons always leave the beam splitter together, while two identical fermions always leave through different output ports. This is the Hong–Ou–Mandel effect and its fermionic counterpart.

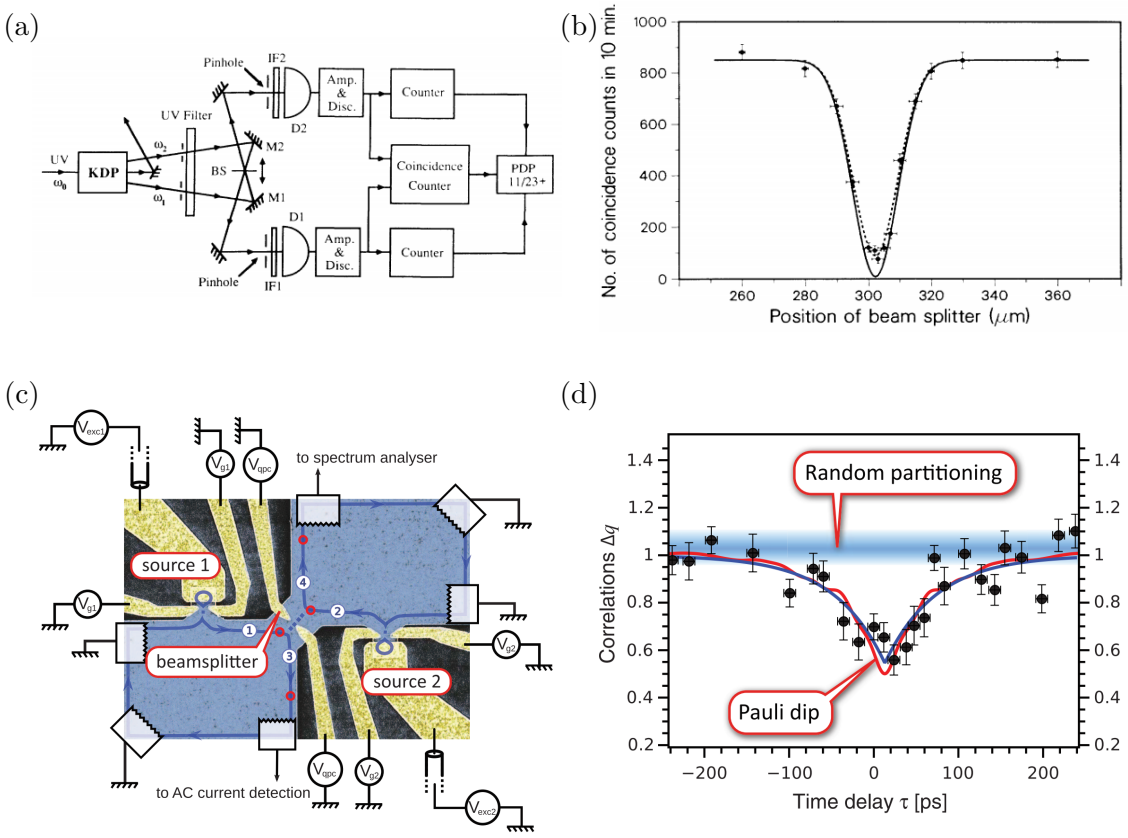


Figure 15: (a) Scheme of the original experiment demonstrating the Hong–Ou–Mandel effect [34]. Photons are emitted in pairs by parametric down-conversion in a nonlinear crystal and are subsequently recombined at a beam splitter. The probability of detecting one photon in each output port is measured through coincidence counting. (b) The observed suppression of coincidences, known as the HOM dip, occurs when the two photons become indistinguishable at the beam splitter. (c) Scheme of an experiment demonstrating the analogous fermionic anti-bunching effect using one-dimensional electronic conduction channels and a quantum point contact as a beam splitter. (d) The suppression of current noise when the arrival times of the two electrons coincide is the fermionic analogue of the HOM dip (from [35]).

The bosonic HOM effect was observed experimentally by Hong, Ou, and Mandel in 1987 [34] (see Figure 15a). They measured the rate of coincident detections at the two output ports and found that coincidences are strongly suppressed when the optical path lengths are adjusted so that the two photons arrive simultaneously at the beam splitter. This suppression is a direct signature of two-particle interference and requires the photons to be indistinguishable in all relevant degrees of freedom. The corresponding fermionic anti-bunching has also been observed using electronic conduction channels [35] (see Figure 15c and d).

Explicit construction of the mode functions. For completeness, we give here a concrete realization of the states used above. It plays no role in the result, and may be skipped.

The stationary scattering states of the beam splitter at wavevector k can be written as

$$\begin{aligned}
\phi_{a,k}(\mathbf{r}) &= \frac{1}{\sqrt{2\pi L\sigma}} \exp\left(-\frac{y^2+z^2}{4\sigma^2}\right) \mathrm{e}^{\mathrm{i}kx} \qquad \text{in } \mathcal{E}_{\text{in}}, \\
&= \frac{1}{\sqrt{2\pi L\sigma}} \frac{1}{\sqrt{2}} \left[\exp\left(-\frac{y^2+z^2}{4\sigma^2}\right) \mathrm{e}^{\mathrm{i}(kx+\theta_{aa'k})} + \exp\left(-\frac{x^2+z^2}{4\sigma^2}\right) \mathrm{e}^{\mathrm{i}(ky+\theta_{ab'k})}\right] \qquad \text{in } \mathcal{E}_{\text{out}}, \\
\phi_{b,k}(\mathbf{r}) &= \frac{1}{\sqrt{2\pi L\sigma}} \exp\left(-\frac{x^2+z^2}{4\sigma^2}\right) \mathrm{e}^{\mathrm{i}ky} \qquad \text{in } \mathcal{E}_{\text{in}}, \\
&= \frac{1}{\sqrt{2\pi L\sigma}} \frac{1}{\sqrt{2}} \left[\exp\left(-\frac{y^2+z^2}{4\sigma^2}\right) \mathrm{e}^{\mathrm{i}(kx+\theta_{ba'k})} + \exp\left(-\frac{x^2+z^2}{4\sigma^2}\right) \mathrm{e}^{\mathrm{i}(ky+\theta_{bb'k})}\right] \qquad \text{in } \mathcal{E}_{\text{out}}.
\end{aligned}$$

Here L is the length of the quantization box and σ characterizes the transverse width of the beams, transverse diffraction being neglected. The states $|\phi_{a,k}\rangle$ and $|\phi_{b,k}\rangle$ are stationary states of energy $\hbar\omega = \hbar ck$; we use a linear dispersion relation for definiteness, as appropriate for photons, although it plays no role here.

The two incoming states are orthogonal provided that

$$\theta_{aa'k} + \theta_{bb'k} - \theta_{ab'k} - \theta_{ba'k} = \pi \mod (2\pi), \tag{2.61}$$

the individual phases being otherwise irrelevant. We choose, for simplicity,

$$\theta_{aa'k} = \theta_{bb'k} = 0, \qquad \theta_{ab'k} = \theta_{ba'k} = \frac{\pi}{2}, \tag{2.62}$$

corresponding to no phase shift upon transmission and a phase shift of $\pi/2$ upon reflection, as is standard for an ideal beam splitter. This is the origin of the factor i in the beam-splitter transformation used above.

Superposing these stationary states with a Gaussian weight of width $1/w$ in wavevector,

$$\phi_a(\mathbf{r}, t) \propto \int \mathrm{d}k\, \mathrm{e}^{-w^2(k-k_0)^2} \phi_{a,k}(\mathbf{r})\, \mathrm{e}^{-\mathrm{i}ckt}, \tag{2.63}$$

produces a packet of spatial width w travelling along x. After normalization, the wavepackets entering the main derivation read

$$\phi_a^{(0)}(\mathbf{r}, t) = \frac{1}{(2\pi)^{3/4}\sigma\sqrt{w}} \exp\left(-\frac{y^2+z^2}{4\sigma^2}\right) \exp\left(-\frac{(x-ct)^2}{4w^2}\right) \mathrm{e}^{\mathrm{i}k_0(x-ct)}, \tag{2.64}$$

$$\phi_b^{(0)}(\mathbf{r}, t) = \frac{1}{(2\pi)^{3/4}\sigma\sqrt{w}} \exp\left(-\frac{x^2+z^2}{4\sigma^2}\right) \exp\left(-\frac{(y-ct)^2}{4w^2}\right) \mathrm{e}^{\mathrm{i}k_0(y-ct)}, \tag{2.65}$$

the prefactor being fixed by $\int |\phi_a^{(0)}|^2 \, \mathrm{d}^3 r = 1$, which uses $\int \exp[-(y^2+z^2)/2\sigma^2] \, \mathrm{d}y \, \mathrm{d}z = 2\pi\sigma^2$ and $\int \exp[-(x-ct)^2/2w^2] \, \mathrm{d}x = \sqrt{2\pi}\, w$.

2 identical spinful particles. Let us now consider two identical particles with internal spin degrees of freedom. We take both particles to have spin s and introduce the coupled spin basis $|S, M\rangle$, where

$$\hat{\mathbf{S}} = \hat{\mathbf{s}}_1 + \hat{\mathbf{s}}_2 \tag{2.66}$$

is the total spin, with $0 \leq S \leq 2s$, and M is its projection along a chosen quantization axis.

Under exchange of the two particles, the spin state $|S, M\rangle$ acquires the phase[2]

$$(-1)^{2s-S}. \tag{2.67}$$

For the familiar case $s = 1/2$, the triplet states with $S = 1$ are symmetric, while the singlet state with $S = 0$ is anti-symmetric.

The total many-body state is a product of orbital and spin degrees of freedom,

$$|\Psi\rangle = |\Psi_{\mathrm{orb}}\rangle \otimes |\Psi_{\mathrm{spin}}\rangle, \tag{2.68}$$

and must satisfy the appropriate exchange symmetry. For bosons, the orbital and spin parts must have the same exchange symmetry: they are either both symmetric or both anti-symmetric. For fermions, their exchange symmetries must be opposite.

This interplay between orbital and spin symmetry is at the origin of the exchange interaction in many condensed-matter systems. As a simple example, consider two electrons occupying two *different* orthogonal orbitals $|\phi_1\rangle$ and $|\phi_2\rangle$ of the same atom. Two orbitals are essential here: a single orbital admits no anti-symmetric orbital state, and would force the two electrons into the singlet. With two orbitals available, both the symmetric and the anti-symmetric orbital combinations exist. The anti-symmetric one vanishes when the two electrons coincide, and therefore suppresses the probability of finding them close to one another, which lowers their Coulomb repulsion. Since for fermions an anti-symmetric orbital state must be paired with a symmetric spin state, the triplet is pushed below the singlet. This is Hund's first rule, and at low energies the resulting splitting is described by an effective spin interaction of the form

$$-J_{\mathrm{ex}} \, \hat{\mathbf{S}}_1 \cdot \hat{\mathbf{S}}_2, \tag{2.69}$$

with $J_{\mathrm{ex}} > 0$ corresponding to a ferromagnetic coupling.

Three identical particles in the same internal state. Finally, let us briefly consider three identical particles. For fermions occupying three orthogonal orbitals $|\phi_1\rangle$, $|\phi_2\rangle$, and $|\phi_3\rangle$, the many-body wave-function is the corresponding 3×3 Slater

[2] A simple way to see this is to consider successively the highest-weight states of the multiplets with $S = 2s, 2s-1, \ldots, 0$. The state with $S = 2s$ is $|s, s\rangle \otimes |s, s\rangle$ and is symmetric. In the subspace with $M = 2s-1$, the $S = 2s$ state is the symmetric combination of $|s, s\rangle \otimes |s, s-1\rangle$ and $|s, s-1\rangle \otimes |s, s\rangle$, while the orthogonal $S = 2s-1$ state is their anti-symmetric combination. More generally, each time S is decreased by one, the exchange symmetry alternates, giving the exchange parity $(-1)^{2s-S}$.

determinant,

$$\psi(\mathbf{r}_1,\mathbf{r}_2,\mathbf{r}_3)=\frac{1}{\sqrt{6}}\Big[\phi_1(\mathbf{r}_1)\phi_2(\mathbf{r}_2)\phi_3(\mathbf{r}_3)+\phi_3(\mathbf{r}_1)\phi_1(\mathbf{r}_2)\phi_2(\mathbf{r}_3)$$
$$+\phi_2(\mathbf{r}_1)\phi_3(\mathbf{r}_2)\phi_1(\mathbf{r}_3)-\phi_3(\mathbf{r}_1)\phi_2(\mathbf{r}_2)\phi_1(\mathbf{r}_3)$$
$$-\phi_1(\mathbf{r}_1)\phi_3(\mathbf{r}_2)\phi_2(\mathbf{r}_3)-\phi_2(\mathbf{r}_1)\phi_1(\mathbf{r}_2)\phi_3(\mathbf{r}_3)\Big]. \tag{2.70}$$

For bosons, the corresponding wave-function is obtained by replacing all relative minus signs by plus signs.

Already for three particles, the explicit construction of the properly symmetrized or anti-symmetrized wave-function becomes cumbersome. For larger particle numbers, this approach rapidly becomes impractical: one has to manipulate $N!$ terms while keeping track of the exchange symmetry and normalization. More importantly, the physically relevant information is not the labels assigned to individual particles, but rather the occupation numbers of the available single-particle states.

This observation motivates a change of language. In the next section, we introduce the formalism of *second quantization*, in which occupation numbers provide the natural labels of many-body states and the symmetrization or anti-symmetrization of the wave-function is built directly into the algebra of creation and annihilation operators.

2.3 Second quantization

The second quantization formalism provides a convenient way of working directly in the symmetric or anti-symmetric Hilbert space of indistinguishable particles. Instead of explicitly symmetrizing or anti-symmetrizing many-body wave-functions, the exchange symmetry is encoded in the algebra of creation and annihilation operators. The formalism also naturally allows for states with different particle numbers, and is therefore particularly well suited to processes involving the creation and annihilation of quanta, such as photons.

2.3.1 Fock space

We consider a single-particle Hilbert space with an orthonormal basis $\{|k_1\rangle,|k_2\rangle,\ldots\}$. A many-body Fock state is specified by the occupation number n_p of each single-particle mode $|k_p\rangle$:

$$|n_1:k_1,n_2:k_2,\ldots,n_p:k_p,\ldots\rangle. \tag{2.71}$$

When there is no ambiguity about the single-particle basis, we use the shorter notation $|n_1,n_2,\ldots\rangle$.

The Fock space contains states with arbitrary particle number and is therefore the direct sum

$$\mathcal{E}=\mathcal{E}_0\oplus\mathcal{E}_1\oplus\cdots\oplus\mathcal{E}_N\oplus\cdots, \tag{2.72}$$

where $\mathcal{E}_N$ is the symmetric or anti-symmetric Hilbert space of N identical particles. In contrast to the Hilbert space of distinguishable particles, the exchange symmetry strongly reduces the number of independent states (see Fig. 16). For a single-particle

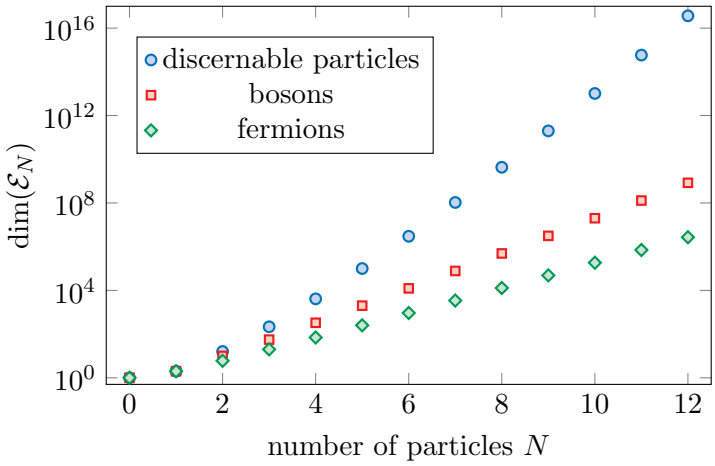


Figure 16: Dimension of the Hilbert space for an ensemble of N particles that can occupy a set of $2N$ single-particle states. The particles are assumed to be either distinguishable (blue disks), indistinguishable bosons (red squares), or indistinguishable fermions (green diamonds). Note the logarithmic scale on the vertical axis.

Hilbert space of dimension d, one has

$$\dim \mathcal{E}_N^{\mathrm{B}} = \binom{N+d-1}{N}, \tag{2.73}$$

$$\dim \mathcal{E}_N^{\mathrm{F}} = \binom{d}{N}, \tag{2.74}$$

for bosons and fermions, respectively.

2.3.2 Creation and annihilation operators

The subspace $\mathcal{E}_0$ contains a single state, the vacuum,

$$|\varnothing\rangle \equiv |n_1 = 0, n_2 = 0, \ldots\rangle. \tag{2.75}$$

It serves as the starting point for constructing the Fock basis. A creation operator $\hat{a}_k^\dagger$ adds one particle to the mode $|k\rangle$, while its Hermitian conjugate $\hat{a}_k$ removes one particle from this mode.

A useful first-quantized definition of the creation operator is

$$\hat{a}_k^\dagger |\psi\rangle = \sqrt{N+1}\,\hat{\Pi}\left(|k\rangle \otimes |\psi\rangle\right), \tag{2.76}$$

where $|\psi\rangle$ contains N particles and $\hat{\Pi} = \hat{S}$ for bosons and $\hat{\Pi} = \hat{A}$ for fermions. The factor $\sqrt{N+1}$ ensures the conventional normalization of Fock states.

Since the definition is linear in the single-particle state, one has

$$\hat{a}^\dagger_{\lambda_1|k_1\rangle+\lambda_2|k_2\rangle} = \lambda_1 \hat{a}^\dagger_{k_1} + \lambda_2 \hat{a}^\dagger_{k_2}. \tag{2.77}$$

The annihilation operator is defined as the Hermitian conjugate,

$$\hat{a}_k = (\hat{a}_k^\dagger)^\dagger. \tag{2.78}$$

Because the label of an annihilation operator is a bra-like single-particle state, it is anti-linear:

$$\hat{a}_{\lambda_1|k_1\rangle+\lambda_2|k_2\rangle} = \lambda_1^* \hat{a}_{k_1} + \lambda_2^* \hat{a}_{k_2}. \tag{2.79}$$

Action on the Fock basis. (i) Fermions. For fermions, each mode can be occupied at most once. Consider a normalized Fock state $|k_1, \ldots, k_N\rangle$, where all k_i are distinct. Applying a creation operator gives

$$\hat{a}_k^\dagger |k_1, \ldots, k_N\rangle = \sqrt{N+1}\, \hat{A}\left(|k\rangle \otimes |k_1, \ldots, k_N\rangle\right). \tag{2.80}$$

If the mode k coincides with one of the occupied modes, say $k = k_1$, the state $|k\rangle \otimes |k_1, \ldots, k_N\rangle$ contains the same single-particle state twice, and its anti-symmetrization vanishes:

$$\hat{a}_{k_1}^\dagger |k_1, \ldots, k_N\rangle = 0. \tag{2.81}$$

This is the Pauli exclusion principle. In operator form it reads

$$\left(\hat{a}_k^\dagger\right)^2 = 0, \tag{2.82}$$

which follows at once from the anticommutation relation $\{\hat{a}_k^\dagger, \hat{a}_k^\dagger\} = 0$ established below: a fermionic mode cannot be filled twice.

If k is not occupied, we obtain

$$\hat{a}_k^\dagger |k_1, \ldots, k_N\rangle = |k, k_1, \ldots, k_N\rangle. \tag{2.83}$$

Consequently, a Fock state can be constructed from the vacuum as

$$|k_1, \ldots, k_N\rangle = \hat{a}_{k_1}^\dagger \cdots \hat{a}_{k_N}^\dagger |\emptyset\rangle. \tag{2.84}$$

The annihilation operator removes a particle from the corresponding mode:

$$\hat{a}_{k_1} |k_1, k_2, \ldots, k_N\rangle = |k_2, \ldots, k_N\rangle. \tag{2.85}$$

The order of the occupied modes is physically irrelevant but fixes the sign convention for the state. For instance,

$$\hat{a}_{k_2} |k_1, k_2\rangle = -|k_1\rangle. \tag{2.86}$$

(ii) Bosons. For bosons, an arbitrary number of particles can occupy the same mode. Consider a Fock state $|n_1 : k_1, \ldots, n_p : k_p\rangle$ with $N = \sum_i n_i$. The creation operator acts as

$$\hat{a}_{k_i}^\dagger |n_1 : k_1, \ldots, n_i : k_i, \ldots, n_p : k_p\rangle = \sqrt{n_i + 1}\, |n_1 : k_1, \ldots, (n_i + 1) : k_i, \ldots, n_p : k_p\rangle. \tag{2.87}$$

The factor $\sqrt{n_i + 1}$ is the characteristic bosonic enhancement factor.

Similarly,

$$\hat{a}_{k_i} |n_1 : k_1, \ldots, n_i : k_i, \ldots, n_p : k_p\rangle = \sqrt{n_i}\, |n_1 : k_1, \ldots, (n_i - 1) : k_i, \ldots, n_p : k_p\rangle. \tag{2.88}$$

The Fock basis can therefore be constructed as

$$|n_1 : k_1, \ldots, n_p : k_p\rangle = \frac{(\hat{a}_{k_1}^\dagger)^{n_1} \cdots (\hat{a}_{k_p}^\dagger)^{n_p}}{\sqrt{n_1! \cdots n_p!}} |\emptyset\rangle. \tag{2.89}$$

Commutation and anticommutation relations. The exchange symmetry of identical particles is encoded directly in the algebra of creation and annihilation operators. For two creation operators, one finds

$$[\hat{a}^\dagger_{k_1}, \hat{a}^\dagger_{k_2}] = 0 \qquad \text{for bosons,} \tag{2.90}$$

$$\{\hat{a}^\dagger_{k_1}, \hat{a}^\dagger_{k_2}\} = 0 \qquad \text{for fermions.} \tag{2.91}$$

Thus, bosonic creation operators commute, while fermionic creation operators anticommute. The same relations hold for annihilation operators.

The mixed relations read

$$[\hat{a}_{k_1}, \hat{a}^\dagger_{k_2}] = \delta_{k_1 k_2} \qquad \text{for bosons,} \tag{2.92}$$

$$\{\hat{a}_{k_1}, \hat{a}^\dagger_{k_2}\} = \delta_{k_1 k_2} \qquad \text{for fermions.} \tag{2.93}$$

More generally, for arbitrary single-particle states $|\phi_1\rangle$ and $|\phi_2\rangle$,

$$[\hat{a}_{\phi_1}, \hat{a}^\dagger_{\phi_2}] = \langle\phi_1|\phi_2\rangle \qquad \text{for bosons,} \tag{2.94}$$

$$\{\hat{a}_{\phi_1}, \hat{a}^\dagger_{\phi_2}\} = \langle\phi_1|\phi_2\rangle \qquad \text{for fermions.} \tag{2.95}$$

The commutation or anticommutation relations are the central ingredient of second quantization: they encode the exchange symmetry without requiring explicit sums over permutations.

Number operators. The occupation of a given mode is measured by the Hermitian *number operator*

$$\hat{n}_k = \hat{a}^\dagger_k \hat{a}_k, \tag{2.96}$$

which, for both statistics, is diagonal in the Fock basis,

$$\hat{n}_k |n_1, n_2, \ldots\rangle = n_k |n_1, n_2, \ldots\rangle. \tag{2.97}$$

Its eigenvalues are $n_k = 0, 1, 2, \ldots$ for bosons. For fermions they are restricted to $n_k \in \{0, 1\}$, as follows from

$$\hat{n}_k^2 = \hat{a}^\dagger_k \hat{a}_k \hat{a}^\dagger_k \hat{a}_k = \hat{a}^\dagger_k \left(1 - \hat{a}^\dagger_k \hat{a}_k\right) \hat{a}_k = \hat{n}_k, \tag{2.98}$$

where we used $\hat{a}_k \hat{a}^\dagger_k = 1 - \hat{a}^\dagger_k \hat{a}_k$ and $(\hat{a}^\dagger_k)^2 = 0$. A projector has eigenvalues 0 and 1 only, which is Pauli exclusion once more.

The total number of particles is

$$\hat{N} = \sum_k \hat{n}_k, \tag{2.99}$$

and the Fock states are its eigenstates, with eigenvalue $N = \sum_k n_k$. The subspaces $\mathcal{E}_N$ introduced above are precisely the eigenspaces of $\hat{N}$.

2.3.3 Field operators

Let us now consider a single-particle basis labelled by position and an internal state, $|\mathbf{r}, \sigma\rangle = |\mathbf{r}\rangle \otimes |\sigma\rangle$, where σ may, for instance, denote a spin projection. We reserve the symbol m for the particle mass. We define the field annihilation operator by

$$\hat{\psi}_\sigma(\mathbf{r}) \equiv \hat{a}_{\mathbf{r},\sigma}. \tag{2.100}$$

The corresponding creation operator is $\hat{\psi}^\dagger_\sigma(\mathbf{r})$. It adds one particle *at the point* $\mathbf{r}$, in the internal state σ.

The position states are not normalizable and satisfy

$$\langle \mathbf{r}, \sigma | \mathbf{r}', \sigma' \rangle = \delta(\mathbf{r} - \mathbf{r}')\delta_{\sigma,\sigma'}. \tag{2.101}$$

Let $|k\rangle$ be a complete orthonormal basis of normalizable single-particle states, with spinor wave-functions

$$\phi_{k,\sigma}(\mathbf{r}) = \langle \mathbf{r}, \sigma | k \rangle. \tag{2.102}$$

Completeness gives

$$|\mathbf{r}, \sigma\rangle = \sum_k \phi_{k,\sigma}(\mathbf{r})^* |k\rangle. \tag{2.103}$$

Using the anti-linearity of the annihilation operator, we obtain

$$\hat{\psi}_\sigma(\mathbf{r}) = \sum_k \phi_{k,\sigma}(\mathbf{r})\hat{a}_k. \tag{2.104}$$

The canonical commutation or anticommutation relations therefore become

$$[\hat{\psi}_\sigma(\mathbf{r}), \hat{\psi}^\dagger_{\sigma'}(\mathbf{r}')] = \delta(\mathbf{r} - \mathbf{r}')\delta_{\sigma,\sigma'} \qquad \text{for bosons,} \tag{2.105}$$

$$\{\hat{\psi}_\sigma(\mathbf{r}), \hat{\psi}^\dagger_{\sigma'}(\mathbf{r}')\} = \delta(\mathbf{r} - \mathbf{r}')\delta_{\sigma,\sigma'} \qquad \text{for fermions.} \tag{2.106}$$

Field operators provide a compact way of writing states. Acting on the vacuum, a single creation operator produces a particle localized at $\mathbf{r}$, and a superposition of such operators produces a particle in an arbitrary orbital: for a normalized single-particle wave-function $\phi(\mathbf{r})$ of a spinless particle,

$$|\phi\rangle = \int \phi(\mathbf{r})\, \hat{\psi}^\dagger(\mathbf{r})|\varnothing\rangle \, \mathrm{d}^3 r. \tag{2.107}$$

More generally, an N-particle state is obtained by applying N field creation operators to the vacuum, the exchange symmetry being automatically enforced by the algebra.

2.3.4 Observables

Single-particle observables. Consider an observable $\hat{b}$ acting on the single-particle Hilbert space. The corresponding observable for N identical particles is the sum

$$\hat{B} = \sum_{i=1}^{N} \hat{b}_i, \tag{2.108}$$

where $\hat{b}_i$ acts as $\hat{b}$ on particle i and as the identity on all other particles.

For example, choosing $\hat{b} = \hat{\boldsymbol{p}}$ gives the total momentum $\hat{\boldsymbol{P}} = \sum_i \hat{\boldsymbol{p}}_i$. Similarly, choosing $\hat{b} = \delta(\hat{\mathbf{r}} - \mathbf{r})$ gives the particle-density operator, which we denote $\hat{\rho}(\mathbf{r})$. Beware of the conflict of notation: $\hat{\rho}(\mathbf{r})$ and $\hat{\rho}_2(\mathbf{r}, \mathbf{r}')$, which carry position arguments, are the density and the pair density, whereas $\hat{\rho}$, $\hat{\rho}_1$ and $\hat{\rho}_2$ without arguments denote density matrices.

The second-quantized form of $\hat{B}$ follows directly from the matrix elements of $\hat{b}$ in a single-particle basis:

$$\hat{B} = \sum_{k,k'} \langle k'|\hat{b}|k\rangle \hat{a}^\dagger_{k'} \hat{a}_k. \tag{2.109}$$

To see this, expand the single-particle operator on the basis $\{|k\rangle\}$ as $\hat{b} = \sum_{k,k'} \langle k'|\hat{b}|k\rangle |k'\rangle\langle k|$, so that

$$\hat{B} = \sum_{k,k'} \langle k'|\hat{b}|k\rangle \sum_{i=1}^{N} |k'\rangle_i \langle k|_i. \tag{2.110}$$

The operator $\sum_i |k'\rangle_i \langle k|_i$ transfers one particle, whichever it is, from the mode k to the mode k'; being symmetric under permutations, it acts within the physical subspace, and one checks on an arbitrary Fock state that it coincides there with $\hat{a}^\dagger_{k'} \hat{a}_k$. In particular, for $k = k'$ it reduces to the number operator (2.96), and summing over k gives $\hat{N}$ as it must.

Formula (2.109) has a transparent interpretation: $\hat{a}_k$ removes a particle from the mode k, the single-particle operator $\hat{b}$ transforms it into the mode k', and $\hat{a}^\dagger_{k'}$ creates the resulting particle.

In terms of field operators, a one-body operator can equivalently be written as

$$\hat{B} = \sum_{\sigma,\sigma'} \int \hat{\psi}^\dagger_\sigma(\mathbf{r}) \langle \mathbf{r}, \sigma|\hat{b}|\mathbf{r}', \sigma'\rangle \hat{\psi}_{\sigma'}(\mathbf{r}') \, \mathrm{d}^3 r \, \mathrm{d}^3 r'. \tag{2.111}$$

The simplest example is the density itself. Taking $\hat{b} = \delta(\hat{\mathbf{r}} - \mathbf{r})$, which is diagonal in position, gives for spinless particles

$$\hat{\rho}(\mathbf{r}) = \hat{\psi}^\dagger(\mathbf{r}) \hat{\psi}(\mathbf{r}), \qquad \hat{N} = \int \hat{\rho}(\mathbf{r}) \, \mathrm{d}^3 r. \tag{2.112}$$

This is the expression that will be used constantly in the following. Together with (2.99), it shows that the two ways of counting particles, mode by mode or point by point, are the same operator.

For the kinetic energy of spinless particles,

$$\hat{T} = \frac{\hat{P}^2}{2m}, \tag{2.113}$$

we need the matrix elements of $\hat{p}^2$ between position states. They are obtained from the fact that, in the position representation, $\hat{p}^2$ acts on a wave-function as $-\hbar^2\Delta$,

$$\langle \mathbf{r}|\hat{p}^2|\phi\rangle = -\hbar^2 \Delta_{\mathbf{r}} \, \phi(\mathbf{r}) = \int \langle \mathbf{r}|\hat{p}^2|\mathbf{r}'\rangle \phi(\mathbf{r}') \, \mathrm{d}^3 r', \tag{2.114}$$

which identifies the kernel as

$$\langle \mathbf{r}|\hat{p}^2|\mathbf{r}'\rangle = -\hbar^2 \, \Delta_{\mathbf{r}} \, \delta(\mathbf{r} - \mathbf{r}'). \tag{2.115}$$

Two remarks are in order. First, (2.115) is a distribution, not a function: the Laplacian of a Dirac distribution only makes sense under an integral. Second, and this is the

essential point, the kernel is proportional to $\delta(\mathbf{r}-\mathbf{r}')$, that is, $\hat{p}^2$ is a *local* operator. This is what will collapse the double integral of a general one-body operator into a single one.

Since $\delta(\mathbf{r}-\mathbf{r}')$ depends only on the difference of its arguments, the derivatives can be transferred from the delta onto the function multiplying it, by integrating by parts twice. This gives the equivalent, and more convenient, form

$$\langle \mathbf{r}|\hat{p}^2|\mathbf{r}'\rangle = -\hbar^2\,\delta(\mathbf{r}-\mathbf{r}')\,\Delta_{\mathbf{r}'}, \tag{2.116}$$

where $\Delta_{\mathbf{r}'}$ is now understood to act on whatever function of $\mathbf{r}'$ stands to its right, here the field operator $\hat{\psi}(\mathbf{r}')$. Inserting this into the general expression for a one-body operator, the delta function removes the integral over $\mathbf{r}'$ and we obtain

$$\hat{T} = \int \hat{\psi}^\dagger(\mathbf{r}) \left(-\frac{\hbar^2}{2m}\Delta\right) \hat{\psi}(\mathbf{r})\,\mathrm{d}^3 r. \tag{2.117}$$

The result has the familiar look of a kinetic-energy expectation value, with the wave-function replaced by the field operator.

Link with the single-body density matrix.

The expectation value of any one-body observable can also be obtained from the one-body reduced density matrix. For an N-particle state $\hat{\rho}$, we define

$$\hat{\rho}_1 = N\,\mathrm{Tr}_{2,\ldots,N}\,\hat{\rho}. \tag{2.118}$$

With this convention, $\mathrm{Tr}(\hat{\rho}_1) = N$, and

$$\langle \hat{B}\rangle = \mathrm{Tr}(\hat{b}\hat{\rho}_1). \tag{2.119}$$

Two-body operators. Consider a two-body observable of the form

$$\hat{C} = \sum_{i\neq j} \hat{c}_{i,j}, \tag{2.120}$$

where $\hat{c}$ acts on the two-particle Hilbert space. In a single-particle basis,

$$\hat{c}_{i,j} = \sum_{k_1',k_2',k_1,k_2} \langle k_1', k_2'|\hat{c}|k_1,k_2\rangle \times |i:k_1'\rangle|j:k_2'\rangle\langle i:k_1|\langle j:k_2|. \tag{2.121}$$

Note that the sum in (2.120) runs over *ordered* pairs $i\neq j$, and therefore counts each pair twice. A pairwise interaction is accordingly written with a compensating factor $1/2$,

$$\hat{V} = \frac{1}{2}\sum_{i\neq j} V(|\hat{\mathbf{r}}_i - \hat{\mathbf{r}}_j|) = \sum_{i<j} V(|\hat{\mathbf{r}}_i - \hat{\mathbf{r}}_j|), \tag{2.122}$$

and this factor $1/2$ will reappear in every expression for an interaction energy below. Another example, without the factor $1/2$, is the pair-density operator

$$\hat{\rho}_2(\mathbf{r},\mathbf{r}') = \sum_{i\neq j} \delta(\hat{\mathbf{r}}_i - \mathbf{r})\delta(\hat{\mathbf{r}}_j - \mathbf{r}'). \tag{2.123}$$

Two-body observables in second quantization.

The second-quantized form of a two-body operator is

$$\hat{C} = \sum_{k_1', k_2', k_1, k_2} \langle k_1', k_2' | \hat{c} | k_1, k_2 \rangle \hat{a}^\dagger_{k_1'} \hat{a}^\dagger_{k_2'} \hat{a}_{k_2} \hat{a}_{k_1}. \tag{2.124}$$

The ordering of the operators is important, in particular for fermions. Reading from right to left, the operator first annihilates a particle in k_1, then one in k_2, and subsequently creates particles in k_2' and k_1'. Note the reversed order of the two annihilation operators relative to the two creation operators; it is this arrangement that makes the fermionic signs come out correctly, and they are then generated automatically by the anticommutation relations.

For a local interaction potential $V(\mathbf{r} - \mathbf{r}')$, this expression becomes

$$\hat{V} = \frac{1}{2} \int \hat{\psi}^\dagger(\mathbf{r}) \hat{\psi}^\dagger(\mathbf{r}') V(\mathbf{r} - \mathbf{r}') \hat{\psi}(\mathbf{r}') \hat{\psi}(\mathbf{r}) \, \mathrm{d}^3 r \, \mathrm{d}^3 r'. \tag{2.125}$$

The same normal ordering applies here: the two creation operators stand to the left of the two annihilation operators. This is what removes any spurious self-interaction of a particle with itself, since $\hat{\psi}(\mathbf{r}')\hat{\psi}(\mathbf{r})$ annihilates two *distinct* particles. Using the commutation relations, the interaction can equivalently be written in terms of the pair density,

$$\hat{V} = \frac{1}{2} \int V(\mathbf{r} - \mathbf{r}') \, \hat{\rho}_2(\mathbf{r}, \mathbf{r}') \, \mathrm{d}^3 r \, \mathrm{d}^3 r', \qquad \hat{\rho}_2(\mathbf{r}, \mathbf{r}') = \hat{\psi}^\dagger(\mathbf{r}) \hat{\psi}^\dagger(\mathbf{r}') \hat{\psi}(\mathbf{r}') \hat{\psi}(\mathbf{r}). \tag{2.126}$$

Link with the two-body density matrix.

As for one-body observables, expectation values can be obtained from a reduced density matrix. We define the two-body reduced density matrix as

$$\hat{\rho}_2 = N(N-1) \, \mathrm{Tr}_{3,\ldots,N} \, \hat{\rho}, \tag{2.127}$$

the prefactor $N(N-1)$ being the number of ordered pairs, consistently with the convention of (2.120). With this choice,

$$\langle \hat{C} \rangle = \mathrm{Tr}(\hat{c} \hat{\rho}_2). \tag{2.128}$$

2.3.5 Evolution of quantum fields

We now have all the ingredients to write the Hamiltonian of a system of spinless particles in second quantization. For particles subject to a one-body potential $U(\mathbf{r})$ and a pairwise interaction $V(\mathbf{r} - \mathbf{r}')$, it reads

$$\hat{H} = \int \hat{\psi}^\dagger(\mathbf{r}) \left[-\frac{\hbar^2}{2m} \Delta + U(\mathbf{r}) \right] \hat{\psi}(\mathbf{r}) \, \mathrm{d}^3 r + \frac{1}{2} \int \hat{\psi}^\dagger(\mathbf{r}) \hat{\psi}^\dagger(\mathbf{r}') V(\mathbf{r} - \mathbf{r}') \hat{\psi}(\mathbf{r}') \hat{\psi}(\mathbf{r}) \, \mathrm{d}^3 r \, \mathrm{d}^3 r'. \tag{2.129}$$

We adopt the Heisenberg picture and define

$$\hat{\psi}_{\mathrm{H}}(\mathbf{r}, t) = \hat{U}^\dagger(t) \hat{\psi}(\mathbf{r}) \hat{U}(t), \tag{2.130}$$

where

$$\hat{U}(t) = \exp\left(-\frac{\mathrm{i} \hat{H} t}{\hbar} \right). \tag{2.131}$$

The Heisenberg equation of motion is

$$\mathrm{i}\hbar\partial_t\hat{\psi}_{\mathrm{H}}(\mathbf{r},t) = [\hat{\psi}_{\mathrm{H}}(\mathbf{r},t), \hat{H}]. \tag{2.132}$$

We henceforth omit the subscript H and the explicit time dependence.

The calculation relies on the canonical commutation or anticommutation relations. Introducing $\varepsilon = 1$ for bosons and $\varepsilon = -1$ for fermions, they can be written compactly as

$$\hat{\psi}(\mathbf{r})\hat{\psi}^\dagger(\mathbf{r}') = \delta(\mathbf{r}-\mathbf{r}') + \varepsilon\hat{\psi}^\dagger(\mathbf{r}')\hat{\psi}(\mathbf{r}). \tag{2.133}$$

This immediately gives

$$[\hat{\psi}(\mathbf{r}), \hat{\psi}^\dagger(\mathbf{r}_1)\hat{\psi}(\mathbf{r}_2)] = \delta(\mathbf{r}-\mathbf{r}_1)\hat{\psi}(\mathbf{r}_2). \tag{2.134}$$

For the quartic term, one similarly finds

$$\begin{aligned}&[\hat{\psi}(\mathbf{r}), \hat{\psi}^\dagger(\mathbf{r}_1)\hat{\psi}^\dagger(\mathbf{r}_2)\hat{\psi}(\mathbf{r}_2)\hat{\psi}(\mathbf{r}_1)] \\ &\quad = \delta(\mathbf{r}-\mathbf{r}_1)\hat{\psi}^\dagger(\mathbf{r}_2)\hat{\psi}(\mathbf{r}_2)\hat{\psi}(\mathbf{r}) + \delta(\mathbf{r}-\mathbf{r}_2)\hat{\psi}^\dagger(\mathbf{r}_1)\hat{\psi}(\mathbf{r}_1)\hat{\psi}(\mathbf{r}).\end{aligned} \tag{2.135}$$

The result is the same for bosons and fermions: the exchange signs cancel inside the complete interaction term.

Combining the one-body and two-body contributions, we obtain

$$\mathrm{i}\hbar\partial_t\hat{\psi}(\mathbf{r}) = \left[-\frac{\hbar^2}{2m}\Delta + U(\mathbf{r}) + \int V(\mathbf{r}-\mathbf{r}')\hat{\psi}^\dagger(\mathbf{r}')\hat{\psi}(\mathbf{r}')\,\mathrm{d}^3r'\right]\hat{\psi}(\mathbf{r}). \tag{2.136}$$

The first two terms have the same structure as the single-particle Schrödinger equation. The crucial difference is that $\hat{\psi}(\mathbf{r})$ is now a quantum operator rather than a classical wave-function. The last term represents the interaction with the other particles through the density operator $\hat{\psi}^\dagger(\mathbf{r}')\hat{\psi}(\mathbf{r}')$.

Equation (2.136) is therefore an operator equation of motion for the quantum field. This is the origin of the terminology "second quantization": rather than quantizing a classical field, the formalism provides a quantum field operator whose excitations correspond to particles.

Finally, we note that the Hamiltonian above contains as many creation as annihilation operators in every term. It therefore commutes with the total number operator,

$$[\hat{N}, \hat{H}] = 0, \tag{2.137}$$

so that the particle number is conserved and the dynamics does not mix the subspaces $\mathcal{E}_N$. The Fock-space description is nevertheless useful even in this case, since it handles the exchange symmetry automatically. It becomes indispensable when the number of particles is genuinely not conserved, as for photons emitted and absorbed by atoms, or for the Bogoliubov excitations encountered later in these notes, whose Hamiltonians do contain terms with unequal numbers of creation and annihilation operators.

2.4 Quantum statistics of composite particles

Many physical particles, such as nuclei, atoms, and molecules, are composite objects made of several elementary constituents. When the internal structure of such an object

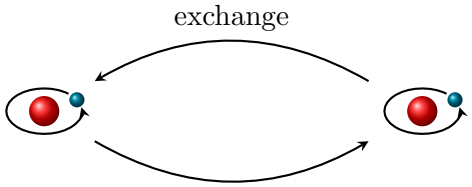


Figure 17: Scheme of the exchange of two identical composite particles, illustrated for two hydrogen atoms. Exchanging the two electrons gives a statistical phase of π, as does exchanging the two protons. The two phases add up to 2π, corresponding to an overall bosonic exchange symmetry.

can be neglected, for instance when its size is much smaller than the relevant interparticle distances, it can be treated as an effective pointlike particle. Its quantum statistics is then determined by the parity of the number of fermionic constituents: a composite object containing an even number of fermions behaves as a boson, while one containing an odd number of fermions behaves as a fermion.

This rule follows from the spin-statistics theorem together with the rules for composing angular momenta. It can also be understood directly by considering the exchange of two identical composite particles. During such an exchange, each set of identical fermionic constituents is effectively exchanged, and therefore contributes a minus sign. The total exchange phase is consequently $(-1)^{N_\mathrm{F}}$, where N_F is the number of fermionic constituents in the composite particle. The composite particle is therefore bosonic for even N_F and fermionic for odd N_F.

An illustration is given in Fig. 17 for the exchange of two hydrogen atoms. The hydrogen atom is composed of one proton and one electron, and therefore contains an even number of fermionic constituents. It can consequently behave as a bosonic particle. This bosonic quantum statistics is experimentally manifested, for instance, by the possibility of forming a Bose–Einstein condensate of hydrogen atoms, in which a macroscopic number of atoms occupy the same quantum state [36].

The most striking illustration of this counting rule is provided by the two stable isotopes of helium, which differ by a single neutron. The ^{4}He atom contains two protons, two neutrons and two electrons, hence six fermions: it is a boson, and becomes superfluid below 2.17 K. The ^{3}He atom contains one neutron less, hence five fermions: it is a fermion, and its superfluid transition requires the formation of Cooper pairs and occurs only in the millikelvin range, three orders of magnitude lower. A single neutron, buried deep inside the nucleus and utterly irrelevant to the chemistry of the atom, thus changes its collective behaviour completely. The same rule governs the choice of species in ultracold-atom experiments, where ^{87}Rb (124 fermions) is bosonic while ^{40}K (59 fermions) is fermionic.

At first sight, this behavior may seem to conflict with Pauli's exclusion principle, which prevents identical fermions from occupying the same single-particle state. The resolution is that the constituents of different composite particles can still be subject to Pauli exclusion, even though the composite particles themselves behave approximately as bosons. This approximation becomes particularly transparent in the dilute limit, where the wave-functions of the constituents belonging to different composite particles have little overlap.

When does a composite particle behave as a boson? To make this quantitative, we consider a many-body system formed by pairs of fermions of two species, denoted 1 and 2. We assume that the two fermions form a bound state described by the two-body wave-function $\phi(\mathbf{r}_1, \mathbf{r}_2)$. For simplicity, we consider pairs with zero center-of-mass momentum and write $\phi(\mathbf{r}_1, \mathbf{r}_2) = \phi(\mathbf{r}_1 - \mathbf{r}_2)$. We introduce the pair creation operator

$$\hat{c}^\dagger = \int \phi(\mathbf{r}_1 - \mathbf{r}_2)\hat{\psi}_1^\dagger(\mathbf{r}_1)\hat{\psi}_2^\dagger(\mathbf{r}_2)\,\mathrm{d}^3r_1\,\mathrm{d}^3r_2, \tag{2.138}$$

and consider a state in which pairs are coherently populated,

$$|\Psi\rangle \propto \exp(\alpha\hat{c}^\dagger)|\varnothing\rangle. \tag{2.139}$$

If the composite pairs behaved exactly as elementary bosons, $\hat{c}^\dagger$ would act as an ordinary bosonic creation operator, and one would expect the mean number of pairs to be $\langle\hat{N}\rangle = |\alpha|^2$. Pauli exclusion between the fermionic constituents can prevent multiple pairs from occupying the same internal state, however, leading to $\langle\hat{N}\rangle < |\alpha|^2$. We now quantify this effect.

We introduce the plane-wave decomposition

$$\phi(\mathbf{r}_1 - \mathbf{r}_2) = \frac{1}{V}\sum_{\mathbf{k}} \phi_{\mathbf{k}} \mathrm{e}^{\mathrm{i}\mathbf{k}\cdot(\mathbf{r}_1 - \mathbf{r}_2)}, \tag{2.140}$$

which gives

$$\hat{c}^\dagger = \sum_{\mathbf{k}} \phi_{\mathbf{k}} \hat{a}_{\mathbf{k},1}^\dagger \hat{a}_{-\mathbf{k},2}^\dagger. \tag{2.141}$$

Pair creation operators associated with different momenta commute. Moreover, because the two constituents are fermions,

$$\left(\hat{a}_{\mathbf{k},1}^\dagger \hat{a}_{-\mathbf{k},2}^\dagger\right)^2 = 0. \tag{2.142}$$

The latter relation expresses Pauli exclusion: a given pair state cannot be occupied more than once.

The coherent state can therefore be factorized into independent momentum sectors,

$$|\Psi\rangle \propto \prod_{\mathbf{k}} \exp\left(\alpha\phi_{\mathbf{k}} \hat{a}_{\mathbf{k},1}^\dagger \hat{a}_{-\mathbf{k},2}^\dagger\right)|\varnothing\rangle. \tag{2.143}$$

Since the square of each pair creation operator vanishes, the exponential truncates after the linear term:

$$|\Psi\rangle = \prod_{\mathbf{k}} \left(u_{\mathbf{k}} + v_{\mathbf{k}} \hat{a}_{\mathbf{k},1}^\dagger \hat{a}_{-\mathbf{k},2}^\dagger\right)|\varnothing\rangle, \tag{2.144}$$

where

$$\frac{v_{\mathbf{k}}}{u_{\mathbf{k}}} = \alpha\phi_{\mathbf{k}}, \qquad |u_{\mathbf{k}}|^2 + |v_{\mathbf{k}}|^2 = 1. \tag{2.145}$$

The mean number of particles of either species is then

$$\langle\hat{N}\rangle = \sum_{\mathbf{k}} \langle\hat{a}_{\mathbf{k},1}^\dagger \hat{a}_{\mathbf{k},1}\rangle \tag{2.146}$$

$$= \sum_{\mathbf{k}} |v_{\mathbf{k}}|^2 \tag{2.147}$$

$$= |\alpha|^2 \sum_{\mathbf{k}} \frac{|\phi_{\mathbf{k}}|^2}{1 + |\alpha|^2|\phi_{\mathbf{k}}|^2}. \tag{2.148}$$

The normalization of the pair wave-function is fixed by requiring the one-pair state $\hat{c}^\dagger|\varnothing\rangle$ to be normalized, which gives

$$\sum_{\mathbf{k}} |\phi_{\mathbf{k}}|^2 = 1. \tag{2.149}$$

We then see that

$$\langle \hat{N} \rangle \simeq |\alpha|^2 \tag{2.150}$$

whenever

$$|\alpha|^2 |\phi_{\mathbf{k}}|^2 \ll 1 \qquad \text{for all } \mathbf{k}. \tag{2.151}$$

Thus, in this regime,

$$\text{bosonic behavior} \quad \Longleftrightarrow \quad \langle \hat{N} \rangle \simeq |\alpha|^2 \quad \Longleftrightarrow \quad |\alpha|^2 |\phi_{\mathbf{k}}|^2 \ll 1 \quad \text{for all } \mathbf{k}. \tag{2.152}$$

Let us express this condition in terms of the spatial size of the composite particle. If σ denotes the characteristic size of the bound state, its momentum-space wave-function typically extends over a volume of order σ^{-3}. In a quantization volume V, this gives the estimate

$$\max_{\mathbf{k}} |\phi_{\mathbf{k}}| \simeq \sqrt{\frac{\sigma^3}{V}}. \tag{2.153}$$

The condition for bosonic behavior then becomes

$$|\alpha|^2 \frac{\sigma^3}{V} \ll 1. \tag{2.154}$$

Since $\langle \hat{N} \rangle \simeq |\alpha|^2$ in this regime and $\rho = \langle \hat{N} \rangle / V$ is the particle density of either species, we obtain the simple criterion

$$\text{bosonic behavior} \quad \Longleftrightarrow \quad \rho \sigma^3 \ll 1. \tag{2.155}$$

This condition has a simple physical interpretation: the composite particle behaves as a pointlike boson when there is, on average, much less than one constituent particle of the same species within the volume σ^3 occupied by the bound state. In this dilute regime, Pauli exclusion between constituents belonging to different composite particles is unlikely to play a role, and the composite objects behave approximately as elementary bosons.

The same criterion is obtained by examining directly the commutation relation of the pair operators. For an ideal bosonic mode one would require $[\hat{c}, \hat{c}^\dagger] = 1$, whereas a short calculation using the fermionic anticommutation relations gives

$$[\hat{c}, \hat{c}^\dagger] = 1 - \sum_{\mathbf{k}} |\phi_{\mathbf{k}}|^2 \left(\hat{n}_{\mathbf{k},1} + \hat{n}_{-\mathbf{k},2} \right), \tag{2.156}$$

where (2.149) has been used and $\hat{n}_{\mathbf{k},s}$ is the occupation of the mode $\mathbf{k}$ of species s. The pair operator is therefore bosonic only up to a correction measuring how much the constituent modes are already occupied. Using $|\phi_{\mathbf{k}}|^2 \simeq \sigma^3/V$ and $\langle \hat{n}_{\mathbf{k},s} \rangle \simeq \rho\sigma^3$ in the dilute regime, this correction is again of order $\rho\sigma^3$, in agreement with the criterion above. A more detailed analysis of the bosonic behavior of composite particles can be found in [37, 38].

The opposite limit and the BEC–BCS crossover. It is instructive to ask what happens when the criterion fails. For $|\alpha|^2|\phi_{\mathbf{k}}|^2 \gg 1$ the occupations saturate, $|v_{\mathbf{k}}|^2 \to 1$, and each pair mode is filled at most once, as Pauli exclusion demands. The mean particle number then grows much more slowly than $|\alpha|^2$, and the pairs can no longer be regarded as independent bosons: their constituents strongly overlap, with many pairs sharing the same region of space.

The reader may recognize in the state obtained above,

$$|\Psi\rangle = \prod_{\mathbf{k}} \left(u_{\mathbf{k}} + v_{\mathbf{k}} \hat{a}^\dagger_{\mathbf{k},1} \hat{a}^\dagger_{-\mathbf{k},2}\right) |\varnothing\rangle, \tag{2.157}$$

exactly the variational wave-function of BCS theory, (7.7), with the two species playing the role of the two spin states of the electron. The two limits considered here are then the two ends of the same physical family: for $\rho\sigma^3 \ll 1$ the pairs are small, tightly bound molecules that condense as elementary bosons, whereas for $\rho\sigma^3 \gg 1$ they are large, strongly overlapping Cooper pairs. The continuous evolution between the two regimes is the BEC–BCS crossover, discussed in Section 7 and illustrated in Fig. 47.

2.5 (∗) From classical to quantum fields: a vibrating string

The quantization of the field operator introduced earlier is a particular example of a more general procedure for transforming a classical field theory into a quantum one. We consider here a simple example, namely a vibrating string. The same procedure can be applied in other contexts, such as the quantization of the electromagnetic field. We do not consider here the quantum field theory of relativistic particles, which is treated in a separate course.

We consider a string stretched between two points separated by a distance L along the x axis (see Fig. 18). We denote by ρ the mass per unit length and by T the string tension. The vibration of the string along the z direction is described by the time-dependent field $\phi(x,t)$, representing the transverse displacement at position x. The Lagrangian of the system is

$$\mathcal{L}_{\text{tot}} = E_{\text{kin}} - E_{\text{pot}} \tag{2.158}$$

$$= \frac{\rho}{2} \int \dot{\phi}^2 \mathrm{d}x - T \int \sqrt{\mathrm{d}x^2 + \mathrm{d}\phi^2} \tag{2.159}$$

$$\simeq \frac{\rho}{2} \int \dot{\phi}^2 \mathrm{d}x - T \int \left[1 + \frac{1}{2}(\partial_x \phi)^2\right] \mathrm{d}x, \tag{2.160}$$

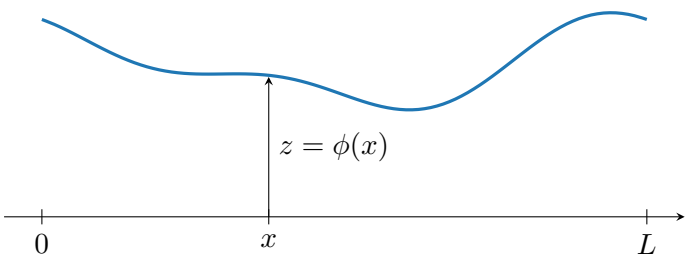


Figure 18: Scheme of a string stretched along the x axis over a distance L. The transverse displacement of the string at position x is described by the field $\phi(x)$.

where we have assumed small transverse displacements, or equivalently small angles between the string and the x axis. Dropping the constant contribution TL, the Lagrangian can be written as the integral of a Lagrangian density,

$$\mathcal{L}_{\text{tot}} = \int \mathcal{L}[\dot{\phi}(x), \phi(x)]\mathrm{d}x, \tag{2.161}$$

$$\mathcal{L}(\dot{\phi}, \phi) = \frac{\rho}{2}\dot{\phi}^2 - \frac{T}{2}(\partial_x \phi)^2. \tag{2.162}$$

The evolution of the field is obtained from the Euler–Lagrange equation. For a field theory, the Lagrangian density depends not only on ϕ and $\dot{\phi}$ but also on the spatial derivative $\partial_x \phi$, which contributes an additional term compared with the familiar equation for a point particle,

$$\partial_t \left(\frac{\partial \mathcal{L}}{\partial \dot{\phi}} \right) + \partial_x \left(\frac{\partial \mathcal{L}}{\partial (\partial_x \phi)} \right) - \frac{\partial \mathcal{L}}{\partial \phi} = 0. \tag{2.163}$$

Here $\mathcal{L}$ does not depend on ϕ itself, and

$$\frac{\partial \mathcal{L}}{\partial \dot{\phi}} = \rho\, \dot{\phi}, \qquad \frac{\partial \mathcal{L}}{\partial (\partial_x \phi)} = -T\, \partial_x \phi, \tag{2.164}$$

so that we obtain

$$\rho\, \ddot{\phi} = T\, \partial_x^2 \phi. \tag{2.165}$$

This is the usual wave equation, with propagation velocity

$$v = \sqrt{\frac{T}{\rho}}. \tag{2.166}$$

Before quantizing the field theory, it is useful to express the Hamiltonian and identify the canonical momentum conjugate to the field $\phi(x, t)$. It is obtained from the Lagrangian density as

$$\pi(x, t) = \frac{\partial \mathcal{L}}{\partial \dot{\phi}} = \rho\, \dot{\phi}. \tag{2.167}$$

The Hamiltonian is then

$$H = \int \mathcal{H}[\phi(x), \pi(x)]\mathrm{d}x, \tag{2.168}$$

where the Hamiltonian density is

$$\mathcal{H}(\phi, \pi) = \pi\dot{\phi} - \mathcal{L}(\dot{\phi}, \phi) \tag{2.169}$$

$$= \frac{\pi^2}{2\rho} + \frac{T}{2}(\partial_x \phi)^2. \tag{2.170}$$

Quantization proceeds by promoting the classical fields to quantum field operators,

$$\phi \to \hat{\phi}, \qquad \pi \to \hat{\pi}, \tag{2.171}$$

and imposing the canonical commutation relations

$$[\hat{\phi}(x), \hat{\phi}(x')] = 0, \tag{2.172}$$

$$[\hat{\pi}(x), \hat{\pi}(x')] = 0, \tag{2.173}$$

$$[\hat{\phi}(x), \hat{\pi}(x')] = \mathrm{i}\hbar\, \delta(x - x'). \tag{2.174}$$

The resulting quantum Hamiltonian is

$$\hat{H} = \int \left[\frac{\hat{\pi}(x)^2}{2\rho} + \frac{T}{2} (\partial_x \hat{\phi}(x))^2 \right] \mathrm{d}x. \tag{2.175}$$

At this stage, one may wonder whether quantizing a classical field can also involve fermionic field operators. The answer is already contained in the canonical relations: $\hat{\phi}$ and $\hat{\pi}$ obey a *commutator*, not an anticommutator, because they descend from classical quantities whose values are ordinary numbers that can be added and measured simultaneously in the classical limit. The ladder operators built from them are therefore necessarily bosonic. More generally, classical fields whose amplitude can take arbitrary values are described by bosonic quantum fields.[3] This is why the collective excitations of a medium – phonons here, but also magnons, plasmons or photons – are always bosonic, whatever the statistics of the underlying constituents.

To determine the spectrum of $\hat{H}$, we exploit the translational invariance of the string and introduce a momentum-space representation. For convenience, we impose periodic boundary conditions, so that

$$k = \frac{2\pi p}{L}, \qquad p \in \mathbb{Z}. \tag{2.176}$$

We define the Fourier components

$$\hat{\phi}_k = \frac{1}{\sqrt{L}} \int_0^L \mathrm{e}^{-\mathrm{i}kx} \hat{\phi}(x) \mathrm{d}x, \tag{2.177}$$

$$\hat{\pi}_k = \frac{1}{\sqrt{L}} \int_0^L \mathrm{e}^{\mathrm{i}kx} \hat{\pi}(x) \mathrm{d}x. \tag{2.178}$$

The opposite sign in the two exponents is deliberate: it is what makes the canonical commutator diagonal, $\propto \delta_{kk'}$ rather than $\delta_{k,-k'}$. With these conventions,

$$[\hat{\phi}_k, \hat{\phi}_{k'}] = 0, \tag{2.179}$$

$$[\hat{\pi}_k, \hat{\pi}_{k'}] = 0, \tag{2.180}$$

$$[\hat{\phi}_k, \hat{\pi}_{k'}] = \mathrm{i}\hbar\, \delta_{kk'}. \tag{2.181}$$

Since $\hat{\phi}(x)$ and $\hat{\pi}(x)$ are Hermitian, their Fourier components satisfy

$$\hat{\phi}_{-k} = \hat{\phi}_k^\dagger, \qquad \hat{\pi}_{-k} = \hat{\pi}_k^\dagger. \tag{2.182}$$

Let us first consider the potential energy. Inverting the Fourier transform,

$$\hat{\phi}(x) = \frac{1}{\sqrt{L}} \sum_k \mathrm{e}^{\mathrm{i}kx} \hat{\phi}_k, \qquad \partial_x \hat{\phi}(x) = \frac{1}{\sqrt{L}} \sum_k \mathrm{i}k\, \mathrm{e}^{\mathrm{i}kx} \hat{\phi}_k, \tag{2.183}$$

and inserting this decomposition, one obtains

$$\int_0^L (\partial_x \hat{\phi})^2 \mathrm{d}x = \sum_{k,k'} (\mathrm{i}k)(\mathrm{i}k') \hat{\phi}_k \hat{\phi}_{k'} \frac{1}{L} \int_0^L \mathrm{e}^{\mathrm{i}(k+k')x} \mathrm{d}x \tag{2.184}$$

$$= \sum_k k^2 \hat{\phi}_{-k} \hat{\phi}_k \tag{2.185}$$

$$= \sum_k k^2 \hat{\phi}_k^\dagger \hat{\phi}_k. \tag{2.186}$$

[3] It is possible to define fermionic coherent states, whose amplitudes are Grassmann numbers. However, these states do not provide a quantum description of a classical field with an ordinary commuting amplitude.

A similar calculation for the kinetic energy gives

$$\hat{H} = \sum_k \hat{H}_k, \tag{2.187}$$

with

$$\hat{H}_k = \frac{1}{2\rho}\hat{\pi}_k^\dagger \hat{\pi}_k + \frac{\rho\omega_k^2}{2}\hat{\phi}_k^\dagger \hat{\phi}_k, \tag{2.188}$$

where

$$\omega_k = v|k|. \tag{2.189}$$

Thus, the Hamiltonian contains no coupling between different momentum modes, as expected from translational invariance.

For every non-zero momentum mode, $\hat{H}_k$ has the form of a harmonic oscillator. We therefore introduce the annihilation operator

$$\hat{a}_k = \sqrt{\frac{\rho\omega_k}{2\hbar}}\left(\hat{\phi}_k + \frac{\mathrm{i}}{\rho\omega_k}\hat{\pi}_k^\dagger\right), \qquad k \neq 0. \tag{2.190}$$

Using the canonical commutation relations, one verifies that

$$[\hat{a}_k, \hat{a}_{k'}^\dagger] = \delta_{kk'}, \qquad [\hat{a}_k, \hat{a}_{k'}] = [\hat{a}_k^\dagger, \hat{a}_{k'}^\dagger] = 0. \tag{2.191}$$

The Hamiltonian can consequently be written as a collection of independent harmonic oscillators,

$$\hat{H} = \sum_{k\neq 0} \hbar\omega_k \left(\hat{a}_k^\dagger \hat{a}_k + \frac{1}{2}\right) + \hat{H}_{k=0}. \tag{2.192}$$

The $k = 0$ mode corresponds to a uniform displacement of the string and has $\omega_0 = 0$; it therefore does not form a harmonic oscillator and must be treated separately. It can be omitted if the overall displacement of the string is fixed.

Each non-zero momentum mode can be populated by an arbitrary integer number of quanta. These quanta are called phonons: each phonon is characterized by a wave-vector k and carries an energy

$$E_k = \hbar\omega_k. \tag{2.193}$$

Thus, quantizing the classical vibrating string transforms its normal modes into quantum harmonic oscillators.

It is worth contrasting this construction with the one of Section 2.3. There, we started from particles and built a field operator $\hat{\psi}(\mathbf{r})$ to describe them; here, we started from a classical field and found that its quantized excitations behave as particles. The two routes meet in the same formalism, which is the reason for the name "second quantization". There is, however, an important difference. The phonons obtained here are not elementary constituents but *emergent* excitations of a medium, and their number is not conserved: the Hamiltonian of an anharmonic string, for instance, contains terms with unequal numbers of $\hat{a}_k$ and $\hat{a}_k^\dagger$, which create and destroy phonons. This is precisely the situation in which the Fock-space description becomes indispensable rather than merely convenient.

Finally, we note that the zero-point contribution $\sum_{k\neq 0} \hbar\omega_k/2$ diverges when arbitrarily large wave-vectors are allowed. For a physical string this is not a difficulty: the continuum description breaks down below the interatomic distance, which provides a natural cutoff on k. Only energy *differences* are measurable, and these are unaffected by the constant zero-point term.

2.6 Gaussian quantum states and Wick theorem

Gaussian states form an important class of many-body states for which expectation values of products of operators can be expressed in terms of two-point correlation functions. They occur naturally in a wide range of contexts, including ideal gases at thermal equilibrium and interacting systems treated within a quadratic mean-field approximation.

A Gaussian state is a state whose density matrix can be written, up to normalization, as the exponential of a quadratic operator,

$$\hat{\rho} = \frac{1}{\mathcal{Z}} \exp(-\hat{H}), \tag{2.194}$$

where $\hat{H}$ is a dimensionless quadratic Hamiltonian. As shown in section 5, such a Hamiltonian can be brought, using a Bogoliubov transformation, to the form

$$\hat{H} = \sum_k E_k \, \hat{a}_k^\dagger \hat{a}_k, \tag{2.195}$$

where the $\hat{a}_k$'s are the ladder operators of the normal modes.

A familiar example is an ideal gas at thermal equilibrium in the grand-canonical ensemble,

$$\hat{\rho} = \frac{1}{\Xi} \exp[-\beta(\hat{H} - \mu \hat{N})], \tag{2.196}$$

which is Gaussian because $\hat{H} - \mu\hat{N}$ is quadratic in the ladder operators. Gaussian states also arise when interacting systems are approximated by an effective quadratic Hamiltonian.

The main simplification provided by Gaussian states is analogous to the familiar property of Gaussian random variables: all higher-order moments can be expressed in terms of two-point moments. This result is known as Wick's theorem.

We consider an observable written as a product

$$\hat{O} = \hat{b}_1 \cdots \hat{b}_p, \tag{2.197}$$

where each $\hat{b}_i$ is a linear combination of creation and annihilation operators. Since a quadratic Hamiltonian preserves fermion-number parity, and similarly for bosons, the density matrix commutes with the parity operator. Consequently, the expectation value of a product containing an odd number of ladder operators vanishes:

$$\langle \hat{b}_1 \cdots \hat{b}_{2n+1} \rangle = 0. \tag{2.198}$$

We therefore restrict our attention to an even number $2n$ of operators.

Wick theorem for fermions. The essential step is to express a $2n$-point expectation value in terms of lower-order ones. We first consider a normal mode of the Hamiltonian (2.195). Since

$$\hat{H} = \sum_k E_k \hat{a}_k^\dagger \hat{a}_k, \tag{2.199}$$

one readily finds

$$\hat{a}_k \, \hat{\rho} = \mathrm{e}^{-E_k} \, \hat{\rho} \, \hat{a}_k, \tag{2.200}$$

$$\hat{a}_k^\dagger \, \hat{\rho} = \mathrm{e}^{E_k} \, \hat{\rho} \, \hat{a}_k^\dagger. \tag{2.201}$$

To establish (2.200), note that $\hat{\rho} \propto \exp(-\sum_j E_j \hat{n}_j)$ factorizes over the modes, and that every factor commutes with $\hat{a}_k$ except the one associated with the mode k itself. For that mode, the elementary relation

$$\hat{n}_k \hat{a}_k = \hat{a}_k (\hat{n}_k - 1), \tag{2.202}$$

which holds for bosons as well as for fermions, implies more generally

$$\hat{a}_k \, f(\hat{n}_k) = f(\hat{n}_k + 1) \, \hat{a}_k \tag{2.203}$$

for an arbitrary function f, as is immediately checked by acting on a Fock state $|n_k\rangle$. Applying this with $f(x) = \mathrm{e}^{-E_k x}$ gives

$$\hat{a}_k \, \mathrm{e}^{-E_k \hat{n}_k} = \mathrm{e}^{-E_k(\hat{n}_k+1)} \, \hat{a}_k = \mathrm{e}^{-E_k} \, \mathrm{e}^{-E_k \hat{n}_k} \, \hat{a}_k, \tag{2.204}$$

which is the announced relation: commuting an annihilation operator through the density matrix simply costs a factor e^{-E_k}, because it lowers by one the occupation of the mode k appearing in the exponent. The second relation follows by taking the Hermitian conjugate of the first and using $\hat{\rho}^\dagger = \hat{\rho}$.

These relations allow us to move a ladder operator through the density matrix inside a trace. Rewriting the first of them as $\hat{\rho} \, \hat{a}_k = \mathrm{e}^{E_k} \hat{a}_k \hat{\rho}$, and taking $\hat{b}_1 = \hat{a}_k$ for definiteness, cyclicity of the trace gives

$$\begin{aligned} \langle \hat{b}_1 \cdots \hat{b}_{2n} \rangle &= \mathrm{Tr}(\hat{\rho} \, \hat{b}_1 \cdots \hat{b}_{2n}) && (2.205) \\ &= \mathrm{e}^{E_k} \, \mathrm{Tr}(\hat{b}_1 \, \hat{\rho} \, \hat{b}_2 \cdots \hat{b}_{2n}) && (2.206) \\ &= \mathrm{e}^{E_k} \, \mathrm{Tr}(\hat{\rho} \, \hat{b}_2 \cdots \hat{b}_{2n} \hat{b}_1). && (2.207) \end{aligned}$$

For a fermionic operator, we now move $\hat{b}_1$ successively through the other operators. At each step we use

$$\hat{b}_i \hat{b}_1 = -\hat{b}_1 \hat{b}_i + \{\hat{b}_i, \hat{b}_1\}. \tag{2.208}$$

This gives

$$\begin{aligned} \hat{b}_2 \cdots \hat{b}_{2n} \hat{b}_1 = \sum_{i=2}^{2n} (-1)^i \{\hat{b}_i, \hat{b}_1\} \hat{b}_2 \cdots \hat{b}_{i-1} \hat{b}_{i+1} \cdots \hat{b}_{2n} \\ - \hat{b}_1 \hat{b}_2 \cdots \hat{b}_{2n}. \end{aligned} \tag{2.209}$$

Taking the expectation value and using the previous relation therefore gives

$$\begin{aligned} \left(1 + \mathrm{e}^{E_k}\right) \langle \hat{b}_1 \cdots \hat{b}_{2n} \rangle = \mathrm{e}^{E_k} \sum_{i=2}^{2n} (-1)^i \{\hat{b}_i, \hat{b}_1\} \\ \times \langle \hat{b}_2 \cdots \hat{b}_{i-1} \hat{b}_{i+1} \cdots \hat{b}_{2n} \rangle. \end{aligned} \tag{2.210}$$

The same calculation applies when $\hat{b}_1 = \hat{a}_k^\dagger$, with the replacement $E_k \to -E_k$. In either case, the coefficient multiplying the anticommutator is precisely the corresponding two-point expectation value. Indeed, applying the above argument to a product of two operators gives

$$\langle \hat{b}_1 \hat{b}_i \rangle = \frac{\{\hat{b}_1, \hat{b}_i\}}{1 + \mathrm{e}^{-E_k}} \qquad \text{for } \hat{b}_1 = \hat{a}_k, \tag{2.211}$$

and the same expression with $E_k \to -E_k$ when $\hat{b}_1 = \hat{a}_k^\dagger$. As a check, the simplest case reproduces the Fermi–Dirac occupation of the normal mode,

$$\langle \hat{a}_k^\dagger \hat{a}_k \rangle = \frac{1}{1+\mathrm{e}^{E_k}}, \qquad \langle \hat{a}_k \hat{a}_k^\dagger \rangle = \frac{1}{1+\mathrm{e}^{-E_k}}, \tag{2.212}$$

whose sum is indeed equal to one. We consequently obtain the recursion relation

$$\langle \hat{b}_1 \cdots \hat{b}_{2n} \rangle = \sum_{i=2}^{2n} (-1)^i \langle \hat{b}_1 \hat{b}_i \rangle \langle \hat{b}_2 \cdots \hat{b}_{i-1} \hat{b}_{i+1} \cdots \hat{b}_{2n} \rangle. \tag{2.213}$$

The argument was presented for a single ladder operator, but the result extends by linearity to arbitrary linear combinations of creation and annihilation operators. This point deserves emphasis. The normal modes $\hat{a}_k$ appearing in (2.195) are the *quasiparticle* operators obtained after the Bogoliubov transformation, and are in general linear combinations of the creation *and* annihilation operators of the original particles. Expressed in terms of the latter, a Gaussian state therefore possesses non-vanishing *anomalous* averages such as $\langle \hat{a}_{\mathbf{k}} \hat{a}_{-\mathbf{k}} \rangle$, in addition to the usual occupations $\langle \hat{a}_{\mathbf{k}}^\dagger \hat{a}_{\mathbf{k}} \rangle$. All of these must be retained as possible pairings when applying the theorem, as will be the case for the Bogoliubov and BCS ground states studied later in these notes.

Iterating the recursion relation gives Wick's theorem for fermions:

$$\langle \hat{b}_1 \cdots \hat{b}_{2n} \rangle = \sum_{\text{pairings } \sigma} \varepsilon(\sigma) \langle \hat{b}_{\sigma(1)} \hat{b}_{\sigma(2)} \rangle \cdots \langle \hat{b}_{\sigma(2n-1)} \hat{b}_{\sigma(2n)} \rangle, \tag{2.214}$$

where the sum runs over all possible pairings of the $2n$ operators, and $\varepsilon(\sigma)$ is the sign of the permutation required to bring the paired operators next to each other. The number of distinct pairings is

$$\frac{(2n)!}{2^n n!}. \tag{2.215}$$

For four operators, there are three possible pairings, giving

$$\langle \hat{b}_1 \hat{b}_2 \hat{b}_3 \hat{b}_4 \rangle = \langle \hat{b}_1 \hat{b}_2 \rangle \langle \hat{b}_3 \hat{b}_4 \rangle - \langle \hat{b}_1 \hat{b}_3 \rangle \langle \hat{b}_2 \hat{b}_4 \rangle + \langle \hat{b}_1 \hat{b}_4 \rangle \langle \hat{b}_2 \hat{b}_3 \rangle. \tag{2.216}$$

Note that the number of distinct pairings increases very fast with the number of operators: for $2n = 6$ there are 15 pairings, and for $2n = 8$ there are 105 pairings.

Bosons. For bosons, the same argument applies, except that exchanging two operators does not produce a minus sign. Wick's theorem therefore takes the form

$$\langle \hat{b}_1 \cdots \hat{b}_{2n} \rangle = \sum_{\text{pairings } \sigma} \langle \hat{b}_{\sigma(1)} \hat{b}_{\sigma(2)} \rangle \cdots \langle \hat{b}_{\sigma(2n-1)} \hat{b}_{\sigma(2n)} \rangle. \tag{2.217}$$

Thus the difference between bosons and fermions is entirely contained in the sign associated with exchanging fermionic operators.

As a simple example, consider the ground state of a harmonic oscillator, which is a Gaussian state: it is the zero-temperature limit of $\hat{\rho} \propto \mathrm{e}^{-E\hat{a}^\dagger \hat{a}}$ for $E \to \infty$. The non-zero second-order moments of the ladder operators are

$$\langle \hat{a} \hat{a}^\dagger \rangle = 1, \tag{2.218}$$

$$\langle \hat{a} \hat{a} \rangle = \langle \hat{a}^\dagger \hat{a}^\dagger \rangle = \langle \hat{a}^\dagger \hat{a} \rangle = 0. \tag{2.219}$$

Introducing the position operator

$$\hat{x} = \sigma(\hat{a} + \hat{a}^\dagger), \qquad \sigma^2 = \frac{\hbar}{2m\omega}, \tag{2.220}$$

we obtain

$$\langle \hat{x}^2 \rangle = \sigma^2 \langle (\hat{a} + \hat{a}^\dagger)^2 \rangle = \sigma^2. \tag{2.221}$$

Wick's theorem then immediately gives

$$\langle \hat{x}^4 \rangle = 3\langle \hat{x}^2 \rangle^2 = 3\sigma^4. \tag{2.222}$$

More generally, Wick's theorem allows higher-order correlation functions to be reduced to products of two-point correlation functions. This property will be used in the following sections to simplify the calculation of many-body correlation functions.

3 Coherence and correlations in many-body systems

Correlation functions play a central role in the description and understanding of quantum many-body systems in terms of simple observables. They can be used to identify phases of matter, characterized for instance by the existence of long-range phase ordering or translation symmetry breaking. They are also intimately linked to the spatial structure of entanglement between particles within a many-body system.

3.1 First-order correlation function and coherence properties

3.1.1 Definition and basic properties

We first consider the first-order spatial correlation function

$$g_1(\mathbf{r},\mathbf{r}') = \langle \hat{\psi}^\dagger(\mathbf{r})\hat{\psi}(\mathbf{r}')\rangle. \tag{3.1}$$

This definition corresponds to the expectation value of a single-particle operator $\hat{B} = \sum_i \hat{b}_i$, with $\hat{b} = |\mathbf{r}\rangle\langle\mathbf{r}'|$ acting on particle i. Indeed, inserting the matrix elements $\langle \mathbf{r}_1|\hat{b}|\mathbf{r}_2\rangle = \delta(\mathbf{r}_1-\mathbf{r})\delta(\mathbf{r}_2-\mathbf{r}')$ into the general second-quantized form of a one-body operator gives precisely $\hat{B} = \hat{\psi}^\dagger(\mathbf{r})\hat{\psi}(\mathbf{r}')$. Using $\langle\hat{B}\rangle = \mathrm{Tr}(\hat{b}\hat{\rho}_1)$, the g_1 function can then be written as

$$g_1(\mathbf{r},\mathbf{r}') = \mathrm{Tr}\left(|\mathbf{r}\rangle\langle\mathbf{r}'|\hat{\rho}_1\right) = \langle\mathbf{r}'|\hat{\rho}_1|\mathbf{r}\rangle,$$

i.e. it is a matrix element of the single-particle density matrix in position space, the two arguments appearing in reverse order. Recalling the definition of the single-particle density matrix

$$\hat{\rho}_1 = N\,\mathrm{Tr}_{2,\ldots,N}\,\hat{\rho}, \tag{3.2}$$

the g_1 function can then be expressed in terms of the wave-function $\psi(\mathbf{r}_1,\ldots,\mathbf{r}_N)$ of a pure many-body state as

$$g_1(\mathbf{r},\mathbf{r}') = \int \psi^*(\mathbf{r}_1=\mathbf{r},\mathbf{r}_2,\ldots,\mathbf{r}_N)\psi(\mathbf{r}_1=\mathbf{r}',\mathbf{r}_2,\ldots,\mathbf{r}_N)\,\mathrm{d}^3r_2\cdots\mathrm{d}^3r_N. \tag{3.3}$$

Three properties follow directly from this definition. First, the diagonal values of g_1 give the particle density,

$$g_1(\mathbf{r},\mathbf{r}) = \langle\hat{\psi}^\dagger(\mathbf{r})\hat{\psi}(\mathbf{r})\rangle = \rho(\mathbf{r}), \tag{3.4}$$

whose integral is the total particle number, $\int g_1(\mathbf{r},\mathbf{r})\,\mathrm{d}^3r = N$. Second, g_1 is Hermitian,

$$g_1(\mathbf{r}',\mathbf{r}) = g_1(\mathbf{r},\mathbf{r}')^*, \tag{3.5}$$

as follows from the Hermiticity of $\hat{\rho}_1$. Third, since $\hat{\rho}_1$ is a positive operator, the Cauchy–Schwarz inequality bounds its off-diagonal elements by the diagonal ones,

$$|g_1(\mathbf{r},\mathbf{r}')| \le \sqrt{\rho(\mathbf{r})\,\rho(\mathbf{r}')}. \tag{3.6}$$

It is therefore natural to introduce the *normalized* first-order correlation function

$$g^{(1)}(\mathbf{r},\mathbf{r}') = \frac{g_1(\mathbf{r},\mathbf{r}')}{\sqrt{\rho(\mathbf{r})\,\rho(\mathbf{r}')}}, \qquad \left|g^{(1)}(\mathbf{r},\mathbf{r}')\right| \le 1, \tag{3.7}$$

which measures the degree of coherence between the two points independently of the local density. It equals unity in modulus for a perfectly coherent field, and the distance over which it decays defines the *coherence length* of the system.

The g_1 function can be used to express the expectation value of any single-particle operator $\hat{B} = \sum_{i=1}^{N} \hat{b}_i$ once given the matrix elements $\langle \mathbf{r}|\hat{b}|\mathbf{r}'\rangle$ of the operator $\hat{b}$. Indeed, one writes

$$\hat{B} = \int \langle \mathbf{r}|\hat{b}|\mathbf{r}'\rangle \hat{\psi}^\dagger(\mathbf{r})\hat{\psi}(\mathbf{r}')\,\mathrm{d}^3r\,\mathrm{d}^3r' \tag{3.8}$$

and take the expectation value

$$\langle \hat{B}\rangle = \int \langle \mathbf{r}|\hat{b}|\mathbf{r}'\rangle g_1(\mathbf{r},\mathbf{r}')\,\mathrm{d}^3r\,\mathrm{d}^3r'. \tag{3.9}$$

3.1.2 Link with the momentum distribution.

We assume in the following a translationally invariant system, such that $g_1(\mathbf{r},\mathbf{r}')$ only depends on the separation $\mathbf{r}'-\mathbf{r}$. One then usually sets the first argument to zero, and writes the first-order correlation function as

$$g_1(\mathbf{r}) = \langle \hat{\psi}^\dagger(\mathbf{0})\hat{\psi}(\mathbf{r})\rangle. \tag{3.10}$$

The g_1 function can be directly linked with the momentum distribution

$$n_{\mathbf{k}} = \langle \hat{a}^\dagger_{\mathbf{k}}\hat{a}_{\mathbf{k}}\rangle, \tag{3.11}$$

where we define the operator

$$\hat{a}_{\mathbf{k}} = \frac{1}{L^{d/2}} \int \mathrm{e}^{-\mathrm{i}\mathbf{k}\cdot\mathbf{r}}\hat{\psi}(\mathbf{r})\,\mathrm{d}^dr \tag{3.12}$$

annihilating a particle of momentum $\mathbf{k}$, where $V = L^d$ is the quantization box volume in dimension d. Inverting this relation,

$$\hat{\psi}(\mathbf{r}) = \frac{1}{L^{d/2}} \sum_{\mathbf{k}} \mathrm{e}^{\mathrm{i}\mathbf{k}\cdot\mathbf{r}}\hat{a}_{\mathbf{k}}, \tag{3.13}$$

one writes

$$g_1(\mathbf{r}) = \langle \hat{\psi}^\dagger(\mathbf{0})\hat{\psi}(\mathbf{r})\rangle \tag{3.14}$$

$$= \frac{1}{L^d} \sum_{\mathbf{k},\mathbf{k}'} \mathrm{e}^{\mathrm{i}\mathbf{k}'\cdot\mathbf{r}} \langle \hat{a}^\dagger_{\mathbf{k}}\hat{a}_{\mathbf{k}'}\rangle. \tag{3.15}$$

We now use translation invariance, which states that the system is unchanged when displaced by an arbitrary vector $\mathbf{a}$. Under such a displacement the field operator becomes $\hat{\psi}(\mathbf{r}-\mathbf{a})$, so that the mode operators merely acquire a phase,

$$\hat{a}_{\mathbf{k}} \longrightarrow \mathrm{e}^{-\mathrm{i}\mathbf{k}\cdot\mathbf{a}}\,\hat{a}_{\mathbf{k}}, \tag{3.16}$$

and the quantity $\langle \hat{a}^\dagger_{\mathbf{k}}\hat{a}_{\mathbf{k}'}\rangle$ gets multiplied by $\mathrm{e}^{\mathrm{i}(\mathbf{k}'-\mathbf{k})\cdot\mathbf{a}}$. Since it must be unchanged for *every* $\mathbf{a}$, it has to vanish unless the two phases compensate, that is unless $\mathbf{k} = \mathbf{k}'$:

$$\langle \hat{a}^\dagger_{\mathbf{k}}\hat{a}_{\mathbf{k}'}\rangle = n_{\mathbf{k}}\,\delta_{\mathbf{k},\mathbf{k}'}. \tag{3.17}$$

Only the populations of the momentum modes survive, and the double sum collapses to a single one,

$$g_1(\mathbf{r}) = \frac{1}{L^d} \sum_{\mathbf{k}} \mathrm{e}^{\mathrm{i}\mathbf{k}\cdot\mathbf{r}} n_{\mathbf{k}}, \tag{3.18}$$

$$= \frac{1}{(2\pi)^d} \int \mathrm{e}^{\mathrm{i}\mathbf{k}\cdot\mathbf{r}} n_{\mathbf{k}} \, \mathrm{d}^d k. \tag{3.19}$$

In other words, the g_1 function is the Fourier transform of the momentum distribution. This relation has an important practical consequence: the coherence length introduced above and the width of the momentum distribution are conjugate quantities, so that a broad momentum distribution corresponds to a short-ranged g_1, and conversely a sharply peaked momentum distribution – as for a Bose–Einstein condensate – to long-range coherence. It also provides the standard experimental route to g_1, since the momentum distribution is directly accessible, for instance by time-of-flight imaging of a released atomic gas.

3.2 Pair-distribution function and particle fluctuations

Pairwise correlations between the positions of particles are characterized by the second-order correlation function

$$g_2(\mathbf{r}, \mathbf{r}') = \langle \hat{\psi}^\dagger(\mathbf{r}) \hat{\psi}^\dagger(\mathbf{r}') \hat{\psi}(\mathbf{r}') \hat{\psi}(\mathbf{r}) \rangle, \tag{3.20}$$

also called the pair-distribution (or pair-correlation) function. This time, the g_2 function corresponds to the expectation value of a two-body observable $\hat{c} = |\mathbf{r}, \mathbf{r}'\rangle\langle \mathbf{r}, \mathbf{r}'|$. This allows one to express it in terms of the two-body reduced density matrix as

$$g_2(\mathbf{r}, \mathbf{r}') = \langle \mathbf{r}, \mathbf{r}' | \hat{\rho}_2 | \mathbf{r}, \mathbf{r}' \rangle. \tag{3.21}$$

For a pure many-body state of wave-function $\psi(\mathbf{r}_1, \ldots, \mathbf{r}_N)$, it is explicitely given by

$$g_2(\mathbf{r}, \mathbf{r}') = N(N-1) \int |\psi(\mathbf{r}_1 = \mathbf{r}, \mathbf{r}_2 = \mathbf{r}', \mathbf{r}_3, \ldots, \mathbf{r}_N)|^2 \, \mathrm{d}^3 r_3 \cdots \mathrm{d}^3 r_N, \tag{3.22}$$

the prefactor $N(N-1)$ being the one entering the definition of $\hat{\rho}_2$, that is the number of ordered pairs of particles.

The normal ordering of the operators, with both creation operators standing to the left, is essential: $g_2(\mathbf{r}, \mathbf{r}')$ is the joint probability density of detecting one particle at $\mathbf{r}$ *and another one* at $\mathbf{r}'$. It differs from the density–density correlation $\langle \hat{\rho}(\mathbf{r}) \hat{\rho}(\mathbf{r}') \rangle$ by a self-detection term $\delta(\mathbf{r} - \mathbf{r}')\rho(\mathbf{r})$, which is precisely what will produce the Poissonian contribution to the number fluctuations below.

Several properties follow immediately. The function is symmetric, $g_2(\mathbf{r}, \mathbf{r}') = g_2(\mathbf{r}', \mathbf{r})$, and positive, being the squared norm of $\hat{\psi}(\mathbf{r}')\hat{\psi}(\mathbf{r})|\Psi\rangle$. Its integral counts ordered pairs,

$$\int g_2(\mathbf{r}, \mathbf{r}') \, \mathrm{d}^3 r \, \mathrm{d}^3 r' = \langle \hat{N}(\hat{N} - 1) \rangle. \tag{3.23}$$

For fermions, $\hat{\psi}(\mathbf{r})\hat{\psi}(\mathbf{r}) = 0$ implies

$$g_2(\mathbf{r}, \mathbf{r}) = 0, \tag{3.24}$$

which is the Pauli hole: two identical fermions in the same internal state are never found at the same point. It is often convenient to normalize g_2 by the uncorrelated result, introducing

$$g^{(2)}(\mathbf{r},\mathbf{r}') = \frac{g_2(\mathbf{r},\mathbf{r}')}{\rho(\mathbf{r})\,\rho(\mathbf{r}')}, \tag{3.25}$$

which tends to one at large separation for a system without long-range order. Values $g^{(2)} > 1$ signal bunching, and $g^{(2)} < 1$ antibunching.

The second-order correlation function can be used to compute the fluctuations of the particle number

$$\hat{N}_\Omega = \int_\Omega \hat{\psi}^\dagger(\mathbf{r})\hat{\psi}(\mathbf{r})\,\mathrm{d}^3 r \tag{3.26}$$

contained in a subregion Ω of the system. Its variance writes

$$\Delta N_\Omega^2 = \langle \hat{N}_\Omega^2 \rangle - \langle \hat{N}_\Omega \rangle^2, \tag{3.27}$$

$$= \int_\Omega [\langle \hat{\psi}^\dagger(\mathbf{r})\hat{\psi}(\mathbf{r})\hat{\psi}^\dagger(\mathbf{r}')\hat{\psi}(\mathbf{r}')\rangle - \rho(\mathbf{r})\rho(\mathbf{r}')]\,\mathrm{d}^3 r\,\mathrm{d}^3 r', \tag{3.28}$$

where $\rho(\mathbf{r})$ is the mean particle density at $\mathbf{r}$ (not to be confused with the density matrix $\hat{\rho}$). In order to express it in terms of the pair-correlation function, one has to move the field operator $\hat{\psi}(\mathbf{r})$ to the right. Taking care of the commutation rules, we have

$$\hat{\psi}(\mathbf{r})\hat{\psi}^\dagger(\mathbf{r}')\hat{\psi}(\mathbf{r}') = \hat{\psi}^\dagger(\mathbf{r}')\hat{\psi}(\mathbf{r}')\hat{\psi}(\mathbf{r}) + \delta(\mathbf{r}-\mathbf{r}')\hat{\psi}(\mathbf{r}') \tag{3.29}$$

for both bosons and fermions, which leads to

$$\Delta N_\Omega^2 = \langle \hat{N}_\Omega \rangle + \int_\Omega [g_2(\mathbf{r},\mathbf{r}') - \rho(\mathbf{r})\rho(\mathbf{r}')]\,\mathrm{d}^3 r\,\mathrm{d}^3 r'. \tag{3.30}$$

The first term is the self-detection contribution mentioned above, and gives the Poissonian result $\Delta N_\Omega^2 = \langle \hat{N}_\Omega \rangle$ expected for uncorrelated particles. The deviation from Poisson statistics is then entirely determined by the deviation of the pair distribution function from the product of densities, that is by $g^{(2)} - 1$. Bunched particles ($g^{(2)} > 1$) produce super-Poissonian fluctuations, while antibunched ones ($g^{(2)} < 1$), such as the fermions considered below, produce sub-Poissonian fluctuations.

3.3 Example 1: ideal Bose and Fermi gases.

We consider ideal (i.e. non-interacting) gases, described in the grand-canonical ensemble by the density matrix

$$\hat{\rho} = \frac{1}{\Xi}\exp[-\beta(\hat{H} - \mu\hat{N})], \tag{3.31}$$

where $\hat{H}$ is the kinetic energy operator.

3.3.1 First-order coherence

The occupation number of the single-particle momentum state $\mathbf{k}$ is given by the distribution

$$n_\mathbf{k} = \langle \hat{a}_\mathbf{k}^\dagger \hat{a}_\mathbf{k} \rangle = \frac{1}{\mathrm{e}^{\beta(\varepsilon_k - \mu)} - \varepsilon}, \tag{3.32}$$

where $\varepsilon = 1$ for bosons (Bose-Einstein distribution with $\mu < 0$) and $\varepsilon = -1$ for fermions (Fermi-Dirac distribution), and where $\varepsilon_k = \hbar^2 k^2/(2m)$ is the single-particle kinetic energy.

Classical gas. In the classical limit $\beta(\varepsilon_k - \mu) \gg 1$, the ± 1 in the denominator becomes negligible and one recovers the Maxwell-Boltzmann distribution

$$n_{\mathbf{k}} = \rho\, \lambda_{\mathrm{dB}}^3\, \exp\left[-\frac{(k\lambda_{\mathrm{dB}})^2}{4\pi}\right], \tag{3.33}$$

where we introduce the thermal de Broglie wavelength

$$\lambda_{\mathrm{dB}} = \frac{h}{\sqrt{2\pi m k_{\mathrm{B}} T}}. \tag{3.34}$$

The prefactor is the fugacity $\mathrm{e}^{\beta\mu}$, fixed by the normalization $\sum_{\mathbf{k}} n_{\mathbf{k}} = N$: it is the phase-space density $\rho\lambda_{\mathrm{dB}}^3$, which is indeed much smaller than one in the classical regime. Taking the Fourier transform of this Gaussian yields the first-order correlation function

$$g_1(\mathbf{r}) = \rho\, \exp\left[-\pi\left(\frac{r}{\lambda_{\mathrm{dB}}}\right)^2\right]. \tag{3.35}$$

One checks that $g_1(\mathbf{0}) = \rho$, as it must. The de Broglie wavelength sets the characteristic decay length of the g_1 function, i.e. the coherence length: in a classical gas, coherence does not extend beyond the thermal wavelength.

Condensed Bose gas. In three dimensions, non-interacting bosonic particles undergo Bose-Einstein condensation at sufficiently low temperature $T < T_{\mathrm{c}}$. The critical temperature is usually expressed in terms of a critical phase space density $n\lambda_{\mathrm{dB,c}}^3 = 2.612$. In the condensed regime, the chemical potential vanishes, and the momentum distribution is given by

$$n_{\mathbf{k}} = n_0\, \delta_{\mathbf{k},0} + \frac{1}{\mathrm{e}^{\beta\varepsilon_k} - 1}. \tag{3.36}$$

The ground-state occupation number n_0 is given by

$$n_0 = N\left[1 - \left(\frac{T}{T_c}\right)^{3/2}\right]. \tag{3.37}$$

The Fourier transform of the momentum distribution yields the first-order correlation function

$$g_1(\mathbf{r}) = \frac{1}{V}\sum_{\mathbf{k}} \mathrm{e}^{\mathrm{i}\mathbf{k}\cdot\mathbf{r}} n_{\mathbf{k}} \tag{3.38}$$

$$= \frac{n_0}{V} + \frac{1}{V}\sum_{\mathbf{k}\neq\mathbf{0}} \mathrm{e}^{\mathrm{i}\mathbf{k}\cdot\mathbf{r}} n_{\mathbf{k}} \tag{3.39}$$

$$= \rho_0 + \frac{1}{(2\pi)^3}\int \mathrm{e}^{\mathrm{i}\mathbf{k}\cdot\mathbf{r}} n_{\mathbf{k}}\, \mathrm{d}^3k, \tag{3.40}$$

where $\rho_0 = n_0/V$ is the condensed particle density, and where the sum over the excited modes has been replaced by an integral.

The Fourier transform of a radially symmetric function is given by the Hankel transform [39], allowing us to write

$$g_1(\mathbf{r}) = \rho_0 + \frac{1}{(2\pi)^{3/2}\sqrt{r}}\int n_k\, k^{3/2} J_{1/2}(kr)\, \mathrm{d}k, \tag{3.41}$$

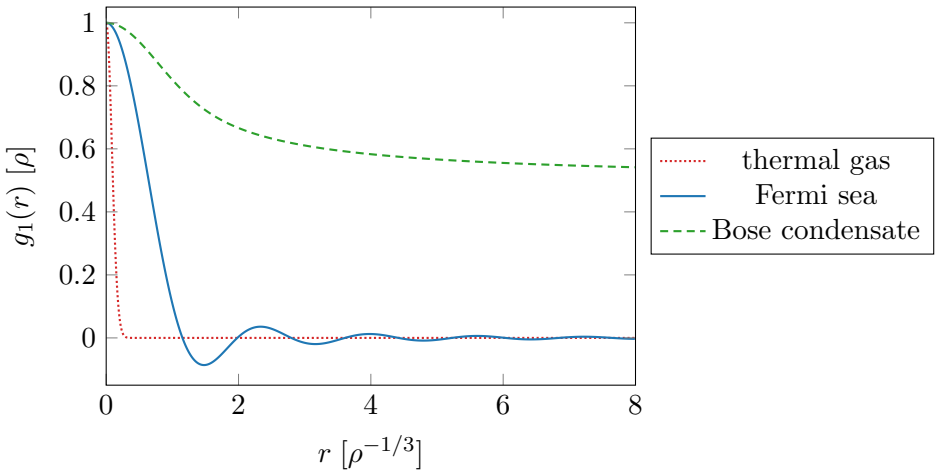


Figure 19: First-order correlation function $g_1(r)$ computed for a thermal gas (red dotted line, with $\rho\lambda_{\mathrm{dB}}^3 = 0.01$ and no discernable effect of quantum statistics), a $T = 0$ Fermi gas and a Bose gas with a 50% condensed fraction in three dimensions.

where $J_{1/2}$ is a Bessel function. The second term in the right hand side represents the contribution of non-condensed particles, which decays towards zero over a characteristic length λ_{dB}. At long distance, the g_1 function tends towards a non-zero value given by the condensed density: the condensate exhibits long-range phase coherence.

Fermi gas at zero temperature. At low temperature, a (spinless) Fermi gas forms a Fermi sea with an occupation number of momentum states given by

$$n_{\mathbf{k}} = 1 \quad \text{for} \quad k < k_{\mathrm{F}}, \tag{3.42}$$

$$= 0 \quad \text{for} \quad k > k_{\mathrm{F}}, \tag{3.43}$$

where k_{F} is the Fermi momentum for a particle density ρ ($k_{\mathrm{F}} = \pi\rho$ in 1D and $k_{\mathrm{F}} = (6\pi^2\rho)^{1/3}$ in 3D).

We begin with the case of a one-dimensional system, for which the momentum distribution is a rectangular function, whose Fourier transform gives

$$g_1(x) = \rho\ \mathrm{sinc}(k_{\mathrm{F}}x) \quad \text{in 1D}. \tag{3.44}$$

The correlation function is an oscillating function decaying to zero over a characteristic length $1/k_{\mathrm{F}}$, but the decay is algebraic only (Friedel oscillations). This can be attributed to the discontinuity of the momentum distribution at the Fermi points $\pm k_{\mathrm{F}}$.

We get a similar behavior in dimension three, for which the first-order correlation function writes

$$g_1(\mathbf{r}) = \frac{\sin(k_{\mathrm{F}}r) - (k_{\mathrm{F}}r)\cos(k_{\mathrm{F}}r)}{2\pi^2 r^3} \quad \text{in 3D}. \tag{3.45}$$

We show in Fig. 19 the g_1 correlation functions of ideal Bose and Fermi gases discussed above.

The g_1 correlation function of weakly-interacting bosonic gases has been measured in atomic gases in various ways. We present in Fig. 20 an experiment probing the matter-wave interference between two distant points of the gas [40]. The measurements are in good agreement with the correlation function computed above.

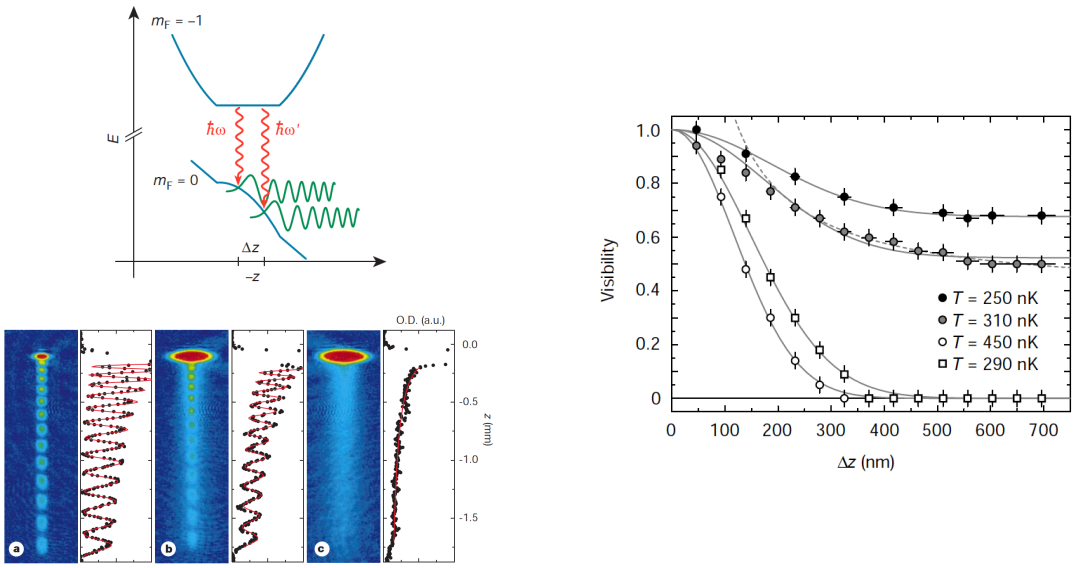


Figure 20: Measurement of the first-order correlation function $g_1(r)$ of a weakly-interacting Bose gas of rubidium atoms [40]. A radiofrequency field driven with two tones selectively outcouples atoms from an ultracold gas at two different spatial positions with a relative distance r. The two emitted atomic beams form an interference pattern whose visibility is proportional to $g_1(r)$. Its variation with r is consistent with the prediction shown in Fig. 19 for a non-interacting Bose gas.

3.3.2 Particle correlations and fluctuations

Bunching and anti-bunching effects. Ideal gases at thermal equilibrium in the grand-canonical ensemble are Gaussian quantum states, hence higher-order correlation functions can be calculated using Wick's theorem. The pair-distribution function can then be expressed in terms of the first-order correlation function as

$$g_2(\mathbf{r},\mathbf{r}') = \langle\hat\psi^\dagger(\mathbf{r})\hat\psi^\dagger(\mathbf{r}')\hat\psi(\mathbf{r}')\hat\psi(\mathbf{r})\rangle \tag{3.46}$$
$$= \langle\hat\psi^\dagger(\mathbf{r})\hat\psi(\mathbf{r})\rangle\langle\hat\psi^\dagger(\mathbf{r}')\hat\psi(\mathbf{r}')\rangle + \varepsilon\langle\hat\psi^\dagger(\mathbf{r})\hat\psi(\mathbf{r}')\rangle\langle\hat\psi^\dagger(\mathbf{r}')\hat\psi(\mathbf{r})\rangle \tag{3.47}$$
$$= \rho(\mathbf{r})\rho(\mathbf{r}') + \varepsilon|g_1(\mathbf{r},\mathbf{r}')|^2, \tag{3.48}$$

where only two of the three pairings of Wick's theorem contribute, the anomalous one $\langle\hat\psi^\dagger\hat\psi^\dagger\rangle$ vanishing for a state of fixed particle number. In terms of the normalized correlation functions (3.7) and (3.25), this relation takes the compact form

$$g^{(2)}(\mathbf{r},\mathbf{r}') = 1 + \varepsilon\left|g^{(1)}(\mathbf{r},\mathbf{r}')\right|^2, \tag{3.49}$$

which shows that for an ideal gas the pair correlations are entirely determined by the first-order coherence.

Non-interacting bosonic and fermionic particles consequently behave very differently at short distance, where $|g^{(1)}| \to 1$:

$$g_2(\mathbf{r},\mathbf{r}) = 2\,\rho(\mathbf{r})^2 \quad \text{for bosons,} \tag{3.50}$$
$$= 0 \quad \text{for fermions.} \tag{3.51}$$

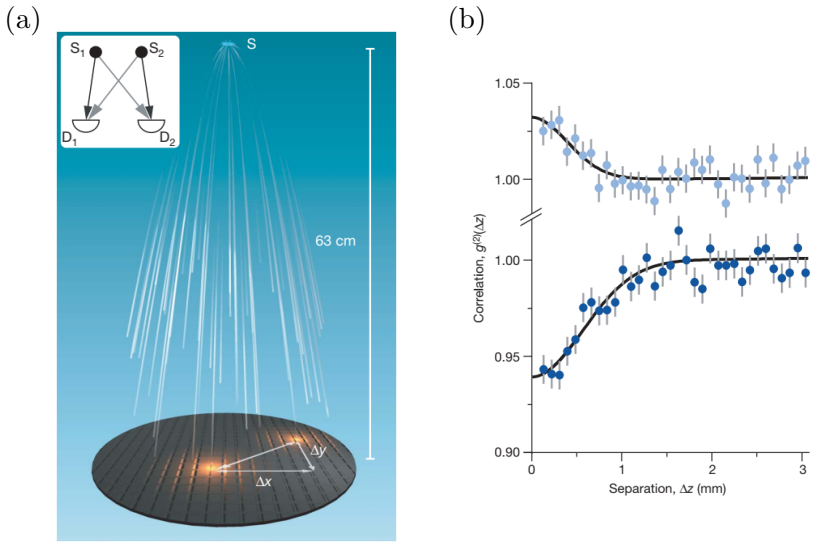


Figure 21: (a) Scheme of the experiment from [41]. An ultracold gas of ^{3}He (fermion) or ^{4}He (bosons) is released from the trap and detected on a multichannel plate. The x and y positions are directly measured via the point of detection on the plate, while the z position is inferred from the arrival times. The pair distribution function can then be reconstructed. (b) Comparison between the correlation functions between fermions (bottom) at bosons (top), showing antibunching and bunching effects, respectively. The deviation to perfect (anti-)bunching is attributed to the finite spatial resolution of the detector.

This result shows that non-interacting bosons tend to group together at short distance (bunching), while two identical fermions cannot be found at the same positions, owing to Pauli's exclusion principle (antibunching). Note that the correlations extend over the coherence length, that is over λ_{dB} for a thermal gas and $1/k_{\mathrm{F}}$ for a degenerate Fermi gas: bunching and antibunching are purely quantum-statistical effects, with no interaction involved.

Bosonic bunching and fermionic antibunching have been observed in a wide range of systems, including photons (Hanbury-Brown and Twiss effect), electrons and ultracold atoms. We present in Fig. 21 an experiment using ultracold atoms of helium, in which particle correlations were measured for two different isotopes, revealing in the same experiment antibunching for the fermionic isotope ^{3}He and bunching for the bosonic isotope ^{4}He [41].

Particle fluctuations in a Fermi gas. We now consider particle fluctuations, focusing on Fermi gases evolving in one dimension. Since the $T = 0$ Fermi gas exhibits Gaussian statistics, its pair correlation function is given by

$$g_2(x) = \rho^2 - |g_1(x)|^2 = \rho^2[1 - \mathrm{sinc}^2(k_{\mathrm{F}}x)]. \tag{3.52}$$

We consider the number of particles in a given volume Ω, given by the operator

$$\hat{N}_\Omega = \int_\Omega \hat{\psi}^\dagger(x)\hat{\psi}(x)\,\mathrm{d}x. \tag{3.53}$$

Its fluctuation is given by the variance

$$\Delta N_\Omega^2 = \langle \hat{N}_\Omega^2 \rangle - \langle \hat{N}_\Omega \rangle^2 \tag{3.54}$$

$$= \int_\Omega [\langle \hat{\psi}^\dagger(x)\hat{\psi}(x)\hat{\psi}^\dagger(x')\hat{\psi}(x')\rangle - \rho^2]\,\mathrm{d}x\,\mathrm{d}x'. \tag{3.55}$$

Using the operator identity $\hat{\psi}^\dagger(x)\hat{\psi}(x)\hat{\psi}^\dagger(x')\hat{\psi}(x') = \hat{\psi}^\dagger(x)\hat{\psi}^\dagger(x')\hat{\psi}(x')\hat{\psi}(x) + \delta(x-x')\,\hat{\psi}^\dagger(x)\hat{\psi}(x)$, whose last term contributes $\langle \hat{N}_\Omega \rangle$ upon integration, we can express the variance in terms of the second-order correlation function as

$$\Delta N_\Omega^2 = \langle \hat{N}_\Omega \rangle + \int_\Omega [g_2(x-x') - \rho^2]\,\mathrm{d}x\,\mathrm{d}x', \tag{3.56}$$

$$= \langle \hat{N}_\Omega \rangle - \rho^2 \int_\Omega \mathrm{sinc}^2[k_\mathrm{F}(x-x')]\,\mathrm{d}x\,\mathrm{d}x'. \tag{3.57}$$

This expression already shows that particle fluctuations are subpoissonian, i.e.

$$\Delta N_\Omega < \sqrt{\langle \hat{N}_\Omega \rangle}. \tag{3.58}$$

Taking Ω as a segment $(0, L)$ (and dropping the index Ω from now on), we obtain the explicit expression

$$\Delta N^2 = \langle N \rangle - \rho^2 \int_{(0,L)\times(0,L)} \mathrm{sinc}^2[k_\mathrm{F}(x-x')]\,\mathrm{d}x\,\mathrm{d}x' \tag{3.59}$$

$$= \langle N \rangle - \rho^2 \int_{-L}^{L} (L - |X|)\,\mathrm{sinc}^2(k_\mathrm{F}X)\,\mathrm{d}X \tag{3.60}$$

$$= \langle N \rangle - (\rho/k_\mathrm{F})^2 \int_{-k_\mathrm{F}L}^{k_\mathrm{F}L} (k_\mathrm{F}L - |u|)\,\mathrm{sinc}^2(u)\,\mathrm{d}u, \tag{3.61}$$

where the triangular weight $L - |X|$ is the overlap of the segment with its translate by X. We use the asymptotic expansion

$$\int_{-A}^{A} (A - |u|)\,\mathrm{sinc}^2(u)\,\mathrm{d}u = \pi A - [\log(2A) + \gamma + 1] + O(A^{-2}), \tag{3.62}$$

where $\gamma = 0.5772...$ is the Euler constant. We obtain the final expression

$$\Delta N^2 = \frac{\log(2\pi\langle \hat{N} \rangle) + \gamma + 1}{\pi^2} + O(1/\langle \hat{N} \rangle^2), \tag{3.63}$$

which can also be written in terms of the length L as

$$\Delta N^2 = \frac{\log(2\pi\rho L) + \gamma + 1}{\pi^2} + O(1/L^2), \tag{3.64}$$

These fluctuations are very small compared to the Poisson law $\Delta N^2 = \langle \hat{N} \rangle$ expected for an uncorrelated system.

A similar behavior occurs in dimension 3, for which one has the large-L scaling [42]

$$\Delta N^2 \propto (k_\mathrm{F}L)^2 \log(k_\mathrm{F}L) \tag{3.65}$$

for a subregion Ω of volume L^3 .

Note that in a system with truly short-range correlations, fluctuations should scale with the area of the boundary of subregion Ω, hence a scaling $\Delta N^2 \propto L^{d-1}$ (so-called *area law*). This would for instance be the case for a band insulator in a lattice potential, for which each site is occupied with a single fermion.

Finally, we mention that particle fluctuations are intimately linked with many-body entanglement. The entanglement between subregion Ω and its complement Ω^c is characterized by the so-called (von Neumann) entanglement entropy $S(\hat{\rho}_\Omega) = -\operatorname{Tr}(\hat{\rho}_\Omega \log \hat{\rho}_\Omega)$, where $\hat{\rho}_\Omega = \operatorname{Tr}_{\Omega^c} \hat{\rho}$ is the reduced density matrix in Ω, obtained by tracing out from the many-body density matrix $\hat{\rho}$ all degrees of freedom localized in Ω^c. The computation of the entanglement entropy for non-interacting fermions shows that, for a system in dimension d and a subregion Ω of volume L^d, one has [43]

$$S(\hat{\rho}_\Omega) \sim L^{d-1} \log L \quad \text{for gapless systems (free fermions, metals)} \tag{3.66}$$

$$\sim L^{d-1} \quad \text{for gapped systems (insulators).} \tag{3.67}$$

The area law $S \sim L^{d-1}$ for gapped systems manifests the short-range character of entanglement in those systems [44].

3.4 Example 2: impenetrable bosons in one dimension

We now consider a more complex example that consists of a system of bosons in one dimension with hardcore interactions. Despite the presence of interactions, this system remains tractable, based on the existence of an exact mapping to free fermions that was first put forward by Girardeau [45].

3.4.1 Definition and mapping to free fermions

Hardcore interactions are defined by the impossibility to find two particles with a relative distance below the hard-core diameter a. This situation also includes the limit $a \to 0$ of impenetrable bosons, which can be formulated as the limit of infinite interaction strength $g \to \infty$ of the Lieb-Liniger model, which describes 1D bosons interacting through a short-range contact potential [46]:

$$\hat{H} = \int \left[-\frac{\hbar^2}{2m} \hat{\psi}^\dagger(x) \partial_x^2 \hat{\psi}(x) + \frac{g}{2} \hat{\psi}^\dagger(x) \hat{\psi}^\dagger(x) \hat{\psi}(x) \hat{\psi}(x) \right] \mathrm{d}x. \tag{3.68}$$

We restrict our discussion to the limit $g \to \infty$ of impenetrable bosons, also called the Tonks-Girardeau regime [47, 45].

The hardcore interaction prevents the occurrence of configurations in which two particles can be found at the same position x. In the first quantization language, it means that we only consider many-body wavefunctions $\psi(x_1, \ldots, x_N)$ that vanish when two positions x_i and x_j coincide.

The formulation of the problem in second quantization raises some difficulties in continuous space. In the remainder of this section, we assume x to be a discrete coordinate, with a spacing $\mathrm{d}x$ between neighbouring coordinates that can be taken arbitrarily small. In this discretized space, the bosonic field operator will be written as $\hat{\psi}_x$, with the commutation rules

$$[\hat{\psi}_x, \hat{\psi}_{x'}] = [\hat{\psi}_x^\dagger, \hat{\psi}_{x'}^\dagger] = 0, \tag{3.69}$$

$$[\hat{\psi}_x, \hat{\psi}_{x'}^\dagger] = \delta_{x,x'}. \tag{3.70}$$

The expression of the many-body Hamiltonian then involves a discretization of the Laplacian operator, leading to

$$\hat{H} = \sum_x \left[-\frac{\hbar^2}{2m\mathrm{d}x^2} \hat{\psi}_x^\dagger (\hat{\psi}_{x-\mathrm{d}x} - 2\hat{\psi}_x + \hat{\psi}_{x+\mathrm{d}x}) + \frac{U}{2} \hat{\psi}_x^\dagger \hat{\psi}_x^\dagger \hat{\psi}_x \hat{\psi}_x \right],$$

where $U \sim g/\mathrm{d}x$ is the onsite interaction energy.

The hardcore constraint occurring in the limit $U \to \infty$ corresponds to the replacement of the interaction term by the action of the projector $\hat{P}$ on many-body states with at most one boson at each point x. The many-body Hamiltonian then becomes

$$\hat{H} = -\frac{\hbar^2}{2m\mathrm{d}x^2} \sum_x \hat{P}\hat{\psi}_x^\dagger \hat{P}(\hat{P}\hat{\psi}_{x-\mathrm{d}x}\hat{P} - 2\hat{P}\hat{\psi}_x\hat{P} + \hat{P}\hat{\psi}_{x+\mathrm{d}x}\hat{P}).$$

At first sight, this Hamiltonian looks like a simple non-interacting model, but one should notice that the operators $\hat{P}\hat{\psi}_x\hat{P}$ do not correspond to bosonic field operators since it is impossible to create a pair of hardcore bosons at the same point, i.e. $(\hat{P}\hat{\psi}_x^\dagger\hat{P})^2 = 0$. Nor do they define fermionic fields, because of the commutation relations inherited from bosons, $[\hat{P}\hat{\psi}_x\hat{P}, \hat{P}\hat{\psi}_{x'}\hat{P}] = [\hat{P}\hat{\psi}_x\hat{P}, \hat{P}\hat{\psi}_{x'}^\dagger\hat{P}] = [\hat{P}\hat{\psi}_x^\dagger\hat{P}, \hat{P}\hat{\psi}_{x'}^\dagger\hat{P}] = 0$ for $x \neq x'$.

Fermionization using a Jordan-Wigner transform. The projected bosonic field $\hat{P}\hat{\psi}_x\hat{P}$ can be mapped to a fermionic field operator $\hat{\psi}_x^F$ by introducing a suitable sign factor defined by the parity of the number of atoms at the left of position x (so-called Jordan-Wigner transformation [48]). More specifically, we define

$$\hat{\psi}_x^F = \hat{\Pi}_{0,x}\hat{P}\hat{\psi}_x\hat{P}, \tag{3.71}$$

where we assume that the system is defined on the segment $[0, L]$ and where

$$\hat{\Pi}_{x,x'} = \exp\left[\mathrm{i}\pi \sum_{x' \leq x'' < x} \hat{\psi}_{x''}^\dagger \hat{\psi}_{x''} \right]$$

is the parity of the number of atoms in the interval $[x, x'[$. Since the mapping from $\hat{P}\hat{\psi}_x\hat{P}$ to $\hat{\psi}_x^F$ involves field operators at all positions $x' < x$, one speaks of a non-local transform, and the parity operator is also known as a string operator.

The parity operator $\hat{\Pi}_{x,x'}$ commutes with the projector $\hat{P}$ and with the field operator $\hat{\psi}_{x''}$ if x'' is outside the interval $[x, x'[$. If $x'' \in [x, x'[$, the field operator flips the parity. Hence, we have the commutation rule

$$\hat{\Pi}_{x,x'}\hat{\psi}_{x''} = \hat{\psi}_{x''}\hat{\Pi}_{x,x'} \quad \text{for} \quad x'' \notin [x, x'[\tag{3.72}$$

$$= -\hat{\psi}_{x''}\hat{\Pi}_{x,x'} \quad \text{for} \quad x'' \in [x, x'[\tag{3.73}$$

Let us check that the operators $\hat{\psi}_x^F$ fulfill the usual fermionic anti-commutation rules. We first consider the anticommutation at a given point x:

$$\{\hat{\psi}_x^F, \hat{\psi}_x^{F\dagger}\} = \hat{\psi}_x^F\hat{\psi}_x^{F\dagger} + \hat{\psi}_x^{F\dagger}\hat{\psi}_x^F \tag{3.74}$$

$$= \hat{P}\hat{\psi}_x\hat{P}\hat{\psi}_x^\dagger\hat{P} + \hat{P}\hat{\psi}_x^\dagger\hat{P}\hat{\psi}_x\hat{P}. \tag{3.75}$$

In hardcore subspace, it is clear that $\hat{P}\hat{\psi}_x\hat{P}\hat{\psi}_x^\dagger\hat{P} = 1-\hat{n}_x$ and $\hat{P}\hat{\psi}_x^\dagger\hat{P}\hat{\psi}_x\hat{P} = \hat{n}_x$, where $\hat{n}_x$ is the occupation number at position x, restricted to 0 and 1. Hence we get $\{\hat{\psi}_x^F, \hat{\psi}_x^{F\dagger}\} = 1$. We then consider the case $x < x'$ and write the anticommutator

$$\{\hat{\psi}_x^F, \hat{\psi}_{x'}^{F\dagger}\} = \hat{\psi}_x^F\hat{\psi}_{x'}^{F\dagger} + \hat{\psi}_{x'}^{F\dagger}\hat{\psi}_x^F \tag{3.76}$$

$$= \hat{P}\hat{\Pi}_{0,x}\hat{\psi}_x\hat{P}\hat{\Pi}_{0,x'}\hat{\psi}_{x'}^\dagger\hat{P} + \hat{P}\hat{\Pi}_{0,x'}\hat{\psi}_{x'}^\dagger\hat{P}\hat{\Pi}_{0,x}\hat{\psi}_x\hat{P}. \tag{3.77}$$

We then use the commutation rule (3.72) and (3.73) to regroup the parity signs on the left, which gives

$$\{\hat{\psi}_x^F, \hat{\psi}_{x'}^{F\dagger}\} = \hat{\Pi}_{x,x'}\left(-\hat{P}\hat{\psi}_x\hat{P}\hat{\psi}_{x'}^\dagger\hat{P} + \hat{P}\hat{\psi}_{x'}^\dagger\hat{P}\hat{\psi}_x\hat{P}\right), \tag{3.78}$$

which gives zero owing to bosonic commutation rules. We would get the same result for $x' < x$, and an identical argument gives $\{\hat{\psi}_x^F, \hat{\psi}_{x'}^F\} = 0$. The field operators $\hat{\psi}_x^F$ then fulfill fermionic anticommutation rules.

As a result, the hard-core Hamiltonian can be reformulated in terms of fermionic fields as

$$\hat{H} = -\frac{\hbar^2}{2m\mathrm{d}x^2}\sum_x \hat{\psi}_x^{F\dagger}(\hat{\psi}_{x-\mathrm{d}x}^F - 2\hat{\psi}_x^F + \hat{\psi}_{x+\mathrm{d}x}^F).$$

which simply corresponds to free fermions.

Fermionization of bosonic wavefunctions. The mapping of impenetrable bosons onto fermions can also be written at the level of the many-body wavefunction. For a bosonic wavefunction $\psi(x_1, \ldots, x_N)$ fulfilling the hardcore constraint (i.e. vanishing if $x_i = x_j$ with $i \neq j$), one defines a fermionic wavefunction

$$\psi_F(x_1, \ldots, x_N) = A(x_1, \ldots x_N)\psi(x_1, \ldots, x_N). \tag{3.79}$$

by multiplying with the 'unit anti-symmetric function' A given by [45]

$$A(x_1, \ldots x_N) = \prod_{i<j}\mathrm{sgn}(x_i - x_j), \tag{3.80}$$

where sgn is the sign function. Note that the sign function is always well-defined since two particles cannot be at the same position.

3.4.2 Many-body ground state

The many-body ground state of impenetrable bosons can then be expressed starting from the ground state of the associated free fermions, which is a Fermi sea. Its wave-function can be expressed as a Slater determinant

$$\psi_F(x_1, \ldots, x_N) = \frac{1}{L^{N/2}\sqrt{N!}}\begin{vmatrix} \mathrm{e}^{\mathrm{i}k_1x_1} & \ldots & \mathrm{e}^{\mathrm{i}k_1x_N} \\ \vdots & \ddots & \vdots \\ \mathrm{e}^{\mathrm{i}k_Nx_1} & \ldots & \mathrm{e}^{\mathrm{i}k_Nx_N} \end{vmatrix}, \tag{3.81}$$

where the k_i's are the momenta forming the Fermi sea, which are the integer multiples of $2\pi/L$ satisfying $|k_i| < k_\mathrm{F} = \pi\rho$, with $\rho = N/L$ the particle density.

The bosonic ground state is then given by

$$\psi(x_1, \ldots, x_N) = A(x_1, \ldots x_N)\psi_F(x_1, \ldots, x_N), \tag{3.82}$$

For the ground state considered here the Slater determinant can be chosen real, up to an irrelevant global phase, so that the construction simply amounts to taking its absolute value,

$$\psi(x_1, \ldots, x_N) = |\psi_F(x_1, \ldots, x_N)|. \tag{3.83}$$

In any case, the two wave-functions always share the same modulus, $|\psi| = |\psi_F|$, since $|A| = 1$.

A number of physical quantities take identical values in the two systems, but for two distinct reasons. The energies coincide because the two Hamiltonians are mapped onto one another, as shown above. Separately, *any* observable that is diagonal in the positions of the particles takes the same value in the two states, because the two wave-functions share the same modulus, $|\psi| = |\psi_F|$. This is the case of the density and, more generally, of all density correlations. In particular, since

$$g_2(x, x') = N(N-1) \int |\psi(x, x', x_3, \ldots, x_N)|^2 \, \mathrm{d}x_3 \cdots \mathrm{d}x_N \tag{3.84}$$

involves only $|\psi|^2$, the pair correlation function of impenetrable bosons is simply that of the free fermions,

$$g_2(x, x') = g_2^F(x, x') = \rho^2 \left[1 - \mathrm{sinc}^2 \left(k_\mathrm{F}(x - x')\right)\right]. \tag{3.85}$$

It is instructive to recover this result directly in second quantization, as the mechanism by which the string operators disappear is the one that will fail for g_1. Inverting the definition (3.71) with the help of $\hat{\Pi}_{0,x}^2 = 1$ gives

$$\hat{P}\hat{\psi}_x\hat{P} = \hat{\Pi}_{0,x}\,\hat{\psi}_x^F, \qquad \hat{P}\hat{\psi}_x^\dagger\hat{P} = \hat{\psi}_x^{F\dagger}\,\hat{\Pi}_{0,x}, \tag{3.86}$$

where the projectors may be omitted since all states considered belong to the hardcore subspace. Substituting into the definition of g_2 and using $\hat{\Pi}_{0,x'}^2 = 1$ for the two central string operators,

$$\begin{aligned} g_2(x, x') &= \langle \hat{\psi}_x^\dagger \hat{\psi}_{x'}^\dagger \hat{\psi}_{x'} \hat{\psi}_x \rangle & (3.87)\\ &= \langle\, (\hat{\psi}_x^{F\dagger}\hat{\Pi}_{0,x})(\hat{\psi}_{x'}^{F\dagger}\hat{\Pi}_{0,x'})(\hat{\Pi}_{0,x'}\hat{\psi}_{x'}^F)(\hat{\Pi}_{0,x}\hat{\psi}_x^F)\,\rangle & (3.88)\\ &= \langle \hat{\psi}_x^{F\dagger}\,\hat{\Pi}_{0,x}\,\hat{\psi}_{x'}^{F\dagger}\hat{\psi}_{x'}^F\,\hat{\Pi}_{0,x}\,\hat{\psi}_x^F \rangle. & (3.89) \end{aligned}$$

It remains to move the first $\hat{\Pi}_{0,x}$ to the right, through the pair $\hat{\psi}_{x'}^{F\dagger}\hat{\psi}_{x'}^F$. If $x' \geq x$, the point x' lies outside the interval $[0, x[$ and the string commutes with each of the two operators. If $x' < x$, it anticommutes with each of them, and the two sign changes compensate. In both cases $\hat{\Pi}_{0,x}$ commutes with the *pair*, so that the two string operators meet and cancel,

$$\begin{aligned} g_2(x, x') &= \langle \hat{\psi}_x^{F\dagger}\hat{\psi}_{x'}^{F\dagger}\hat{\psi}_{x'}^F\,\hat{\Pi}_{0,x}\hat{\Pi}_{0,x}\,\hat{\psi}_x^F \rangle & (3.90)\\ &= \langle \hat{\psi}_x^{F\dagger}\hat{\psi}_{x'}^{F\dagger}\hat{\psi}_{x'}^F\hat{\psi}_x^F \rangle = g_2^F(x, x'), & (3.91) \end{aligned}$$

in agreement with the wave-function argument. The essential point is that $\hat{\psi}^{F\dagger}_{x'}$ and $\hat{\psi}^{F}_{x'}$ appear *in pairs* at the same point, so that whatever sign the string picks up is immediately undone.

The bunching previously found for non-interacting bosons is lost since $g_2(0) = 0$, as expected for impenetrable bosons.

By contrast, many other observables take different expectation values in the bosonic many-body states and its fermionized counterpart. For instance, let us consider the first-order correlation function of a bosonic state

$$g_1(x, x') = \langle \hat{\psi}^\dagger_x \hat{\psi}_{x'} \rangle \tag{3.92}$$

$$= \langle \hat{\psi}^{F\dagger}_x \hat{\Pi}_{x,x'} \hat{\psi}^F_{x'} \rangle. \tag{3.93}$$

Here the two field operators sit at *different* points, so the compensation at work in g_2 does not occur: the two strings $\hat{\Pi}_{0,x}$ and $\hat{\Pi}_{0,x'}$ no longer cancel but combine into $\hat{\Pi}_{x,x'}$, which counts the parity of the number of particles lying between the two points. This operator cannot be discarded, and the expression does not reduce to the correlation function of the fermionized state. This is consistent with the wave-function picture: g_1 is not diagonal in the positions, and therefore probes the *phase* of the many-body wave-function, which is precisely what the sign function A changes. The momentum distribution, being the Fourier transform of g_1, differs as well between impenetrable bosons and fermions. The momentum distribution n_k [49, 50, 51], as well as the first-order correlation function g_1 [52], can be computed in the thermodynamic limit after rather tedious calculations that are beyond the scope of this course. We show in Fig. 22 these two quantities, and give the analytical expressions of infrared asymptotic behaviors [50, 51]

$$n_k \sim A\rho \sqrt{\frac{2\pi}{k_{\mathrm{F}} k}} \quad \text{for} \quad k \ll k_{\mathrm{F}}, \tag{3.94}$$

$$g_1(x) \sim \frac{A\rho}{\sqrt{k_{\mathrm{F}}|x|}} \quad \text{for} \quad k_{\mathrm{F}} x \gg 1, \tag{3.95}$$

where $A = 0.92418....$ The two expressions are consistent with each other: the Fourier transform of $|x|^{-1/2}$ being $\sqrt{2\pi/|k|}$, the second asymptotic law implies the first. The momentum distribution n_k diverges for $k \to 0$, but the $k = 0$ momentum is not macroscopically populated: there is no Bose-Einstein condensation [52]. This is confirmed by the decay to zero of the g_1 function at large distances.

The Tonks–Girardeau regime has been reached with ultracold rubidium atoms confined to one dimension by a tight transverse trapping [53, 54]. In particular, the antibunching characteristic of impenetrable bosons, $g^{(2)}(0) \to 0$, has been observed in the strongly interacting regime [55], see Fig. 23.

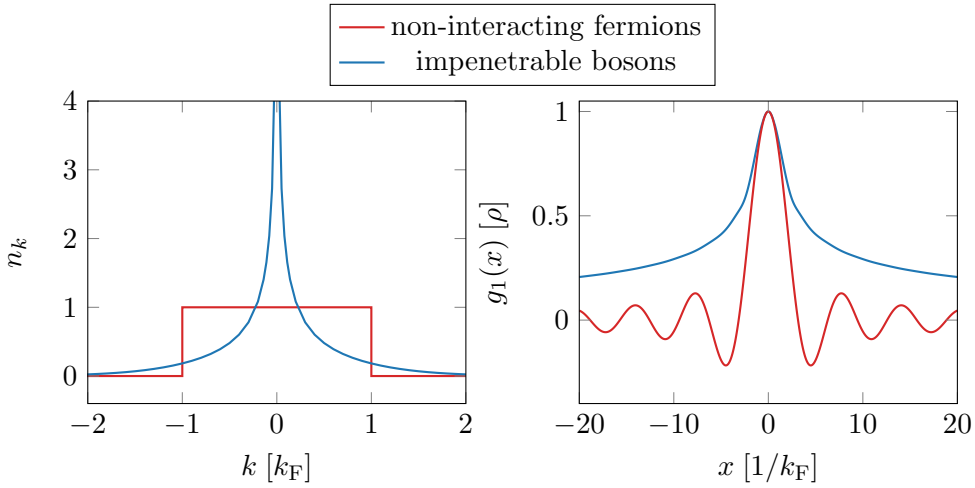


Figure 22: Momentum distribution and first-order correlation function of one-dimensional systems of non-interacting fermions (red lines) or impenetrable bosons (blue lines).

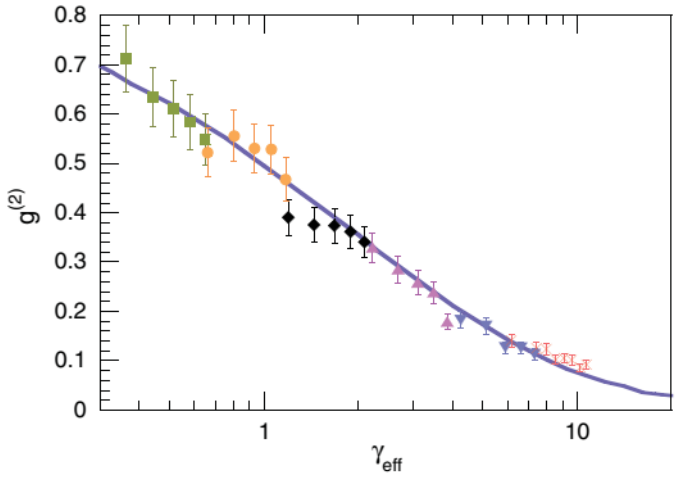


Figure 23: Local pair correlation $g^{(2)}(0)$ of a one-dimensional Bose gas, measured as a function of the effective Lieb–Liniger parameter $\gamma_{\text{eff}} = m^* g_{1D}/(\hbar^2 \rho)$ (where g_{1D} is the one-dimensional coupling constant, ρ the linear density, and m^* the effective mass of the atoms in the optical lattice), which describes the strength of interactions and grows both with the coupling and at low density. The antibunching of the Tonks–Girardeau regime is revealed in the strongly interacting limit $\gamma_{\text{eff}} \to \infty$. Figure taken from [55].

3.5 Example 3: superfluid helium

The final example considered here is superfluid (liquid) helium. Superfluidity was discovered in 1937 by P. Kapitza, J.F. Allen, and D. Misener, who studied the viscosity of liquid helium at cryogenic temperatures [56, 57]. This phenomenon was soon attributed to the formation of a Bose-Einstein condensate of helium atoms.

3.5.1 Coherence properties and condensed fraction

Neutron-scattering experiments, which study the resonant transfer of energy and momentum between a neutron beam and liquid helium, can be used to measure the atomic momentum distribution n_k [58]. Its central peak, corresponding to the $n_0\,\delta_{\mathbf{k},\mathbf{0}}$ term convolved with experimental broadening, gives a condensed fraction of $f_0 = \rho_0/\rho = 7\%$ at zero temperature and saturating vapor pressure. The fact that the system is not fully condensed at $T = 0$ comes from the strong interactions between atoms. We will develop in section 6 the Bogoliubov theory, which describes the elementary excitations of a Bose-Einstein condensate and offers a theoretical framework for understanding partial condensation at $T = 0$ in an idealized model. It is important to note that the partial nature of condensation does not preclude the system from being fully superfluid. Indeed, it exhibits no viscosity and remains unresponsive to moderate rotations of its container at zero temperature.

The measured condensed fraction is consistent with a computation of the g_1 function using quantum Monte-Carlo simulations, shown in Fig. 24 [59, 60].

3.5.2 Pair distribution function

The pair distribution function $g^{(2)}(r)$ was also measured using neutron scattering experiments. As shown in Fig. 24b, it compares very well with a numerical computation using quantum Monte-Carlo simulations [60]. At short distances, $g^{(2)}(r)$ tends towards zero because of the short-range repulsion between helium atoms. It exceeds one for $r \simeq 3.5\,\text{Å}$, but this bunching should not be considered as a smoking gun of bosonic quantum statistics, as checked using Monte-Carlo simulations of an equivalent system without bosonic exchange statistics [60].

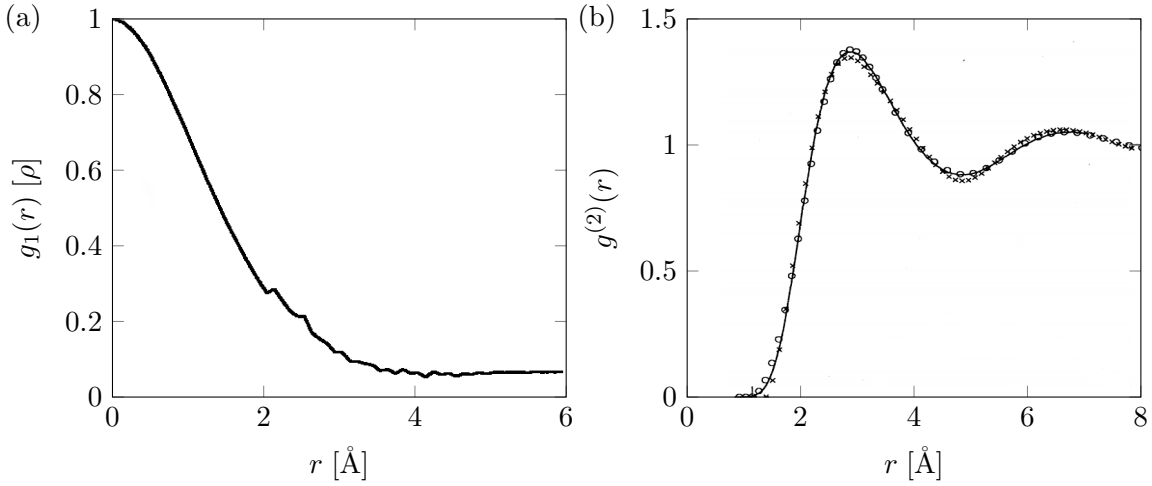


Figure 24: (a) First-order correlation function of superfluid helium, computed using quantum Monte-Carlo simulations (adapted from [59, 60]). The asymptotic value $g_1(r \to \infty)/\rho \simeq 7\%$ corresponds to the condensed fraction. (b) Normalized pair distribution function $g^{(2)}(r)$ computed using Monte-Carlo simulations (solid line) and measured using neutron scattering experiments (symbols) [60].

4 Describing interactions: quantum scattering

The description of a typical quantum many-body system involves single-particle operators (e.g. kinetic energy, lattice potential) as well as the binary interaction between pairs of particles. This section describes the quantum theory of scattering between two particles. We do not treat the more complex case of genuine three-body interactions, that play a role in more exotic systems.

4.1 The two-body problem: definitions

We consider two particles labelled 1 and 2, of masses m_1 and m_2. Their dynamics is described by the Hamiltonian

$$\hat{H} = \frac{\hat{p}_1^2}{2m_1} + \frac{\hat{p}_2^2}{2m_2} + V(\hat{\mathbf{r}}_2 - \hat{\mathbf{r}}_1), \tag{4.1}$$

where $V(\mathbf{r})$ is the interaction potential. We assume that the interaction potential decays at long distance towards an asymptotic zero value.

The invariance of the system under global translations leads to a separation between the center-of-mass and relative motions. More precisely, we define the center-of-mass operators

$$\begin{aligned}\hat{\mathbf{R}} &= \frac{m_1\,\hat{\mathbf{r}}_1 + m_2\,\hat{\mathbf{r}}_2}{M},\\ \hat{\mathbf{P}} &= \hat{\mathbf{p}}_1 + \hat{\mathbf{p}}_2,\end{aligned}$$

where $M = m_1 + m_2$ is the total mass, and the relative motion operators

$$\begin{aligned}\hat{\mathbf{r}} &= \hat{\mathbf{r}}_2 - \hat{\mathbf{r}}_1,\\ \hat{\mathbf{p}} &= \mu\left(\frac{\hat{\mathbf{p}}_2}{m_2} - \frac{\hat{\mathbf{p}}_1}{m_1}\right),\end{aligned}$$

where $\mu = m_1 m_2/(m_1 + m_2)$ is the reduced mass. The Hamiltonian can be expressed as

$$\hat{H} = \frac{\hat{P}^2}{2M} + \frac{\hat{p}^2}{2\mu} + V(\hat{\mathbf{r}}), \tag{4.2}$$

which corresponds to free motion of the center of mass and the dynamics of a fictitious particle of mass μ evolving in the potential $V(\mathbf{r})$. We can look for eigenstates of the Hamiltonian as a product of a plane wave $|\mathbf{P}\rangle$ for the center-of-mass motion and an eigenstate $|\psi\rangle$ of the relative motion

$$|\Psi\rangle = |\mathbf{P}\rangle \otimes |\psi\rangle. \tag{4.3}$$

We will disregard hereafter the trivial motion of the center of mass and focus on the relative motion. Following the standard treatment of particle dynamics in a potential, we can distinguish two types of eigenstates:

- discrete bound states of energy $E < 0$,

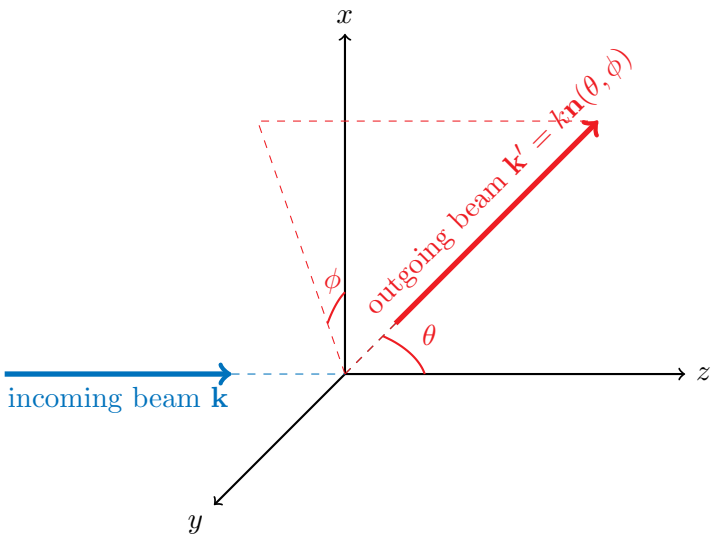


Figure 25: Scheme of the cartesian and spherical coordinates conventions used to describe scattering processes in this course.

- a continuum of scattering states of energy $E > 0$.

In the following we will focus on the description of the most subtle case of scattering and discuss the existence of bound states more quickly.

Scattering has played a prominent role in the development of our knowledge on the structure of matter, from Rutherford's discovery of the nucleus to the exploration of sub-atomic physics in high-energy particle colliders. In low-energy physics, it plays an important role in the study of solid-state systems through neutron-, electron- or X-ray scattering.

A scattering process corresponds to the problem of the interaction between a beam of particles onto a target. We can distinguish inelastic from elastic scattering, for which the particle remains in the same internal state and exits with the same kinetic energy as the incoming one. We focus here on the description of elastic scattering.

Differential scattering cross-section The amplitude of scattering is globally quantified by the scattering cross-section σ, which counts the rate of particles $\dot{N}$ that undergo the collision for an incoming flux j , according to

$$\dot{N} = j\sigma. \tag{4.4}$$

For a hard sphere target of radius R and a point-like incoming particle, classical dynamics predicts that the cross section corresponds to the actual area of the geometric cross section $\sigma = \pi R^2$ [61].

The scattering process is more precisely characterized by the differential cross section $(\mathrm{d}\sigma/\mathrm{d}\Omega)$, which quantifies the angular scattering pattern. It is defined by the rate of particles $\mathrm{d}\dot{N}$ scattered towards the direction $\mathbf{n} = (\theta, \phi)$ with a solid angle $\mathrm{d}^2\Omega$, given by

$$\mathrm{d}\dot{N} = j \left(\frac{\mathrm{d}\sigma}{\mathrm{d}\Omega} \right) \mathrm{d}^2\Omega. \tag{4.5}$$

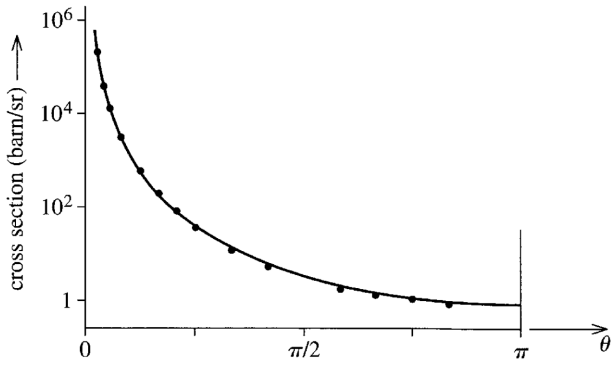


Figure 26: Historical measurement of the differential cross section of alpha particles on a thin gold foil by Geiger and Marsden. The excellent agreement with Rutherford's formula strongly supported Rutherford's planetary model of the atom.

We use the standard convention of an angle θ defined relative to the axis of the incident beam (see Fig. 25).

Reminder of classical physics. We remind some well-known examples of scattering in classical physics [61]. We focus on isotropic scattering potentials, for which the scattering cross-section only depends on the polar angle θ. The deflection of a classical trajectory of impact parameter b is characterized by the exit angle $\theta(b)$. We can easily show the relationship

$$\left(\frac{\mathrm{d}\sigma}{\mathrm{d}\Omega}\right) = \left|\frac{\mathrm{d}(\pi b^2)}{\mathrm{d}[2\pi(1-\cos\theta)]}\right| = \frac{1}{4}\left|\frac{\mathrm{d}b^2}{\mathrm{d}\sin^2(\theta/2)}\right|. \tag{4.6}$$

For a point projectile bouncing off a hard sphere of radius R, one can show that the differential cross section is isotropic, with

$$\left(\frac{\mathrm{d}\sigma}{\mathrm{d}\Omega}\right) = \frac{R^2}{4}. \tag{4.7}$$

In the famous collision experiment performed by Rutherford, the scattering of alpha particles onto gold nuclei involves the Coulomb potential $V(\mathbf{r}) = qQ/(4\pi\varepsilon_0 r)$. It is a standard exercise to derive the expression for the differential cross section

$$\left(\frac{\mathrm{d}\sigma}{\mathrm{d}\Omega}\right) = \left(\frac{qQ}{16\pi\varepsilon_0 E\sin^2(\theta/2)}\right)^2, \tag{4.8}$$

where E is the energy. This formula was tested with great accuracy by Rutherford's assistants Geiger and Marsden, who contributed to the acceptance of Rutherford's planetary model of the atom (see Fig. 26).

Extension to quantum scattering. We now turn to the quantum-mechanical problem. In order to define the differential scattering cross section, we consider a scattering eigenstate $\psi_{\mathbf{k}}(\mathbf{r})$ of energy $E = \hbar^2 k^2/2\mu$ (with $E > 0$). More specifically, it is a stationary eigenstate of the Schrödinger equation

$$E\psi_{\mathbf{k}}(\mathbf{r}) = \left[-\frac{\hbar^2}{2\mu}\Delta + V(\mathbf{r})\right]\psi_{\mathbf{k}}(\mathbf{r}) \tag{4.9}$$

that can be decomposed into an incoming (non-normalized) plane wave and a scattered wave

$$\psi_{\mathbf{k}}(\mathbf{r}) = \mathrm{e}^{\mathrm{i}\mathbf{k}\cdot\mathbf{r}} + \psi_{\mathrm{sc}}(\mathbf{r}), \tag{4.10}$$

where $\mathbf{k} = k\,\mathbf{e}_z$ is the incoming wave-vector.

For a sufficiently localized scattering potential, the scattered wave takes the asymptotic form

$$\psi_{\mathrm{sc}}(\mathbf{r}) \simeq f(\mathbf{k},\mathbf{k}')\frac{\mathrm{e}^{\mathrm{i}kr}}{r} \tag{4.11}$$

in the far-field region, i.e. for r much larger than the potential range b (and than kb^2), where $f(\mathbf{k},\mathbf{k}')$ is the scattering amplitude for an outgoing momentum $\mathbf{k}' = k\,\mathbf{n}$, parametrized by the outgoing direction $\mathbf{n}$ or equivalently the polar angles (θ,ϕ). The computation of the particle flux involves the probability current $\mathbf{j} = \frac{\hbar}{2\mu\mathrm{i}}(\psi^*\nabla\psi - \psi\nabla\psi^*)$, which can be decomposed into three terms:

1. the incoming particle flux
$$\mathbf{j}_{\mathrm{in}} = \frac{\hbar\mathbf{k}}{\mu}. \tag{4.12}$$

2. the scattered flux
$$\mathbf{j}_{\mathrm{sc}}(\mathbf{n}) = \frac{\hbar k}{\mu}\frac{|f(\mathbf{k},\mathbf{k}')|^2}{r^2}\mathbf{n}. \tag{4.13}$$

3. the cross product involving the product of the incoming plane wave and the scattered spherical wave. Except for forward scattering $\theta \simeq 0$, the cross product involves interference terms $\mathrm{e}^{\pm\mathrm{i}kr(1-\cos\theta)}$ that oscillate on very small angular scale as $kr \to \infty$, so that can be safely neglected.

The differential cross section can be obtained from the particle flux scattered through the area sustained by a solid angle $\mathrm{d}^2\Omega$ around $\mathbf{n}$, as

$$\mathbf{j}_{\mathrm{sc}} \cdot \mathbf{n}\, r^2 \mathrm{d}^2\Omega = j_{\mathrm{in}}|f(\mathbf{k},\mathbf{k}')|^2\mathrm{d}^2\Omega, \tag{4.14}$$

which leads to

$$\left(\frac{\mathrm{d}\sigma}{\mathrm{d}\Omega}\right) = |f(\mathbf{k},\mathbf{k}')|^2. \tag{4.15}$$

4.2 The Lippmann-Schwinger equation

We can rewrite the Schrödinger equation as follows

$$\frac{\hbar^2}{2\mu}(\Delta + k^2)\psi_{\mathbf{k}}(\mathbf{r}) = V(\mathbf{r})\psi_{\mathbf{k}}(\mathbf{r}), \tag{4.16}$$

which can be solved formally using Green's functions by considering the right hand side as a source term. For this, we define the Green function $\mathcal{G}_0(\mathbf{r})$ as the solution of the partial differential equation

$$\frac{\hbar^2}{2\mu}(\Delta + k^2)\mathcal{G}_0(\mathbf{r}) = \delta(\mathbf{r}). \tag{4.17}$$

This equation exhibits two linearly independent solutions corresponding to incoming and outgoing spherical waves

$$\mathcal{G}_0^{(\pm)}(\mathbf{r}) = -\frac{\mu}{2\pi\hbar^2}\frac{\mathrm{e}^{\pm \mathrm{i}kr}}{r}. \tag{4.18}$$

For our scattering problem, we retain solely the outgoing spherical wave, and obtain after integration the Lippmann-Schwinger equation [62]

$$\psi_{\mathbf{k}}(\mathbf{r}) = \mathrm{e}^{\mathrm{i}\mathbf{k}\cdot\mathbf{r}} + \int \mathcal{G}_0^{(+)}(\mathbf{r}-\mathbf{r}')V(\mathbf{r}')\psi_{\mathbf{k}}(\mathbf{r}')\mathrm{d}^3r'. \tag{4.19}$$

Note that the wave-function $\psi_{\mathbf{k}}(\mathbf{r})$ is involved in the integral, so that this equation cannot be considered as an explicit expression for the scattering state.

The scattering amplitude can be expressed by looking at the scattered wave in the far-field region. We approximate $|\mathbf{r}-\mathbf{r}'| \simeq r - \mathbf{n}\cdot\mathbf{r}'$ (with $\mathbf{n} = \mathbf{r}/r$), and

$$\frac{\mathrm{e}^{\mathrm{i}k|\mathbf{r}-\mathbf{r}'|}}{|\mathbf{r}-\mathbf{r}'|} \simeq \frac{\mathrm{e}^{\mathrm{i}kr}}{r}\mathrm{e}^{-\mathrm{i}\mathbf{k}'\cdot\mathbf{r}'}, \tag{4.20}$$

where we use the expression $\mathbf{k}' = k\mathbf{n}$ for the outgoing wave-vector. This leads to the scattering wave-function

$$\psi_{\mathbf{k}}(\mathbf{r}) \simeq \mathrm{e}^{\mathrm{i}\mathbf{k}\cdot\mathbf{r}} - \frac{\mu}{2\pi\hbar^2}\frac{\mathrm{e}^{\mathrm{i}kr}}{r}\int \mathrm{e}^{-\mathrm{i}\mathbf{k}'\cdot\mathbf{r}'}V(\mathbf{r}')\psi_{\mathbf{k}}(\mathbf{r}')\,\mathrm{d}^3r'. \tag{4.21}$$

Normalization conventions. In order to express this result in terms of operators, we use, as in the rest of these lecture notes, plane waves normalized in a cubic box of volume L^3 with periodic boundary conditions,

$$\langle\mathbf{r}|\mathbf{k}\rangle = \frac{\mathrm{e}^{\mathrm{i}\mathbf{k}\cdot\mathbf{r}}}{L^{3/2}}, \quad \langle\mathbf{k}|\mathbf{k}'\rangle = \delta_{\mathbf{k},\mathbf{k}'}, \quad \sum_{\mathbf{k}}|\mathbf{k}\rangle\langle\mathbf{k}| = \hat{\mathbb{1}}, \tag{4.22}$$

with the continuum limit $\sum_{\mathbf{k}} \to L^3\int \mathrm{d}^3k/(2\pi)^3$ for $L\to\infty$. The scattering state $|\psi_{\mathbf{k}}\rangle$ is normalized in the same manner as the incoming plane wave, i.e. $\langle\mathbf{r}|\psi_{\mathbf{k}}\rangle = \psi_{\mathbf{k}}(\mathbf{r})/L^{3/2}$.

We define the transition operator $\hat{T}$ by its action on plane waves as

$$\hat{T}|\mathbf{k}\rangle = \hat{V}|\psi_{\mathbf{k}}\rangle. \tag{4.23}$$

The matrix elements of $\hat{V}$ and $\hat{T}$ between plane waves scale as $1/L^3$. Since the scattering amplitude, which is a physical quantity, does not depend on L, it is convenient to work with the box-independent quantities

$$\tilde{V}(\mathbf{k}'-\mathbf{k}) \equiv L^3\langle\mathbf{k}'|\hat{V}|\mathbf{k}\rangle = \int \mathrm{e}^{-\mathrm{i}(\mathbf{k}'-\mathbf{k})\cdot\mathbf{r}}V(\mathbf{r})\,\mathrm{d}^3r, \qquad \mathcal{T}(\mathbf{k}',\mathbf{k}) \equiv L^3\langle\mathbf{k}'|\hat{T}|\mathbf{k}\rangle, \tag{4.24}$$

where $\tilde{V}(\mathbf{q})$ is the Fourier transform of the potential. We then identify the scattering amplitude as

$$f(\mathbf{k},\mathbf{k}') = -\frac{\mu}{2\pi\hbar^2}\,\mathcal{T}(\mathbf{k}',\mathbf{k}). \tag{4.25}$$

This expression justifies the name of transition matrix for the operator $\hat{T}$. In the following, all formulas are expressed in terms of $\tilde{V}$ and $\mathcal{T}$, with momentum sums written as integrals $\int \mathrm{d}^3k/(2\pi)^3$, so that the box size L no longer appears. These formulas are identical to those obtained with non-normalized plane waves $\mathrm{e}^{\mathrm{i}\mathbf{k}\cdot\mathbf{r}}$.

4.3 Born approximation and perturbative expansion

The Lippmann-Schwinger equation can be used as the starting point of a perturbative treatment with respect to the scattering potential V, known as the Born expansion. This approach is particularly useful when considering scattering at high energy, for which the scattering probability remains small. More quantitatively, for a potential of typical magnitude $|V_0|$ and range b, the first-order correction to the wave-function remains small near the scattering center provided that

$$|V_0| \ll \frac{\hbar^2}{\mu b^2} \quad \text{at low energy } (kb \lesssim 1),$$
$$|V_0|\, b \ll \hbar v = \frac{\hbar^2 k}{\mu} \quad \text{at high energy } (kb \gg 1).$$

The first condition expresses that the potential is too weak to bind a particle, while the second one shows that the Born approximation always becomes valid at sufficiently high energy (for a regular potential).

4.3.1 Born approximation

At zero order in V, the scattering potential is neglected and the scattering state reduces to the incoming plane wave

$$\psi_{\mathbf{k}}(\mathbf{r}) \simeq \mathrm{e}^{\mathrm{i}\mathbf{k}\cdot\mathbf{r}}. \tag{4.26}$$

At first order, one replaces in the integral the scattering state by its zero-order expression, leading to

$$\psi(\mathbf{r}) \simeq \mathrm{e}^{\mathrm{i}\mathbf{k}\cdot\mathbf{r}} + \int \mathcal{G}_0^{(+)}(\mathbf{r}-\mathbf{r}')V(\mathbf{r}')\mathrm{e}^{\mathrm{i}\mathbf{k}\cdot\mathbf{r}'}\mathrm{d}^3r'. \tag{4.27}$$

As a result, the scattering amplitude is obtained by replacing the scattering state $|\psi_{\mathbf{k}}\rangle$ by the incoming plane wave, leading to

$$f(\mathbf{k},\mathbf{k}') = -\frac{\mu}{2\pi\hbar^2}\tilde{V}(\mathbf{k}'-\mathbf{k}), \tag{4.28}$$

which involves the matrix element of the scattering potential between the incoming and outgoing wave-vectors. This shows that, within the Born approximation, the T matrix is simply given by the matrix elements of the scattering potential V in momentum space, $\mathcal{T}(\mathbf{k}',\mathbf{k}) \simeq \tilde{V}(\mathbf{q})$, i.e. by the Fourier transform of the scattering potential at the transferred momentum $\mathbf{q} \equiv \mathbf{k}' - \mathbf{k}$.

Note that the differential cross section $|f(\mathbf{k},\mathbf{k}')|^2$ obtained within the Born approximation can also be obtained using Fermi's Golden rule giving the transition rate between the incoming plane wave $\mathbf{k}$ and the continuum of states with wave-vectors $\mathbf{k}'$.

Example 1: Yukawa/Coulomb potentials. We consider the Yukawa potential

$$V(r) = \alpha\frac{\mathrm{e}^{-r/R}}{r}, \tag{4.29}$$

which is extensively used in particle physics, e.g. for modeling the strong interaction between hadrons. It is also relevant in condensed matter physics to describe interactions

between electrons, where their mutual Coulomb interaction is screened by the ionic lattice. Its Fourier representation is given by a Lorentzian

$$\tilde{V}(\mathbf{k}'-\mathbf{k}) = \frac{4\pi\alpha R^2}{1+|\mathbf{k}-\mathbf{k}'|^2R^2} = \frac{4\pi\alpha R^2}{1+4k^2R^2\sin^2(\theta/2)}, \tag{4.30}$$

hence the differential cross section

$$\left(\frac{\mathrm{d}\sigma}{\mathrm{d}\Omega}\right) = \left(\frac{2\alpha\mu}{\hbar^2}\frac{R^2}{1+4k^2R^2\sin^2(\theta/2)}\right)^2. \tag{4.31}$$

In the limit $R\to\infty$, the potential becomes the Coulomb potential. For $\alpha = qQ/(4\pi\varepsilon_0)$, we recover the Rutherford formula given in (4.8).

Example 2: Bragg scattering from periodic potential. The scattering from a periodic potential plays a prominent role in the study of crystalline structure. The Fourier transform of a periodic potential is constituted of discrete momenta, which can be decomposed as

$$\mathbf{g}_{n_1,n_2,n_3} = n_1\,\mathbf{g}_1 + n_2\,\mathbf{g}_2 + n_3\,\mathbf{g}_3, \tag{4.32}$$

where $(\mathbf{g}_1,\mathbf{g}_2,\mathbf{g}_3)$ are the primitive vectors of the reciprocal lattice and the n_i's are integers.

The scattering of an incoming plane wave of momentum $\mathbf{k}$ gives rise to discrete Bragg diffraction peaks at

$$\mathbf{k}'_{n_1,n_2,n_3} = \mathbf{k} + \mathbf{g}_{n_1,n_2,n_3}, \tag{4.33}$$

provided that the outgoing wave-vector satisfies the energy conservation condition $|\mathbf{k}'| = |\mathbf{k}|$ of elastic scattering, i.e.

$$2\mathbf{k}\cdot\mathbf{g}_{n_1,n_2,n_3} + |\mathbf{g}_{n_1,n_2,n_3}|^2 = 0. \tag{4.34}$$

This Laue condition is equivalent to Bragg's law. For a generic incoming wave-vector, it is not fulfilled by any non-zero reciprocal lattice vector, and diffraction peaks are observed only for specific orientations of the crystal or by using a polychromatic beam or a powder sample.

Note that this Bragg diffraction solely relies on the fact that the Fourier transform of the potential is restricted to discrete momenta. It also applies to quasi-crystals, which are precisely defined by a Fourier transform restricted to

$$\mathbf{g}_{n_1,\ldots,n_p} = \sum_{i=1}^{p} n_i\mathbf{g}_i, \tag{4.35}$$

where the number p of incommensurate vectors $\mathbf{g}_i$ exceeds the spatial dimension. In general, the potential $V(\mathbf{r})$ is not spatially periodic, but it exhibits a so-called quasi-crystalline order [63].

4.3.2 Extending the Born expansion

The Born expansion can also be performed systematically to higher orders. For this, a formulation of the Lippmann-Schwinger equation in terms of operators is more adapted. The starting point of its derivation, given by (4.16), can be formulated as

$$(E-\hat{H}_0)|\psi_{\mathbf{k}}\rangle = \hat{V}|\psi_{\mathbf{k}}\rangle, \tag{4.36}$$

where $\hat{H}_0 = \hat{p}^2/(2\mu)$ is the free particle Hamiltonian. It is tempting to define the inverse of the operator $(E - \hat{H}_0)$, but this operator is not invertible for $E > 0$. We regularize it by adding an infinitesimal imaginary part $\mathrm{i}\eta$ before taking the inverse (with $\eta > 0$ an infinitesimal positive real number). By adding the incoming plane wave as an obvious solution of the homogeneous equation, we obtain the formal expression for the scattering state

$$|\psi_{\mathbf{k}}\rangle = |\mathbf{k}\rangle + \hat{G}_0^{(+)}\hat{V}|\psi_{\mathbf{k}}\rangle, \tag{4.37}$$

where we introduce the Green operator (also called the resolvent operator, already introduced in section 1.3.2)

$$\hat{G}_0^{(+)} = \frac{1}{E - \hat{H}_0 + \mathrm{i}\eta}. \tag{4.38}$$

In order to express the matrix elements of the Green operator, we write

$$(E + \mathrm{i}\eta - \hat{H}_0)\hat{G}_0 = \hat{\mathbb{1}} \tag{4.39}$$

and take the matrix elements between $\langle\mathbf{r}'|$ and $|\mathbf{r}\rangle$, which gives

$$\frac{\hbar^2}{2\mu}\left[(k + \mathrm{i}\eta')^2 + \Delta\right]\langle\mathbf{r}'|\hat{G}_0^{(+)}|\mathbf{r}\rangle = \delta(\mathbf{r} - \mathbf{r}'), \tag{4.40}$$

where we write $E + \mathrm{i}\eta = \hbar^2(k + \mathrm{i}\eta')^2/(2\mu)$, with $\eta' = \mu\eta/(\hbar^2 k)$ another positive infinitesimal, that we rename η hereafter. The matrix element $\langle\mathbf{r}'|\hat{G}_0^{(+)}|\mathbf{r}\rangle$ is nothing but a Green function $\mathcal{G}_0(|\mathbf{r} - \mathbf{r}'|)$ solution of (4.17), which can be expanded over incoming and outgoing spherical waves

$$\mathcal{G}_0(r) = A_- \frac{\mathrm{e}^{-\mathrm{i}(k+\mathrm{i}\eta)r}}{r} + A_+ \frac{\mathrm{e}^{\mathrm{i}(k+\mathrm{i}\eta)r}}{r}. \tag{4.41}$$

Because of the imaginary term $\mathrm{i}\eta$, the incoming wave diverges for $r \to \infty$, so that $A_- = 0$. We eventually find that the matrix elements $\langle\mathbf{r}'|\hat{G}_0^{(+)}|\mathbf{r}\rangle$ are given by the Green function $\mathcal{G}_0^{(+)}(|\mathbf{r} - \mathbf{r}'|)$ representing an outgoing spherical wave. This justifies a posteriori the choice of the infinitesimal term $\mathrm{i}\eta$.

The formal expression for the scattering state (4.37) allows for a systematic Born expansion in powers of V, as

$$|\psi_{\mathbf{k}}\rangle = |\mathbf{k}\rangle + \hat{G}_0^{(+)}\hat{V}|\mathbf{k}\rangle + (\hat{G}_0^{(+)}\hat{V})^2|\mathbf{k}\rangle + \dots. \tag{4.42}$$

We introduce the transition operator

$$\hat{T} = \hat{V} + \hat{V}\hat{G}_0^{(+)}\hat{V} + \hat{V}(\hat{G}_0^{(+)}\hat{V})^2 + \dots, \tag{4.43}$$

such that the scattering state writes

$$|\psi_{\mathbf{k}}\rangle = |\mathbf{k}\rangle + \hat{G}_0^{(+)}\hat{T}|\mathbf{k}\rangle. \tag{4.44}$$

Comparing this expression with the Lippmann-Schwinger equation (4.37), we identify $\hat{T}|\mathbf{k}\rangle = \hat{V}|\psi_{\mathbf{k}}\rangle$, which corresponds to the definition of the T matrix introduced in (4.23).

Based on the expansion (4.43) of the T matrix, we can decompose the scattering amplitude between two states $\mathbf{k}$ and $\mathbf{k}'$ as a sum of contributions involving several

elementary scattering events. For instance, at order 2 in V, we account for two scattering events involving an intermediate momentum state $\mathbf{k}''$, leading to the expression

$$\langle \mathbf{k}'|\hat{T}|\mathbf{k}\rangle = \langle \mathbf{k}'|\hat{V}|\mathbf{k}\rangle + \sum_{\mathbf{k}''} \frac{\langle \mathbf{k}'|\hat{V}|\mathbf{k}''\rangle\langle \mathbf{k}''|\hat{V}|\mathbf{k}\rangle}{E - \hbar^2 k''^2/(2\mu) + \mathrm{i}\eta} + \dots \tag{4.45}$$

In terms of the box-independent quantities (4.24), and in the continuum limit, it writes

$$\mathcal{T}(\mathbf{k}', \mathbf{k}) = \tilde{V}(\mathbf{k}' - \mathbf{k}) + \int \frac{\tilde{V}(\mathbf{k}' - \mathbf{k}'')\tilde{V}(\mathbf{k}'' - \mathbf{k})}{E - \hbar^2 k''^2/(2\mu) + \mathrm{i}\eta} \frac{\mathrm{d}^3 k''}{(2\pi)^3} + \dots \tag{4.46}$$

The relevance of the Born expansion relies on the convergence of the series, whose study can be quite complex [64]. It can be shown that, if the scattering potential decays sufficiently fast with distance, there exists an energy E_* above which the Born series converges. Moreover, the series is convergent at all energies if the attractive potential $-|V(\mathbf{r})|$ is sufficiently shallow to exhibit no bound state. Conversely, when the potential V supports a bound state, the Born series necessarily diverges at low energy, since a finite-order expansion cannot reproduce the pole of the scattering amplitude associated with the bound state (see section 4.4.2).

However, there exists situations for which the Born expansion is not useful, for instance when the scattering occurs at low energy and for an interaction potential sufficiently strong to allow for bound states. This is the case for the van der Waals interaction between neutral atoms in the ultracold regime, for which the interaction potential typically hosts dozens of bound states.

4.4 Partial wave decomposition

When the Born approximation is not useful, the determination of the scattering amplitude requires solving directly the Schrödinger equation, which may be difficult. The problem is significantly simplified in the case of a spherically symmetric potential $V(r)$. Thanks to the rotational symmetry of the problem, it is convenient to decompose the incoming plane wave into spherical harmonics, so that the scattering problem can be decomposed into scattering between spherical waves of given angular momentum.

4.4.1 Definition of the partial wave decomposition

We remind that we use the convention of an incoming plane wave directed along $\mathbf{e}_z$. The so-called partial wave decomposition of the plane wave writes (formula 10.60.7 of the NIST Digital Library of Mathematical Functions)

$$\mathrm{e}^{\mathrm{i}kz} = \sum_{\ell=0}^{\infty} (2\ell + 1)\, \mathrm{i}^\ell j_\ell(kr) P_\ell(\cos\theta), \tag{4.47}$$

where j_ℓ are the spherical Bessel functions and $P_\ell(\cos\theta) = \sqrt{\frac{4\pi}{2\ell+1}} Y_{\ell 0}(\theta)$ denote the Legendre polynomials. Using the asymptotic behavior $j_\ell(kr) \simeq \sin(kr - \ell\pi/2)/(kr)$ for $kr \gg 1$, we obtain at large distance

$$\mathrm{e}^{\mathrm{i}kz} \simeq \frac{1}{2\mathrm{i}kr} \sum_{\ell=0}^{\infty} (2\ell + 1) \left[(-1)^{\ell+1} \mathrm{e}^{-\mathrm{i}kr} + \mathrm{e}^{\mathrm{i}kr}\right] P_\ell(\cos\theta). \tag{4.48}$$

The plane wave is thus decomposed into a series of incoming and outgoing spherical waves of different angular momentum ℓ. We note that the projection of the angular momentum m is equal to $m = 0$ for all terms, because we have aligned the propagation axis of the plane wave with the z axis.

Rotational symmetry of the potential $V(r)$ ensures that an incoming spherical wave of angular momentum ℓ can only be scattered towards the outgoing spherical wave with the same value of ℓ. Consequently, the scattering state can be expressed, at large distance from the scattering center, as

$$\psi_{\mathbf{k}}(\mathbf{r}) \simeq \frac{1}{2\mathrm{i}kr} \sum_{\ell=0}^{\infty} (2\ell+1) \left[(-1)^{\ell+1} \mathrm{e}^{-\mathrm{i}kr} + S_\ell \mathrm{e}^{\mathrm{i}kr} \right] P_\ell(\cos\theta), \tag{4.49}$$

where S_ℓ characterizes the scattering within a given partial wave ℓ. The conservation of particle flux imposes that S_ℓ is of modulus 1, hence we write it as

$$S_\ell = \mathrm{e}^{2\mathrm{i}\delta_\ell}. \tag{4.50}$$

Elastic scattering can then be fully characterized by the values of scattering phase shifts δ_ℓ. Akin to atomic orbital notations, the successive partial waves $\ell = 0, 1, 2, \ldots$ are usually referred to as $s, p, d \ldots$-wave channels.

The scattering amplitude, which only depends on the polar scattering angle θ, is given by

$$f(\theta) = \frac{1}{2\mathrm{i}k} \sum_{\ell=0}^{\infty} (2\ell+1)(\mathrm{e}^{2\mathrm{i}\delta_\ell} - 1) P_\ell(\cos\theta). \tag{4.51}$$

The scattering cross-section σ is obtained by integrating the modulus square of the scattering amplitude over the scattering angles (θ, ϕ). The orthogonality between Legendre polynomials allows one to separate the contribution from each partial wave, as

$$\sigma = \sum_{\ell=0}^{\infty} \sigma_\ell, \quad \text{where} \quad \sigma_\ell = \frac{4\pi}{k^2}(2\ell+1)\sin^2\delta_\ell. \tag{4.52}$$

We note that each partial wave exhibits a maximal value for the scattering cross-section, known as the unitary limit. It is reached when the phase shift is equal to $\delta_\ell = \pi/2 \,(\mathrm{mod}\ \pi)$, and is given by

$$\sigma_\ell^{\max} = \frac{4\pi}{k^2}(2\ell+1). \tag{4.53}$$

The total cross section can be directly linked with the amplitude $f(\theta = 0)$ in the forward direction. Using $P_\ell(1) = 1$ for all partial waves ℓ, we can easily check the relation

$$\mathrm{Im}\, f(\theta = 0) = \frac{k}{4\pi}\sigma, \tag{4.54}$$

known as the optical theorem. This identity simply reflects the conservation of probability: one can check that the forward scattering amplitude gives rise to a reduction of the probability current in the forward direction, precisely by the amount scattered in all other directions.

The computation of scattering phase shifts requires solving the Schrödinger equation for a wave-function of given angular momentum ℓ. Decomposing the wave-function

as $Y_\ell^m(\theta,\phi)u_\ell(r)/r$, the problem can be reduced to a 1D Schrödinger equation for the radial wave-function

$$u_\ell''(r) + \left[k^2 - \frac{\ell(\ell+1)}{r^2} - \frac{2\mu V(r)}{\hbar^2}\right] u_\ell(r) = 0, \tag{4.55}$$

with $u_\ell(r=0)=0$. The large-r expansion of the solution, which can be expressed as

$$\begin{aligned} u_\ell(r) &\propto (-1)^{\ell+1}\mathrm{e}^{-\mathrm{i}kr} + \mathrm{e}^{2\mathrm{i}\delta_\ell}\mathrm{e}^{\mathrm{i}kr} && (4.56)\\ &\propto \sin(kr - \ell\pi/2 + \delta_\ell) && (4.57)\\ &\propto \sin(kr-\ell\pi/2) + \tan\delta_\ell \cos(kr-\ell\pi/2), && (4.58) \end{aligned}$$

then provides the value of the phase shift δ_ℓ.

4.4.2 Bound states and poles of the scattering amplitude

Let us consider a given scattering channel ℓ. A bound state of energy $E = -\hbar^2 q^2/(2\mu)$ (with $q>0$) decays at large distances as $Y_\ell^m(\theta,\phi)\mathrm{e}^{-qr}/r$ (up to power-law corrections for $\ell>0$), which can be seen as a spherical outgoing wave $Y_\ell^m(\theta,\phi)\mathrm{e}^{\mathrm{i}kr}/r$ with an imaginary wave-vector $k=\mathrm{i}q$. One can then formally characterize the discrete spectrum of bound states as the values of q for which the scattering amplitude diverges, so that the relative weight of the incoming plane wave vanishes, leaving solely the spherical wave of imaginary wave-vector as the bound-state wave-function.

In other words, the spectrum of bound states can be obtained as the poles of the scattering amplitude (or equivalently of $S_\ell(k)$, analytically continued to complex k) on the imaginary semi-axis $\mathrm{i}\mathbb{R}_+$.

4.4.3 Low-energy limit and scattering length

Except for s-wave ($\ell=0$) scattering, the radial equation given in (4.55) involves a centrifugal barrier that suppresses the density probability in the classically forbidden region

$$r < r_E = \sqrt{\frac{\hbar^2\ell(\ell+1)}{2\mu E}}. \tag{4.59}$$

Let us consider the case of a potential whose range is limited to a finite range $r<b$. When the collision energy E is small enough for the radius r_E to exceed the range b, the interaction potential ceases to affect the radial wave-function, leading to a vanishing of the scattering phase shift δ_ℓ.

A more precise understanding of the low-energy regime $k \ll 1/b$ can be studied by solving the radial equation

$$u_\ell''(r) + \left[k^2 - \frac{\ell(\ell+1)}{r^2}\right] u_\ell(r) = 0 \tag{4.60}$$

for $r>b$, for which the potential can be neglected. This differential equation admits two linearly independent solutions as Bessel functions of the first and second kind, leading to the generic solution

$$u_\ell(r) = A\sqrt{kr}J_{\ell+1/2}(kr) + B\sqrt{kr}Y_{\ell+1/2}(kr). \tag{4.61}$$

At long distance $r \gg 1/k$, one uses the asymptotic expansion of Bessel functions to find [4]

$$u_\ell(r) \simeq \sqrt{2/\pi}[A \sin(kr - \ell\pi/2) - B \cos(kr - \ell\pi/2)]. \tag{4.62}$$

Comparing with (4.58), we obtain $B/A = -\tan\delta_\ell$. In the regime $b \ll r \ll 1/k$, we use the small-argument behavior of Bessel functions to obtain the asymptotic form

$$u_\ell(r) \simeq k^{\ell+1} \left[c_1 \, A \, r^{\ell+1} + c_2 \, \frac{B}{k^{2\ell+1}} \, r^{-\ell} \right], \tag{4.63}$$

where c_1 and c_2 are numerical constants. Since this functional form is valid over distances smaller than the inverse momentum $1/k$, it is determined by the zero-energy solution of the radial equation, and we expect it to be independent from the value of k (up to a global factor). This requires that the scattering phase shifts follow the scaling

$$\tan\delta_\ell(k) \propto k^{2\ell+1} \tag{4.64}$$

as $k \to 0$.[5] This confirms that the suppression of scattering phase shifts at low energy is more and more pronounced as ℓ increases. This behavior justifies the interest of the partial wave decomposition when studying collisions at low energy, where we expect that only a few partial waves need to be involved.

Let us consider the *cold collision* regime, for which the interaction is dominated by the s-wave channel. Quantum scattering then becomes isotropic, and it can be characterized in a very simple manner by the proportionality constant between $\tan\delta_0(k)$ and k, given by the so-called scattering length

$$a = -\lim_{k\to 0} \frac{\tan\delta_0(k)}{k}. \tag{4.65}$$

The scattering amplitude, given in the s-wave channel by $f = (\mathrm{e}^{2\mathrm{i}\delta_0} - 1)/(2\mathrm{i}k)$, takes the asymptotic form

$$f = -\frac{a}{1 + \mathrm{i}ka} \tag{4.66}$$

upon the approximation $\tan\delta_0 \simeq -ak$. Note that the scattering length can be positive, negative, and even infinite (this simply corresponds to a scattering phase shift $\delta_0 \to \pi/2 \pmod\pi$ in the limit $k \to 0$).

The expression of the scattering amplitude (4.66) can also be used to look for bound states. The scattering amplitude exhibits a single pole for $k = \mathrm{i}/a$, which is on the semi-axis $\mathrm{i}\mathbb{R}_+$ for $a > 0$. The corresponding energy writes

$$E = -\frac{\hbar^2 q^2}{2\mu} = -\frac{\hbar^2}{2\mu a^2}. \tag{4.67}$$

Note that this prediction is only relevant at low energy since the expression (4.66) of the scattering amplitude was derived in the low-k limit. It is thus meaningful only

[4] Note that for s-wave scattering, for which there is no centrifugal potential, the Bessel functions reduce to harmonic functions, so that the functional forms given in (4.56), (4.57) and (4.58) are exact for $\ell = 0$.

[5] This argument assumes that the potential decays sufficiently fast at large distances, namely faster than $1/r^{2\ell+3}$. For the van der Waals potential $V(r) \propto 1/r^6$, the scaling $\tan\delta_\ell \propto k^{2\ell+1}$ holds for $\ell = 0$ and $\ell = 1$, while $\tan\delta_\ell \propto k^4$ for all $\ell \geq 2$.

when the pole lies in the low-momentum region $q \ll 1/b$, i.e. for a scattering length large compared to the potential range, $a \gg b$. For $a \sim b$, the pole is an artefact of the low-energy expansion: for example, the hard-sphere potential discussed below has a positive scattering length $a = R$, but no bound state. One also cannot exclude the existence of additional strongly-bound states, outside the range of validity of (4.66).

We see that the binding energy of this weakly bound state vanishes when $a \to +\infty$. This behavior is generic: when the depth of an attractive potential is increased, each new bound state appears at the threshold $E = 0$, and the scattering length diverges at this point. This is related to Levinson's theorem, which states that the zero-energy phase shift is given by $\delta_0(0) - \delta_0(\infty) = N_\mathrm{b}\pi$, where N_b is the number of s-wave bound states: each time a new bound state appears, $\delta_0(0)$ increases by π, passing through the value $\pi/2$ at which a diverges.

The cold collision regime is typically encountered in the following situations:

- The nuclear interaction between neutrons involves a potential of range $b \simeq 2\,\mathrm{fm}$, which defines a cold-collision regime for $E \ll E_\star = \hbar^2/(2\mu b^2) = \hbar^2/(m_n b^2) \simeq 10\,\mathrm{MeV}$. This energy exceeds the typical energy of 'slow' neutron beam experiments. The low-energy regime is also relevant for the ultra-dense matter that constitute neutron stars. Since free neutron targets are not available, the neutron-neutron scattering length is determined indirectly, from nuclear reactions producing two neutrons in the final state, such as the radiative capture $\pi^- + d \to n + n + \gamma$, leading to the value $a \simeq -18.6\,\mathrm{fm}$ [65].

- The interaction between atoms is dominated, at long distance, by the van der Waals interaction potential $V(r) = -C_6/r^6$. The characteristic energy $E_\star$ below which collisions dominantly occur in s-wave can be obtained by dimensional analysis. One first forms the van der Waals length $R_\mathrm{vdW} = (2\mu C_6/\hbar^2)^{1/4}$, and then the energy $E_\star = \hbar^2/(2\mu R_\mathrm{vdW}^2) = \hbar^3/[(2\mu)^{3/2}\sqrt{C_6}]$, which takes typical values $E_\star \sim k_B \times 100\,\mu\mathrm{K}$ for alkali atoms. Dilute atomic gases can be cooled down to very low temperatures, well below the micro-kelvin. In such conditions, van der Waals interactions are very well in the cold collision regime and, except in exotic situations, they can be fully characterized by the s-wave scattering length a.

4.5 Scattering between identical particles

Up to now, we have not paid attention to the exchange symmetry of the wave-function, implicitly assuming that the two particles are distinguishable. We now consider scattering between identical particles, and restrict the discussion to the case where they share the same internal state.

We remind that we have separated the center-of-mass motion from the relative one. The center-of-mass motion being always symmetric upon exchange, the effect of particle exchange statistics is only relevant for the relative motion, which should be written in the (anti-)symmetrized form

$$\psi_\mathbf{k}(\mathbf{r}) = \frac{1}{\sqrt{2}}\left(\mathrm{e}^{\mathrm{i}\mathbf{k}\cdot\mathbf{r}} + \varepsilon\,\mathrm{e}^{-\mathrm{i}\mathbf{k}\cdot\mathbf{r}} + [f(\mathbf{k},\mathbf{k}') + \varepsilon f(\mathbf{k},-\mathbf{k}')]\frac{\mathrm{e}^{\mathrm{i}kr}}{r}\right), \tag{4.68}$$

where $\mathbf{k}' = k\mathbf{r}/r$ is the outgoing wave-vector and where $\varepsilon = 1$ for bosons and -1 for

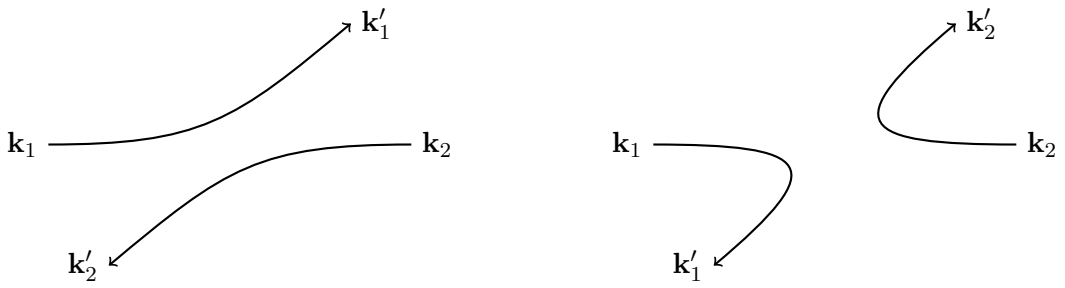


Figure 27: Scheme of the two scattering processes that cannot be distinguished for identical particles, leading to an interference.

fermions. The scattering cross-section then writes

$$\frac{\mathrm{d}\sigma}{\mathrm{d}\Omega} = \frac{1}{2}|f(\mathbf{k},\mathbf{k}') + \varepsilon\, f(\mathbf{k},-\mathbf{k}')|^2. \tag{4.69}$$

This expression reflects the interference between the two scattering processes shown in Fig. 27. For scattering at 90°, i.e. $\mathbf{k}' \perp \mathbf{k}$, the two amplitudes $f(\mathbf{k},\mathbf{k}')$ and $f(\mathbf{k},-\mathbf{k}')$ are equal, and the interference is constructive for bosons and destructive for fermions. Such interferences have been observed in collisions between carbon nuclei, with the isotopes ^{12}C (bosons) and ^{13}C (fermions) [66], see Fig. 28. In this experiment, a beam of carbon nuclei is sent onto a target at rest. For equal masses, a scattering angle of 90° in the center-of-mass frame corresponds to an angle of 45° in the laboratory frame.

The ^{13}C nucleus carries a spin 1/2, and the nuclei used in the experiment are not spin-polarized, so that the restriction to identical internal states does not hold. The two-nucleus spin state is a statistical mixture of the singlet state (probability 1/4), whose antisymmetric spin wave-function imposes a symmetric spatial wave-function, and of the triplet states (probability 3/4), associated with an antisymmetric spatial wave-function. The interference term is thus weighted by $1/4 - 3/4 = -1/2$, leading to

$$\frac{\mathrm{d}\sigma}{\mathrm{d}\Omega} = \frac{1}{2}\left(|f(\mathbf{k},\mathbf{k}')|^2 + |f(\mathbf{k},-\mathbf{k}')|^2 - \mathrm{Re}[f(\mathbf{k},\mathbf{k}')f^*(\mathbf{k},-\mathbf{k}')]\right), \tag{4.70}$$

i.e. a destructive interference with a contrast reduced by a factor 2 compared to spin-polarized fermions.

Indistinguishability plays a fundamental role in describing scattering in different partial waves. Notably, a wave-function with angular momentum ℓ exhibits spatial parity $(-1)^\ell$. Consequently, symmetric wave-functions for identical bosons can only be constructed using even values of ℓ, whereas identical fermions are restricted to odd partial waves. This constraint has significant implications in the cold collision regime: for identical fermions, the scattering wave-function is limited to higher (odd) partial waves $\ell \geq 1$, where the centrifugal barrier suppresses scattering, resulting in minimal interactions. This behavior has been observed by comparing the scattering cross-section for spin-polarized fermions and for a spin mixture as a function of temperature [67] (see Fig. 29).

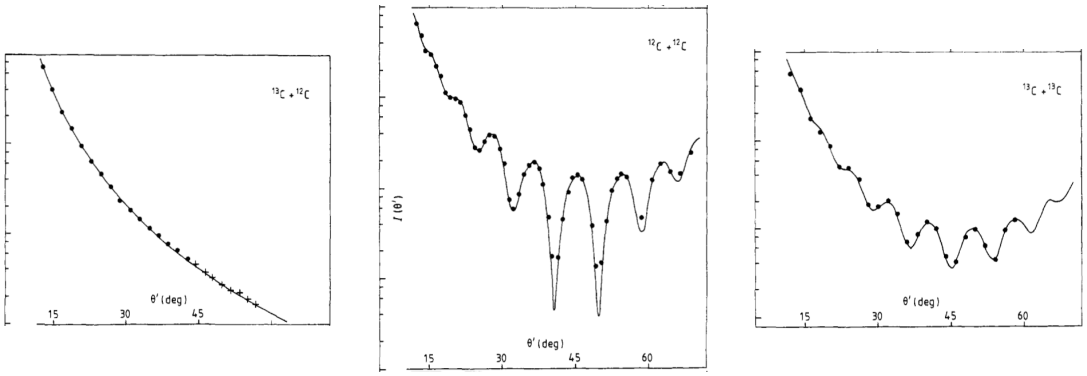


Figure 28: Differential scattering cross-section measured for the collision between different isotopes of carbon nuclei. The collision between two different isotopes (left panel) is well described by the Rutherford formula (4.8). Interferences are observed for collisions between identical isotopes. At 90° in the center-of-mass frame (45° in the laboratory frame used in the figure), the interference is constructive for bosons and destructive for fermions. The lower interference contrast for fermions results from the spin 1/2 of the ^{13}C nuclei: for unpolarized nuclei, the spatial wave-function is symmetric in the singlet spin state and antisymmetric in the triplet states, which reduces the interference contrast by a factor 2.

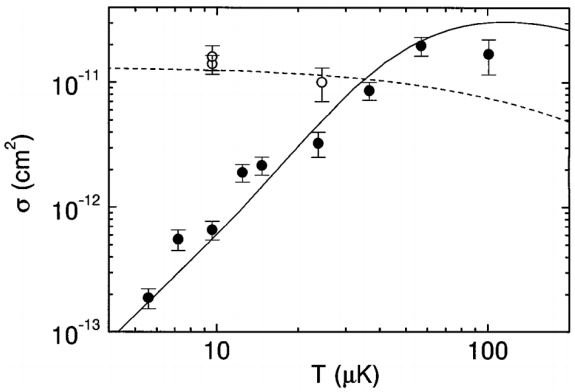


Figure 29: Elastic scattering cross-section measured as a function of temperature for a spin-polarized Fermi gas (filled circles) and for a mixture of spin states (open circles) [67]. Spin-polarized fermions, whose pairwise relative motion only involves odd partial wave, exhibit a strong reduction of scattering at low temperature.

4.6 Examples

We consider several examples of scattering potentials that allow for a complete analytic treatment.

4.6.1 Hard-sphere potential

We first consider the hard-sphere potential, defined by the expressions

$$V(r) = +\infty \quad \text{for} \quad r < R, \tag{4.71}$$
$$= 0 \quad \text{for} \quad r > R. \tag{4.72}$$

The hard-sphere constraint is equivalent to imposing the boundary condition $\psi_{\mathbf{k}}(R) = 0$ on the wave-function of the scattering state. We look separately for the stationary states in different partial waves ℓ. We write the radial part of the wave-function as $u_\ell(r)/r$, where $u_\ell(r)$ is solution of

$$u''_\ell(r) + \left[k^2 - \frac{\ell(\ell+1)}{r^2}\right] u_\ell(r) = 0. \tag{4.73}$$

We have already shown that the solutions to this equation can be expressed in terms of Bessel functions as

$$u_\ell(r) = A_\ell[\cos\alpha_\ell \sqrt{kr} J_{\ell+1/2}(kr) - \sin\alpha_\ell \sqrt{kr} Y_{\ell+1/2}(kr)]. \tag{4.74}$$

The large-r expansion in terms of spherical wave is given by

$$u_\ell(r) \propto \cos\alpha_\ell \sin(kr - \ell\pi/2) + \sin\alpha_\ell \cos(kr - \ell\pi/2) = \sin(kr - \ell\pi/2 + \alpha_\ell). \tag{4.75}$$

By comparing with (4.57), we can identify the angle α_ℓ with the scattering phase shift δ_ℓ. Its value is determined by the hard-sphere constraint $u_\ell(R) = 0$, which gives

$$\cos\delta_\ell J_{\ell+1/2}(kR) = \sin\delta_\ell Y_{\ell+1/2}(kR), \tag{4.76}$$

which can be written as

$$\tan\delta_\ell = \frac{J_{\ell+1/2}(kR)}{Y_{\ell+1/2}(kR)}. \tag{4.77}$$

For $\ell = 0$, the spherical Bessel functions can be expressed in terms of standard harmonic functions, and we get the exact expression $\delta_0 = -kR$. At low energy $k \to 0$, this gives the value of the scattering length

$$a = R. \tag{4.78}$$

We note that this value is necessarily positive. More generally, one can show that any potential $V(r)$ which is everywhere positive with respect to its asymptotic value gives rise to a positive scattering length.

4.6.2 Square-well potential

The square-well potential is slightly more complex than the hard sphere, but we will see that it allows for richer behavior, such as the possibility to have positive or negative scattering lengths depending on the potential parameters. It is defined by the expressions

$$V(r) = -U \quad \text{for} \quad r < R, \tag{4.79}$$
$$= 0 \quad \text{for} \quad r > R. \tag{4.80}$$

We focus here on the determination of the s-wave scattering length. For this, we look for the expression of the zero-energy scattering state $u_0(r)$, which is solution of the system

$$u_0''(r) + k_0^2 u_0(r) = 0 \quad \text{for} \quad r < R, \tag{4.81}$$
$$u_0''(r) = 0 \quad \text{for} \quad r > R, \tag{4.82}$$

where we define k_0 from the relation $U = \hbar^2 k_0^2/(2\mu)$. We write the solution as

$$u_0(r) = A \sin(k_0 r) \quad \text{for} \quad r < R, \tag{4.83}$$
$$= \alpha r + \beta \quad \text{for} \quad r > R. \tag{4.84}$$

We remind the expression of the asymptotic behavior expected for large r,

$$u_0(r) \propto \sin(kr) + \tan\delta_0 \cos(kr) \tag{4.85}$$
$$\propto r - a \quad \text{for} \quad k \to 0. \tag{4.86}$$

The scattering length is thus given by the ratio $a = -\beta/\alpha$. By imposing the continuity of the wave-function and of its derivative, we obtain the formula

$$a = R - \frac{\tan(k_0 R)}{k_0}. \tag{4.87}$$

We show in Fig. 30 the variation of the scattering length with the depth U of the potential.

We can compare it with the prediction of the Born approximation

$$a = -f(k=0) = \frac{\mu}{2\pi\hbar^2}\int V(r)\mathrm{d}^3 r = -\frac{k_0^2 R^3}{3}. \tag{4.88}$$

It is consistent with the exact result (4.87) in the limit of small depth $U \ll \hbar^2/(2\mu R^2)$, but it does not provide a useful estimate for larger depths.

For larger values of U, one finds a series of resonances, given by $k_0 R = (n+1/2)\pi$, i.e. $k_0 = (2n+1)\pi/(2R)$, with $n \in \mathbb{N}$, at which the scattering length diverges $a \to \infty$. Those resonances are also characterized by a zero-energy phase shift $\delta_0 = (n+1/2)\pi$, and the cross-section saturates to the unitary limit $\sigma_0 = 4\pi/k^2$. As discussed earlier, each divergence occurring when increasing U coincides with the appearance of a bound state in the square well. Such zero-energy resonances are discussed in a more general context in section 4.7.

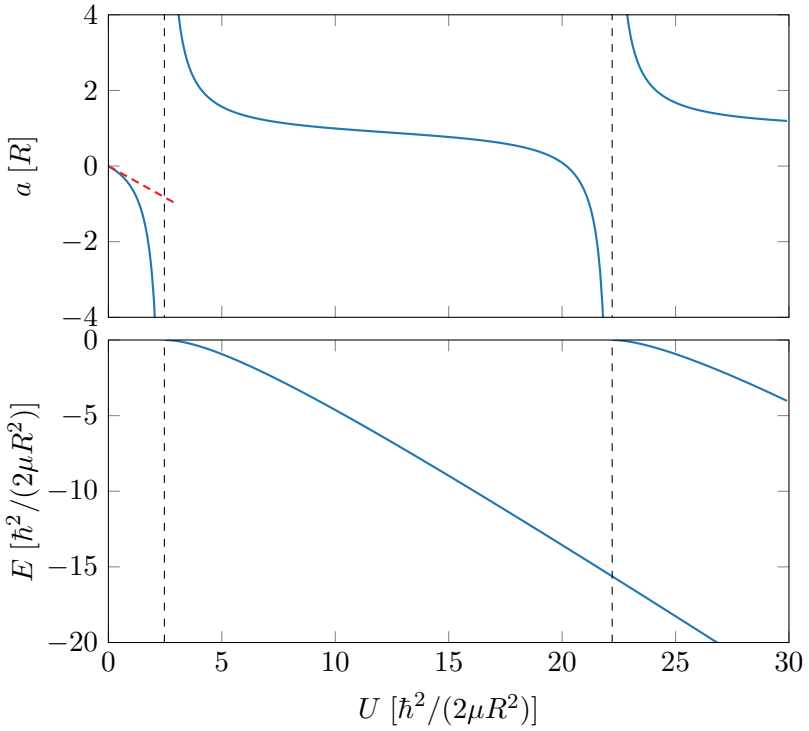


Figure 30: Evolution of the scattering length and bound state energies for the square-well potential as a function of its depth U. The blue lines are the exact results and the dashed red line is the Born approximation. The dashed black lines indicate two resonances at which the scattering length diverges and a bound state emerges from the continuum.

4.7 Scattering resonances

The square-well example shows that the scattering length diverges each time a bound state crosses the collision threshold $E = 0$. More generally, a scattering resonance corresponds to a strong enhancement of the scattering cross-section, possibly restricted to a narrow energy range, which is associated with the existence of a bound or quasi-bound state at an energy close to the collision energy. These features can be understood in a unified manner from the analytic structure of the scattering matrix elements $S_\ell(k) = \mathrm{e}^{2\mathrm{i}\delta_\ell(k)}$, extended to complex values of k.

4.7.1 Bound states, virtual states and resonances

We first consider the low-energy s-wave scattering amplitude (4.66), which corresponds to

$$S_0(k) = 1 + 2\mathrm{i}kf = \frac{1 - \mathrm{i}ka}{1 + \mathrm{i}ka}. \tag{4.89}$$

It exhibits a single pole at $k = \mathrm{i}/a$, whose interpretation depends on the sign of the scattering length:

- For $a > 0$, the pole lies on the positive imaginary axis, and it corresponds to the bound state of energy $E = -\hbar^2/(2\mu a^2)$ discussed in section 4.4.2.
- For $a < 0$, the pole lies on the negative imaginary axis, $k = -\mathrm{i}/|a|$. The corresponding wave-function $\mathrm{e}^{\mathrm{i}kr}/r = \mathrm{e}^{r/|a|}/r$ diverges at large distance, so that it does not describe a physical state. It is called a *virtual state*. Although it does not belong to the spectrum of the Hamiltonian, a virtual state close to threshold (i.e. for $|a| \gg b$) strongly enhances low-energy scattering, with a cross-section $\sigma_0 = 4\pi a^2/(1 + k^2a^2)$ largely exceeding the geometric cross-section $\sim b^2$.

The neutron-neutron interaction discussed above provides an example of virtual state: with $a \simeq -18.6\,\mathrm{fm}$, there is no bound state of two neutrons (the dineutron does not exist), but the virtual state lies at an energy $\hbar^2/(m_n a^2) \simeq 0.1\,\mathrm{MeV}$ only, much smaller than the energy scale $E_\star \simeq 10\,\mathrm{MeV}$ associated with the potential range.

A third type of pole can occur in the lower half of the complex plane, close to the positive real axis, at $k = k_r - \mathrm{i}\gamma$ with $0 < \gamma \ll k_r$. The corresponding complex energy writes

$$E = \frac{\hbar^2(k_r - \mathrm{i}\gamma)^2}{2\mu} \simeq E_r - \frac{\mathrm{i}\hbar\Gamma}{2}, \quad \text{with} \quad E_r = \frac{\hbar^2 k_r^2}{2\mu}, \quad \Gamma = \frac{2\hbar k_r \gamma}{\mu}. \tag{4.90}$$

Such a pole describes a *quasi-bound state*, i.e. a state of positive energy E_r that remains localized in the potential region for a finite lifetime $1/\Gamma$, before decaying towards the continuum of scattering states. For real energies E close to E_r, the scattering matrix element can be approximated as

$$S_\ell(E) \simeq \mathrm{e}^{2\mathrm{i}\delta_{\mathrm{bg}}} \frac{E - E_r - \mathrm{i}\hbar\Gamma/2}{E - E_r + \mathrm{i}\hbar\Gamma/2}, \tag{4.91}$$

where the phase shift δ_{bg} describes the slowly-varying background scattering. This expression is compatible with the unitarity constraint $|S_\ell| = 1$ for real energies, and it

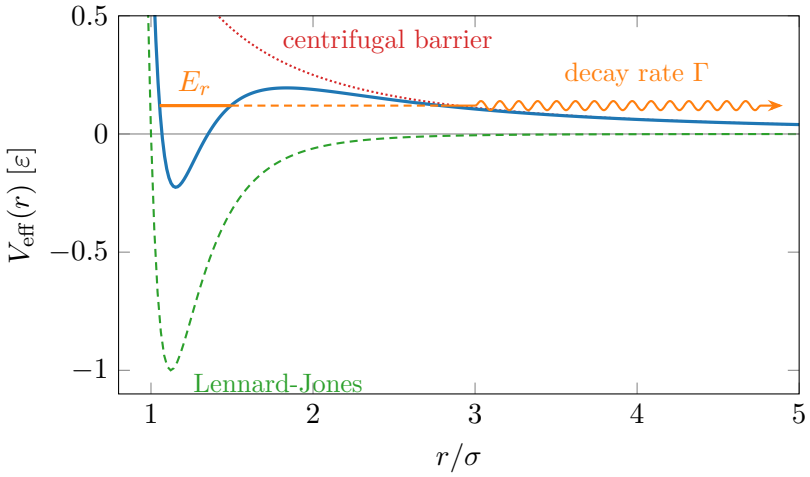


Figure 31: Effective radial potential $V(r) + \hbar^2\ell(\ell+1)/(2\mu r^2)$ (blue line) for a Lennard-Jones potential $V(r) = 4\varepsilon[(\sigma/r)^{12} - (\sigma/r)^6]$, with a centrifugal strength $\hbar^2\ell(\ell+1)/(2\mu\sigma^2) = \varepsilon$. The dashed green line is the bare Lennard-Jones potential, and the dotted red line the centrifugal potential alone. The centrifugal barrier traps a quasi-bound state of positive energy E_r (orange line, schematic), which decays towards the continuum by tunneling through the barrier, with a rate Γ.

exhibits the expected pole at $E = E_r - \mathrm{i}\hbar\Gamma/2$. The scattering phase shift is then given by $\delta_\ell = \delta_{\text{bg}} + \delta_{\text{res}}$, with

$$\tan\delta_{\text{res}} = \frac{\hbar\Gamma/2}{E_r - E}. \tag{4.92}$$

The resonant contribution δ_{res} increases by π when the energy is scanned across the resonance, over an energy range of width $\hbar\Gamma$, and it crosses the value $\pi/2$ at $E = E_r$. For negligible background scattering ($\delta_{\text{bg}} = 0$), the partial cross-section takes the Breit-Wigner form

$$\sigma_\ell(E) = \frac{4\pi}{k^2}(2\ell+1)\,\frac{(\hbar\Gamma/2)^2}{(E-E_r)^2 + (\hbar\Gamma/2)^2}, \tag{4.93}$$

i.e. a Lorentzian peak of width $\hbar\Gamma$, reaching the unitary limit at $E = E_r$. This line shape is reminiscent of the Lorentzian profile associated with the decay of a discrete state coupled to a continuum, discussed in section 1.3.4: the quasi-bound state plays the role of the discrete state, and the continuum of scattering states the role of the reservoir.

A typical mechanism leading to quasi-bound states is provided by the centrifugal barrier in partial waves $\ell \geq 1$. An attractive potential at short distance, surrounded by the centrifugal barrier, can host a state of positive energy, which is trapped behind the barrier and decays by tunneling (see Fig. 31). Such *shape resonances* become narrower as E_r decreases, since the tunneling probability through the barrier vanishes in the low-energy limit (one can show that $\Gamma \propto k_r^{2\ell+1}$).

4.7.2 Feshbach resonances

In atomic physics, scattering resonances can also be induced by the coupling between different internal states of the colliding atoms. We consider two atoms colliding in a

given internal state, which defines the so-called *open channel*, of energy threshold $E = 0$. We assume that the atoms can be coupled, via the interaction potential, to another internal state, the *closed channel*, whose threshold lies at a higher energy, so that two atoms in the closed channel cannot propagate to infinity at the considered collision energy. The closed-channel potential can nevertheless host a molecular bound state $|b\rangle$, whose energy E_b lies close to the open channel threshold. When the magnetic moments of the open and closed channels differ by $\delta\mu$, the bound-state energy can be tuned with an external magnetic field B, as

$$E_b(B) \simeq \delta\mu\,(B - B_c), \tag{4.94}$$

where B_c is the field at which the bound state crosses the open-channel threshold.

The coupling $\hat{W}$ between the open and closed channels gives rise to an effective interaction in the open channel. Eliminating the closed channel at second order in $\hat{W}$ (see section 1.1.1), the open-channel collisions at energy E experience the effective potential

$$\hat{V}_{\rm eff}(E) = \hat{V}_{\rm bg} + \frac{\hat{W}|b\rangle\langle b|\hat{W}}{E - E_b}, \tag{4.95}$$

where $\hat{V}_{\rm bg}$ is the open-channel potential, characterized by a background scattering length $a_{\rm bg}$. Treating the resonant term within the Born approximation at zero energy, we obtain its contribution to the scattering length

$$a - a_{\rm bg} \simeq \frac{\mu}{2\pi\hbar^2}\,\frac{|W_0|^2}{-E_b}, \tag{4.96}$$

where $W_0 \equiv L^{3/2}\langle b|\hat{W}|\mathbf{k} = \mathbf{0}\rangle$ is the coupling between the normalized molecular state $|b\rangle$ and the zero-energy open-channel wave of unit amplitude, independent of the box size. The resonant contribution is negative when the bound state lies above threshold ($E_b > 0$), and positive when it lies below. It diverges when $E_b \to 0$. This heuristic argument captures the generic form of the scattering length close to a Feshbach resonance,

$$a(B) = a_{\rm bg}\left(1 - \frac{\Delta}{B - B_0}\right), \tag{4.97}$$

where Δ is the width of the resonance (see Fig. 32). A complete treatment, beyond the Born approximation, shows that this form remains valid, with a resonance position B_0 shifted from B_c by the coupling to the open channel [68].

On the side of the resonance where $a > 0$ and $a \gg b$, the closed-channel bound state is dressed by the coupling to the open channel into a weakly bound molecular state of energy $E = -\hbar^2/(2\mu a^2)$, whose wave-function mostly lies in the open channel, in agreement with the universal behavior discussed in section 4.4.2. Such *Feshbach molecules* play a central role in the BEC-BCS crossover discussed in section 7.

Feshbach resonances were first observed with ultracold atoms in a Bose-Einstein condensate of sodium atoms [69]. They have since become the main tool to tune the interaction strength in ultracold atomic gases, from strongly repulsive to strongly attractive. A well-known example is the broad resonance of fermionic ^{6}Li atoms around $B_0 \simeq 832\,$G, used in most studies of the BEC-BCS crossover.

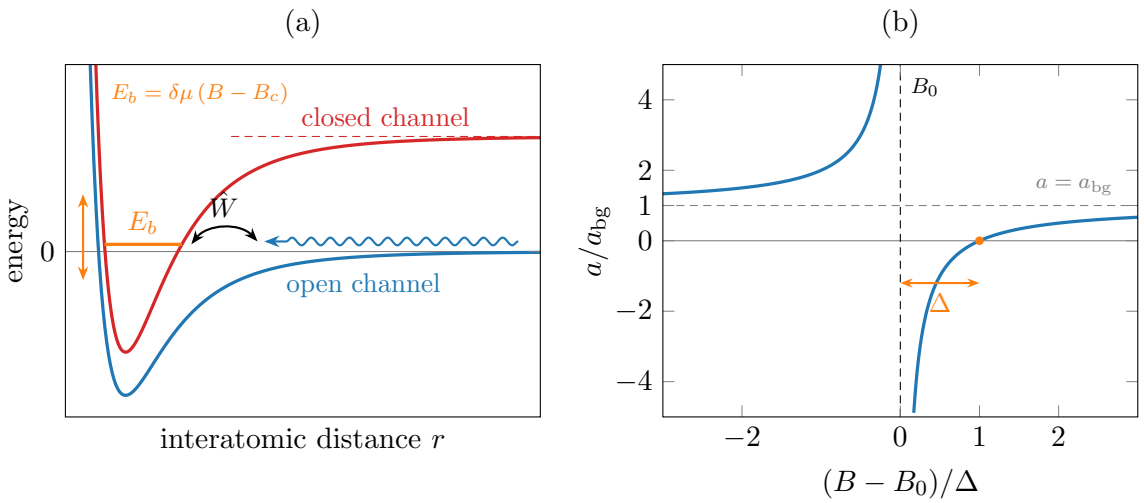


Figure 32: (a) Scheme of a Feshbach resonance. Two atoms collide at low energy in the open channel (blue), and are coupled by $\hat{W}$ to a molecular state $|b\rangle$ of the closed channel (red), whose energy E_b relative to the open-channel threshold is tuned with the magnetic field. (b) Variation of the scattering length with the magnetic field, according to (4.97), for a positive background scattering length $a_{\rm bg}$. The scattering length diverges at $B = B_0$ and vanishes at $B = B_0 + \Delta$.

4.8 Zero-range model: the Fermi-Huang pseudopotential

In the low-energy regime where s-wave interaction dominates, the scattering is fully determined by a single parameter, the scattering length a. The irrelevance of the details of the interaction potential calls for the introduction of a model interaction potential which can be used to describe low-energy collisions in a simplified manner.

The square-well potential introduced earlier is already a very simple potential, solely characterized by two quantities, its range R and depth U. However, the expression (4.87) shows that there are plenty of choices of R and U leading to the same value of a. This motivates the introduction of an even simpler potential parametrized by a single quantity.

4.8.1 Definition of the pseudopotential

Our objective is to introduce a potential whose range is shrunk to zero, so that the low-energy form of the scattering eigenstates

$$\psi_{\mathbf{k}}(\mathbf{r}) = \mathrm{e}^{\mathrm{i}\mathbf{k}\cdot\mathbf{r}} - \frac{a}{1 + \mathrm{i}ka}\frac{\mathrm{e}^{\mathrm{i}kr}}{r} \tag{4.98}$$

is an exact solution for all $r > 0$. Rather than postulating its expression, we reverse-engineer the potential from this requirement.

What the potential must compensate. For $r > 0$, the wave-function (4.98) solves the free Schrödinger equation $(\Delta + k^2)\psi_{\mathbf{k}} = 0$. This is not the case at the origin: using the identity $(\Delta + k^2)\,\mathrm{e}^{\mathrm{i}kr}/r = -4\pi\delta(\mathbf{r})$, valid in the sense of distributions over $\mathbb{R}^3$, we obtain

$$\left(-\frac{\hbar^2}{2\mu}\Delta - E\right)\psi_{\mathbf{k}}(\mathbf{r}) = -\frac{2\pi\hbar^2 a}{\mu}\,\frac{1}{1 + \mathrm{i}ka}\,\delta(\mathbf{r}), \tag{4.99}$$

with $E = \hbar^2 k^2/(2\mu)$. The scattering state is thus an eigenstate of $-\frac{\hbar^2}{2\mu}\Delta + V$ provided that the potential compensates this term, i.e.

$$V[\psi_{\mathbf{k}}] = \frac{g}{1 + \mathrm{i}ka}\,\delta(\mathbf{r}), \qquad \text{with} \qquad g = \frac{2\pi\hbar^2 a}{\mu}. \tag{4.100}$$

The potential must therefore act as $V[\psi] = g\,\delta(\mathbf{r})\,L[\psi]$, where L is a linear functional depending only on the behavior of ψ close to the origin. A simple delta potential $g\,\delta(\mathbf{r})$, for which $L[\psi] = \psi(\mathbf{0})$, is not acceptable: the scattering state diverges at the origin, and the required weight $1/(1 + \mathrm{i}ka)$ depends on k.

The Fermi-Huang pseudopotential. The functional L can be read from the short-distance expansion of the scattering state

$$\psi_{\mathbf{k}}(\mathbf{r}) = \frac{c}{r} + B + O(r), \qquad c = -\frac{a}{1 + \mathrm{i}ka}, \qquad B = \frac{1}{1 + \mathrm{i}ka}. \tag{4.101}$$

The regular part B coincides with the required weight for all values of k. We are thus led to the s-wave (also called Fermi-Huang) pseudopotential [70], which extracts the regular part of the wave-function at the origin:

$$V_{\mathrm{pp}}[\psi(\mathbf{r})] = g\,\delta(\mathbf{r})\frac{\partial(r\psi(\mathbf{r}))}{\partial r}, \qquad g = \frac{2\pi\hbar^2 a}{\mu}. \tag{4.102}$$

Indeed, for a wave-function that can be decomposed as

$$\psi(\mathbf{r}) = \frac{c}{r} + \psi_{\mathrm{reg}}(\mathbf{r}), \tag{4.103}$$

where the regular part has a well-defined limit at $\mathbf{r} = \mathbf{0}$, we have

$$V_{\mathrm{pp}}[\psi(\mathbf{r})] = g\,\psi_{\mathrm{reg}}(\mathbf{0})\delta(\mathbf{r}). \tag{4.104}$$

For a regular wave-function ($c = 0$), such as a plane wave, the pseudopotential acts as a simple delta potential $g\,\delta(\mathbf{r})$.

Interpretation as a boundary condition. The coefficients of the short-distance expansion satisfy $c = -aB$ for all k, i.e.

$$\psi(\mathbf{r}) \underset{r\to 0}{\propto} 1 - \frac{a}{r}, \qquad \text{or equivalently} \qquad \frac{u'(0)}{u(0)} = -\frac{1}{a} \quad \text{for} \quad u(r) = r\psi(r). \tag{4.105}$$

This is the Bethe-Peierls boundary condition. It states that the radial wave-function behaves as the zero-energy solution $u_0(r) \propto r - a$ found above. The zero-range model is thus fully specified by the free Schrödinger equation for $r > 0$, supplemented by this boundary condition, and the pseudopotential is a way to encode it in the Hamiltonian. This also clarifies in which sense the pseudopotential is unique [71]. Any other local functional $L[\psi] = \alpha c + \beta B$ would reduce to $(\beta - \alpha a)B$ on wave-functions satisfying (4.105), so that it defines the same operator once its normalization is fixed by (4.100).

Bound state. Bound states of the pseudopotential are solutions of the free Schrödinger equation for $r > 0$ that decay at infinity, $\psi(\mathbf{r}) = \mathrm{e}^{-qr}/r$ with $E = -\hbar^2 q^2/(2\mu)$. Their short-distance expansion $\psi = 1/r - q + O(r)$ satisfies the boundary condition (4.105) for $q = 1/a$. A single bound state thus exists for $a > 0$, of wave-function

$$\psi(\mathbf{r}) = \frac{\mathrm{e}^{-r/a}}{r} \tag{4.106}$$

and energy $E = -\hbar^2/(2\mu a^2)$, while no bound state exists for $a < 0$. This result coincides with the pole of the scattering amplitude $f = -a/(1 + \mathrm{i}ka)$ at $k = \mathrm{i}/a$. We check again that the bound state disappears in the continuum ($E \to 0$) simultaneously to the divergence of the scattering length.

4.8.2 Momentum-space representation

The pseudopotential is not a multiplicative potential $V(\mathbf{r})\psi(\mathbf{r})$, so that it does not admit a Fourier transform $\tilde{V}(\mathbf{k}' - \mathbf{k})$ in the usual sense. It is a separable operator, of the form $V_{\mathrm{pp}}[\psi] = g\,\delta(\mathbf{r})\,L[\psi]$, where the linear functional $L[\psi] = \psi_{\mathrm{reg}}(\mathbf{0})$ extracts the regular part of the wave-function at the origin. Its momentum-space representation is thus obtained by expressing this functional in terms of the Fourier transform $\tilde{\psi}(\mathbf{k}) = \int \psi(\mathbf{r})\mathrm{e}^{-\mathrm{i}\mathbf{k}\cdot\mathbf{r}}\mathrm{d}^3 r$. We write it as

$$L[\psi] = \int \Lambda(k)\,\tilde{\psi}(\mathbf{k})\,\frac{\mathrm{d}^3 k}{(2\pi)^3}, \tag{4.107}$$

and determine the weight $\Lambda(k)$ from two requirements:

- For a regular wave-function, we need $L[\psi] = \psi(\mathbf{0}) = \int \tilde{\psi}(\mathbf{k})\,\mathrm{d}^3 k/(2\pi)^3$, hence $\Lambda(k) = 1$ for any finite k. If one stops here, the pseudopotential cannot be distinguished from a delta potential $g\,\delta(\mathbf{r})$.
- The two potentials differ by their action on the singular function $1/r$: we need $L[1/r] = 0$. Using the Fourier transform $4\pi/k^2$ of $1/r$, this condition reads

$$\int \frac{\Lambda(k)}{k^2}\,\mathrm{d}^3 k = 4\pi \int_0^\infty \Lambda(k)\,\mathrm{d}k = 0. \tag{4.108}$$

These two requirements are incompatible for an ordinary function, and $\Lambda(k)$ must involve a singular contribution at $k = \infty$. In practice, one introduces a momentum cutoff k_c and defines

$$\Lambda_{k_c}(k) = \theta(k_c - k) - k_c\,\delta(k - k_c), \tag{4.109}$$

where θ is the Heaviside function, and where the second term ensures that $\int_0^\infty \Lambda_{k_c}(k)\,\mathrm{d}k = 0$. Calculations are performed at finite k_c, and the limit $k_c \to +\infty$ is taken at the end. Formally, this limit defines the generalized distribution [72]

$$\Lambda(k) = \lim_{k_c\to\infty} \left[\theta(k_c - k) - k_c\,\delta(k - k_c)\right] \tag{4.110}$$

$$= \lim_{k_c\to\infty} \left[\theta(k_c - k) - \frac{1}{k}\,\delta(1/k - 1/k_c)\right] \tag{4.111}$$

$$= 1 - \frac{\delta(1/k)}{k}. \tag{4.112}$$

Since the action of the pseudopotential on any wave-function is proportional to $\delta(\mathbf{r})$, whose Fourier transform is uniform, the matrix elements between box-normalized plane waves read

$$\langle \mathbf{k}'|\hat{V}_{\rm pp}|\mathbf{k}\rangle = \frac{g}{L^3}\,\Lambda(k). \tag{4.113}$$

They do not depend on the outgoing momentum $\mathbf{k}'$, and the factor Λ only involves the incoming momentum $\mathbf{k}$. This is the form used in the second-quantized Hamiltonians of Bogoliubov and BCS theories (sections 6 and 7), where the box volume L^3 is denoted V and $\mathbf{k}$ is the incoming relative momentum of the colliding pair.

We note that these matrix elements are not symmetric under the exchange of $\mathbf{k}$ and $\mathbf{k}'$: the pseudopotential is not Hermitian on the whole Hilbert space. The Hamiltonian is nevertheless Hermitian on the physical domain of wave-functions satisfying the Bethe-Peierls boundary condition (4.105). In practice, the factor $\Lambda(k)$ is never manipulated directly: one only uses $\Lambda(k) = 1$ at finite k together with the relation $\int_0^\infty \Lambda(k)\,\mathrm{d}k = 0$.

In the following we discuss two examples of calculations involving the momentum-space representation of the pseudo-potential, namely the calculations of the bound state energy and the Born expansion of the scattering amplitude. These examples illustrate how to handle the momentum space representation of the pseudo-potential, which will be used later when discussing interacting Bose-Einstein condensates and BCS fermionic superfluids. We then show that this approach is equivalent to the renormalization of the coupling constant, commonly used in the literature.

4.8.3 Bound state of the pseudo-potential

We first discuss how to determine the bound states of the contact potential from the momentum representation, as a check of the formalism (the result was already obtained in position space). We look for a stationary state of the Schrödinger equation

$$E\psi(\mathbf{r}) = -\frac{\hbar^2}{2\mu}\Delta\psi(\mathbf{r}) + V_{\rm pp}[\psi(\mathbf{r})] \tag{4.114}$$

with a negative energy $E = -|E|$. Since $V_{\rm pp}[\psi] = g\,\delta(\mathbf{r})\,\mathcal{I}$, with $\mathcal{I} = L[\psi]$ given by (4.107), the Schrödinger equation reads in momentum space

$$\left(|E| + \frac{\hbar^2 k^2}{2\mu}\right)\tilde{\psi}(\mathbf{k}) + g\,\mathcal{I} = 0, \qquad \mathcal{I} = \int \Lambda(k)\tilde{\psi}(\mathbf{k})\frac{\mathrm{d}^3k}{(2\pi)^3}. \tag{4.115}$$

It allows us to formally write the momentum-space wave-function as

$$\tilde{\psi}(\mathbf{k}) = \frac{-g\mathcal{I}}{|E| + \hbar^2k^2/(2\mu)}, \tag{4.116}$$

which is the Fourier transform of e^{-qr}/r with $|E| = \hbar^2q^2/(2\mu)$. We then compute the integral $\mathcal{I}$ as

$$\mathcal{I} = -g\,\mathcal{I}\int \frac{\Lambda(k)}{|E| + \hbar^2k^2/(2\mu)}\frac{\mathrm{d}^3k}{(2\pi)^3}. \tag{4.117}$$

For a non-trivial solution ($\mathcal{I} \neq 0$), we obtain the equation

$$\frac{-2\pi^2}{g} = \int \frac{\Lambda(k)k^2}{|E| + \hbar^2k^2/(2\mu)}\mathrm{d}k. \tag{4.118}$$

We note that the integral is divergent if one simply sets $\Lambda(k) = 1$, which shows the importance of the diverging term at $k = \infty$. In order to calculate the integral, we use the fact that $\int \Lambda(k)\mathrm{d}k = 0$ to transform the integral so that it can be safely integrated when setting $\Lambda(k) = 1$. More precisely, we write

$$\frac{-2\pi^2}{g} = \int \Lambda(k) \left[\frac{k^2}{|E| + \hbar^2 k^2/(2\mu)} - \frac{1}{\hbar^2/(2\mu)} \right] \mathrm{d}k \tag{4.119}$$

$$= -\frac{2\mu|E|}{\hbar^2} \int \frac{\Lambda(k)}{|E| + \hbar^2 k^2/(2\mu)} \mathrm{d}k \tag{4.120}$$

$$= -\frac{2\mu|E|}{\hbar^2} \int \frac{1}{|E| + \hbar^2 k^2/(2\mu)} \mathrm{d}k \tag{4.121}$$

$$= -\frac{\pi}{2} \left(\frac{2\mu}{\hbar^2} \right)^{3/2} \sqrt{|E|}. \tag{4.122}$$

This solution is only possible for a positive scattering length $a > 0$, and we recover the bound state energy $E = -\hbar^2/(2\mu a^2)$ given above.

4.8.4 Born expansion of the scattering amplitude

The simplicity of the pseudopotential allows for an analytic calculation of all orders of the Born expansion of the scattering amplitude (or equivalently the T-matrix). We focus here on the two first orders $\mathcal{T}_1$ and $\mathcal{T}_2$, for which we already gave explicit expressions for a generic potential in (4.46), replacing $\tilde{V}(\mathbf{k}' - \mathbf{k})$ by the box-independent matrix elements $L^3 \langle \mathbf{k}' | \hat{V}_{\mathrm{pp}} | \mathbf{k} \rangle = g\Lambda(k)$.

The first-order term is simply given by the matrix element of the potential, hence

$$\mathcal{T}_1(\mathbf{k}', \mathbf{k}) = g\Lambda(k) = g, \tag{4.123}$$

since the incoming momentum k is finite.

The second-order term involves the intermediate momenta $\mathbf{k}''$ as incoming momenta of the second collision, hence

$$\mathcal{T}_2(\mathbf{k}', \mathbf{k}) = \int \frac{g\Lambda(k'')\, g\Lambda(k)}{\hbar^2(k^2 - k''^2)/(2\mu) + \mathrm{i}\eta} \frac{\mathrm{d}^3 k''}{(2\pi)^3} \tag{4.124}$$

$$= \frac{g^2}{(2\pi)^3} \int \frac{\Lambda(k'')}{\hbar^2(k^2 - k''^2)/(2\mu) + \mathrm{i}\eta} \mathrm{d}^3 k'' \tag{4.125}$$

$$= \frac{g^2}{2\pi^2} \int \Lambda(k'') \left[\frac{k''^2}{\hbar^2(k^2 - k''^2)/(2\mu) + \mathrm{i}\eta} + \frac{2\mu}{\hbar^2} \right] \mathrm{d}k'' \tag{4.126}$$

$$= \frac{g^2 \mu k^2}{\pi^2 \hbar^2} \int \frac{\Lambda(k'')}{k^2 - k''^2 + \mathrm{i}\eta} \mathrm{d}k'' \tag{4.127}$$

$$= \frac{g^2 \mu k^2}{\pi^2 \hbar^2} \int \frac{1}{k^2 - k''^2 + \mathrm{i}\eta} \mathrm{d}k''. \tag{4.128}$$

This integral can be computed using the residue theorem, yielding the result

$$\mathcal{T}_2(\mathbf{k}', \mathbf{k}) = -\mathrm{i}g^2 \frac{\mu k}{2\pi\hbar^2} = -\mathrm{i}gka. \tag{4.129}$$

These results are consistent with the series expansion of the exact scattering amplitude

$$\mathcal{T}(\mathbf{k}',\mathbf{k}) = \frac{g}{1+\mathrm{i}ka} \simeq g - \mathrm{i}gka + \dots \tag{4.130}$$

In fact, the pseudopotential being separable, each order of the Born series involves the same integral over intermediate momenta, so that $\mathcal{T}_{n+1} = \mathcal{T}_1(-\mathrm{i}ka)^n$, and the series sums up to the exact result. We note that the first-order (Born) amplitude $\mathcal{T}_1 = g$ is real. According to the optical theorem, the imaginary part of the forward scattering amplitude is proportional to the total cross-section, which is non-zero. The Born approximation thus violates the conservation of probability, and this inconsistency is cured at second order: the term $\mathcal{T}_2$ provides precisely the imaginary part $\mathrm{Im}\, f(0) = ka^2 = k\sigma/(4\pi)$ required by the optical theorem, with $\sigma = 4\pi a^2$ the low-energy cross-section.

4.8.5 Equivalence with a renormalized coupling constant

The use of the generalized distribution $\Lambda(k)$ is equivalent to a more common procedure, which consists in describing the interaction by a contact potential $g_0\,\delta(\mathbf{r})$ regularized by a momentum cutoff k_c, i.e. with a Fourier transform $\tilde{V}(\mathbf{k}'-\mathbf{k}) = g_0$ for $k, k' < k_c$, and in adjusting the bare coupling constant g_0 so as to reproduce the scattering length a.

For such a separable potential, the Born series (4.46) can be summed exactly. Each term involves the same integral over the intermediate momenta, so that

$$\mathcal{T}(\mathbf{k}',\mathbf{k}) = g_0 + g_0^2\Pi(E) + g_0^3\Pi(E)^2 + \dots = \frac{g_0}{1-g_0\Pi(E)}, \tag{4.131}$$

where

$$\Pi(E) = \int_{k''<k_c} \frac{1}{E - \hbar^2 k''^2/(2\mu) + \mathrm{i}\eta} \frac{\mathrm{d}^3k''}{(2\pi)^3}. \tag{4.132}$$

The integral $\Pi(E)$ diverges linearly with the cutoff k_c. We fix the bare coupling by imposing the zero-energy value $\mathcal{T} = g = 2\pi\hbar^2 a/\mu$, i.e. $f(k=0) = -a$, which gives

$$\frac{1}{g_0} = \frac{1}{g} + \Pi(0) = \frac{1}{g} - \int_{k<k_c} \frac{2\mu}{\hbar^2k^2} \frac{\mathrm{d}^3k}{(2\pi)^3} = \frac{\mu}{2\pi\hbar^2 a} - \frac{\mu k_c}{\pi^2\hbar^2}. \tag{4.133}$$

The bare coupling constant thus depends on the cutoff, and it tends to zero (from negative values) when $k_c \to \infty$, whatever the sign of the scattering length. The T-matrix at finite energy then reads

$$\frac{1}{\mathcal{T}(\mathbf{k}',\mathbf{k})} = \frac{1}{g} - [\Pi(E) - \Pi(0)]. \tag{4.134}$$

The difference $\Pi(E) - \Pi(0)$ is convergent, and its value for $k_c \to \infty$, computed as for the term $\mathcal{T}_2$ above, is $-\mathrm{i}\mu k/(2\pi\hbar^2)$. We thus recover the exact result $\mathcal{T}(\mathbf{k}',\mathbf{k}) = g/(1+\mathrm{i}ka)$, at all orders.

This calculation shows that the physical quantities depend on the bare coupling g_0 and on the cutoff k_c only through the scattering length a. The relation (4.133) plays the same role as the prescription $\int_0^\infty \Lambda(k)\,\mathrm{d}k = 0$: in both cases, the ultraviolet divergence of the integrals is compensated by the subtraction of the counterterm $\int \mathrm{d}^3k/k^2$. In practice, a calculation performed with the coupling $g\Lambda(k)$ can be translated into the renormalized-coupling language by replacing g by g_0 and using (4.133) to eliminate g_0 in favor of a.

A Density matrix of a quantum system

In this appendix we introduce the density matrix and the reduced density matrix of a quantum subsystem. These notions are particularly useful when a quantum system is coupled to additional degrees of freedom, such as an electromagnetic field, a thermal reservoir, or a many-body environment. The main point is that even when the total system is in a pure quantum state, a subsystem generally cannot be described by a pure state. The appropriate description is instead given by a density operator.

A.1 Density matrix of a quantum system

Consider first an isolated quantum system described by a Hilbert space $\mathcal{H}$. A pure state is represented by a normalized vector $|\psi\rangle \in \mathcal{H}$. It is often convenient to associate with this state the density operator

$$\hat{\rho} = |\psi\rangle\langle\psi|. \tag{A.1}$$

The expectation value of an observable $\hat{O}$ can then be written as

$$\langle \hat{O} \rangle = \langle\psi|\hat{O}|\psi\rangle = \mathrm{Tr}(\hat{\rho}\hat{O}). \tag{A.2}$$

The density-operator formulation is more general than the description in terms of a state vector, since it also allows us to describe statistical mixtures. Consider a collection of pure states $|\psi_n\rangle$ occurring with probabilities Π_n, with

$$\Pi_n \geq 0, \qquad \sum_n \Pi_n = 1. \tag{A.3}$$

The corresponding density operator is

$$\hat{\rho} = \sum_n \Pi_n |\psi_n\rangle\langle\psi_n|. \tag{A.4}$$

The expectation value of any observable is then

$$\langle \hat{O} \rangle = \mathrm{Tr}(\hat{\rho}\hat{O}) = \sum_n \Pi_n \langle\psi_n|\hat{O}|\psi_n\rangle. \tag{A.5}$$

Thus, the density matrix provides a unified description of both pure states and statistical mixtures.

The density operator satisfies three important algebraic properties:

$$\hat{\rho}^\dagger = \hat{\rho}, \qquad \hat{\rho} \geq 0, \qquad \mathrm{Tr}\,\hat{\rho} = 1. \tag{A.6}$$

A state is pure if and only if

$$\hat{\rho}^2 = \hat{\rho}, \tag{A.7}$$

or, equivalently,

$$\mathrm{Tr}(\hat{\rho}^2) = 1. \tag{A.8}$$

The quantity

$$\gamma(\hat{\rho}) = \mathrm{Tr}(\hat{\rho}^2) \tag{A.9}$$

is called the *purity*. It satisfies $0 < \gamma \leq 1$, with $\gamma = 1$ for pure states.

Another measure of mixedness is the von Neumann entropy,

$$S(\hat{\rho}) = -\,\mathrm{Tr}(\hat{\rho}\log\hat{\rho}). \tag{A.10}$$

It vanishes for pure states and is positive for mixed states.

A.2 Subsystems and the reduced density matrix

We now consider a composite system made of a subsystem $\mathcal{S}$ and an environment or reservoir $\mathcal{E}$. The total Hilbert space has the tensor-product structure

$$\mathcal{H} = \mathcal{H}_S \otimes \mathcal{H}_E. \tag{A.11}$$

An observable acting only on the subsystem has the form

$$\hat{O}_S \otimes \hat{\mathbb{1}}_E. \tag{A.12}$$

For a total density matrix $\hat{\rho}$ describing $\mathcal{S} + \mathcal{E}$, its expectation value is therefore

$$\langle \hat{O}_S \rangle = \mathrm{Tr}_{S+E} \left[\hat{\rho} (\hat{O}_S \otimes \hat{\mathbb{1}}_E) \right]. \tag{A.13}$$

We would like to describe all measurements performed on $\mathcal{S}$ without explicitly keeping track of the degrees of freedom of $\mathcal{E}$. This is achieved by introducing the *reduced density matrix*

$$\hat{\rho}_S = \mathrm{Tr}_E \, \hat{\rho}. \tag{A.14}$$

The expectation value of any observable acting on $\mathcal{S}$ can then be written solely in terms of $\hat{\rho}_S$:

$$\langle \hat{O}_S \rangle = \mathrm{Tr}_S \left(\hat{\rho}_S \hat{O}_S \right). \tag{A.15}$$

Thus, $\hat{\rho}_S$ contains precisely the information required to predict all measurements performed on the subsystem.

The partial trace can be defined by choosing any orthonormal basis $\{|\xi_n\rangle\}$ of $\mathcal{H}_E$:

$$\mathrm{Tr}_E \, \hat{\rho} = \sum_n \langle \xi_n | \hat{\rho} | \xi_n \rangle, \tag{A.16}$$

where the matrix elements on the right-hand side are operators acting on $\mathcal{H}_S$. Although this expression uses a particular basis, the resulting reduced density matrix is independent of the choice of basis.

A.3 Reduced state of an entangled pure state

The physical meaning of the reduced density matrix becomes particularly clear when the total system is in a pure state. Let

$$|\Psi\rangle \in \mathcal{H}_S \otimes \mathcal{H}_E \tag{A.17}$$

be a normalized state of the composite system. Its density matrix is

$$\hat{\rho} = |\Psi\rangle\langle\Psi|, \tag{A.18}$$

and the reduced state of the subsystem is

$$\hat{\rho}_S = \mathrm{Tr}_E |\Psi\rangle\langle\Psi|. \tag{A.19}$$

To illustrate this construction, choose an orthonormal basis $\{|\xi_n\rangle\}$ of the reservoir and write

$$|\Psi\rangle = \sum_n c_n |\psi_n\rangle \otimes |\xi_n\rangle, \tag{A.20}$$

where the states $|\psi_n\rangle$ need not be orthogonal. Taking the partial trace gives

$$\hat{\rho}_S = \sum_n |c_n|^2 |\psi_n\rangle\langle\psi_n|. \tag{A.21}$$

Consequently,

$$\langle \hat{O}_S \rangle = \sum_n |c_n|^2 \langle\psi_n|\hat{O}_S|\psi_n\rangle. \tag{A.22}$$

From the point of view of the subsystem, the state therefore has the same measurement statistics as an incoherent mixture of the states $|\psi_n\rangle$.

This does not mean that the total state is itself an incoherent mixture. The distinction is important: the total system can be in a perfectly well-defined pure state, while the subsystem is described by a mixed state because information about correlations with the environment has been discarded.

A particularly simple case is a product state,

$$|\Psi\rangle = |\psi_S\rangle \otimes |\chi_E\rangle. \tag{A.23}$$

The reduced density matrix is then

$$\hat{\rho}_S = |\psi_S\rangle\langle\psi_S|, \tag{A.24}$$

which is pure. By contrast, if $|\Psi\rangle$ is entangled, the reduced state is generally mixed.

For example, consider the entangled state

$$|\Psi\rangle = \frac{1}{\sqrt{2}} \left(|0\rangle_S |0\rangle_E + |1\rangle_S |1\rangle_E \right). \tag{A.25}$$

The total state is pure, but tracing over the reservoir gives

$$\hat{\rho}_S = \frac{1}{2} \left(|0\rangle\langle 0| + |1\rangle\langle 1| \right), \tag{A.26}$$

which is maximally mixed for a two-level subsystem. The loss of purity is therefore a direct consequence of entanglement with degrees of freedom that are not observed.

A.4 Populations, coherences, and entropy

In a chosen orthonormal basis $\{|n\rangle\}$ of the subsystem, the density matrix can be written as

$$\hat{\rho}_S = \sum_{n,m} \rho_{nm} |n\rangle\langle m|, \qquad \rho_{nm} = \langle n|\hat{\rho}_S|m\rangle. \tag{A.27}$$

The diagonal elements

$$\rho_{nn} \tag{A.28}$$

are called *populations*, while the off-diagonal elements

$$\rho_{nm}, \qquad n \neq m, \tag{A.29}$$

are called *coherences*.

The reduced density matrix is therefore particularly useful for describing the loss of coherence and the redistribution of populations that can occur when a subsystem

interacts with an environment. These effects will be central in the discussion of open quantum systems.

The von Neumann entropy of the subsystem,

$$S(\hat{\rho}_S) = -\operatorname{Tr}\left(\hat{\rho}_S \log \hat{\rho}_S\right), \tag{A.30}$$

provides a quantitative measure of its mixedness. For a bipartite pure state, the entropies of the two subsystems are equal,

$$S(\hat{\rho}_S) = S(\hat{\rho}_E), \tag{A.31}$$

and quantify the entanglement between them.

More generally, the von Neumann entropy obeys the subadditivity inequality

$$S(\hat{\rho}_{SE}) \leq S(\hat{\rho}_S) + S(\hat{\rho}_E), \tag{A.32}$$

and, for a product state,

$$\hat{\rho}_{SE} = \hat{\rho}_S \otimes \hat{\rho}_E, \tag{A.33}$$

it is additive:

$$S(\hat{\rho}_S \otimes \hat{\rho}_E) = S(\hat{\rho}_S) + S(\hat{\rho}_E). \tag{A.34}$$

The reduced density matrix thus provides the natural language for describing a subsystem independently of the detailed state of its environment. In the main text, we will use it to formulate the effective dynamics of open quantum systems, where the evolution of $\hat{\rho}_S$ is generally no longer described by a unitary Schrödinger equation.

References

[1] M. W. Ray, E. Ruokokoski, K. Tiurev, M. Möttönen, and D. S. Hall. Observation of isolated monopoles in a quantum field. *Science*, 348:544–547, 2015.

[2] Victor Frederick Weisskopf and Eugene Paul Wigner. Calculation of the natural brightness of spectral lines on the basis of Dirac's theory. *Z. Phys.*, 63:54–73, 1930.

[3] Edward Mills Purcell. Spontaneous Emission Probabilities at Radio Frequencies. *Phys. Rev.*, 69:681, 1946.

[4] Philippe Lalanne, Wei Yan, Kevin Vynck, Christophe Sauvan, and Jean-Paul Hugonin. Light Interaction with Photonic and Plasmonic Resonances. *Laser Photonics Rev.*, 12:1700113, 2018.

[5] P. Goy, J. M. Raimond, M. Gross, and S. Haroche. Observation of Cavity-Enhanced Single-Atom Spontaneous Emission. *Phys. Rev. Lett.*, 50:1903–1906, 1983.

[6] J. M. Gérard, B. Sermage, B. Gayral, B. Legrand, E. Costard, and V. Thierry-Mieg. Enhanced Spontaneous Emission by Quantum Boxes in a Monolithic Optical Microcavity. *Phys. Rev. Lett.*, 81:1110–1113, 1998.

[7] Pascale Senellart, Glenn Solomon, and Andrew White. High-performance semiconductor quantum-dot single-photon sources. *Nature Nanotech*, 12:1026–1039, 2017.

[8] Randall G. Hulet, Eric S. Hilfer, and Daniel Kleppner. Inhibited Spontaneous Emission by a Rydberg Atom. *Phys. Rev. Lett.*, 55:2137–2140, 1985.

[9] W. Jhe, A. Anderson, E. A. Hinds, D. Meschede, L. Moi, and S. Haroche. Suppression of spontaneous decay at optical frequencies: Test of vacuum-field anisotropy in confined space. *Phys. Rev. Lett.*, 58:666–669, 1987.

[10] Eli Yablonovitch. Inhibited Spontaneous Emission in Solid-State Physics and Electronics. *Phys. Rev. Lett.*, 58:2059–2062, 1987.

[11] M. D. Leistikow, A. P. Mosk, E. Yeganegi, S. R. Huisman, A. Lagendijk, and W. L. Vos. Inhibited Spontaneous Emission of Quantum Dots Observed in a 3D Photonic Band Gap. *Phys. Rev. Lett.*, 107:193903, 2011.

[12] Sajeev John and Jian Wang. Quantum electrodynamics near a photonic band gap: Photon bound states and dressed atoms. *Phys. Rev. Lett.*, 64:2418–2421, 1990.

[13] Ulrich Hoeppe, Christian Wolff, Jens Küchenmeister, Jens Niegemann, Malte Drescher, Hartmut Benner, and Kurt Busch. Direct Observation of Non-Markovian Radiation Dynamics in 3D Bulk Photonic Crystals. *Phys. Rev. Lett.*, 108:043603, 2012.

[14] Yanbing Liu and Andrew A. Houck. Quantum electrodynamics near a photonic bandgap. *Nature Phys*, 13:48–52, 2017.

[15] Ludwig Krinner, Michael Stewart, Arturo Pazmiño, Joonhyuk Kwon, and Dominik Schneble. Spontaneous emission of matter waves from a tunable open quantum system. *Nature*, 559:589–592, 2018.

[16] Vinicius S. Ferreira, Jash Banker, Alp Sipahigil, Matthew H. Matheny, Andrew J. Keller, Eunjong Kim, Mohammad Mirhosseini, and Oskar Painter. Collapse and Revival of an Artificial Atom Coupled to a Structured Photonic Reservoir. *Phys. Rev. X*, 11:041043, 2021.

[17] B.-W. Li, Q.-X. Mei, Y.-K. Wu, M.-L. Cai, Y. Wang, L. Yao, Z.-C. Zhou, and L.-M. Duan. Observation of Non-Markovian Spin Dynamics in a Jaynes-Cummings-Hubbard Model Using a Trapped-Ion Quantum Simulator. *Phys. Rev. Lett.*, 129:140501, 2022.

[18] Jean Dalibard, Yvan Castin, and Klaus Mølmer. Wave-function approach to dissipative processes in quantum optics. *Phys. Rev. Lett.*, 68:580, 1992.

[19] Andrew J. Daley. Quantum trajectories and open many-body quantum systems. *Adv. Phys.*, 63:77–149, 2014.

[20] Yuto Ashida, Zongping Gong, and Masahito Ueda. Non-Hermitian physics. *Adv. Phys.*, 69:249–435, 2020.

[21] Sébastien Gleyzes, Stefan Kuhr, Christine Guerlin, Julien Bernu, Samuel Deléglise, Ulrich Busk Hoff, Michel Brune, Jean-Michel Raimond, and Serge Haroche. Quantum jumps of light recording the birth and death of a photon in a cavity. *Nature*, 446:297–300, 2007.

[22] Christine Guerlin, Julien Bernu, Samuel Deléglise, Clément Sayrin, Sébastien Gleyzes, Stefan Kuhr, Michel Brune, Jean-Michel Raimond, and Serge Haroche. Progressive field-state collapse and quantum non-demolition photon counting. *Nature*, 448:889–893, 2007.

[23] Serge Haroche. Nobel Lecture: Controlling photons in a box and exploring the quantum to classical boundary. *Rev. Mod. Phys.*, 85:1083–1102, 2013.

[24] Serge Haroche and Jean-Michel Raimond. *Exploring the Quantum: Atoms, Cavities, and Photons*. Oxford university press, 2006.

[25] A. M. L. Messiah and O. W. Greenberg. Symmetrization Postulate and Its Experimental Foundation. *Phys. Rev.*, 136:B248–B267, 1964.

[26] W. Pauli. The Connection Between Spin and Statistics. *Phys. Rev.*, 58:716–722, 1940.

[27] Robert C. Hilborn. Answer to Question ♯7 ["The spin-statistics theorem," Dwight E. Neuenschwander, Am. J. Phys. 62 (11), 972 (1994)]. *American Journal of Physics*, 63:298–299, 1995.

[28] M. D. Girardeau. Permutation Symmetry of Many-Particle Wave Functions. *Phys. Rev.*, 139:B500–B508, 1965.

[29] J. M. Leinaas and J. Myrheim. On the theory of identical particles. *Nuovo Cim B*, 37:1–23, 1977.

[30] Gregory Moore and Nicholas Read. Nonabelions in the fractional quantum hall effect. *Nuclear Physics B*, 360:362–396, 1991.

[31] R. Hanbury Brown and R. Q. Twiss. Correlation between Photons in two Coherent Beams of Light. *Nature*, 177:27–29, 1956.

[32] M. Reznikov, M. Heiblum, Hadas Shtrikman, and D. Mahalu. Temporal Correlation of Electrons: Suppression of Shot Noise in a Ballistic Quantum Point Contact. *Phys. Rev. Lett.*, 75:3340–3343, 1995.

[33] Harald Kiesel, Andreas Renz, and Franz Hasselbach. Observation of Hanbury Brown–Twiss anticorrelations for free electrons. *Nature*, 418:392–394, 2002.

[34] C. K. Hong, Z. Y. Ou, and L. Mandel. Measurement of subpicosecond time intervals between two photons by interference. *Phys. Rev. Lett.*, 59:2044–2046, 1987.

[35] E. Bocquillon, V. Freulon, J.-M Berroir, P. Degiovanni, B. Plaçais, A. Cavanna, Y. Jin, and G. Fève. Coherence and Indistinguishability of Single Electrons Emitted by Independent Sources. *Science*, 339:1054–1057, 2013.

[36] Dale G. Fried, Thomas C. Killian, Lorenz Willmann, David Landhuis, Stephen C. Moss, Daniel Kleppner, and Thomas J. Greytak. Bose-Einstein Condensation of Atomic Hydrogen. *Phys. Rev. Lett.*, 81:3811–3814, 1998.

[37] C. K. Law. Quantum entanglement as an interpretation of bosonic character in composite two-particle systems. *Phys. Rev. A*, 71:034306, 2005.

[38] Christopher Chudzicki, Olufolajimi Oke, and William K. Wootters. Entanglement and Composite Bosons. *Phys. Rev. Lett.*, 104:070402, 2010.

[39] Alexander D. Poularikas. *Transforms and Applications Handbook*. CRC Press, 2018.

[40] I. Bloch, T. W. Hänsch, and T. Esslinger. Measurement of the spatial coherence of a trapped Bose gas at the phase transition. *Nature*, 403:166–170, 2000.

[41] T. Jeltes, J. M. McNamara, W. Hogervorst, W. Vassen, V. Krachmalnicoff, M. Schellekens, A. Perrin, H. Chang, D. Boiron, A. Aspect, and C. I. Westbrook. Comparison of the Hanbury Brown-Twiss effect for bosons and fermions. *Nature*, 445:402–405, 2007.

[42] Yvan Castin. Basic theory tools for degenerate Fermi gases. *ArXivcond-Mat0612613*, 2006.

[43] Michael M. Wolf. Violation of the Entropic Area Law for Fermions. *Phys. Rev. Lett.*, 96:010404, 2006.

[44] J. Eisert, M. Cramer, and M. B. Plenio. *Colloquium* : Area laws for the entanglement entropy. *Rev. Mod. Phys.*, 82:277–306, 2010.

[45] M. Girardeau. Relationship between Systems of Impenetrable Bosons and Fermions in One Dimension. *Journal of Mathematical Physics*, 1:516–523, 1960.

[46] Elliott H. Lieb and Werner Liniger. Exact Analysis of an Interacting Bose Gas. I. The General Solution and the Ground State. *Phys. Rev.*, 130:1605–1616, 1963.

[47] Lewi Tonks. The Complete Equation of State of One, Two and Three-Dimensional Gases of Hard Elastic Spheres. *Phys. Rev.*, 50:955–963, 1936.

[48] P. Jordan and E. Wigner. Über das Paulische Äquivalenzverbot. *Z. Physik*, 47:631–651, 1928.

[49] A. Lenard. Momentum Distribution in the Ground State of the One-Dimensional System of Impenetrable Bosons. *Journal of Mathematical Physics*, 5:930–943, 1964.

[50] H. G. Vaidya and C. A. Tracy. One particle reduced density matrix of impenetrable bosons in one dimension at zero temperature. *Journal of Mathematical Physics*, 20:2291–2312, 1979.

[51] M. Olshanii. Atomic Scattering in the Presence of an External Confinement and a Gas of Impenetrable Bosons. *Phys. Rev. Lett.*, 81:938–941, 1998.

[52] T. D. Schultz. Note on the One-Dimensional Gas of Impenetrable Point-Particle Bosons. *Journal of Mathematical Physics*, 4:666–671, 1963.

[53] Toshiya Kinoshita, Trevor Wenger, and David S. Weiss. Observation of a One-Dimensional Tonks-Girardeau Gas. *Science*, 305:1125–1128, 2004.

[54] Belén Paredes, Artur Widera, Valentin Murg, Olaf Mandel, Simon Fölling, Ignacio Cirac, Gora V. Shlyapnikov, Theodor W. Hänsch, and Immanuel Bloch. Tonks–Girardeau gas of ultracold atoms in an optical lattice. *Nature*, 429:277–281, 2004.

[55] Toshiya Kinoshita, Trevor Wenger, and David S. Weiss. Local Pair Correlations in One-Dimensional Bose Gases. *Phys. Rev. Lett.*, 95:190406, 2005.

[56] P. Kapitza. Viscosity of Liquid Helium below the λ-Point. *Nature*, 141:74–74, 1938.

[57] J. F. Allen and A. D. Misener. Flow Phenomena in Liquid Helium II. *Nature*, 142:643–644, 1938.

[58] H. R. Glyde, S. O. Diallo, R. T. Azuah, O. Kirichek, and J. W. Taylor. Atomic momentum distribution and Bose-Einstein condensation in liquid ^{4}He under pressure. *Phys. Rev. B*, 84:184506, 2011.

[59] D. M. Ceperley and E. L. Pollock. The momentum distribution of normal and superfluid liquid 4He. *Can. J. Phys.*, 65:1416–1420, 1987.

[60] D. M. Ceperley. Path integrals in the theory of condensed helium. *Rev. Mod. Phys.*, 67:279–355, 1995.

[61] John R. Taylor. *Classical Mechanics*. University Science Books, Sausalito, Calif, null edition edition, 2005.

[62] B. A. Lippmann and Julian Schwinger. Variational Principles for Scattering Processes. I. *Phys. Rev.*, 79:469–480, 1950.

[63] Dov Levine and Paul Joseph Steinhardt. Quasicrystals: A New Class of Ordered Structures. *Phys. Rev. Lett.*, 53:2477–2480, 1984.

[64] Roger G Newton. *Scattering Theory of Waves and Particles*. Springer Science & Business Media, 2013.

[65] Q. Chen, C. R. Howell, T. S. Carman, W. R. Gibbs, B. F. Gibson, A. Hussein, M. R. Kiser, G. Mertens, C. F. Moore, C. Morris, A. Obst, E. Pasyuk, C. D. Roper, F. Salinas, H. R. Setze, I. Slaus, S. Sterbenz, W. Tornow, R. L. Walter, C. R. Whiteley, and M. Whitton. Measurement of the neutron-neutron scattering length using the ${\ensuremath{\pi}}^{\ensuremath{-}}d$ capture reaction. *Phys. Rev. C*, 77:054002, 2008.

[66] G.-R. Plattner and I. Sick. Coherence, interference and the Pauli principle: Coulomb scattering of carbon from carbon. *Eur. J. Phys.*, 2:109, 1981.

[67] B. DeMarco, J. L. Bohn, J. P. Burke, M. Holland, and D. S. Jin. Measurement of p-Wave Threshold Law Using Evaporatively Cooled Fermionic Atoms. *Phys. Rev. Lett.*, 82:4208–4211, 1999.

[68] Cheng Chin, Rudolf Grimm, Paul Julienne, and Eite Tiesinga. Feshbach resonances in ultracold gases. *Reviews of Modern Physics*, 82:1225–1286, 2010.

[69] S. Inouye, M. R. Andrews, J. Stenger, H.-J. Miesner, D. M. Stamper-Kurn, and W. Ketterle. Observation of Feshbach resonances in a Bose–Einstein condensate. *Nature*, 392:151–154, 1998.

[70] Kerson Huang and C. N. Yang. Quantum-Mechanical Many-Body Problem with Hard-Sphere Interaction. *Phys. Rev.*, 105:767–775, 1957.

[71] Maxim Olshanii and Ludovic Pricoupenko. Rigorous Approach to the Problem of Ultraviolet Divergencies in Dilute Bose Gases. *Phys. Rev. Lett.*, 88:010402, 2001.

[72] Manuel Valiente. Tan's distributions and Fermi-Huang pseudopotential in momentum space. *Phys. Rev. A*, 85:014701, 2012.

[73] D. F. Walls and Gerard J. Milburn. *Quantum Optics*. Springer, Berlin, Heidelberg, 2 edition, 2008.

[74] B. Andrei Bernevig and Taylor L. Hughes. *Topological Insulators and Topological Superconductors*. Princeton University Press, Princeton, 2013.

[75] F. Nicacio. Williamson theorem in classical, quantum, and statistical physics. *Am. J. Phys.*, 89:1139–1151, 2021.

[76] M. H. Anderson, J. R. Ensher, M. R. Matthews, C. E. Wieman, and E. A. Cornell. Observation of Bose-Einstein Condensation in a Dilute Atomic Vapor. *Science*, 269:198–201, 1995.

[77] K. B. Davis, M. O. Mewes, M. R. Andrews, N. J. van Druten, D. S. Durfee, D. M. Kurn, and W. Ketterle. Bose-Einstein Condensation in a Gas of Sodium Atoms. *Phys. Rev. Lett.*, 75:3969–3973, 1995.

[78] J. Kasprzak, M. Richard, S. Kundermann, A. Baas, P. Jeambrun, J. M. J. Keeling, F. M. Marchetti, M. H. Szymańska, R. André, J. L. Staehli, V. Savona, P. B. Littlewood, B. Deveaud, and Le Si Dang. Bose–Einstein condensation of exciton polaritons. *Nature*, 443:409–414, 2006.

[79] Alberto Amo, Jérôme Lefrère, Simon Pigeon, Claire Adrados, Cristiano Ciuti, Iacopo Carusotto, Romuald Houdré, Elisabeth Giacobino, and Alberto Bramati. Superfluidity of polaritons in semiconductor microcavities. *Nature Phys*, 5:805–810, 2009.

[80] Dmytro A. Bozhko, Alexander A. Serga, Peter Clausen, Vitaliy I. Vasyuchka, Frank Heussner, Gennadii A. Melkov, Anna Pomyalov, Victor S. L'vov, and Burkard Hillebrands. Supercurrent in a room-temperature Bose–Einstein magnon condensate. *Nature Phys*, 12:1057–1062, 2016.

[81] Jan Klaers, Julian Schmitt, Frank Vewinger, and Martin Weitz. Bose–Einstein condensation of photons in an optical microcavity. *Nature*, 468:545–548, 2010.

[82] R. Y. Chiao, E. Garmire, and C. H. Townes. Self-Trapping of Optical Beams. *Phys. Rev. Lett.*, 13:479–482, 1964.

[83] L. Khaykovich, F. Schreck, G. Ferrari, T. Bourdel, J. Cubizolles, L. D. Carr, Y. Castin, and C. Salomon. Formation of a Matter-Wave Bright Soliton. *Science*, 296:1290–1293, 2002.

[84] Kevin E. Strecker, Guthrie B. Partridge, Andrew G. Truscott, and Randall G. Hulet. Formation and propagation of matter-wave soliton trains. *Nature*, 417:150–153, 2002.

[85] Cheng-An Chen and Chen-Lung Hung. Observation of Universal Quench Dynamics and Townes Soliton Formation from Modulational Instability in Two-Dimensional Bose Gases. *Phys. Rev. Lett.*, 125:250401, 2020.

[86] B. Bakkali-Hassani, C. Maury, Y.-Q. Zou, É. Le Cerf, R. Saint-Jalm, P. C. M. Castilho, S. Nascimbene, J. Dalibard, and J. Beugnon. Realization of a Townes Soliton in a Two-Component Planar Bose Gas. *Phys. Rev. Lett.*, 127:023603, 2021.

[87] J. L. Roberts, N. R. Claussen, S. L. Cornish, E. A. Donley, E. A. Cornell, and C. E. Wieman. Controlled Collapse of a Bose-Einstein Condensate. *Phys. Rev. Lett.*, 86:4211–4214, 2001.

[88] Elizabeth A. Donley, Neil R. Claussen, Simon L. Cornish, Jacob L. Roberts, Eric A. Cornell, and Carl E. Wieman. Dynamics of collapsing and exploding Bose–Einstein condensates. *Nature*, 412:295–299, 2001.

[89] J. Steinhauer, R. Ozeri, N. Katz, and N. Davidson. Excitation Spectrum of a Bose-Einstein Condensate. *Phys. Rev. Lett.*, 88:120407, 2002.

[90] Raphael Lopes, Christoph Eigen, Nir Navon, David Clément, Robert P. Smith, and Zoran Hadzibabic. Quantum Depletion of a Homogeneous Bose-Einstein Condensate. *Phys. Rev. Lett.*, 119:190404, 2017.

[91] R. E. Grisenti, W. Schöllkopf, J. P. Toennies, G. C. Hegerfeldt, T. Köhler, and M. Stoll. Determination of the Bond Length and Binding Energy of the Helium Dimer by Diffraction from a Transmission Grating. *Phys. Rev. Lett.*, 85:2284–2287, 2000.

[92] K. T. Tang, J. P. Toennies, and C. L. Yiu. Accurate Analytical He-He van der Waals Potential Based on Perturbation Theory. *Phys. Rev. Lett.*, 74:1546–1549, 1995.

[93] M. H. Kalos, D. Levesque, and L. Verlet. Helium at zero temperature with hard-sphere and other forces. *Phys. Rev. A*, 9:2178–2195, 1974.

[94] S. Giorgini, J. Boronat, and J. Casulleras. Ground state of a homogeneous Bose gas: A diffusion Monte Carlo calculation. *Phys. Rev. A*, 60:5129–5132, 1999.

[95] V. I. Yukalov and E. P. Yukalova. Bose-Einstein-condensed gases with arbitrary strong interactions. *Phys. Rev. A*, 74:063623, 2006.

[96] T. D. Lee, Kerson Huang, and C. N. Yang. Eigenvalues and Eigenfunctions of a Bose System of Hard Spheres and Its Low-Temperature Properties. *Phys. Rev.*, 106:1135–1145, 1957.

[97] T. D. Lee and C. N. Yang. Many-Body Problem in Quantum Mechanics and Quantum Statistical Mechanics. *Phys. Rev.*, 105:1119–1120, 1957.

[98] Nir Navon, Swann Piatecki, Kenneth Günter, Benno Rem, Trong Canh Nguyen, Frédéric Chevy, Werner Krauth, and Christophe Salomon. Dynamics and Thermodynamics of the Low-Temperature Strongly Interacting Bose Gas. *Phys. Rev. Lett.*, 107:135301, 2011.

[99] D. S. Petrov. Quantum Mechanical Stabilization of a Collapsing Bose-Bose Mixture. *Phys. Rev. Lett.*, 115:155302, 2015.

[100] C. R. Cabrera, L. Tanzi, J. Sanz, B. Naylor, P. Thomas, P. Cheiney, and L. Tarruell. Quantum liquid droplets in a mixture of Bose-Einstein condensates. *Science*, 359:301–304, 2018.

[101] Nicolas Dupuis. *Field Theory of Condensed Matter and Ultracold Gases-Volume 1.* World Scientific, 2023.

[102] A. J. Leggett. Can a Solid Be "Superfluid"? *Phys. Rev. Lett.*, 25:1543–1546, 1970.

[103] Alessio Recati and Sandro Stringari. Supersolidity in ultracold dipolar gases. *Nat Rev Phys*, 5:735–743, 2023.

[104] C. Raman, M. Köhl, R. Onofrio, D. S. Durfee, C. E. Kuklewicz, Z. Hadzibabic, and W. Ketterle. Evidence for a Critical Velocity in a Bose-Einstein Condensed Gas. *Phys. Rev. Lett.*, 83:2502–2505, 1999.

[105] D. E. Miller, J. K. Chin, C. A. Stan, Y. Liu, W. Setiawan, C. Sanner, and W. Ketterle. Critical velocity for superfluid flow across the BEC-BCS crossover. *Physical Review Letters*, 99:070402, 2007.

[106] H.K. Onnes. The superconductivity of mercury. *Comm. Phys. Lab. Univ. Leiden*, 122:124, 1911.

[107] John Bardeen, Leon N Cooper, and J Robert Schrieffer. Microscopic theory of superconductivity. *Phys. Rev.*, 106:162–164, 1957.

[108] R. Combescot, M. Yu. Kagan, and S. Stringari. Collective mode of homogeneous superfluid Fermi gases in the BEC-BCS crossover. *Phys. Rev. A*, 74:042717, 2006.

[109] Yvan Castin, Igor Ferrier-Barbut, and C. Salomon. The Landau critical velocity for a particle in a Fermi superfluid. *Comptes Rendus Phys.*, 16:241–253, 2015.

[110] P. W. Anderson. Random-Phase Approximation in the Theory of Superconductivity. *Phys. Rev.*, 112:1900–1916, 1958.

[111] LD Landau. Oscillations in a fermi liquid. *Sov. Phys. Jetp-Ussr*, 5:101–108, 1957.

[112] D. van Oosten, P. van der Straten, and H. T. C. Stoof. Quantum phases in an optical lattice. *Phys. Rev. A*, 63:053601, 2001.

[113] Ana Maria Rey, Keith Burnett, Robert Roth, Mark Edwards, Carl J. Williams, and Charles W. Clark. Bogoliubov approach to superfluidity of atoms in an optical lattice. *J. Phys. B: At. Mol. Opt. Phys.*, 36:825, 2003.

[114] K. Xu, Y. Liu, D. E. Miller, J. K. Chin, W. Setiawan, and W. Ketterle. Observation of Strong Quantum Depletion in a Gaseous Bose-Einstein Condensate. *Phys. Rev. Lett.*, 96:180405, 2006.

[115] Jacob F. Sherson, Christof Weitenberg, Manuel Endres, Marc Cheneau, Immanuel Bloch, and Stefan Kuhr. Single-atom-resolved fluorescence imaging of an atomic Mott insulator. *Nature*, 467:68–72, 2010.

[116] V. J. Emery. Theory of the quasi-one-dimensional electron gas with strong "on-site" interactions. *Phys. Rev. B*, 14:2989–2994, 1976.

[117] Y. Claveau, B. Arnaud, and S. Di Matteo. Mean-field solution of the hubbard model: The magnetic phase diagram. *Eur. J. Phys.*, 35:035023, 2014.

[118] JM Radcliffe. Some properties of coherent spin states. *J. Phys. Gen. Phys.*, 4:313, 1971.

[119] T. Holstein and H. Primakoff. Field Dependence of the Intrinsic Domain Magnetization of a Ferromagnet. *Phys. Rev.*, 58:1098–1113, 1940.

[120] Anders W. Sandvik. Finite-size scaling of the ground-state parameters of the two-dimensional Heisenberg model. *Phys. Rev. B*, 56:11678–11690, 1997.

[121] Anders W. Sandvik and Hans Gerd Evertz. Loop updates for variational and projector quantum Monte Carlo simulations in the valence-bond basis. *Phys. Rev. B*, 82:024407, 2010.